

City Research Online

City St George's, University of London

Citation: Counihan, J. (1973). The structure and simulation of adiabatic boundary layers. (Unpublished Doctoral thesis, The City University)

This is the accepted version of the paper.

This version of the publication may differ from the final published version. To cite this item please consult the publisher's version.

Permanent repository link: https://openaccess.city.ac.uk/id/eprint/38378/

Copyright and Reuse: Copyright and Moral Rights remain with the author(s) and/or copyright holders. Copies of full items can be used for personal research or study, educational, or not-for-profit purposes without prior permission or charge, unless otherwise indicated, provided that the authors, title and full bibliographic details are credited, a hyperlink and/or URL is given for the original metadata page and the content is not changed in any way. For full details of reuse please refer to City Research Online policy.

City Research Online: http://openaccess.city.ac.uk/ publications@citystgeorges.ac.uk

The structure and Simulation of Adiabatic Boundary layers

by

J. Counihan

Part 2. Wind Tunnel Simulation of Adiabatic Boundary Layers

("The best and safest method of philosophising certainly seems to be, first, to enquire diligently into the properties of things and then to establish these properties by experiments". I. Newton - 1672)

A Thesis submitted for the degree of

Doctor of Philosophy

of

The City University

September 1973.

THE CITY UNIVERSITY LIBRARY,
ST. JOHN STREET, LONDON, E.C.1.

Department of Aeronautics,
City University,
London. E. C. 1.

ABSTRACT

It has been established that Industrial Aerodynamic wind tunnel tests should be carried out in flows which model atmospheric boundary layers. In order that the models being tested should be of an adequate size these boundary layers should be as deep as possible. Such a boundary layer can be produced naturally in a wind tunnel having a very long working section; the object of this work has been to devise a system which would reproduce flows having the structure of Adiabatic boundary layers in a few boundary layer heights.

There are some conflicting opinions in the literature as to the nature of the boundary layer structure for various terrain types or, how the flow structure varies as a function of the terrain roughness. Consequently, the first part of the work was concerned with deriving the boundary layer structure appropriate to flow over various types of terrain. This was done by reviewing and analysing the available meteorological literature for the period 1880 - 1972. The analysed data are finally presented as a function of the roughness lengths appropriate to various types of terrains and these data are considered to be the most representative available for Adiabatic boundary layers.

Many methods of simulating such flows have been attempted; these have been briefly reviewed in the second part of the work and were generally found to produce flows which did not have all of the required turbulence characteristics. The method described here produced all of the mean and turbulent flow properties required in a length of between three and four and one half boundary layer

heights. In the first instance the flow appropriate to rural terrain was produced and subsequently, with the system for producing the flow partly modified, the flow characteristics of urban terrain were simulated. The structure of both of these boundary layers was consistent with that predicted by the analysed atmospheric data.

CONTENTS

Notation.

List of figures.

1. Introduction.

2. Other Methods of Producing Simulated Boundary Layers.

2.1 Production of Sheared or Turbulent Flows.

2.2 Production of Sheared/Turbulent Flows.

3. Design Philosophy of the Boundary Layer Simulation system developed at the Central Electricity Research Laboratories.

4. Wind Tunnel and Instrumentation.

4.1 The Wind Tunnell.

4.2 Instrumentation.

5. Development of the Simulated Rural Boundary Layer.

5.1 Models.

5.2 Test Programme.

5.2.1 Wind Tunnel Calibration.

5.2.2 Barrier and Generator Wake Flow Characteristics.

5.2.3 Rural Simulated Flow Tests - Part 1.

5.2.4 Rural Simulated Flow Tests - Part 2.

5.3 Experimental Results.

5.3.1 Wind Tunnel Calibration.

5.3.2 Barrier and Generator Wake Flow Characteristics.

5.3.3 Rural Simulated Flow Tests - Part 1.

5.3.4 Rural Simulated Flow Tests - Part 2.

5.4 Discussion.

5.4.1 Wind Tunnel Calibration.

5.4.2 Barrier and Generator Wake Flow Characteristics.

5.4.3 Rural Simulated Flow Tests - Part 1.

CONTENTS (contd)

5.4.4 Rural Simulated Flow tests - Part 2.

5.4.5 Flow Visualisation Tests.

6. Determination of Roughness Element Characteristics.

6.1 Model and Test details.

6.2 Method of Analysis .

6.3 Results and Discussion.

6.3.1 Measurements at h_r/f_e = 0.014

6.3.2 Measurements at other Fetches.

7. Development of the Simulated Urban Boundary Layer.

7.1 Problems to be considered in Modelling an Urban Boundary Layer.

7.2 Models.

7.2.1 Roughness Element details.

7.2.2 The Barriers.

7.3 Test Programme.

7.4 Experimental Results.

7.5 Defining the Urban Boundary Layer.

7.5.1 The Velocity Profile.

7.5.2 The Turbulence Intensities.

7.5.3 The Power Spectral Densities.

7.5.4 The Reynolds Stresses.

7.5.5. The Co-Spectrum of the Reynolds Stresses.

7.5.6 The Probability Density Distribution.

7.5.7 The Scales of Turbulence.

7.5.8 The typical Urban Terrain Boundary Layer.

7.6 Discussion.

7.6.1 Effect of increasing the Barrier Height.

7.6.2 Mean Velocity and Turbulence Intensity Measurements.

CONTENTS (contd)

7.6.3 Correlation Measurements and Turbulence Scales.

7.6.4 The Power Spectral Densities.

7.6.5 The Co-spectra of the Reynolds Stresses.

7.6.6 The Probability Density Distributions.

7.6.7 Variation of the Power Index with the Roughness Length.

7.6.8 Wind Tunnel Axial Static Pressure Gradient.

8. General Comparison of the Simulated and Full-scale Adiabatic Boundary Layers.

9. Application of these Simulated Boundary Layers in Industrial Aerodynamics.

10. Conclusions.

11. Acknowledgements.

12. References.

APPENDIX 1

NOTATION.

A	Total plan surface area.
A_R	Plan surface area of roughness elements.
d	Zero-plane displacement.
f	Non-dimensional frequency-- $\frac{nh}{\bar{u}}$ or $\frac{ny}{\bar{u}}$
f_e	Fetch.
f_m	Non-dimensional frequency at which peak $nS(n)$ or $nS_{uv}(n)$ occur.
F	Coriolis parameter $(\cong 10^{-4}$ /sec.)
h	Vertical distance from ground level, $(=y)$
h_r	Roughness height.
h_1, h_2	Barrier height to base and top of castellations respectively.
H	Generator height = Boundary layer height $(=\delta)$.
H_D	Height of Adiabatic atmospheric boundary layer.
k	Von Karman's constant.
l	Width of square mesh of gauze.
$Lu_{x,y,z}$	Longitudinal turbulence length scales.
Lv_x	Vertical turbulence length scales.
$\mathcal{L}$	Semi-empirical constant.
n	Frequency.
n_p	Frequency at which peak $nS(n)$ occur.
$p(x)$	Probability density
q	Dynamic head $--\frac{1}{2}\rho\bar{u}^2$.
r	Separation distance.
R_o	Rossby number.
$Rii(r_1,r_2,r_3)$	Correlation coefficients.
$Rii(\tau)$	Auto-correlation coefficient.
$S(n)$	Power spectral density at frequency (n).
$S_{uv}(n)$	Power cospectral density at frequency (n).
u	Longitudinal velocity.
v	Vertical velocity.
w	Lateral velocity.

$\bar{U}$ Freestream velocity; or $\bar{U}_{max.}$.

U_* Friction velocity.

x Streamwise direction.

$\bar{x}$ Non-dimensional frequency-- $\frac{n\ell}{\bar{u}_{10}}$ ($\bar{u}_{10}$ = VEL. AT y = 10 m.)

X Model or full-scale building dimension.

y Vertical distance from ground level (=h).

y_L Vertical distance from zero plane, (=y - d).

y_o Roughness length.

z Across-wind direction.

$1/\alpha$ Power index of velocity power law.

α_G Generator incidence.

α_w Semi-wedge angle.

β Porosity of gauze screens.

γ Intermittency factor.

δ Boundary layer height.

μ Mean value (ref. to probability density).

ν Kinematic viscosity.

ρ Density.

σ Standard deviation (ref. to probability density).

τ Time increment.

τ_o Ground level shear stress.

C_p Pressure coefficient- $\frac{p_s - p_o}{q}$: p_s=tunnel static pressure
p_o=atmospheric pressure.

Suffix: M.S. - Model scale.

F.S. - Full scale.

Bar: denotes an average w.r.t. time.

Prime: denotes afluctuating contribution.

LIST OF FIGURES

Number	Contents
1.	Vortex system produced from barrier and generators.
2.	Diagrammatic presentation of momentum losses and turbulence production by simulation system components.
3.	Layout of wind tunnel and simulation system.
4.	Circuit diagram for measurement of mean and fluctuating velocities.
5.	Circuit diagram for measurement of intermittency factors.
6.	Range of generators investigated.
7.	Final arrangement of simulation system.
8.	Sign convention for correlation measurements.
9.	Wind tunnel calibration, mean velocity data.
10.	Wind tunnel calibration, turbulence intensity data.
11.	Determination of optimum integration time.
12.	Measurements in wake of Triangular Generators.
13.	Measurements in wake of Cranked Triangular Generators.
14.	Measurements in wake of Plane Elliptical Generator.
15.	Triangular Generator - contours of constant turbulence intensity.
16.	Plane Elliptic Generator - contours of constant turbulence intensity.
17.	Plane Elliptic Generator - contours of constant turbulence intensity.
18.	Elliptic-Wedge Generator - turbulence intensity in wake.
19.	Elliptic-Wedge Generator - contours of constant turbulence intensity.
20.	Measurements in wakes of Barriers.
21.	Measurements in wakes of Barrier/Generator combinations.

LIST OF FIGURES (cont.)

Number	Contents
22.	Comparison of wakes of Barrier and Barrier/Elliptic Generator.
23.	Effects of varying Generator spacing - 5° Elliptic Generator.
24.	Effects of varying Generator spacing - 6° Elliptic Generator.
25.	Effects of varying axial positions the Barrier and Generators.
26.	Effects of varying the Barrier/Generator spacing.
27.	Rough boundary layer characteristics - 'Lego' baseboard.
28.	Flat-plate boundary layer characteristics.
29.	Flat-plate boundary layer characteristics.
30.	Mean Velocity; Reynolds stress - Barrier height = 19.05 m.m.; Generator spacing = 88.9 m.m.
31.	Turbulence intensity - Barrier height = 19.05 m.m.; Generator spacing = 88.9 m.m.
32.	Mean Velocity; Reynolds stress - Barrier height = 19.05 m.m.; Generator spacing = 76.2 m.m.
33.	Turbulence intensity - Barrier height = 19.05 m.m.; Generator spacing = 76.2 m.m.
34.	Turbulence intensity - Barrier height = 19.05 m.m.; Generator spacing = 76.2 m.m.
35.	Mean Velocity; Reynolds stress - Barrier height = 22.2 m.m.; Generator spacing = 88.9 m.m.
36.	Turbulence intensity - Barrier height = 22.2 m.m.; Generator spacing = 88.9 m.m.
37.	Mean Velocity; Reynolds stress - Barrier height = 22.2 m.m.; Generator spacing = 76.2 m.m.

LIST OF FIGURES (cont.)

Number	Contents
38.	Turbulence intensity - Barrier height = 22.2 m.m.; Generator spacing = 76.2 m.m.
39.	Mean Velocity; Reynolds stress - Mod. Barrier; Generator spacing = 76.2 m.m.
40.	Turbulence intensity - Mod. Barrier; Generator spacing = 76.2 m.m.
41.	Turbulence intensity - Mod. Barrier; Generator spacing = 76.2 m.m.
42.	Measurements of mean velocity and Reynolds stress - Variation of axial position.
43.	Measurements of turbulence intensity - Variation of axial position.
44.	Measurements of mean velocity and Reynolds stress - Variation of axial position.
45.	Measurements of turbulence intensity - Variation of axial position.
46.	Measurements of Power Spectral Densities.
47.	Mean velocity contours behind roughness.
48.	Repeatibility of correlation measurements.
49.	$R_{uu}(o,r,o)$ at Generator mid-span, various heights, Station A.
50.	$R_{uu}(o,r,o)$ at Generator mid-span, various heights, Station A.
51.	$R_{uu}(o,r,o)$ at Generator mid-span, various heights, Station A.
52.	$R_{uu}(o,r,o)$ at Generator centre-line, various heights, Station A.
53.	$R_{uu}(o,r,o)$ at Generator centre-line, various heights, Station A.
54.	$R_{uu}(o,r,o)$ at Generator centre-line, various heights, Station A.
55.	$R_{uu}(o,r,o)$ at Generator mid-span, various heights, Station B.
56.	$R_{uu}(o,r,o)$ at Generator mid-span, various heights, Station B.
57.	$R_{uu}(o,r,o)$ at Generator mid-span, various heights, Station B.
58.	$R_{uu}(o,r,o)$ at Generator centre-line, various heights, Station B.

LIST OF FIGURES (cont.)

Number	Contents
59.	$R_{uu}(o,r,o)$ at Generator centre-line, various heights, Station B.
60.	$R_{uu}(o,r,o)$ at Generator centre-line, various heights, Station B.
61.	Test for symmetry of $R_{uu}(o,o,r)$ measurements, Station A.
62.	$R_{uu}(o,o,r)$ at various spanwise fixed points, y/H = 0.10, Station A.
63.	$R_{uu}(o,o,r)$ at various spanwise fixed points, y/H = 0.20, Station A.
64.	$R_{uu}(o,o,r)$ at various heights, Station A.
65.	Test for symmetry of $R_{uu}(o,o,r)$ measurements, Station B.
66.	$R_{uu}(o,o,r)$ at various spanwise fixed points, y/H = 0.10, Station B.
67.	$R_{uu}(o,o,r)$ at various spanwise fixed points, y/H = 0.20, Station B.
68.	$R_{uu}(o,o,r)$ at various heights, Station B.
69.	Comparison of $R_{uu}(o,r,o)$ with flat-plate boundary layer data.
70.	Comparison of $R_{uu}(o,o,r)$ with flat-plate boundary layer data.
71.	Comparison of $R_{uu}(o,r,o)$ with full-scale data, Generator mid-span.
72.	Comparison of $R_{uu}(o,r,o)$ with full-scale data, Generator centre-line.
73.	Comparison of $R_{uu}(o,o,r)$ with full scale data.
74.	Full scale $R_{uu}(o,r,o)$ corrected for possible spurious input effects.
75.	Full scale $R_{uu}(o,r,o)$ corrected for possible spurious input effects.
76.	Theoretical power spectral densities.
77.	Theoretical power spectral densities.
78.	Longitudinal spectra at various spanwise positions, Station A.
79.	Longitudinal spectra at various heights, Generator quarter-span, Station A.

LIST OF FIGURES (cont.)

Number	Contents
80.	Lateral spectra at various heights, Generator quarter-span, Stn. A.
81.	Lateral spectra at various heights, Generator quarter-span, Stn. A.
82.	Vertical spectra at various spanwise positions, Station A.
83.	Vertical spectra at various heights, Generator quarter-span, Stn. A.
84.	Longitudinal spectra at various spanwise positions, Station B.
85.	Longitudinal spectra at various heights, Generator quarter-span, Station B.
86.	Intermittency factors of longitudinal turbulence at Stns. A and B.
87.	Intermittency factors of all turbulence components at Station B.
88.	Mean velocity and Reynolds Stress at Station A.
89.	Mean velocity and Reynolds Stress at Station B.
90.	Longitudinal turbulence intensity measurements at Station B.
91.	Comparison of simulated and full scale longitudinal turbulence intensity.
92.	Diagrammatic results of flow visualisation tests.
93.	Mean velocity profiles in the wakes of large roughness elements.
94.	Variation of mean roughness length with roughness element density.
95.	Variation of mean roughness length with fetch and roughness element density.
96.	Theoretical and measured mean velocity profiles.
97.	Variation of turbulence intensity with Barrier height.
98.	Mean velocity and Reynolds Stress, Urban barrier, Station B.
99.	Turbulence intensities, Urban barrier, Station B.
100.	Effects of roughness on mean velocity and Reynolds stress profiles.
101.	Effects of roughness on turbulence intensity profiles.

LIST OF FIGURES (cont.)

Number	Contents
102.	Mean velocity and Reynolds stress, Urban barrier, Station A.
103.	Turbulence intensities, Urban barrier, Station A.
104.	Main velocity and Reynolds Stress, Urban barrier, Station C.
105.	Turbulence intensities, Urban barrier, Station C.
106.	$R_{uu}(0,r,0)$ at various heights, Generator centre-line, Station B.
107.	$R_{uu}(0,r,0)$ at various heights, Generator centre-line, Station B.
108.	$R_{uu}(0,r,0)$ at various heights, Generator mid-span, Station B.
109.	$R_{uu}(0,r,0)$ at various heights, Generator mid-span, Station B.
110.	Comparison of $R_{uu}(0,r,0)$ in simulated Rural and Urban flows.
111.	Test for symmetry of $R_{uu}(0,0,r)$ measurements, Station B.
112.	$R_{uu}(0,0,r)$ at various heights, Station B.
113.	$R_{uu}(0,0,r)$ at various heights, Station B.
114.	Comparison of $R_{uu}(0,0,r)$ in simulated Rural and Urban flows.
115.	Longitudinal scale of turbulence as a function of terrain type.
116.	Longitudinal spectra at various heights, Generator centre-line, Station B.
117.	Longitudinal spectra at various heights, Generator centre-line, Station C.
118.	Local effects of roughness on longitudinal spectra.
119.	Normalised longitudinal spectra.
120.	Lateral spectra at various heights, Generator centre-line, Stn. B.
121.	Vertical spectra at various heights, Generator centre-line, Stn.B.
122.	Vertical spectra at various heights, Generator centre-line, Stn.B.
123.	Comparison of spectra in simulated Rural and Urban flows.

LIST OF FIGURES (cont.)

Number	Contents
124.	Co-spectra of longitudinal and vertical velocities in simulated flows.
125.	Probability density distributions of longitudinal velocities in simulated flows.
126.	Wind tunnel axial static pressure gradient in simulated flows.
127.	Comparison of full-scale and simulated flows - $1/\alpha \sim y_o$
128.	Comparison of full-scale and simulated flows - $\sqrt{\overline{u^2}}/\bar{u} \sim y_o$
129.	Comparison of full-scale and simulated flows - $\overline{uv}/\bar{U}_o \sim y_o$
130.	Comparison of full-scale and simulated flows - $L_{u_x} \sim y \sim y_o$

1. INTRODUCTION

The main scope of the work of this thesis has previously been outlined in the introduction to Part 1; this also gave a more detailed background to the work on the structure of Adiabatic boundary layers. The following introduction outlines the reason for, and the scope of, the work on the simulation of these Adiabatic boundary layers in a wind tunnel.

The main reasons for needing to simulate such boundary layers have been noted previously. Briefly these can be attributed to the fact that modern high-rise and other buildings, being of a lighter structure, tend to be more vulnerable to the effects of high winds, i.e. those winds which produce a state of Adiabatic equilibrium. Consequently, both mean and fluctuating load components are of importance, and their respective magnitudes need to be determined, if possible, at model scale prior to construction of the relevant building.

In the initial stages of wind tunnel work on Industrial Aerodynamics problems, the majority of investigations were carried out in either a shear flow or a flow having uniform turbulence. Such flows were produced by arrangements of rods, gauze screens and turbulence grids. Clearly, rods and screens which were designed to produce shear profiles also produced some turbulence. However such turbulence was necessarily of a small scale and decayed rapidly. For various reasons model results from such tests cannot always be relied upon to be truly indicative of full-scale phenomena, although they can isolate the individual effects of shear and turbulence. Therefore even though tests in such flows can help in the understanding of some problems, it is not possible

to deduce from them the combined effects of shear and turbulence. Hence the flow produced in a wind tunnel needs to be representative of a shear/turbulent flow i.e. turbulent boundary layer flow.

Some methods were available by which shear turbulent flows could be produced before the work presented here was started; other methods were also devised during and after completion of this work. One of the first methods used was that devised by Jensen which was based on growing turbulent boundary layers over various types of rough surfaces. All of the systems devised have been briefly reviewed here. Generally it was found that many of the systems were based on either inadequate or invalid assumptions regarding the type of flow to be simulated. In many cases the resultant flows did not conform to the flow characteristics specified in Part 1 of this work. Some of the more recent methods devised have specified that only the lower part of the boundary layer need be simulated. These systems, as far as can be deduced, produce just the small-scale turbulence at the high frequency end of the spectrum. Therefore it is difficult to justify their use without the support of extensive model and full-scale test data.

In general, the most common fault of the various systems was that the required mean velocity profile was produced correctly but the accompanying intensities and scales of turbulence were arbitrary and not matched to the mean velocity profile (see Part 1). In many cases the precise terrain roughness simulated was either unspecified or unmeasured. Such a state clearly precludes the eventual correlation of research data on, say, wind loadings on buildings from various wind tunnels since the approach flows to the models being considered depends on the simulation system used.

The Universities of Colorado (U.S.A.) and Western Ontario (Canada) produce turbulent boundary layer flows in wind tunnels having very long working sections. Typically a boundary layer of height δ can be grown naturally over a rough surface in a distance of 25δ. Clearly, if it is assumed that the boundary layer height needs to be at least of the order of one metre, in order that models of adequate size may be used, then the cost of building an Industrial Aerodynamics wind tunnel of suitable dimensions becomes prohibitive.

The necessity of having an Industrial Aerodynamics wind tunnel was foreseen at the Central Electricity Research Laboratories. Consequently, a wind tunnel suitable for investigating problems encountered by the Central Electricity Generating Board was designed and constructed. This was available for research shortly after the collapse of the Ferrybridge cooling towers in 1965. Partly on the basis of current knowledge at that time and on the basis of the results of the Ferrybridge investigation it was decided that the wind tunnel measurement of both mean and fluctuating load components was essential in wind loading investigations. It followed that both the mean velocity profile and the turbulence intensity profiles should be simulated in the approach flow in wind tunnel model tests. It was assumed that representation of the fluctuating wind component implied simulation of both the turbulence intensities and the scales of turbulence contained in Adiabatic boundary layers. This gave the first main requirement of the simulation and essentially implied a representation of the complete gust spectrum. In addition, simulation of the large scales of turbulence was considered to be of importance since they are of

the same order of magnitude as conventional C.E.G.B. cooling towers.

The second main requirement was that the simulated flow should be in a state of equilibrium on approaching the model under test. It is considered that this should be a common requirement of all simulated flows; in which case research data from various wind tunnels should be capable of being correlated, at least on the basis of similarity of flow over the model. The remaining requirement was dictated by the design of the C.E.R.L. Industrial Aerodynamics wind tunnel and specified that the required flows should be produced in a distance of three to four and one half boundary layer heights. Therefore a system was required which would produce an accelerated rate of boundary layer growth and simulate flow over terrains varying from rural to urban. Although the analysis presented in Part 1 of this thesis was not complete when starting the experimental work, the choice of representative values of the power index and roughness length for the simulated rural and urban flows were seen to be fully justified on completion of the analysis presented in Part 1.

Hence this part of the thesis presents a brief review of the many types of systems now available for producing Adiabatic boundary layers and a detailed account of the philosophy behind, and the development of, the system described here for simulating Adiabatic atmospheric boundary layers.

2. OTHER METHODS OF PRODUCING SIMULATED BOUNDARY LAYERS.

2.1 Production of shear or turbulent flows

The production of either a shear or a turbulent flow relies on such devices as gauze screens, grids of rods and turbulence grids.

The effects of using gauze screens to modify non-uniform flows in wind tunnels has been considered by Collar (1939). Following on this Wieghardt (1953) showed that screen characteristics could be related to their geometry expressed as the porosity:-

$$\beta = (1 - d/\ell)^2$$

(where d = wire diam. ℓ = width of square mesh)

Winternitz and Ramsey (1957) attempted to produce velocity gradients using gauze screens and the theoretical aspects of this were later investigated by Elder (1959). Following this, greater success was achieved by Baines (1963) in producing velocity gradients; he later devised a method of estimating the shapes of screens required to produce specific velocity gradients.

Although reasonable velocity profiles can be produced using the above technique, the associated turbulance has a purely arbitrary value and is of a small scale.

The possibility of using grids of rods, having varying vertical spacings, to produce linear velocity gradients was first investigated by Owen and Zienkiewicz (1957). They derived a method of estimating theoretically the grid configurations needed to produce particular degrees of shear flow in wind tunnels. The generated shear flows were found to remain constant over downstream distances of at least,

$$1.2 \leq x/H \leq 4.2$$

(where H = height of shear flow generated)

Thus a more practical method was provided for studying the effects of shear flow. It was used successfully, e.g. by Livesey and Turner (1969)to produce symmetral velocity profiles in a two-dimensional duct.

A study to determine whether a homogeneous turbulent flow field could be produced in such grid flows was later carried out by Rose (1966). He showed, as had previous workers, that the mean shear flow produced was self-preserving in the streamwise direction. However his measurements also showed that the length scales of the turbulence were small, being about 1.5 to 2 times the rod diameter $(\text{or } L_{ux} \simeq M/8)$, and that the turbulence intensities were low; in addition these quantities tended to vary both in the streamwise and vertical directions. A further method for predicting how these flows can be produced experimentally was developed by Cowdrey (1967); however the resulting flows were still subject to the same limitations, regarding the turbulence in the flow, as stated above. These methods allow the effects of a mean shear flow to be studied where the background turbulence intensity is relatively low.

The effects of various degrees of turbulence intensity and scale can be studied independently of mean shear flows by the use of turbulence grids. Such grids produce turbulence which is constant at any spanwise section downstream of them. The scales and intensities of turbulence produced are, as in the case of gauze screens, a function of the geometry of the square meshes. A number of such grids were investigated in detail by Baines and Peterson (1949) who showed that the turbulence intensity

decreased and the turbulence scales increased with increase of distance downstream of the grids. They also made the interesting comment that the flow through such grids "has been represented as a number of jets which form independently and then gradually spread and coalesce with neighbouring jets" - (of interest relative to Teunisson's (1972) method of simulating boundary layer flows using jets).

The characteristics of such grids were further investigated by Vickery (1965). The limitations of the flows produced by them in investigating problems in Industrial Aerodynamics were illustrated in Whitbread (1968). His results showed that only the high frequency end of grid-produced power spectral densities were comparable to the full-scale spectra measured in the atmospheric boundary layer. However, in the uniform turbulent flow produced by such grids, the effects of turbulence can be isolated from those of mean shear.

From the above assessment it can be seen that the next logical step is to produce a shear-turbulent flow, or turbulent boundary layer flow, in which Industrial Aerodynamic tests can be carried out at a large scale and the combined effects of shear and turbulence determined.

2.2 The production of turbulent boundary layer flow in wind tunnels.

Many of the attempts to artificially produce thick turbulent boundary layer flows in Wind Tunnels were commenced either during or after completion of the method described in this thesis. Therefore the intention in the following text is to note the

various methods investigated, or being investigated, and to indicate what are considered to be their main faults without discussing them in excessive detail.

Probably one of the first attempts to carry out an Industrial Aerodynamics test in thickened turbulent boundary layer flow was that of Jensen (see Jensen and Martin 1958, and Jensen and Franck 1963), although Klebanoff and Diehl (1952) had previously attempted to produce thick boundary layers. Jensen grew the boundary layers naturally over surfaces roughened with various degrees of surface roughness. Thus flows with different values of the roughness length could be modelled. The required degree of surface roughness was dictated by the modelling low that Jensen proposed:-

$$(y_o)_{F.S.} / (y_o)_{M.S.} = X_{F.S.} / X_{M.S.}$$

However, although the models were completely immersed in the boundary layer flow they were not always scaled relative to the boundary layer height (i.e. the model height for houses etc. could be up to 0.3 to 0.4 δ). Detailed measurements of the turbulence intensity in the flows produced are not available. The heights of the boundary layers produced varied between 10 and 25cm. in a wind tunnel working section length of about 5.5m. Clearly, using this method to produce thick boundary layers (say δ of 1m.) requires exceptionally long wind tunnel working sections.

This method of producing thick boundary layers has been used by a number of research centres. The first to adopt the method was the Colorado State University under the direction of Cermak. The work has been reported on in detail in Plate and Cermak (1963), Cermak et al (1965), Sandborn and Marshall (1965) and Cermak (1966 a,b).

Typically, a one metre high boundary layer is produced in a distance of 29m (i.e. 29 δ). The work of the C.S.U. has mainly been concerned with thermal effects and their measurements of the flow properties are usually presented as a function of the Monin-Obukhov length, and only in the lower 0.15 of the boundary layer height. The measured spectra show a rapid decrease in the energy at low frequencies and Cermak recommends the introduction of large scale disturbances at the beginning of the test section as a remedy; vortex generators are in fact used in some of the work reported on in Cermak (1971). The C.S.U. also adopt the higher power law indices recommended by Davenport (see Part 1 of thesis) which have been shown to be unsatisfactory. The roughness lengths of the flows modelled are not usually indicated. The dimensions of the C.S.U. meteological wind tunnel working section are as follows:-

Length - 30m

Width - 1.8m

Height - 1.8m

A similar method of producing thick boundary layers was used by Davenport at the University of Western Ontario. The characteristics of the Adiabatic boundary layer flow over terrains having various degrees of surface roughness were initially established in Davenport (1963) and the wind tunnel modelling of such flows in Davenport (1966) and Davenport and Isyumov (1967). The dimensions of the U.W.O. tunnel are:-

Length - 26m

Width - 2.6m

Height - 1.8 - 2.5m

Typically the boundary layer height required is produced in a

distance of about 25δ and the system includes the use of a fence or barrier at the upstream end of the fetch of roughness elements. On some occasions a grid of bars has also been added (Davenport and Isyumov 1967). Due to the narrowness of the above wind tunnel working sections (i.e. C.S.U. and U.W.O.) the possibility of three-dimensional flow effects occurring must be considered. However, regardless of this, it has been shown previously that the flow characteristics modelled for the rougher terrain types do not agree with the analysis contained in the first part of this thesis.

Extensive theoretical and experimental work was also carried out at Cornell Aeronautical Laboratory on the simulation of atmospheric boundary layers. These studies have been variously reported on in McVehil et al (1967), Ludwig and Sundaram (1969), Ludwig et al (1971) and Sundaram et al (1971). The boundary layers were grown naturally over rough surfaces but also included a boundary layer trip, in the form of a barrier (also used by U.W.O.) at the beginning of the working section. At one stage triangular vortex generators were also used as mixing devices which were of the same order of magnitude as the roughness elements; in which case the vortex shed by the individual generators was broken up by the interaction with the roughness elements. The authors here stated that they are only interested in producing the constant stress layer of the atmospheric boundary layer, which was taken as being of the order of 50 to 100m thick. For similarity of the model and full-scale flows they proposed that the following quantities should be equal in both flows:-

$$\frac{\sqrt{\overline{u^2}}}{U_R} \quad , \quad \frac{L_R}{y_R}$$

(where e.g. L_R indicates a length scale of turbulence at a

reference height indicated by 'R').

Thick constant stress layers were produced, however, the shear stress, turbulence intensity and roughness length were not matched according to the analysis of Part 1 of this thesis, e.g.

$$\sqrt{\overline{u^2}}/\bar{u} \simeq 0.14 \quad \text{for} \quad y_o \simeq 0.5\text{m}.$$

The production of the thick constant stress layer would also appear to be partly due to the use of large roughness elements. The length scales of turbulence were not measured hence it cannot be deduced if the latter of the above criteria was fulfilled.

There is also some doubt as to whether just a part of a boundary layer can be modelled and still contain in it the characteristics of the whole boundary layer flow. This point is discussed later in this section ie - Cook (1972, '73). The power spectral density measurements in the above flow model also tend to show that some of the flow properties have not been adequately modelled. The dimensions of the tunnel proposed by C.A.L. are:-

Length - 24m

Width - 2.75m

Height - 1.8m

Finally there is the attempt to grow a boundary layer naturally by Gandemar (1973). Generally the measurements of mean velocity and turbulence intensity have not been made sufficiently for downstream for the flow to have reached an equilibrium condition. In addition, the authors specifications of $\frac{1}{2}$ and y_o for various terrain types, are not consistent with the results of the first part of this thesis e.g. and $\frac{1}{2} = 0.2$ and $y_o = .23\text{m}$ for countryside were adopted by Gandemar.

It can be seen that use of the above system, despite the inclusion of barriers, demands in most cases prohibitively long working sections. The remaining part of this section describes various methods proposed, and used, to accelerate the rate of boundary layer growth in order to avoid the cost of building the large wind tunnels described above.

One method of producing such flows was proposed by Armitt (1966). However, inadequacies were found in the system by Counihan (1967) and these were reported on in detail in Armitt and Counihan (1968). The system involved the use of a fence or barrier, triangular vortex generators and surface roughness and was intended to produce the vortex system and physical processes which occur in a natural boundary layer as proposed by Townsend (1957). The vortex generators were intended primarily to produce mixing through the large vortices shed by them; the generators were set at alternate angles of incidence and produced sets of contrary rotating vortices (see Townsend 1937). The barrier was intended to extract the required momentum loss from the flow.

Vortex generators, however, used in the above context as mixing devices were previously shown by Taylor (1950) to produce strong vortices which persisted for downstream in the flow; this was also shown to be the case here (Armitt and Counihan 1968). The result was that the simulated flow contained unacceptable spanwise and vertical discontinuities in the mean and turbulent measured flow characteristics. In addition it was shown in Part 1 of this thesis that the true form of the vortex motions

in Adiabatic boundary layers has not yet been adequately established. Hence a reliable model on which to base a simulation cannot be accurately defined. It was suggested also that the large vortex pairs envisaged by Townsend (1957) had a relatively slow motion; the type of vortex produced by triangular generators can be considered to have a relatively large rotational motion, which in fact helps them to preserve their identity over long distances downstream.

The method adopted by Lloyd (1966) at Bristol University was a modified version of the flat plate grid system used by Strom and Kaplin (1960) to produce essentially shear flows having low turbulence intensities (i.e. of the order of 0.01 - 0.02 as measured by Lloyd). Turbulence generators in the form of small square blocks were added by Lloyd to the back ends of the flat plates. In addition the wind tunnel floor was roughened downstream of the flat plates. Thus turbulence levels of the order of 0.06 to 0.12 were produced near ground level. The measured data showed that a non-decaying shear flow was produced. However the turbulence produced was isotropic and the Reynolds stresses considerably lower than they should be; in addition the measured length scales of turbulence were too small, as could be anticipated from the use of a grid system.

The National research Council of Canada produced another system which is reported on in detail in Templin (1969), and Standen (1969), Standen et al (1971) and Standen (1972). This consisted of a row of spire-shaped flat plates normal to the wind which were modified to produce various mean velocity profiles by drilling a number of arrangements of holes in them. However they produce flows having several undesirable characteristics.

The flows in the upper and lower parts of the generated boundary layer were found to have different power indices; this results in a discontinuity in the variation of the turbulence intensity with height. It was also found that in the upper half of the flow the Reynolds stresses increased rapidly with increase of height. These characteristics have been attributed to regular vortex shedding from the upper half of the spires.

Using a similar method to that used at N.R.C. (Canada) Melbourne (1971) attempted to produce a simulated boundary layer flow in a wind tunnel at Monash University. The system consisted of flat triangular spires followed by surface roughness on the wind tunnel floor. However as in the case of the N.R.C. the inner and outer flow regimes do not seem to match up i.e. there are variable spectral characteristics above a height of 0.25 δ . There are also inconsistencies in the flow characteristics of the lower layer as the characteristics do not agree with the analysis of the first part of this thesis.

A further method was investigated by Wilson (1971) at the Von Karman Institute (Brussels). The system initially consisted of flat spires (as at N.R.C.), to these splitter plates were added and finally the spaces between the splitter plates and spires were completely faired in. These devices were positioned upstream of a grid of rods, the floor downstream of the rods being covered by roughness elements. Since only mean velocity measurements are available, the flow produced by the above system cannot properly be assessed, however the presence of a grid would suggest that the flow will not contain large scale turbulence.

A different approach to simulating neutral boundary layers was attempted by Schon and Mery (1971) on behalf of the Ecole Controle Lyonnaise and the French E.D.F. respectively. This consisted of injecting air into the airflow, at right angles to it, from the wind tunnel floor. The intention of the authors was to simulate the lower 100m of the boundary layer, the validity of which is open to doubt. There are many deficiencies in the flow produced e.g. the turbulence intensities and scales are much too small. In addition the length of working section required to produce this flow is of the order of 27δ (Cf. 25δ taken by Davenport at U.W.O. to grow a boundary layer naturally).

The use of jets was again employed by Morkovin et al. (1972) at the Illinois Institute of Technology. On this occasion the row of air jets was directed parallel to and against the mainstream flow (i.e. counter-jet technique). The initial results from these tests, i.e. mean velocity and turbulence intensity measurements look promising. However, at a distance of about 7δ downstream, the flow does not appear to have yet reached a state of aquilibrium; it is also considered to be doubtful whether the correct turbulence scales can be produced by the introduction of air jets into the flow.

A multiple air jet system was used by Teunisson (1972) at the University of Toronto to produce a simulated flow; the jets in this instance were ejecting downstream in the flow direction. Again many of the measured flow characteristics look plausible. However if an analogy is drawn between flow through screens, as representing a number of jets (see Sect. 2.1. comments from Baines and Peterson 1949), and between the flow of Teunisson's jet system then the length scales of turbulence would be expected to increase

with increase of distance downstream, which they in fact do. In addition they appear to be relatively invariant with height.

A different method was proposed by Wills (1972) at the National Physical Laboratory and this involved curving the roof of the tunnel used in order to produce rapid growth of the floor boundary layer downstream of it. The available data show that the variation of the Reynolds stresses with height is unacceptable and, in addition, the turbulence intensities produced are too low. The use of such a technique would clearly involve the use of an adjustable roof section in order to produce the flows appropriate to various terrain types.

Finally, an attempt has also been made by Cook (1972, 1973) at Bristol University to model the constant stress layer (i.e. the lower 50 to 100m) of the atmospheric boundary layer using a barrier, a grid of rods and floor roughness. The arguments that have been put forward against this type of approach are mainly based on the supposition that the proper turbulence scales could not be produced in such a flow; correct representation of these scales is considered to be of importance if true similarity between model and full-scale flows is to be achieved. This was subsequently shown to be the case in the data presented in Cook's (1973) paper; it can be seen that the longitudinal scales of turbulence are smaller than they should be and the discrepancy increases with increase of distance from the ground. What in fact appears to have been produced is just the lower section of a mean velocity profile with which is associated some arbitrary scales and intensities of turbulence. Hence, as previously mentioned, it would not appear

to be possible to simulate just a part of a boundary layer which will have the correct flow characteristics represented in it.

Therefore it can be seen from the above discussion that prior to, and during, development of the boundary layer simulation system described in the following sections various attempts were made to produce the required boundary layer flow. These have been considered here to produce, for various reasons, inaccurate representations of the flow required. In most cases insufficient measurements were presented from which the true nature of the flows produced could be established. In addition, in many cases, no attempts were made to produce flows appropriate to various terrain types.

3. DESIGN PHILOSOPHY OF THE BOUNDARY LAYER SIMULATION SYSTEM DEVELOPED AT THE CENTRAL ELECTRICITY RESEARCH LABORATORIES.

From the previous section it can be seen that two basic methods exist for producing simulated Adiabatic boundary layers. One method consists of growing the boundary layer naturally over a rough surface and extracting some momentum from the flow initially by placing a barrier upstream of the surface roughness. The second method consists of the addition of a row of obstructions of the same height as the required boundary layer height; these being normally positioned between the barrier and surface roughness are intended to accelerate the rate of boundary layer growth. In this instance a method using the latter technique is to be considered here and it will therefore consist of a barrier, surface roughness and some type of obstructions.

Clearly, for the purposes of comparing such simulated boundary layer flows with full scale boundary layers some criteria are needed as a basis from which to work. Therefore it is suggested here that in order to obtain a satisfactory wind tunnel simulation of the atmospheric boundary layer that the simulated surface layer should comply with the following equation:-

$$\bar{u}/U_* = 1/k \log_e \left(\frac{y-d}{y_o}\right)$$

Correct simulation of the zero-plane displacement 'd' is not too important in the case of the rural simulation but it is considered to be an essential requirement in the case of the urban boundery layer simulation. Therefore it is to be expected that the following quantities should be correctly modelled:-

$$y_o/\delta \;,\; d/\delta \;,\; h_r/\delta \qquad (h_r = \text{roughness element height})$$

If a boundary layer having these quantities accurately simulated can be grown rapidly, then the next requirement, in order to maintain this flow, is reproduction of the large scale eddies, or flow structure, through the full boundary layer height. If these can be produced then the simulated boundary layer should satisfy the main similarity requirements with the atmospheric boundary layer.

On the above basis it can be seen that both the mean and fluctuating flow quantities need to be reproduced in the simulated flow. With respect to the latter quantity, the complete spectrum should be simulated and this implies that the large scales of turbulence, in the longitudual, lateral and vertical directions, should be represented in the flow. This should then give similarity of the simulated and full-scale flow structure which essentially consists of eddies of various sizes. However in considering the problem of trying to produce such flows artificially it seems more practical to approach it by saying "how can a certain mean velocity and turbulence intensity be produced" (while still keeping the large scale turbulence requirements in mind) rather than consider "how can turbulent eddies or vortex systems of some particular shape or size be produced". Therefore it was assumed that the appropriate velocity defects and turbulence intensities to be simulated needed to be produced initially at all heights in the boundary layer. Then as the flow progressed downstream the production of turbulence at ground level would need to balance the natural dissipation of turbulence in the boundary layer. In doing so it is assumed that a natural process of upward diffusion of turbulence from ground level would be set up. Hence the large

circulatory motions present in boundary layers (Townsend 1957) might be induced to form naturally as a consequence.

The function of the ground roughness and the barrier will be defined now before going on to consider the design of the obstructions. It is assumed that the lower region of the boundary layer is of importance since, in this region, the ground roughness should provide for the continual production of turbulent energy. In addition, since the roughness length of the ground roughness is indicative of the terrain type being modelled it is essential that it should be matched to the velocity profile and turbulence intensities being modelled (see Part 1 of thesis). In the case of rural terrain this should not prove to be too difficult a problem and for many cases sand-roughness of the relevant grade will probably be sufficient. However in the case of simulating an urban terrain it will clearly be necessary to determine initially the effects of roughness element (i.e. building) density and fetch on the roughness length and zero plane displacement. Then having decided on a representative value for an urban roughness length a typical urban area will need to be defined, in terms of the ratio of built-up to open area, which will have this roughness length value. Hence it can be seen that the correct definition of the terrain to be modelled in terms of the roughness length, of the ground roughness, is of importance. The function of the barrier is likewise of importance in the simulation of atmospheric boundary layers. In general it has previously been regarded as merely providing a method of extracting momentum from the mean flow. However this applies only over a limited height of the boundary layer to be

simulated. It should, in addition, provide a degree of mixing by means of the vortex which it produces which has its axis across the flow direction, parallel to the ground. It will also provide some contribution to the final degree of turbulence intensity required in the simulated boundary layer. The interaction of its shed vortex with the obstructions downstream should also prevent the formation of a regular vortex pattern in the flow. If a barrier is not included in the simulation system it can be anticipated that the lower sections of the obstructions will need to present a considerable frontal area to the flow in order to produce the required momentum loss. In which case spanwise and vertical non-uniformities can be expected to form in the flow and therefore a longer downstream distance would be required to reduce their effects (e.g. see system developed at N.R.C. Canada).
At an early state in the development of the system at C.E.R.L. it was deduced that a refinement to the shape of the barrier, in the form of the addition of castellations immediately upstream of the obstructions, would be advantageous. It was considered that the castellations would effectively "break-up" the barrier vortex, thus producing a greater amount of mixing in the flow before it reached the obstructions. The ultimate effect should then be to induce earlier coalescence of adjacent obstruction wakes and thereby reduce the downstream distance needed to obtain spanwise uniformity of the flow. Thus it can be seen that the function of the barrier is of more importance than previously considered.

The type of obstruction required to produce an accelerated boundary layer growth can now be considered. The previous types

of obstructions used can essentially be defined as "mixing devices" or "vortex generators". By this is meant that the primary characteristic of the obstruction wake is the strong vortex it produces having its axis in the streamwise direction and the fact that such vortices have been shown to be persistent in the downstream flow; a quality which is desirable for some applications of such devices. As a consequence, although they act as mixing devices directly in redistributing the turbulent energy created a ground level through the boundary layer and extracting energy from the external mean flow, their presence leads to undesirable non-uniformities in the downstream flow. This being so, this type of vortex system cannot be representative of the circulatory motions present in the full-scale boundary layer.

It is assumed from the above that what is needed is an obstruction which would produce in its wake the required vortex, or mixing system, as a secondary rather than primary effect; in which case it should have the relatively slower movements typical of those observed in the full-scale boundary layers (see Part 1 of thesis). Therefore such an obstruction cannot be termed a mixing device on the basis of the above definition. The approach towards defining the obstruction shape needed was based on the assumption that it should in the first instance produce momentum losses and turbulence intensities which when combined with the barrier and surface roughness contributions would result in the required mean velocity and turbulence intensity profiles being produced. It was assumed that the production of these profiles would assist in the formation of the associated eddy system

through the transfer of turbulent energy from ground level to other sections of the boundary layer. In the second instance it was assumed that the obstruction should produce in its wake a graded distribution of vorticity, that is having vortices of varying strength in the vertical direction which also have their axes in the vertical direction. It was expected that such a distribution could then induce, as a secondary effect the formation of the large circulatory movements specified above having their axes in the streamwise direction. These movements and those arising from the turbulent energy transfer would be additive. In addition, since the barrier and surface roughness are not expected to contribute initially to the formation of the outer section of the boundary layer, the obstructions will be expected to produce the required momentum losses and turbulence intensities here which will of course reduce to zero at the top of the boundary layer. For $0 \leqslant \delta \leqslant 0{\cdot}5$ the production of these quantities can be virtually constant and clearly less than the values needed in the final simulated flow.

The type of obstruction which it was envisaged would produce a flow having the characteristics defined above is described in the following text. Its side view shape is a quarter of an ellipse whose major axis is twice its minor axis. Since its change of geometrical form is relatively small over the lower half of the section then its wake characteristics can be expected to be relatively constant in this region. The momentum loss and turbulence intensity should decrease more rapidly with increase of height over the top half of the section and reduce to zero at the top of the ellipse major axis, i.e. the proposed top of the

simulated boundary layer. In plan view the obstruction is wedge shaped, the wedge angle being constant at all horizontal sections. The wedge angle apex points in the flow direction and therefore no asymmetries should be introduced into the wake flow. As a consequence the flow characteristics should be identical at equal distances either side of the wedge centre-line. Hence it could be anticipated that a row of these obstructions could be so spaced across the flow such that the measured characteristics at any height would be uniform in the spanwise direction. However there is obviously a limit to the amount by which this spacing can be reduced in order to avoid possible reduction and distortion of the turbulent scales occurring. Wedge angles of the order of 10-12^{o} seemed reasonable in order to avoid having excessive frontal area and too much base drag which would lead to reduced spanwise uniformity. The wedge angle was maintained constant, as the chord length decreased with increase of height as it was felt that this was essential for the continuous production of vorticity, or turbulence, over the full height range.

The vortex patterns which should be produced from the barrier (without castellations) and obstructions combined as shown diagramatically in Fig. 1; this figure also clearly shows the shape of obstruction derived which is called an elliptic wedge vorticity generator or just a vorticity generator. It can also be seen that a degree of mixing is indicated in all three planes. The large circulatory motion to be produced as a secondary effect is indicated and hence this device cannot be termed "a vortex generator" or mixing device based on the definition given above.

Such a circulatory motion will also encourage, and be encouraged by, the natural transfer of turbulent energy from ground level to other parts of the boundary layer. The contributions of the barrier, vorticity generators and surface roughness towards producing the required simulated mean velocity and turbulence intensity profiles were considered to be of the form shown diagrammatically in Fig 2, on the assumption that the contributions from the various components blend together to form smooth profiles.

It was assumed that the flow appropriate to various terrain types could be produced, using the system described above, by merely changing the barrier height and the size and geometry of the floor roughness elements; no changes to the generator spacing or geometry were envisaged.

The following sections are concerned with development of the initial lay-out and assessment of the system and the subsequent measurements in the simulated rural and urban Adiabatic boundary layers.

4. WIND TUNNEL AND INSTRUMENTATION.

4.1 The Wind Tunnel.

All of the experimental work was carried out in the boundary layer wind tunnel at the Central Electricity Research Laboratories. This wind tunnel has a two-dimensional contraction in the vertical plane, having a contraction ratio of approximately 5:1 (i.e. wind tunnel inside height reduces from 926mm to 187mm through the contraction). Hence, it is ideally suited to the present project since the floor and roof boundary layers in the working section should be comparitively thin and the turbulence intensity in the section comparitively low. The working section dimensions are as follows:-

Length - 1480m.m. (58.4in.)

Width - 618m.m. (24.3in.)

Height - 187m.m. (7.35in.)

The working section roof panels interlock with each other and are interchangeable. Therefore the section which carried the traverse gear could be moved readily to various positions along the wind tunnel working section in increments of 228 m.m. (9 in.). The power unit to drive the wind tunnel consisted of two contra-rotating fans of 0.72 H.P./unit (i.e. Total H.P. of 1.44). Speed control was obtained by means of an adjustable iris positioned downstream of the fans. This was followed by a wide angle diffuser which, since the tunnel is of the straight through type, ejected the air into the atmosphere.

The building which contained the wind tunnel was virtually

underground on three of its four sides. This had the very useful advantage that the ambient temperature remained constant to within a few degrees centigrade on an annual average. Therefore the temperature during a normal day of tunnel running did not vary significantly and as a result hot-wire anemometer readings did not need to be corrected for errors due to ambient temperature changes. The relevant features of the wind tunnel are shown in Fig. 3.

4.2 Instrumentation

The interference effects associated with the presence of a pitot-static tube in the working section was avoided by monitoring the tunnel wind speed using two reference static pressure tappings. These were positioned at the upstream and downstream ends of the contraction and were initially calibrated against a pitot-static tube positioned in the working section.

All of the mean and fluctuating velocity measurements were made using a standard D.I.S.A. miniature X-wire probe; two D.I.S.A. miniature single wire probes were used for the correlation measurements. The traverse gear which carried the probe was mounted on a section of the roof which could slide laterally (Fig. 3), thus the probe could be positioned at any point across the working section. The traverse gear permitted vertical traversing of the probe over the full height of the tunnel in increments of 0.0254 m.m. (0.001 in). The vertical and lateral traverses could be made at four axial stations in the working section as follows:-

228.6 m.m. (9 in.) ; 457.2 m.m. (18 in.) ;

685.8 m.m. (27 in.) and 914.4 m.m. (36 in.).

The probe could be located in the probe holder at 0°, or rotated about its axis by 90°, for measurements of lateral and vertical turbulence components respectively.

The mean and fluctuating velocity measurements were analysed using a P.A.C.E. TR20.R analogue computer. A diagram of the circuit used in the analysis is shown in Fig. 4. Since linearisers were not used with the D.I.S.A. equipment the calibration curves of the individual hot-wires were set up on the P.A.C.E. function generators. Using the circuit shown in Fig. 4 the mean velocities, the mean square fluctuating velocities and the products of the longitudinal and either the lateral or vertical fluctuating velocities could be obtained. The turbulence intensities, for example, were then derived as follows:-

If the output reading in volts is R,

then,

$$R \times G_o = T G_1^2 \overline{u'^2}$$

where, G_o = System gain.

T = Integration time in seconds.

G_1 = External variable gain.

u' = Fluctuating longitudinal velocity.

$$\therefore \sqrt{\overline{u'^2}} = \frac{1}{G_1}\sqrt{\frac{RG_o}{T}}$$

$$= \frac{1}{G_1}\sqrt{\frac{R \times 10 \times 10}{T \times 10}}$$

$$\text{or} \quad \frac{\sqrt{\overline{u'^2}}}{\bar{U}_o} = \frac{1}{G_1 \bar{U}_o}\sqrt{\frac{R}{5}}$$

where, $\bar{U}_o$ = Free-stream velocity

T = 50 secs.

and Gains (G_o) of 10 arise from multiplication, integration and timing circuits.

An accurate measurement of the time is obtained from an electro-mechanical comparator in the P.A.C.E. computer which also stops all integrations at the integrating time specified.

The measurements of the intermittency factors were also made using the analogue computer. The associated circuit diagram is shown in Fig. 5 and this effectively measures the fraction of time, of the total integrating time, that the signal being analysed is totally turbulent or fluctuating. The circuit includes a D.C. bias control since the mean signals are usually subject to some low frequency oscillations which need to be offset. The degree to which this control is used is necessarily subjective to some extent.

The initial measurements of the power spectral densities were obtained by recording the hot-wire anemometer signals using a combined system of an Epsaylon F.M. tape recorder and loop recorder. The loop recorder signals were subsequently processed on a Fenlow low frequency spectrum analyser to obtain the power spectra of the three fluctuating velocity components. More extensive spectra measurements were later made by recording the signals on a Sangamo 3500 tape recorder and subsequently analysing the signals on a Honeywell analyser. The auto-correlations for the longitudinal fluctuating velocity and the probability density distributions were also produced from the Honeywell analyser.

5. DEVELOPMENT OF THE SIMULATED RURAL BOUNDARY LAYER.

5.1 Models.

In order to establish the basic wake differences between "vortex generators" and the vorticity generator proposed here the wake characteristics of four types of generators (Fig. 6) were investigated in some detail. The height of all the generators was taken as 152.4 mm (6 in.) in order to make the maximum use of the available tunnel height. It was assumed that the height of the simulated boundary layer would be the same as the generator height, in which case there should be no interaction between the simulated flow and the boundary layer on the wind tunnel roof. The generator details are as follows:-

(a) Flat-plate triangular generator.

(b) Flat-plate cranked generator.

(c) Flat-plate elliptic generator.

(d) Elliptic wedge generators having wedge angles of 10° and 12°.

The wake characteristics of barriers of various heights were also determined as follows:-

(a) Height = 12.7 m.m. (0.50 in.)

(b) Height = 15.875 m.m. (0.625 in.)

(c) Height = 19.050 m.m. (0.750 in.)

At a later stage of the work the barrier was re-designed. The height was increased to 22.225 m.m. (0.875 in.), with local increases of 6.35 m.m. (0.25 in.) immediately upstream of the generator centre lines thus making the total height at those sections

28.575 m.m. (1.125 in.). The final model configeration (Fig. 7) consisted of this barrier followed by a row of seven elliptic wedge generators, having 12° wedge angles, downstream of it. The generators were spaced 76.2 m.m. (3 in.) apart and positioned in line with the local height increases on the barrier (Fig. 3).

5.2 Test Programme.

5.2.1 Wind Tunnel Calibration.

As a preliminary to the main test programme the flow characteristics of the wind tunnel working section were first determined. This simply involved measurements of the mean velocity and the longitudinal turbulent velocity at the following three axial stations:-

228.6 mm (9 in.); 457.2 m.m. (18 in.) and 685.8 m.m (27 in.) The measurements were made at a nominal reference velocity of approximately 8.5 m/sec. (28 ft/sec).

5.2.2 Barrier and generator wake flow characteristics.

All of these tests were carried out with the probe positioned at the axial station 457.2 mm (18 in.). They included initial traverses made in the wake of a generator to determine the minimum possible integration time to be used in obtaining the mean square values of the fluctuating velocities and correlations. The wake tests were then begun by making vertical traverses in line with the various generator centre-lines; these were followed by similar tests with the generators set at various degrees of incidence. These vertical traverses generally covered a height of 171.5 mm (6.75 in.) from the wind tunnel floor in increments of 6.35 m.m.

(0.250 in.).

More extensive traverses were then made in the wakes of the flat-plate triangular and elliptic generators set at various incidences and covering a distance of $\pm$ 76.2 m.m. ($\pm$ 3 in.) in increments of 6.35 m.m. to 12.7 m.m. (0.25 to 0.5 in.) on each side of the generator centre lines. Similar traverses were made behind the elliptic wedge generators having wedge angles of 10° and 12°.

The wake characteristics of barriers of various heights in isolation were then determined and then the characteristics of various combinations of barriers and either triangular or elliptic wedge generators.

The elliptic wedge generator/barrier combination was tested in more detail, in an attempt to determine the contribution of each of the components to the resultant characteristics. This was followed by a brief investigation to determine whether the axial position of the barrier relative to the beginning of working section was of importance.

The spanwise variations of the resultant flow will clearly depend on the spacing of the generators relative to each other, as previously discussed. Therefore, the next step, in these tests, was to make vertical traverses in-line with both the generator centre-line and the span centre-line, for various span lengths between two generators. These tests were restricted to just the elliptic wedge generators. In addition, similar tests were carried out with the barrier positioned upstream of the generators, for generators having both 10° and 12° wedge angles. Finally, the effects of varying the distance between the barrier and the

elliptic wedges were briefly examined.

It should be noted that extensive tests were not carried out on those aspects of the work which were considered to be of secondary importance e.g. the axial position of the barrier and of the barrier relative to the generators. On the other hand, the wake characteristics and the spacing of the generators were investigated in more detail.

Artificial surface roughness was not used in any of the above tests.

5.2.3 Rural simulated flow tests - Part 1.

For all of these tests the position of the barrier and the position of the elliptic generators relative to the barrier were fixed from the results of the preceding test program.
The barrier was positioned at a distance of 50.8 mm (2 in.) from the beginning of the working section, and the leading edges of the generators were 127.0 m.m. (5 in.) from the barrier as shown in Fig. 7. The elliptic generators having a wedge angle of 12° were used for these tests, based on the results of the previous tests. The surface roughness was represented by standard 'Lego' base boards as shown in Fig. 3 and 7. As a preliminary, the characteristics of the boundary layer grown naturally on this artificial roughness were determined.

The barrier height for the tests was initially 19.05 m.m. (0.75 in.). Measurements taken in the simulated flow below a height of 12.7 m.m. (0.50 in.) were taken in increments of the order of 0.762 m.m. (0.030 in.) to 3.556 m.m. (0.140 in.), and above this

height in increments of 6.350 mm (0.250 in.), up to a height of 152.4 m.m. (6 in.). At these positions the mean velocity, the fluctuating velocities and the shear stress distributions were measured in the simulated flow at the axial station 457.2 m.m. (18 in.). Generator spacings of 76.2 m.m. (3 in.) and 88.9 m.m. (3.5 in.) were investigated. The measurements were made at spanwise positions coincident with the generator centre-line, the span centre-line and the semi-span centre line i.e. at half and one quarter of the generator spacing.

After these tests, the barrier height was increased to 22.225 m.m. (0.875 in.) and the above tests were repeated for generator spacings of 76.2 m.m. (3 in.) and 88.9 m.m. (3.5 in.). Further tests followed in which local increases in barrier height were made at various spanwise positions on the 19.05 m.m. (0.750 in.) and the 22.225 m.m. (0.875 in.) high barriers. The outcome of these tests (in which only the velocity profiles were measured) was the adoption of a 22.225 m.m. (0.875 in.) high barrier which had its height increased locally by 6.35 m.m. (0.25 in) to 28.575 m.m. (1.125 in.) at sections directly in line with the generator centre lines.

With the final configuration for producing the simulated flow in the wind tunnel the following measurements were made. The mean velocity, the fluctuating longitudinal, lateral and vertical velocities and the shear stresses were then measured at the axial stations 228.6 m.m. (9 in.), 457.2 m.m. (18 in.) and 685.8 m.m. (27 in.). These measurements were made at the spanwise stations indicated previously, with the generators set 76.2 m.m. (3 in.)apart.

Finally, the power spectral densities of the longitudinal, lateral and vertical components of turbulence were measured at the 457.2 m.m. (18 in.) station, at mid-span point of the generators, and at a height of 25.4 m.m. (1 in.) from the ground. The mean roughness length of the simulated rural terrain was then determined.

The axial stations 457.2 m.m. (18 in.) and 685.8 m.m. (27 in.) in fact correspond respectively to the leading edge and centre of the C.E.R.L. Low-speed Wind Tunnel turntable; the simulation system considered here was being developed for this wind tunnel. The distances which define various axial stations are the actual distances from the trailing edges of the elliptic generators to the tip of the hot-wire anemometer.

5.2.4 Rural simulated flow tests - Part II.

This part of the test programme was intended to extend the power spectral density measurments in order to establish that they were sensibly invariant in spanwise and axial directions at a constant height and to establish the form of their variation with height. Measurements of the correlations were made in the simulated flow in order to determine whether the scales of turbulence, and hence the flow structure, was correctly modelled. Finally the variations of the intermittancy factors, over the simulated flow height, were measured.

The extension of the power spectre density measurements included the following conditions:-

Station 457.2 m.m. (18 in.):-

Measurement of the longitudinal, lateral and vertical power spectral densities at,

(i) Generator centre-line, quarter-span and mid-span at,

$$y/H = y/\delta = 0.167$$

(ii) Quarter-span position,

$$y/\delta = 0.10, 0.30, 0.50$$

Station 685.8 m.m. (27 in.) :-

Measurement of the longitudinal power spectral densities at,

(i) Generator centre-line, quarter-span and mid-span at,

$$y/\delta = 0.167$$

(ii) Quarter-span position,

$$y/\delta = 0.30, 0.50$$

The scales of turbulence can be determined from space-correlation measurements, the correlation coefficient being defined as:-

$$\overline{u'_A u'_B} \Big/ \sqrt{\overline{u'^2_A}} \sqrt{\overline{u'^2_B}}$$

where, u'_A = the turbulent velocity at a fixed point A

u'_B = the turbulent velocity at a point B

distance r from A.

Clearly when $r = 0$ the correlation coefficient = 1.0.

The correlation coefficient can be written in the general form:-

$$R_{ij}(r_1, r_2, r_3)$$

where r_1, r_2, r_3 are separations on the X, Y and Z axis respectively. The present measurements are confined to cases where $i = j$, hence the definition is reduced to:-

$$R_{ii}(r_1, r_2, r_3)$$

For example, the correlation coefficient of the variation of

longitudinal turbulent velocity for vertical separations is simply:-

$$R_{uu}(0, r, 0)$$

The sign convention adopted for traversing on either side of a fixed point when measuring the correlation coefficients is shown in Fig. 8.

Normally the fixed point, or position of the fixed probe, is defined as the ratio of its distance from the wall or floor relative to the physical thickness of the boundary layer. In this case, as indicated above, the boundary layer thickness (δ) has been assumed to be the same as the height of the generators (H). Since the spanwise uniformity of the flow is also being investigated here, it is necessary to measure correlations relative to additional fixed points. These points are defined by the position of the fixed probe relative to the span of the generators (Fig. 8). The distributions of two correlation coefficients were determined in the simulated boundary layer. These were the correlations of the longitudinal turbulent velocity for vertical and lateral separations. The extent of the measurements made at both axial stations is as follows:-

Correlation $R_{uu}(0, r, 0)$.

These correlations were measured at the generator centre-line and mid-span positions at the axial stations 457.2 m.m. (18 in.) and 685.8 m.m. (27 in.) for the following range of fixed points:- $y/\delta (= y/H)$: 0.030 , 0.083 , 0.167, 0.250, 0.334
0.416 , 0.500, 0.666, 0.834 , 1.000

Correlation $R_{uu}(0, 0, r)$

These correlations were measured at the axial stations 457.2 m.m. (18 in.) and 685.8 m.m. (27 in.) for the

following range of conditions:-

(i) y/H = 0.10 and 0.20,

Spanwise fixed points: 0m.m. (0 in.); 12.7 m.m. (0.50 in.); 25.4 mm (1.0 in.); 38.1 m.m. (1.5 in.); 50.8 m.m. (2.0 in.); 63.5 m.m. (2.5 in.); 76.2 m.m. (3.0 in.)

(ii) Spanwise fixed point = 0m.m. (0 in.)

Vertical fixed point range,

y/H = 0.03 ; 0.04 ; 0.06 ; 0.40 ; 0.50.

(iii) Vertical fixed point y/H = 0.20;

Spanwise fixed points,

0 m.m. (0 in.); 19.05 m.m. (0.75 in.); 38.1mm (1.50 in.)

for traverses of $\pm$ 76.2 m.m. ($\pm$3 in.) from each point i.e, covering a wider range than the tests of (i) above.

The intermittency factors of all the turbulent fluctuating velocities were also measured in the simulated flow. This factor is defined as the proportion of time that high frequency turbulence is present in the velocity signal at a given height in the boundary layer. For example the intermittency factor should have a value of unity in the lower section of the boundary layer and should be approximately zero at the top of the boundary layer, assuming that there is a negligible amount of background or free-stream turbulence. The intermittency factor of the longitudinal component of turbulence was measured at the generator centre-line, quarter-span and mid-span positions at the 457.2 m.m. (18 in.) axial station. The intermittency factors of all three components of the turbulence were determined at similar positions at the 685.8 m.m. (27 in.) station.

5.3 EXPERIMENTAL RESULTS

5.3.1 Wind Tunnel Calibration

The mean velocity measurements at three axial stations are shown in Fig. 9. These are presented as the percent incremental velocity relative to the mean velocity at the section ($\Delta\bar{u}/\bar{u}$ %) at the various measuring points. The measurements of the longitudinal turbulence intensity are shown in Fig. 10 for the section 457.2 m.m. (18 in.).

5.3.2 Barrier and generator wake flow characteristics.

Only the mean velocity and the longitudinal turbulence component were measured in these tests and the results are presented in Fig. 11 to 26.

The effects of integrating the fluctuating signals for various time periods are shown in Fig. 11. The results of vertical traverses in the wakes of various types of generators at various incidence settings are presented in Fig. 12 to 19. These data are shown as mean velocity ratios and longitudinal turbulence intensities plotted against non-dimensional height. In some cases, series of traverses have been plotted as contours of constant turbulence intensity.

The results of the investigations on barriers and on different barrier/generator combinations are shown in Fig. 20 to 22.

The final section of these tests deals with optimisation of the positions of the generators relative to each other and of the axial positioning of the barrier. The test results are shown in Fig. 23 to 26.

5.3.3 Rural simulated flow tests - Part 1.

The data, obtained from various sources, of measurements made in naturally grown, smooth, and rough-wall boundary layers are shown in Fig. 27 to 29.

The results of the tests in which artificial surface roughness was fitted to the wind tunnel working section floor are presented in Fig. 30 to 46. All three components of turbulence and the Reynolds stress were measured.

Variations of the velocity ratio, Reynolds stresses and turbulence intensities with height at various spanwise stations and for generator spacings of 76.2 m.m. (3 in.) and 88.9 m.m. (3.5 in.) are shown in Fig. 30 to 34. These tests were repeated after increasing the barrier height from 19.05 m.m. (0.75 in.) to 22.225 (0.875 in.) and these data are presented in Fig. 35 to 38.

The barrier was then further modified to have local height increases immediately upstream of the generator centre lines. With the generators set at 76.2 m.m. (3 in.) apart, mean and fluctuating quantities were then measured at the axial stations 228.6 m.m. (9 in.), 437.2 m.m. (18 in.) and 685.8 m.m. (27 in.). These results are shown in Fig. 39 to 45. The power spectral density measurements of the three fluctuating velocity components are shown in Fig. 46. The affects of the surface roughness on the local mean velocity are shown in Fig. 47.

5.3.4 Rural simulated flow tests - Part 11.

In order to check on the accuracy of the integration time, used in Part 1 of these tests, in the measurement of correlations, the

degree of repeatibility of some correlation measurements was obtained. The measured data are shown in Fig. 48. The correlations of the longitudinal turbulent velocity for vertical separations are shown in Fig. 49 to 60. These data include measurements at the 457.2 m.m. (18 in.) Fig. 49 to 54 station and the 685,8 m.m. (27 in.) station, Fig. 55 to 60. The correlations for spanwise separations are shown in Fig. 61 to 68. Measurements at the 457.2 m.m. (18 in.) station are shown in Fig. 61 to 64 and at the 685.8 m.m. (27 in.) station in Fig. 65 to 68.

The correlation measurements are compared with similar measurements by Grant (1958) in a natural boundary layer in Fig. 69 and 70 and with similar measurements by Harris (1968) in an atmospheric boundary layer in Fig. 71 to 73. Since some of the full-scale data on auto-correlation measurements do not go asymptotically to zero a correction, applicable to both auto and space correlations, has been derived by Scriven (1969) and applied to the space correlations measured in the simulated flow. These corrected data are shown in Fig. 74 and 75.

Measurements of the longitudinal, lateral and vertical power spectral densities at various spanwise positions and heights in the simulated boundary layer at the 457.2 m.m. (18 in.) station are shown in Fig. 76 to 83. These include estimations of the theoretical power spectra for various values of the longitudinal length scale $\mathcal{L}$, as defined by Davenport (1963), and of the boundary layer height (δ). Measurements of the longitudinal spectra at several spanwise positions and heights at the 685 mm. (27 in.) station as shown in Fig 84 and 85.

The intermittency factors measured in the simulated boundary layer are shown in Fig. 86 and 87.

The previously measured velocity and longitudinal turbulence profiles are compared with Harris's (1968) data on the assumption of a six hundred metre (2000 ft.) high boundary layer in Fig. 88 to 90. A comparison of the simulated turbulence intensities with a more refined set of Harris's and other full-scale data is shown in Fig. 91.

At a later date some flow visualisation tests were carried out at the N.P.L., and from these the schematic representation of the flow produced by the flow simulation devices was produced as shown in Fig. 92.

5.4 DISCUSSION.

5.4.1 Wind Tunnel Calibration.

The results of calibrating the working section of the wind tunnel are shown in Fig. 9 and 10. The mean velocity data show that there are no excessive non-uniformities in the flow at any of the sections considered. Similarly, the turbulence intensity measurements do not show any significant deviations at the axial station considered. In addition, the turbulence intensity levels are relatively low in comparison to what is intended to be produced in the simulated flow. As expected, there are indications that the side wall boundary layers are thicker than those on the wall and roof of the working section.

5.4.2 Barrier and generator wake flow characteristics.

All of the following tests were made with just a vortex generator in the wind tunnel. The tests to establish a representative integrating time for the fluctuating signals indicated 20 sec. as being acceptable (Fig. 11).

The results of the traverses on the centre-line of the triangular generator, for various generator incidences, are shown in Fig. 12. The region up to $y/H = 0.10$ is that which contains the floor boundary layer. At a generator incidence of 10° there is little longitudinal turbulence above this until a height of $y/H = 0.30$ is reached. Between 0.30 ($= y/H$) and 1.00, a large turbulent area clearly exists, which reaches a peak of approximately 8.0% turbulence intensity at approximately $y/H = 0.62$.

Similarly, a large velocity defect occurs between $0.4 \leq y/H \leq 0.90$ which at approximately $y/H = 0.64$ reaches a peak value of 0.13 of the free-stream velocity. This is clearly the source of the large discontinuities found in tests using these generators. As the incidence is reduced to 5°, the extent and magnitude of the turbulent and velocity-defect areas decrease, and this is accompanied by some movement outwards of the vortex centre. At the generator incidence of 5°, the peak values of turbulence intensity and velocity ratio are respectively 4.25% and 0.91.

Similar results are shown for the cranked triangular and flat plate elliptic generators in Fig. 13 and 14 respectively. It was thought that with the cranked generator the vortex might be induced to shed itself from the generator at the point where the sweep angle changes. Since it would then be in the highly turbulent region created by the barrier and the floor roughness it could be expected to break up. However the results show no indications of this and, as can be seen, the results are very similar to those obtained from the triangular generator. There is some evidence that, at an incidence of 5°, turbulence is being produced below the vortex core area. In the case of the flat-plate elliptic generator (Fig. 14) the vortex strength is reduced, and its centre is moved nearer to the generator tip. At an incidence of 5° the turbulence intensity is tending to reach a constant value over the generator height, but there is still evidence of a vortex whose centre is at approximately $y/H = 0.95$.

Traverses on either side of the generator centre lines:

The results of these tests are given in Fig. 15 to 17 for the triangular and flat-plate elliptic generators. They are presented as contours of constant longitudinal turbulence intensity at the axial station 457.2 m.m. (18 in.). In the case of the triangular generator, it can be seen that the vortex core is concentrated at $h/H = 0.62$ and extends over a spanwise distance of a quarter of a generator height. However, the complete effects of the vortex extend spanwise over a distance equivalent to a full generator height. At this axial station in the wind tunnel there is no evidence of break-up of the vortex, and quite severe turbulence gradients still exist. The asymmetry of the wake on either side of the generator centre-line is clearly indicated. This is obviously the source of the spanwise variations in the velocity and turbulence profiles obtained in the tests of Armitt and Counihan (1968).

The contours for the flat-plate elliptic generator at incidence settings of 10° and 5° are shown in Fig. 16 and 17 respectively. Similar effects are apparent, though these are not as pronounced as in the case of the triangular generator, and at an incidence of 5° the gradients in the turbulence produced are not excessive. Asymmetry about the generator centre-line still persists for all the cases, but, as previously stated, this appears to be unavoidable where the generators are set at incidence to the wind direction.

These results show that these generators do not produce the type of vortex motions considered to be in the atmospheric boundary layer e.g. as suggested by Townsend (1957). This concept implies

the existence of large eddies, both in the inner or constant shear stress section of the boundary layer and in the outer layer. However, the two sets of large eddies are not necessarily of a similar structure. It is assumed that these large eddies are of comparable size to the respective sections of the boundary layer in which they exist and that they are relatively slow motions.

However, the results of a more recent study (Tritton 1967) are not consistent with the concept of a large eddy structive existing in the boundary layer, and suggest that separate descriptions of large eddies for both boundary layer regions may be inappropriate. Further work by Kline, Reynolds, Schraub and Runstadler (1967) has shown the existence of secondary vorticity, presumably the large-scale eddies described by Townsend, in the inner region of the boundary layer. It is suggested that the action of these secondary vortices on the spanwise vorticity gives rise to the formation of wall streaks. The subsequent ejection of fluid away from the wall is considered to be the main mechanism for the transfer of energy, momentum and vorticity between the inner and outer regions of the boundary layer. Therefore, as concluded in Part 1 of this thesis, it seems that one cannot say from the present knowledge of the physics of the flow in the boundary layer whether or not large-scale eddies exist or if they do what their precise form is. As indicated previously this also leads to difficulty in defining the low frequency end of power spectra without adequate full-scale data. If they do exist, they could also be the result of outward diffusion of turbulence from ground level, which it is assumed could set up large circulatory motions. It is also assumed that

the boundary layer explored by the above sources was that of a smooth wall, whereas the structure of a moderately rough or rough-wall boundary layer might be slightly different, especially in the inner section of the boundary layer.

However, it is finally considered that, even if different vortex systems had been produced by the above types of generators, some degree of asymmetry would still exist in the flow produced because of the generators being set at an incidence to the approach flow.

Wake characteristics of elliptic wedge generators:

The wake characteristics of these generators are presented in Fig. 18 and 19. In Fig. 18 the intensity of longitudinal turbulence is plotted at various distances from the generator centre-line for generators having wedge angles of 10° (semi-wedge angle 5°) and 12° (semi-wedge angle 6°). These generators produce a vertical distribution of turbulence in their wakes of the type which was postulated in Sect. 3.0 to be of the required form, bearing in mind that the present assessment is being based purely on a survey of longitudinal turbulence. The characteristics of both generator wakes are similar, except that the wake from the generator with the higher wedge angle has a slightly higher turbulence intensity. Similarly the wake from the generator with the higher wedge angle will be wider at any given axial station.

The results plotted in contour form in Fig. 19 show the spanwise extent of the wake more clearly. This distance corresponds to nearly a generator height for both generators.

The second significant wake characteristic of these generators is that at any given height the spanwise turbulence intensity is sensibly constant over a good proportion of the spanwise extent of the wake; again this is consistent with the requirements proposed in Sect. 3.0. For example, with an elliptic wedge generator having a wedge angle of 12°, the turbulence intensity is reasonably constant, at most heights, over a spanwise distance of nearly half a generator height. Hence, at this stage of the tests, it could be seen that an array of such generators should not produce large spanwise variations of the quantities to be simulated, and should also produce the type of wake characteristics which, it was assumed, were required. A generator spacing of the order of 76.2 m.m. (3 in.) to 88.90 m.m. (3.5 in.) also appeared to be tolerable, based on the above measurements.

Barrier wake traverses:

It was thought that the height of the barrier might influence the shape of the vertical distributions, as well as the magnitudes, of the velocity and turbulence profiles. Therefore measurements were made in the wakes of barriers of various heights, the results of these measurements are shown in Fig. 20. As anticipated in the previous discussion, the momentum loss in the outer half of the boundary layer is negligible, but there will be a contribution to the eventual total turbulence intensity. There is little change to the forms of the contributions with increase of barrier height. The results also provide a useful datum for future tests where it is desirable to know the change of the velocity defect obtained for a given change of barrier height.

Comparison of barrier/generator combinations:

Comparitive tests were made on combinations of a triangular generator and an elliptic wedge generator with a barrier; the results are shown in Fig. 21. These data give an indication of the spanwise variations in the profiles obtained by using each type of generator. In the case of the triangular generator/barrier combination the extensive vertical and spanwise variations the turbulence intensity in the wake flow are evident; these are relatively negligible in the case of the elliptic wedge generator/barrier combination.

As assessment is made in Fig. 22 of the individual contributions made by an elliptic wedge and a barrier to the profiles achieved by combining the two components. The contributions are essentially as anticipated and shown diagrammatically in Fig. 2. with the exception that the barrier does produce some turbulent flow in the outer half of the boundary layer. Since ground roughness has not yet been included in the tests at this stage, there is some lack of turbulence intensity in the lower region of the flow. However at this stage of the tests it was concluded that the velocity and turbulence profiles obtained in the absence of ground roughness were fairly satisfactory.

Positioning of the generators and barrier in the tunnel:

The combination of the elliptic wedge generators with a barrier was adopted for the remainder of the tests. However, before commencing the main tests a brief assessment was made of the effects of positioning the generators and barrier at different positions relative to each other, and relative to the contraction/working

section intersection. In particular the effect of generator spacing was investigated.

It was indicated previously that the spanwise uniformity of the flow finally produced is of importance and that it would be dependent on the spacing of the generators. In which case it is necessary to define what one considers to be an acceptable degree of lateral non-uniformity. It was decided that a spanwise variation of turbulence of the order of 1 per cent of turbulence intensity would be tolerable at any given height in the boundary layer. It was also considered that the generator spacing should be as wide as possible, consistent with the above limits, as it was felt that too close a spacing might have some undesirable effect on the power spectral densities of the turbulent velocity components. Consequently, the variation of turbulence intensity with height was determined at positions in line with the generator centre-line and at the mid-span point of the generators, for a number of different generator spacings. All of the measurements were made at the 457.2 m.m. (18 in.) station and they indicate the maximum lateral variations of the longitudinal turbulence intensity. The results of these tests for elliptic wedge generators having wedge angles of 10° and 12° are shown in Fig. 23 and 24 respectively. Based on the above arguments it was decided that the generators having the wedge angle of 12° , at a spacing of between 76.2 m.m. (3 in.) and 88.9 m.m. (3.5 in.), i.e. between 0.5 and 0.6 boundary layer heights, was the most acceptable.

The effects of varying the axial positions of the barrier and generator alone are shown in Fig. 25. In the case of the barrier

it was thought that, if it was placed at, or too near, the intersection of the contraction and working section, it could influence the flow through and from the contraction. In the case of a wind tunnel in which there is no contraction, or where the contraction is produced on the side walls, the point to be considered is that there will be a relatively thick flow boundary layer and that the momentum loss due to this will have to be taken into account when deciding on the height of the barrier. From the results shown in Fig. 25 it was decided to fix the barrier a distance of 50.8mm (2 in.) downstream of the contraction/working section intersection in the C.E.R.L. boundary layer wind tunnel. However, if the working section length of a wind tunnel is short, the barrier could be moved closer to the contraction without seriously affecting the end results.

The effects of varying the axial position of the generators relative to the barrier are shown in Fig. 26. The barrier was fixed at the position indicated above. These results showed that the determination of the position of the generators was to some extent arbitrary, as in the case of the barrier. In this case, where it was positioned was based on what it was thought the shape and magnitude of the final vertical distribution of turbulence intensity should assume. What these should be was in turn based on an assessment of existing measurements in natural flat-plate boundary layers and on predicted or measured values of turbulence intensity at or near ground level in full-scale conditions. In this case, from the data of Fig. 26, it was decided to position the leading edges of the generators 127 m.m. (5 in.) from the

barrier. If the generators are closer to the barrier, then the intensities of turbulence at the same measuring position will clearly be lower. Therefore, as in the case of the barrier, if the wind tunnel working section is short and a lower turbulence level can be tolerated, the generators can be moved closer to the barrier without seriously affecting the shape of the vertical distribution of turbulence. The experimental results of Arie and Rouse (1957) indicate that the vertical spread of the wake behind such a barrier reaches its maximum at a distance of about eight barrier heights downstream. In this instance, the generator leading edges are approximately this distance from the barrier, hence the maximum interference effect should be obtained from both components.

5.4.3 Rural simulated flow tests - Part 1.

The surface roughness was installed for all of these tests, and, as already described, consisted of 'Lego' base boards (Fig. 3 and 7). The velocity profiles, the three components of turbulence and the Reynolds stress were measured using a D.I.S.A. miniature x-wire probe. The elliptic wedge generators of 12° wedge angle were chosen for these tests, and were positioned with their leading edges 127 m.m. (5 in.) from the barrier. The barrier shape and height were modified during the course of the tests. The majority of the tests were made at the axial station corresponding to the turntable leading edge of the C.E.R.L. low speed wind tunnel i.e. at the station 457.2 m.m. (18 in.) from the generator trailing edges. Clearly the simulated flow would need to have

been adequately established and have reached the required degree of spanwise uniformity at this section in order to be acceptable. The results of these tests are discussed in the following text.

Characteristics of 'rough' and 'smooth' boundary layers:

These characteristics are presented as a basis for comparison with the simulated boundary layer profiles, i.e. regarding the shape of vertical distributions and the relative magnitude of the three components of turbulence intensity, and are shown in Fig. 27 to 29. They consist of measurements, made in the boundary layer wind tunnel, in a rough boundary layer grown naturally on just the 'Lego' baseboards, and typical results from a smooth boundary layer from Schlichting (1960). The turbulence intensities of the rough boundary layer are higher, but generally the characteristics of the two boundary layers are comparable. Similar results are presented in Fig. 29 from Hinze (1959) for rough and smooth boundary layers. It can be seen that the magnitude of the three turbulent components relative to each other, in the lower region of the boundary layer and for the case of the rough and smooth boundary layers considered, are not exactly the same. The reasons for this are not apparent.

Simulated Boundary Layer with first barrier:

These tests were carried out using a barrier of height 19.05 m.m. (0.75 in.). All of the quantities indicated above were measured for generator spacings of 76.2 m.m. (3 in.) and 88.9 m.m. (3.5 in.). Normally the measurements were taken at the generator centre-line and at the span centre-line, since such measurements established the

maximum spanwise variations of the measured data.

The results with the generators spaced 88.9 m.m. (3.5 in.) apart are shown in Fig. 30 and 31. The one-seventh power law profile ($1/7 = 0.143$) is plotted for comparison with the measured mean velocity profile in Fig. 30. Although the velocity profiles clearly show an excessive variation between the two spanwise measuring stations, they are basically similar in shape, which suggests that farther downstream, when the velocity defect differences between them have reduced, spanwise non-uniformities should be minimal. The mean wall shear stress is approximately of the right order (ref. Part 1 of thesis) and the vertical distribution of the shear stress suggests that the contributions to the flow from the barrier and generators have blended together reasonably well at this stage. Figure 31 shows that there are no great spanwise variations of the turbulent components at lower levels, however, the variations tend to be excessive in the outer section of the boundary layer. It can be assumed that the wakes of adjacent generators have not yet completely interacted at this section. In general, the magnitudes of the three components of turbulence intensity are of the right order.

Similar measurements at a spacing of 76.2 m.m. (3 in.) are presented in Fig. 32 to 34; data also being obtained at a position corresponding to the generator semi-span centre-line. At this spacing, the discrepancy between the velocity profiles at different spanwise positions has been noticeably reduced and the mean of the measured profiles is nearer to the proposed one seventh power law profile. As expected, the profile mainly

affected is that measured at mid-span, while the profile measured on the generator centre-line has not changed significantly. The Reynolds stress measurements follow a similar pattern to that obtained with the wider spacing. Although there are also improvements in the spanwise variations of the turbulence components, these variations are still not as low as required. Comparison of these results, Fig. 34, with those of the rough boundary layer data from Hinze (1959), Fig. 29, shows that a fair degree of similarity is being achieved.

Referring again to Fig. 32, it was decided that, even though it might not be possible to improve on the shape of these profiles, the average velocity defect should be increased so that the one-seventh power law profile would be the approximate mean of the measured profiles. With this object in mind, the barrier height was increased to 22.225 m.m. (0.875 in.)

Effects of increasing the barrier height:

A similar set of results to those obtained with the previous barrier is presented in Fig. 35 to 38. With the generator spaced at 88.9 m.m. ($3\frac{1}{2}$ in.), Fig. 35 and 36, an increased velocity defect is apparent in both profiles, although the difference between the curves is of the same order as that obtained with the lower barrier. However, the distribution of the shear stress through the boundary layer has improved. There is very little change apparent in the turbulence intensity components, except in the case of the vertical turbulence.

Similar comments apply in the case where the generator spacing

was reduced to 76.2 m.m. (3 in.), Fig. 37 and 38. From these results it was decided to adopt a permanent generator spacing of 76.2 m.m. (3 in.), and that the general forms of the turbulence components and Reynolds stresses in the simulated boundary layer flow were acceptable. However, it was felt that a further reduction in the local velocities at the mid-span section was very desirable if it could be obtained without seriously affecting the other flow properties. The following section considers the results of the investigation to achieve this.

Tests using the modified barrier:

It was considered that, to obtain a velocity defect at the centre-span position, a further increase of barrier height was needed upstream of this point. Consequently, local increases to the barrier height were made, and the effects were assessed by measuring just the resultant velocity profile at the centre span position. However, it was found that increases to the barrier height of up to 6.35 m.m. (0.25 in.) produced no measurable difference in the measured velocity profile. Therefore it was concluded that, if a separate wake is produced by the local height increase of the barrier and is carried downstream between the generators, it could effectively delay coalescence of adjacent generator wakes, and would thus have little or no effect on the velocity profile at the centre-span position. Consequently, it was deduced that the height increase should be added to the barrier directly upstream of the generator centre-lines. Therefore if it is assumed that this section of the barrier wake wraps itself round

the generator in a horseshoe shape, then its subsequent interaction with the generator wakes should accelerate the coalescence of these wakes.

The results shown in Fig. 39 to 41 are those of the system with the barrier modified by a local height increase of 6.35 m.m. (0.25 in.), which is 25.4 m.m. (1 in.) wide, at sections immediately upstream of the generators (see Fig. 7 for details). The lateral uniformity and close approximation to the one-seventh power law of the resulting velocity profiles were considered acceptable. The distribution of the Reynolds stresses has improved and the spanwise variations of the turbulence components are still within acceptable limits over the majority of the simulated boundary layer depth. However, the turbulence component variations near the top of the layer are still considered to be excessively high. Comparison of Fig. 41 with Fig. 24 again shows that the shape of the distribution of turbulence intensity through the simulated boundary layer agrees closely with that of a naturally grown 'rough' boundary layer.

Measurements at other axial stations:

For completion, and for purposes of comparison, similar sets of measurements were made, with the modified barrier and a generator spacing of 76.3 m.m. (3 in.) at the axial stations of 228.6 m.m. (9 in.) and 685.8 m.m. (27 in.).

As expected, the generator wakes have not yet begun to interact at the 228.6 m.m. (9 in.) section, and there are large spanwise variations in all of the components (see Fig. 42 and 43). At the station farther downstream i.e. 685.8 m.m. (27 in.), the spanwise

variation in the velocity ratio, which had been taken to be acceptable at the 457.2 m.m. (18 in.) station, has improved considerably; similarly, the form of the Reynolds stress distribution has improved as shown in Fig. 44. The degree of spanwise non-uniformity in the three turbulent components has also decreased and has reached acceptable limits through the full height of the simulated boundary layer. This latter section is equivalent to the centre of the turntable of the C.E.R.L. low-speed wind tunnel.

Measurements of the power spectral densities:

The power spectral densities of the longitudinal, lateral and vertical fluctuating velocities were measured at a height of 25.4 m.m. (1 in.) at the mid-span point of the generators and at the axial station 457.2 m.m. (18 in.). The results of the measurements are shown in Fig. 46 and are generally in agreement with the proposed spectral shapes of Harris (1963) and Davenport (1963) and of Panofsky and Mc Cormick (1960) for the longitudinal and vertical spectra respectively. At the low frequencies the measured longitudinal data fall between the proposed curves of Harris and Davenport. It is of interest to note that the relatively close spacing of the generators does not appear to effect the spectral shapes adversely. The scatter in some of the lateral component data is attributed to errors arising from use of the Fenlow low frequency analyser in processing the data. Otherwise, the results presented in Fig. 46 are considered to be of an acceptable form to complete the list of parameters which it was thought necessary to reproduce in the first instance in a simulated boundary layer.

Determination of roughness length:

Because the local mean velocity is dependent, to some extent, on the position of the measuring probe relative to the individual roughness elements (Fig. 47), the roughness length was derived at a number of spanwise sections. From these the mean roughness length was derived as being of the order of 0.10 to 0.12 m (full scale). The method used to derive the roughness length was that used by Perry & Joubert (1963) which is discuesed in more detail in Sect. 6.

Some comparisons with theory and full-scale data:

A simple theoretical assessment has been made in Appendix 1 of the extent to which the simulated boundary layer compares with a naturally grown boundary layer of similar height. This comparison was made using the velocity defect law in conjunction with some of the measurements made in a natural rough boundary layer (Fig. 27). It can be seen that the theoretical predictions for the wall shear stress and the velocity ratios compare reasonably well with those measured in the simulated boundary layer flow. Some of the discrepancy could be due to the fact that the natural rough boundary layer may not have yet reached a complete state of equilibrium.

At this stage of the work the comparison with full-scale data is restricted to just particular cases which are assumed to be representative of the conditions being modelled. The data used in this instance are those of Harris (1963) which satisfied the above condition and were also the most up-to-date and comprehensive

available. However, as will be shown in a later section, these full scale data were re-estimated and provided a much closer agreement between full-scale and simulated flows. The present comparison of the data on the mean velocity and turbulence intensity variations with height is shown in Fig. 39 and 41. The agreement between measured velocity profiles is not as close as desirable. However it is taken as being acceptable bearing in mind that the surface roughness of both tests may not be exactly equivalent (see Part 1 of thesis). In any case the present comparison is intended merely to establish that the simulated flow characteristics have the right form and the right order of magnitude; a more exact comparison will be made in a later section. Finally, reference is made to Davenport's (1963) paper where results are summarised for pipe flow and natural wind experiments. The summarised data give a power law exponent of one-seventh for a surface shear-stress coefficient which is in fair agreement with the results in the simulated boundary layer flow.

Assessment of the system as a working method for boundary layer simulation:

The main points to be emphasised concerning the simulation system at this stage are as follows. The simulated rural atmospheric boundary layer, in its present form, clearly does not possess any significant spanwise variations, or discontinuities, of the measured parameters. A very slight tip effect from the generators may be present near the top of the boundary layer at the 457.2 m.m. (18 in.) section. However, this effect rapidly

reduces and is considered to be negligible at the 685.8 m.m. (27 in.) section. The measured quantities also remain sensibly constant in the streamwise direction over that section of the tunnel which it is anticipated would be occupied by the model under test.

The attainment of a velocity profile approximating to the one-seventh power law profile was not the 'sine qua non' of the simulation, but was merely chosen as a convenient basis about which the simulation system could be developed at this stage. In addition, this profile is regarded as being typical of that occurring over an average type of rural area (ref. Part 1 of thesis). It is assumed that the principles of the system adopted here can be developed to include the simulation of flow over a wide range of conditions varying from built-up areas to flow over relatively flat terrain.

A review of the present methods of boundary layer simulation by Lawson (1968) suggests that the available methods do not achieve correct representation of all of the flow properties simultaneously, and in many cases reproduction of a velocity profile only is achieved. Similar conclusions can be deduced from the data reviewed here in Section 2. It is suggested however, even at this stage of development of the system described here, that the method reproduces the quantities discussed in the above text to a degree of accuracy that makes the simulated boundary layer comparable to a naturally grown rough boundary layer. The downstream distance required, from the trailing edges of the generators, for development of this flow is between three to four and one half boundary layer heights.

In the next stage of this work the structure of the simulated flow will be considered and power-spectral density measurements extended to cover a wider range of conditions.

5.4.4. Rural simulated flow tests - Part II.

The first part of these tests was intended to establish simularity of the full-scale and simulated flow structure by measuring the correlations, as previously defined, and establishing their variations with height. Initially it may appear that the measurements of the correlation coefficient distributions have been excessive. However the extensiveness of the tests was intended to fulfil a number of purposes apart from the primary one of establishing the variation of the length scales of turbulence in the simulated boundary layer flow. It was considered that the availability of a wide range of measurements would make it possible to make a more positive analysis of the flow by being able to cross-check any conclusions reached, and thus make it easier to distinguish between main and secondary influences in the simulated boundary layer. It was also thought that some insight could be gained into how the system as a whole works in order to produce an approximate boundary layer flow. In addition, it was also considered necessary to establish that the spanwise uniformity of the flow structure was acceptable.

The analysis of the results with respect to the flow in the simulated boundary layer will be generalised, since no definite conclusions can be drawn without measuring some of the remaining

twenty-five correlation coefficients. At a later stage of the programme it was thought that the correlation of lateral and vertical velocities for various separations would be measured in an attempt to explain the method of production of the simulated boundary layer flow. However it was considered eventually that this would become too time consuming in terms of production of constructive data. The measurements that have been made here are sufficient to demonstrate that the simulated flow resembles natural boundary layer flow. However, from the measured data, it has been possible to indicate what it is thought are the main peculiarities of the simulated flow. These are effects which would not normally be present in a true boundary layer flow. They are here considered to be second order effects and not to seriously influence the main flow.

Correlations of the longitudinal Turbulent Velocity for Vertical Separations:

The first measurements made were merely to establish the repeatibility of the correlation measurements and indicate whether the integration time of 20 secs., previously decided on, was sufficient. The results presented in Fig. 48 showed that this time was adequate for the present purposes.

Consider first the variation of the correlations relative to fixed points in the range $0.03 \leq y/H \leq 0.25$ as shown in Fig. 49, 52, 55 and 58. These show the correlation measurements at the generator mid-span and centre line, at station 457.2 m.m. (18 in.), Fig. 49 and 52, and station 685.8 m.m. (27 in.), Fig. 55 and 58. Since the majority of the measurements will, in the future programme, be

obtained at stations 457.2 m.m. (18 in.) and 685.8 m.m. (27 in.) these will be referred to as Sections A and B, respectively, for convenience in the following text. At large separation distances the correlations presented in the figures referred to above tend to be slightly negative, and this effect is seen to be much more pronounced at the mid-span positions than at the generator centre-line positions. Reference to Fig. 49 and 55 also shows the correlations to be slightly more negative at Section A than at Section B. It was initially thought that this effect could be attributed to some interaction of the simulated flow with the tunnel roof boundary layer. However, since the effect is reduced, and is less well-defined, at the downstream section it is concluded that it is not a dominant motion and that it is relatively localised.

It can be seen that the variation of the turbulent length scale (i.e. the area under the correlation curves) with fixed point, y/H , is more marked at the mid-span positions than at the generator centre lines. Presumably this is due to the fact that the generator wakes have not yet completely expanded or diffused at Section A since the effect is much less obvious at Section B.

The trend of increasing length scale with increase of the fixed point value, y/H , is reversed for the range of $0.334 \leq y/H \leq 0.50$ as shown in Fig. 50, 53, 56 and 59, but is not very pronounced particularly at Section B (Fig. 56 and 59. In general, the mean length scale is of the same order of magnitude as that obtained at the lower fixed point values. The correlations for negative (downward) separations indicate similar trends and length scales to those given by the positive (upward) separations. The correlations

measured at the generator centre-line (Fig. 53 and 59) clearly indicate a peculiarity of the flow not measurable from points lower down in the boundary layer and which again is more prominent at Section A than at Section B. It is indicative of a secondary eddy in the flow. However, since it was not detected in traverses from lower fixed points in the boundary layer, it can be assumed not to be a dominant effect and to be confined to the region specified near the top of the boundary layer. If it is assumed that there is some inward flow to the base of the generator in this region which effectively increases the local velocity, then the correlation results can be associated with a generator 'tip effect'. Reference to Fig. 88 shows that there is a sudden increase in the velocity gradient (du/dy) near the top of the boundary layer at the generator centre-line and a measurable increase of shear stress (τ) in the same region. Since the production of turbulence is a function of the product of these quantities ($\tau\, du/dy$) it can be assumed that the 'hump' on the correlation measurements is associated with this effect. It tends to lead to an apparent extension of the turbulence length scale and is again, fortunately, less distinguishable as a secondary eddy at Section B, as shown in Fig. 59 and 89.

This peculiarity of the flow can be expected to become more pronounced for fixed points higher up in the boundary layer and is clearly shown in the results for the range of $0.666 \leq y/H \leq 1.00$ as shown in Fig. 51, 54, 57 and 60. The measurements on the generator centre-line. Fig. 54 and 60, show this effect clearly for positive separations at Sections A and B and for negative (downward)

separations at $y/H = 1.00$ at Section A.

As in the case of the positive separations at lower fixed points there is no significant tendency for the correlations to go negative at the generator centre-line. This effect is again confined to the mid-span traverses and is shown at the negative separations in Fig. 51 and 57.

A result open to doubt is probably that obtained at $y/H = 1.0$ in Fig. 51. Although the presence of a deviation in the rate of change of slope for the same conditions at Section B, Fig. 57, does provide some support for this irregularity it does not follow the pattern of the other measurements.

Correlations of the Longitudinal Turbulent Velocity for Lateral separations:

The correlations for lateral separation distances are shown in Fig. 61 to 68. In order to determine the degree of spanwise uniformity of the length scale of turbulence, lateral traverses of $\pm$ 76.2mm ($\pm$ 3 in.) were made from various fixed spanwise positions at $y/H = 0.20$ as shown in Fig. 61 and 65. At this height the spanwise uniformity is acceptable at Section A and has improved at Section B. The integral length scales of turbulence are smaller in this direction than those indicated for vertical separations.

These results were then extended to cover fixed points at the two heights $y/H = 0.10$ and 0.20 in more detail over a wider range of fixed spanwise positions, as shown in Fig. 62, 63, 66 and 67, at Sections A and B. The two sets of curves on each figure would in fact be mirror images of each other for true lateral uniformity of

the flow, the results for 38.1 m.m. (1.50 in.) being common to both sets of readings. The degree of spread of the experimental points indicates the order of non-uniformity in the simulated flow. The results at y/H = 0.10 show a reasonable degree of uniformity apart from those for the fixed point at 0 m.m. (0 in.) at Section A. The more detailed results at y/H = 0.20 show some improvement in uniformity due to the increase of height. It was considered that the degree of uniformity obtained was satisfactory for all of the conditions investigated.

The variation of the length scale with height was then established at one fixed spanwise position at Sections A and B as shown in Fig. 64 and 68 respectively. The results obtained indicate an increase of length scale with height which is far more pronounced than that shown by the vertical separation measurements. This trend is persistent up to a height of about y/H = 0.40. These correlations also show a clearly defined trend in going negative, and as shown later the same type of correlation is obtained in both natural and full-scale boundary layer flows. In contrast, a close examination of the experimental points giving the negative correlations for vertical separations shows that they are randomly distributed, unlike those for the lateral separations which have a well defined order. The similarity of the results at Sections A and B is considered to be satisfactory.

Comparison of the correlations with those of a Natural Flat-Plate Boundary Layer:

In order to establish whether in fact the measured correlations

were typical of those obtained in a boundary layer flow, the results were compared with similar measurements by Grant (1958), made in a natural boundary layer. The comparison of the correlations for vertical separations is shown in Fig. 69. Clearly, the correlations are of a similar type to those obtained by Grant. The only discrepancy is that higher up in the boundary layer Grant's length scales tend to be slightly larger. This may be due to the fact that the relative ground roughnesses of the two boundary layers are not the same. However, the important point is that the correlations are of the same form and show similar trends to those of the natural boundary layer.

The same conclusions can be made from Fig. 70 where the correlations for lateral separations are shown compared with some of Grants (1958) data. Grants measurements show the well defined trend of these data in going negative at large separation distances. Thus it can be assumed that the flow structure in the simulated boundary layer approximates reasonably well to that in a natural boundary layer on the above basis.

Comparison of the Correlations with those of an Atmospheric Boundary Layer:

Since the measured correlations have been established as being similar to those measured in a natural boundary layer, they can now be compared with those measured by Harris (1968) in an atmospheric boundary layer as shown in Fig. 71 to 73.

In accordance with Davenports (1963a) work regarding the dependence of the atmospheric boundary layer height on the surface

roughness length (y_o) it was assumed that the height appropriate to the terrain of Harris's measurements was of the order of three hundred metres (one thousand feet). On this basis, the comparison of Harris's results with those in the simulated boundary layer showed that there was a factor of approximately two between the results i.e. the length scales of turbulence in the atmospheric boundary layer were approximately twice those of the simulated boundary layer. On the basis of the conclusions of the previous section a boundary layer height of approximately six hundred metres (two thousand feet) was then assumed for comparison of the correlation data with those of Harris. Reference to the results shown in Fig. 71 to 73 shows that reasonable agreement is then obtained. In Fig. 71, one set of Harris's results has been plotted to illustrate the effects of assuming different boundary layer heights. On average, the length scales of turbulence in the atmospheric boundary layer are slightly larger than those of the simulated boundary layer, as were the results of Grant, previously discussed. However, it can be assumed that a satisfactory simulation of the length scales obtained in the atmospheric boundary layer has been achieved.

It was noted that Harris's (1968) autocorrelation data does not tend asymptotically to zero for large time delays. This suggests that some error is present in these results. Approximate corrections have been derived for these by Scriven (1969) assuming that uncorrelated spurious data has been added to the signal; the corrections are applicable to either auto or space correlations. These corrections have been applied and the corrected curves are

shown in Fig. 74 and 75. The effects of the correction in comparison to that obtained by the assumption of an approximate 600 metres (2000 ft.) high boundary layer are indicated on the same figures. Reference to Fig. 71 and 72 shows that, in general, the result of applying the correction is to obtain closer agreement with the simulated boundary layer measurements on the assumption of a boundary layer height of 600 m. (2000 ft.).

It should be noted that Grant's (1958) measurements of the correlation of the longitudinal turbulent velocity for longitudinal separations tend to suggest that the correlation takes longer to reach zero than theoretically predicted. The indications from this are that Harris's results may be over-corrected in Fig. 74 and 75. Clearly more atmospheric boundary layer data is desirable in order to prove or disprove this argument.

Another point worth noting also arises from the preceding analysis. If the ratio of the length scale of turbulence to the boundary layer thickness is the same for both the atmospheric boundary layer and natural boundary layers, then measurement of the atmospheric boundary layer length scales may provide a suitable method by which the thickness of the relevant boundary layer may be defined.

The proposed Theoretical Power Spectra:

Theoretical forms for the power spectra have been proposed by Davenport (1961) and Harris (1968) and have been used previously for comparison with the experimental data. The proposed forms of the power spectra are as follows:=

$$\frac{n S_u(n)}{} \propto \frac{\bar{x}^2}{(1+\bar{x}^2)^{4/3}} \qquad \text{- Davenport}$$

and,

$$\frac{n S_u(n)}{} \propto \frac{\bar{x}}{(2+\bar{x}^2)^{5/6}} \qquad \text{- Harris}$$

where, $\bar{x} = \frac{n}{\bar{U}_{10}} \mathcal{L}$, $\mathcal{L}$ is a length scale having a value of 1200 m. (4000 ft.) which was derived semi-empirically by Davenport.

Since the height of the atmospheric boundary layer has been assumed to be 600 m. (2000 ft.), based on analysis of the correlation data, the scale of the simulated boundary layer relative to the atmospheric boundary layer is now 4000 : 1 instead of 2000 : 1. Therefore the theoretical spectra were re-calculated for these conditions for comparison with the spectra of the simulated boundary layer. The theoretical spectra shown in Fig. 46 were based on a scale of 2000 : 1.

However, two of the quantities which fix the position of the spectra on the frequency scale cannot be assumed to be defined very precisely. For instance, Harris (1968) suggests that the length $\mathcal{L}$ could possibly be increased to a value of 1800 m. (6000 ft.). The theoretical spectra have therefore been calculated for various values of the boundary layer thickness, as shown in Fig. 76, and the length $\mathcal{L}$, as shown in Fig. 77, in order to assess the degree of error arising from errors either in the assumed boundary layer height, or the length $\mathcal{L}$, or both. These were estimated for the scaling conditions applicable to the simulated boundary layer. For the range of values investigated the effects are not considered to be excessive.

Comparison of the measured Longitudinal Spectra with the proposed Theoretical Spectra:

The measured and theoretical longitudinal power spectral densities are shown in Fig. 78. The spectra were measured at three different spanwise positions at y/H = 0.167 at Section A. Generally the same form of the spectrum is obtained at the various positions; however the total energy content of the spectra should vary in accordance with the small spanwise variation in turbulence intensity, as shown in Fig. 40 and 45. The differences in energy content are shown to occur in the lower and middle frequency ranges in Fig. 78.

The comparison with the theoretical spectra has been made using the mean spectrum of the measured spectra as a basis, i.e. the spectrum measured at the quarter-span position. The agreement between the curves is still satisfactory on the assumption of a 600 m. (2000 ft.) high boundary layer and taking the value of $\mathcal{L}$ to be 1800 m. (4000 ft.). The values of the maximum energy per octave frequencies do not agree exactly, but this is not considered to be particularly significant since the assumption of a slightly higher boundary layer, or larger length $\mathcal{L}$ can offset this effect.

The variation of the spectra with height at Section A is shown in Fig. 79. The forms of the spectra are reasonably invariant with height and will reduce to approximately the same curve if normalised, at a given height, by the ratio of the square of the turbulence intensities at the relavent heights. The spectra have not been normalised here as they are considered to be more informative in this state, for the purpose of comparisons, as regards their actual

variation in the simulated boundary layer. For a comparison of the spectra of boundary layers having different surface roughnesses the process of normalising the energy content would be more appropriate.

Additional spectral measurements at Sections A and B:

The measurements of the lateral and vertical spectra at Section A are shown in Fig. 80 to 83 and of the longitudinal spectra at Section B in Fig. 84 and 85. The spanwise variations of the lateral spectra are of a similar order of magnitude to those of the longitudinal spectra and are not significant enough to be unacceptable. The variation of the spectra with height, as shown in Fig. 81, is also considered to be satisfactory.

The measured vertical power spectral densities are shown in Fig. 82 and 83. The spanwise variation of the spectra at constant height is virtually negligible, as is the variation of the vertical intensity of turbulence at this height as shown in Fig. 40 and 45. Similarly, the variation of the energy content of the spectra with height follows the pattern of the variation with height of the intensity of vertical turbulence. Hence, these spectra were assumed to be satisfactory.

The spanwise variation of the longitudinal turbulence spectra at Section B is shown in Fig. 84 and its variation with height in Fig. 85. These follow similar trends to the longitudinal spectra as measured at Section A.

From this assessment of the power spectral densities it was concluded that the representation of the spectra was satisfactory

in the simulated boundary layer both in the spanwise and axial directions.

Measurement of the Intermittency Factors in the Simulated Boundary Layer:

The intermittency factors of the longitudinal turbulence were measured at Sections A and B and are shown in Fig. 86, where they are compared with similar measurements in a natural boundary layer by Corrsin and Kistler (1954). These factors are of importance in relation to the variation of the length scale of turbulence with height in the boundary layer (see Part 1 of thesis).

As shown in Fig.86, the spanwise variation of the factor is fairly considerable in some parts of the boundary layer at Section A; however, it is acceptable at Section B, as is its comparison with the data from a natural boundary layer. It is apparent that a spanwise position having the highest intermittency factor does not necessarily have the highest intensity of turbulence.

The variation of the intermittency factors of the lateral and vertical turbulence in the simulated boundary layer were also measured at Section B and are shown in Fig. 87. The forms of the distributions, as can be seen, are very similar for all three components of the turbulence and were considered to be satisfactory in the simulated boundary layer flow.

Comparison of the mean Velocity and Longitudinal Turbulence Profiles:

The mean velocity and longitudinal turbulence intensity profiles

measured in the simulated boundary layer have been compared with Harris's (1968) revised data, assuming the relevant thickness of the atmospheric boundary layer for these date to be 600 m. (2000 ft.) and are shown in Fig. 88 to 90. The full-scale mean velocity measurements fit a curve obeying a power law for the distribution of mean velocity in the boundary layer whose power exponent is 0.176 ($1/\alpha = 1/5.68$). The profiles measured at Section A and B have been compared with the profile calculated for this power law and the agreement was considered to be satisfactory at both of these sections.

The intensity of longitudinal turbulence based on both free-stream and local velocity has been compared with the atmospheric boundary layer data in Fig. 90. The comparison of the turbulence measurements based on local velocities is probably the more realistic one to make. On this basis, the forms of the distributions compare reasonably well although the turbulence intensities in the simulated boundary layer are higher. The discrepancy at the bottom section of the boundary layer is greater, since the velocity gradient of the simulated boundary is greater than that of the atmospheric boundary layer in this region. Finally the turbulence intensities based on the local velocities are compared with the most recent data of Harris (1971) and measurements from Sale (see Part 1 of thesis) as shown in Fig. 91. The agreement between the data is seen to be satisfactory.

Implications of the change of Boundary Layer height:

The assumption of an atmospheric boundary layer 600 m. (2000 ft.) in height has still resulted in satisfactory agreement between the simulated and atmospheric boundary layer data. Obviously some sources of error still remain since the height cannot be defined as precisely as one would like and since the choice of the value of the length $\mathcal{L}$ seems, to some extent, to be open to doubt.

However, on the basis of the present knowledge (see Part 1 of thesis) it can be assumed that the scale of the simulated to the atmospheric boundary layer is of the order 4000 : 1 and not 2000 : 1. This point is of importance since it effects the scaling of models in boundary layer flow in wind tunnel tests for measurements of both static and dynamic loads on structures. With regard to the correlation of dynamic load of structures it is important that the ratio of turbulent eddy to building sizes be correct. This aspect of wind loading has been previously discussed by Davenport (1963b). It is also of interest to note the effects of this change of boundary layer height with respect to plume dispersion tests in the simulated flow. The current height of large chimneys is of the order of one third of the boundary layer height, i.e. 180 m. (600 ft.). Therefore, in a scaled 600 m. (2000 ft.) boundary layer the small secondary flow effects of the simulated boundary layer should not influence the plume since these irregularities are confined to the upper section of the boundary layer. If the plume moves into the higher part of the boundary layer, this would normally be some distance downstream, in which case secondary flow effects will be negligible.

If it could be assumed that the atmospheric boundary layer in neutral conditions has a mean height of say 600 m. (2000 ft.), regardless of surface roughness, this would considerably simplify the design of wind tunnel models for measurements of wind loading and other tests. Shellards (1963) paper, in fact, suggests that better agreement with meteorological readings is obtained by the adoption of a common height for the atmospheric boundary layer and with the present lack of data this seems to be the more realistic approach to take. A recent paper by Hanna (1969) on the estimation of boundary layer heights quotes the expression,

$$H_D = \frac{0.006\,\bar{U}_o}{F}$$

where F = the Coriolis parameter $\simeq 10^{-4}$/sec.

This gives a boundary layer height for Adiabatic conditions of the order of 550 m. (1800 ft.) which agrees with the findings of this work. Again, as stated previously, measurement of the integral length scales of turbulence in the atmospheric boundary layer may provide a more tangible method of obtaining the required boundary layer height.

At this stage of the work it can be assumed that Adiabatic boundary layer flow over rural terrain can be simulated satisfactorily in a wind tunnel. The small secondary flow effects associated with this simulation technique are not thought to be of importance in most wind applications and in any case they tend to become negligible as the flow development continues downstream.

5.4.5. Flow visualisation tests.

Some flow visualisation tests were made both at C.E.R.L. and the N.P.L. to see if a clearer picture could be obtained of how the simulation system basically worked. However, as anticipated, it was not very easy to obtain reliable or consistent evidence due to the highly complex flow processes involved. A schematic presentation of some of the deductions from the tests is shown in Fig. 92. However this should only be regarded as being indicative of the general flow processes involved and may be influenced to some extent by pre-conceived ideas of what these flow patterns should look like.

6. DETERMINATION OF ROUGHNESS ELEMENT CHARACTERISTICS.

When attempting to simulate neutral atmospheric boundary layer flows it is essential to represent the values of the roughness length appropriate to the different types of terrain being considered. In the case of open countryside the problem is not too difficult, since the height of typical obstructions is not great. It then follows that the roughness length will be small and, at model scale, could even be represented by "sand roughness". In the case of urban or suburban areas the roughness elements involved, namely buildings, are considerably larger and more densely distributed. Hence there are difficulties not only in modelling the roughness but also in deciding on the value of the roughness length to be represented in the model. This problem has recently been discussed by Fekete (1967) and Pasquill (1970). In addition, modelling of the zero-plane displacement must also be considered.

Since it is eventually required to produce an equilibrium flow which is representative of urban terrain, it is also necessary to establish how the equilibrium value of the roughness length is related to the height and the distribution of roughness elements.

Clearly, a prohibitive fetch is needed to produce equilibrium conditions naturally; therefore all of the present tests were conducted at non-equilibrium conditions and the results extrapolated to obtain equilibrium data. The rural simulated flow system was then used to obtain the near-equilibrium roughness length for comparison with the extrapolated values.

When this section of the work was completed the review paper of Wooding et al (1969) was discovered. Their analysis and the

data analysed obtained here agree; however these authors did not consider the effects of fetch and did not consider the zero-plane displacement.

6.1 Model and test details.

For these tests 'Lego' baseboard, having 1.60 mm (.0625 in.) high protrusions, was fitted to the floor of the wind tunnel and 'Lego' bricks were used as roughness elements. These bricks were 9.5 m.m. (0.375 in.) high and 15.9 mm (0.625 in.) square. By using 'Lego' bricks as roughness elements the number and arrangement of roughness elements in a given area of baseboard could easily be varied.

The test Reynolds number was 0.60×10^4 based on the free-stream velocity and the roughness element height. With regular arrays of bricks the area ratios, i.e. brick plan-area/total area, considered were as follows:-

A_R/A : 0.077 ; 0.116 ; 0.152 ; 0.157 ;
0.206 ; 0.234 ; 0.304 ; 0.426 :

For some cases considered, the area-ratios were kept the same and the bricks were distributed randomly.

The range of brick height/fetch ratios considered were as follows:-

$\frac{h_r}{f_e}$: 0.0106 ; 0.0140 ; 0.0278 :

6.2. Method of Analysis.

Some work has been reported by Perry and Joubert (1963) on two-dimensional roughness strips and their method for the

determination of the roughness length and the zero-plane displacement thickness was used here. This method involves the following procedure. If $(\bar{u}/u_*)$ is plotted against $(\log_e y_L)$, the resultant curve should be linear over the constant stress layer of the boundary layer, if the zero-plane displacement, d, is zero. If it is not zero, then successive values for it are assumed until a value is found which produces a linear variation of $(\bar{u}/u_* \sim \log_e y_L)$. Extrapolation of this line to the $\log_e y_L$ axis then gives the value of $\log_e y_o$.

In the case of the three dimensional roughness elements which were used here, the problem becomes more complicated. It was found necessary to measure the velocity profiles at several spanwise stations varying from the mid-point of the element spacing to the centre-line of a roughness element. For most distributions an average of four roughness length values at four different spanwise stations were obtained from which the average roughness length, $\bar{y}_o$, was then evaluated. As a consequence the mean zero-plane displacement, $\bar{d}$, was also derived. The analysis was carried out by the graphical method described above and, as can be appreciated, was fairly extensive in order to produce the final data presented here.

6.3 Results and Discussion.

6.3.1 Measurements at $h/\delta_e = 0.014$.

The spanwise variation of the velocity profile for a typical roughness distribution is shown in Fig. 93. For heights up to $1\frac{1}{2}$ times the roughness element height, this variation is fairly

large (see also Fig. 47). A mean velocity profile has been derived from the measured profiles and has been extrapolated to zero velocity allowing for the effect of the zero-plane displacement. It can be seen that a power law profile having an index of 0.40 provides a reasonable fit over the lower part of the mean velocity profile i.e. up to a height to which full-scale measurements might be expected to be taken. This index has in fact been suggested by Davenport (1963a) as being applicable to an urban area. However, if a better comparison is required over the full boundary layer height then a power law having a different index, or a log-law, would provide a more appropriate representation. These results are typical of those analysed to obtain the spanwise variations of the roughness length and the zero-plane displacement, and hence to obtain the mean roughness length and mean zero-plane displacement, of a distribution of roughness.

The variation of $\bar{y}_o/h_r$ and $\bar{d}/h_r$ with the roughness element density, A_R/A, at the fetch of 685 m.m. (27 in.) is shown in Fig. 94. For some values of A_R/A the arrangement of roughness elements was changed, but this did not produce any significant trend in the estimated values of $\bar{y}_o/h_r$. This result can be expected to be applicable provided the roughness elements are distributed in the given area in such a way as to avoid large non-uniformities in the distribution. The practical implications of this in modelling, say, a suburban area is that the location considered need not be modelled exactly provided the appropriate A_R/A is represented.

At $A_R/A = 0$, Fig. 94, the roughness length indicated is

that of the 'Lego' baseboard alone. Since the tops of the roughness elements have a similar distribution of protrusions to those of the baseboard, then the roughness length at $A_R/A = 1.0$ is again the same as that measured on the baseboard alone.

As the roughness element density increases, $\bar{y}_o/h_r$ increases until a value of $A_R/A \simeq 0.25$ is reached. Above this value, $\bar{y}_o/h_r$ decreases rapidly as the roughness element density increases. Two flow regimes can therefore be defined, one for $0 \leq A_R/A \leq 0.25$ and one for $0.25 \leq A_R/A \leq 1.0$, which will be referred to as flow regimes A and B respectively. In the work of Parry, Schofield and Joubert (1968) a change in flow characteristics was also observed as the gap between adjacent two-dimensional roughness strips was reduced below a certain value. This is analogous to an increase of A_R/A using three-dimensional roughness elements. It is suggested that in flow regime A each roughness element produces its maximum effect and contributes to the production of turbulent energy. Secondary flow effects, which are assumed to be small, do not have a signifcant effect in the flow regime. As the roughness element density is increased, the full mixing effect of the elements becomes gradually more suppressed by their closeness to each other (Regime B). Thus, secondary flow regions can develop more freely between the elements. In the extreme case (i.e. $A_R/A \rightarrow 1$) it is suggested that the major part of the free-stream flows over the tops of the elements and that secondary flows extend to nearly the full element height. In this condition the production of turbulent energy would not be very great. It was considered that flow regime A was more representative of suburban or urban areas, hence regime B

was not considered further.

Figure 94 also shows the variation of $\bar{d}/h_r$ with A_R/A. Up to A_R/A of about 0.50 to 0.60 the variation is linear and in the range of main interest, $0.10 \leq A_R/A \leq 0.25$, $\bar{d}/h_r$ and $\bar{y}_o/h_r$ are, conveniently, of the same order of magnitude. At the higher values of the element density an arbitrary curve has been fitted on the assumption that at $A_R/A = 1.0$, $\bar{d}/h_r = 1.0$.

6.3.2 Measurements at other Fetches

The above variation of the roughness parameter with the roughness element density is applicable to non-equilibrium flow conditions. The additional data required is the variation of the roughness parameter with both A_R/A and h_r/f_e so that an extrapolation can be made to the near-equilibrium conditions i.e. $h_r/f \rightarrow 0$. Additional measurements were obtained at constant A_R/A by alteration of the fetch distance.

The variation of $\bar{y}_o/h_r$ with A_R/A and h_r/f_e was derived from Fig. 94 and the above additional test points and is shown in Fig. 95. The data of this figure can be represented approximately by the expression:-

$$\bar{y}_o/h_r \simeq 8.2\, h_r/f_e + 1.08\, A_R/A - 0.08$$

hence for the condition of equilibrium when $h_r/f_e \rightarrow 0$,

$$\bar{y}_o/h_r \simeq 1.08\, A_R/A - 0.08$$

Clearly, the above expressions apply only in the range,

$$0.10 \leq A_R/A \leq 0.25$$

At roughness element densities below 0.10 measured roughness lengths will be very dependent on the spacing of the individual roughness elements. It has in fact been shown by Roberson and Chen (1970), that for $A_R/A < 0.10$ the predominant contribution to the total drag comes from the local surface rather than the roughness elements. In some cases the wake properties of individual elements would be measured rather than the integrated effects produced by a number of roughness elements. However, such conditions would not be representative of built-up suburban or urban areas. At roughness densities above about 0.25 a linear variation of $\bar{y}_o/h_r$ with A_R/A would clearly not be acceptable and the form of presentation would necessarily differ from that of Fig. 95. In addition, one may argue as to the validity of representing the results as a set of straight parallel lines. The representation may not be strictly true due to the fact that a linear variation of $\bar{y}_o/h_r$ with A_R/A was assumed from the results of Fig. 94. Additionally, if it is considered that at say h_r/f_e of 0.01, element density distributions of 0.25 and 0.10 have reached 70 and 30 per cent of their respective equilibrium values, it moght be agreed that the lines in Fig. 95 should converge. However, it was considered that the experimental results did not justify a more refined representation than that adopted. Therefore it was decided that the results and expressions derived were valid for the conditions stated to be of interest.

It has previously been suggested by Davis (1970) that,

$$\underline{y_o/h_r \simeq A_R/2A}$$

However, the above results show that this is applicable only at near-equilibrium conditions for density ratios of the order of 0.15.

The system developed for producing a simulated rural atmospheric boundary layer has been assumed to produce near equilibrium flow conditions. Therefore, this system was used to obtain $\bar{y}_o$ of the roughness element densities of 0.15 and 0.20. Combined with the other experimental data, these points were considered to give the best fit on the curves of Fig. 95 when plotted at $h/f_e = 0.001$. From this it can be deduced, that near-equilibrium conditions should be attained in a distance of about 1000 roughness element heights.

From the above data, the roughness element layout chosen as being representative of an average type of urban situation is as follows:-

$$A_e/A = 0.15.$$

which gives a full-scale urban roughness length of,

$$\bar{y}_o \simeq 2.6\text{m}$$ (see Part 1 of thesis)

The following section deals with the modifications to the existing system to produce the urban terrain boundary layer and presents the mean and fluctuating velocity measurements made in this flow.

7. DEVELOPMENT OF THE SIMULATED URBAN BOUNDARY LAYER.

7.1 Problems to be considered in modelling an Urban Boundary Layer.

As has been stated previously, the wind loading on a building or a group of buildings depends on the turbulence and shear in the approaching flow; these properties are determined by the terrain roughness for the case of adiabatic equilibrium. Therefore, in a wind tunnel in which wind loadings are to be investigated, it is essential that the boundary layers appropriate to flow over both moderately rough and very rough surfaces should be reproducible. The problem of simulating moderately rough surface flow (i.e. rural terrain) has been considered in Sect. 5. and an adequate simulation has been obtained.

When considering the simulation of the very rough surface (i.e. urban terrain, which is taken as the extreme rough case), the first problem to resolve was modelling the buildings (i.e. the large roughness elements) to obtain the appropriate roughness length. It was noted that the roughness length was a function of the density distribution of the buildings and of the fetch. Therefore, its variation as a function of these two quantities was determined in Sect. 6. Hence, knowing the degree of roughness, or the roughness length to be simulated, the appropriate distribution of roughness elements could be selected from these data to represent equilibrium flow over that particular terrain; the equilibrium state being defined as one in which the boundary layer characteristics do not change appreciably along the flow direction.

Typically such flow would not normally occur in an urban area due to insufficient fetch being available. However, as a basis from which to work, the equilibrium state is considered here.

As stated previously, the work of Part 1 of this thesis had not been completed when the urban boundary layer was being initially considered. Therefore there was difficulty in defining this boundary layer since the full-scale measurements readily available for such sites appeared to be relatively sparse and uncorrelated. In many cases the measuring sites varied considerably, and measurements were affected to some to some degree by the proximity of local buildings. This being so, local effects have sometimes been measured rather than the integrated effects appropriate to a particular mean urban condition. Usually it was impossible to assess such effects since detailed knowledge of the site topography was not always available.

Urban wind measurements and their analysis are also affected by the magnitude of the local roughness length and the zero-plane displacement as shown in Sect. 6. Allowances for these quantities have, until recently, tended to be neglected in the literature; exceptions to this are included in the work of e.g. Paeschke and Pasquill (1950). However, it is possible that more consistent results would be obtainable if, as stated by Chandler (1968), "a standard non-standard site" could be defined, or if more care were to be taken in the selection of sites for full-scale measurements.

The rural simulated boundary layer was produced as shown in Sect. 6 by the use of a barrier, vorticity generators and surface roughness; the approach adopted being to consider how a certain

mean velocity profile and turbulence intensity distribution could be modelled. It was assumed that such a system would produce the complete spectrum of frequencies required, which it did. The ground roughness was matched to the barrier and provided for the continuing production of turbulence at ground level.

Therefore, on the basis of the above simulation it was anticipated that, having decided on the urban terrain characteristics to be simulated, the geometry and spacing of the generators would not need to be changed to produce the required boundary layer flow. The only alterations envisaged to the system were a change of the barrier height and the use of large roughness elements. The following text presents the main points which were considered in choosing a typical urban terrain, how it was represented in a wind tunnel and the measurements made in this simulated urban boundary layer.

7.2 Models

7.2.1 Roughness element details.

The roughness elements used were those as previously described in Sect. 6 i.e. 'Lego' bricks measuring 9.5 m.m. (0.375 in.) high and 15.9 m.m. (0.625 in.) square which were fitted to a 'Lego' baseboard on the floor of the wind tunnel. The spacing of the bricks used to represent the urban terrain was two brick widths between brick centres in a spanwise direction and three brick widths in a streamwise direction. The resultant ratio between the brick plan area (A_R) and the total plan area (A) was approximately 0.15.

7.2.2 The barriers.

As in the case of the rural simulation the wake characteristics of barriers of various heights were considered. These are as follows:-

h_1/H : 0.167 ; 0.1875 ; 0.208

where h_1 is measured to the base of the castellations.

The geometry of the castellations was the same as in the rural simulation. Therefore, the corresponding range of barrier heights to the tops of the castellations is as follows:-

h_2/H : 0.208 ; 0.229 ; 0.250 :

where h_2 is measured to the tops of the castellations. The barrier finally chosen for the urban simulation is as follows:-

h_1/H = 0.208 ; h_2/H = 0.250

7.3 Test programme.

Measurements of the mean and fluctuating quantities were made over the full boundary layer height at Stations A and B (i.e. at 3 and $4\frac{1}{2}$ boundary layer heights, respectively, downstream of the generators. Some additional measurements were made at Station C which was six boundary layer heights downstream of the generators. These measurements were made at spanwise positions in-line with the generator centre-line and the generator mid-span. In order to assess any local effects of the roughness on the above measurements, additional measurements were made at Station B at various spanwise positions relative to a roughness element.

The definition of the correlation coefficient is as stated previously (Sect. 5.2.4. and Fig. 8) and the details of the

correlation measurements made at Station B are as follows:-

Correlation R_{uu} (0, r, 0)

These correlations are measured at the generator centre-line and mid-span positions for the following range of fixed points:-

y/δ (= y/H) : 0.030 ; 0.083 ; 0.167 ;
0.250 ; 0.334.

Correlation R_{uu} (0, 0, r)

These correlations were measured at the spanwise fixed point at 0 m.m. (0. in.) (i.e. in-line with the generator centre-line for the following range of vertical fixed points:-

y/δ (= y/H): 0.04 ; 0.06 ; 0.10 ;
0.20 ; 0.40 ; 0.50.

The power spectral densities of the fluctuating velocities were measured for the following conditions:-

The longitudinal spectrum:-

y/δ, Generator Centre-line	y/δ, Generator Mid-Span
0.060	0.060
0.083	0.083
0.167	0.167
0.300	-
0.500	-

The lateral and vertical spectra:-

These were measured at the generator centre-line for,

y/δ : 0.060 ; 0.083 ; 0.167 ;
0.300 ; 0.500.

Additional measurements of the longitudinal spectrum were

also made at different spanwise positions at y/δ = 0.083 to determine any local effects due to the roughness elements. These were made at sections in-line with a roughness element centre-line and at the mid-span and quarter-span positions between this element and an adjacent one.

The power co-spectral densities of the Reynolds stresses were measured at Station B, on the generator centre-line, for the following range of heights:-

y/δ : 0.060 ; 0.083 ; 0.167 ;
0.300 ; 0.500 .

The probability density distributions of the fluctuating velocities were measured at Station B for the following range of heights:-

Generator Centre-line - y/δ : 0.060 ; 0.083 ; 0.167;
0.300 ; 0.500.

Generator Mid-span - y/δ : 0.060 ; 0.083 ; 0.167

7. 4. Experimental Results.

The experimental results from the above tests are presented in Fig. 96 to 125.

Fig. 96 and 97 show the theoretical power law velocity profiles suggested for terrain conditions varying from rural to urban and the variation of the measured velocity and turbulence intensity profiles with change of barrier height. The measurements at Station B of the velocity profile, Reynolds Stresses and turbulence intensities in the simulated urban boundary layer are shown in Fig. 98 and 99. Their variation at a number of spanwise positions, which was

determined in order to illustrate local effects due to the large roughness elements, is shown in Fig. 100 and 101. Similar measurements at Station A and C are shown in Fig. 102 to 105.

The correlation measurements for vertical separations are shown in Fig. 106 to 109 and a comparison between the urban and rural data in Fig. 110. The correlation measurements for lateral separations are shown in Fig. 111 to 113. Again, some of the urban and rural measurements are shown compared in Fig. 114. The scales of turbulence in the longitudinal direction were derived from auto-correlation measurements and are shown, compared with rural terrain measurements, in Fig. 115.

Measurements of the power spectral density of the longitudinal fluctuating velocity are shown in Fig. 116 to 118. The spectra, normalised with respect to the mean square fluctuating velocities at the respective heights are shown in Fig. 119. The lateral and vertical fluctuating velocity spectra are shown in Fig. 120 and 121 respectively and some of the spectra of the vertical velocity from the rural simulation, for purposes of comparison, in Fig. 122. Fig. 123 shows a comparison of the spectra of the three fluctuating velocity components for the urban and rural simulated boundary layer flows. The power co-spectral densities of the Reynolds Stresses are shown for the urban and rural simulated boundary layers in Fig. 124. Finally, the probability density distributions of the longitudinal fluctuating velocity measured in the urban simulated boundary layer and compared with those measured in the rural boundary layer as shown in Fig. 125.

7.5 Defining the Urban Boundary Layer.

As stated in Sect. 1, all of the analysis of Part 1 of this thesis had not been completed when developing the Urban boundary layer simulation. Therefore, because of the wide variations in the various definitions of Urban boundary layer structure, in comparison to those for Rural boundary layer structure, it was considered necessary to first establish a more positive definition of the characteristics of the boundary layer. This definition was based on the data of just a number of selected references, which were considered to be fairly generalised and therefore more appropriate for the purpose. The main characteristics of the boundary layer are considered individually in the following text.

7.5.1 The Velocity Profile.

It was assumed, in the first instance, that the variation of velocity with height in an urban area could be represented by a power law, as in the case of the rural terrain. Initially it was thought that a power law having an exponent of 0.40 should be considered; this was suggested by Davenport (1963) as being appropriate to heavily built-up urban areas. However, this was later reconsidered for the following reasons.

Firstly, the initial survey of a selection of the available literature showed that urban power law exponents varying from 0.21 to 0.40 had been measured at various urban sites as follows;

Site	$1/\alpha$	Reference
Liverpool	0.21	Jones et al. (1971)
London	0.23	Shellard (1963)
Kokubunji	0.25	Shiotani (1962)
Suburbs	0.28	Davenport (1960b)
Japanese towns	0.33	Kamei (1955)
City centre	0.40	Davenport (1963)

The prevailing vertical temperature gradients appropriate to the above data have not always been quoted in the literature; however, the measurements were mostly obtained during high winds, implying near-adiabatic conditions.

Secondly, from the measurements previously made in rough boundary layers where the roughness height was a significant part of the total boundary layer height (Sect. 6.0), it was shown that a wide range of indices could be fitted to the measured profiles. This depended on where the measurements were made relative to a particular roughness element and the height range over which the profile was fitted. For example, if measurements were not made to a height great enough to be free of the local effects of the roughness, variations in the local mean velocity of ± 15 per cent could be measured over small spanwise distances. Some of the measurements of Kamei (1955) quoted above may be subject to errors of this type. Additionally, in the measurement of velocity profiles in rough-wall boundary layers (see Sect. 6.0), high values of the power law index were found only in non-equilibrium flows. Similar conditions probably applied to the cases where such exponents had been obtained from full-scale measurements.

The final point considered was that an exponent of about 0.28 had been measured previously in a rough-wall equilibrium boundary layer, in which the ratio of the roughness height to the boundary layer height was similar to that for the intended urban boundary layer simulation.

Taking all the above points into consideration, an exponent of 0.28 was chosen for the urban site in a near-equilibrium state. Local modifications caused by large obstructions can be obtained by representing these in the model and thereby producing local areas having a greater shear flow and indices up to 0.40.

Furthermore, the 0.28 index has been chosen by Commonwealth Aeronautical Advisory Research Committee (C.A.A.R.C.) (Wardlaw and Moss, 1970) as being typical of sites having obstructions of about 25 m. high and is to be used on the shear flow requirement for some basic industrial aerodynamic investigations.

7.5.2 The turbulence intensities.

The available data on urban turbulence measurements are not very extensive and are insufficiently detailed to present graphically, as a function of height, as in the case of the rural data. This is probably due to the fact that the main effort has been directed towards trying to define a representative velocity profile, as a first step, in the understanding of the urban environment. Estimates of the longitudinal turbulence by Davenport (1960) and Harris (1970) suggest that the turbulence intensities, based on the gradient velocity, for urban sites, are not significantly greater than those associated with rural sites.

Based on local velocities, however, they should be 20 to 30 per cent in the lower regions of the boundary layer.

Typical measurements of longitudinal turbulence intensity made in 'rough' terrain are given by Shiotani and Yamamoto (1948) and by Singer (1960). Generally these fall in the range of values quoted above. More recent measurements by Helliwell (1971) in the London area have indicated values ranging from 10 to 30 per cent based on local velocities. There is naturally a greater amount of scatter in the urban measurements than in the case of rural measurements due to the fact that the measured intensities, like the mean velocities, are more dependent on the measuring position relative to the local buildings.

It is assumed that the flat-plate data applicable to the lower 10 to 15 per cent of the boundary layer can also be applied here. In which case, the ratios of the lateral and vertical turbulence intensities to the longitudinal turbulence intensity should be of the order of 0.75 and 0.54 respectively.

7.5.3 The power spectral densities.

The available measurements and discussions of urban power spectra (e.g. see Davenport 1963, 1967 and Panofsky 1969) all suggest that the forms of the urban and rural spectra should be similar. Therefore it is to be expected, for example, that the high frequency end of the spectrum, when plotted in the $n\,S(n)$ form, will follow Kolmogoroffs $-^{2}/_{3}$ law (Kolmogoroff 1941). The longitudinal spectra should also be invariant with height, except possibly at heights which are low in comparison to local building

heights. Here, a shift of the peak $nS_u(n)$ value to a higher frequency would be expected. Additionally, a secondary peak $nS_u(n)$ value may be detected at a frequency associated with a building addy shedding frequency where measurements are made at heights comparable to local building heights.

With these exceptions, the spectral form should be as proposed by Harris (1968):-

$$\frac{nS_u(n)}{} \propto \frac{\bar{x}}{(2+\bar{x}^2)^{5/6}}$$

where,

$\bar{x} = \frac{n\mathcal{L}}{\bar{U}_{10}}$; $\mathcal{L}$ = 1800 m. (in preference to 1200 m. previously suggested); $\bar{U}_{10}$ = Reference velocity at a height of 10 m. This form of the spectrum is more often used in preference to that suggested by Davenport (1967) which appears to underestimate the energy in the low range of frequencies.

The form of the vertical spectrum is assumed to be that proposed by Busch and Panofsky (1968):-

$$\frac{nS_v(n)}{} \propto \frac{1.075\, f/f_m}{1+1.5\,(f/f_m)^{5/3}}$$

and the lateral spectrum, as in the rural simulation, is assumed to lie between the longitudinal and vertical spectra.

7.5.4 The Reynolds Stresses.

Full-scale measurements of the Reynolds stresses are relatively few for Rural terrain and are even more sparse in the case of Urban terrain (see Part 1 of thesis). However, the ratio of the Rural to Urban stresses can be derived on a semi-theoretical basis from data which predicts the variation of the Reynolds stresses with the Rossby Number ($R_o = \bar{U}_o / f y_o$). The Rossby Number mostly reflects

variations in the roughness lengths of the surfaces considered. Therefore, the choice of a reasonable mean value of the roughness length for an urban area is desirable if a good estimate of the stresses is to be obtained; in which case the following points need to be considered.

When a moderately rough surface is being considered, local variations in the roughness length are not significant. However, with a very rough surface, i.e. urban terrain, the roughness length is very dependent on the position at which it is measured. Additionally, it is a function of the distribution of roughness, i.e. whether the area is lightly or heavily built-up (see Sect. 6). Therefore, in the first instance, it is necessary to adopt some mean value for the roughness length which specifies a typical urban site, and it was decided that this should be between 2 to 3 m. full-scale. This is consistent with Slade (1969) for example. On this basis the ratio of the Urban to Rural shear stresses near ground level can be estimated as approximately 1.5 from either Smith (1971) or Pasquill (1971), for the same free-stream velocity in an atmosphere in adiabatic equilibrium.

From the analysis of some full-scale measurements by Deland and Panofsky (1957) it is possible to obtain an estimate of the ratio of the stresses based on local velocities. For heights comparable to the height of the roughness this ratio is about 10.

An additional point that may be considered is that if the turbulence scales and intensity are correctly modelled, it can be assumed that the dissipation term is scaled correctly (Taylor 1935). The corresponding rate of turbulent energy production, which is

proportional to the product of the shear stress and the velocity gradient, should also be simulated correctly and should equal the dissipation. If the scales and intensities of turbulence and the velocity profile, associated with the above terms, are correctly simulated and are constant in a streamwise direction, then the resulting shear stresses should be correctly scaled.

7.5.5 The Co-spectrum of the Reynolds Stresses.

The available co-spectral data for Rural situations have been correlated and analysed by Panofsky and Mares (1968) who derived a semi-empirical expression to describe the co-spectrum:-

$$n S_{uw}(n) \propto \frac{-f/f_m}{(1.06 + f/f_m)^{5/3}}$$

where f_m is the normalised frequency corresponding to the peak value of $nS_{uw}(n)$ and is taken as -0.08. The above expression is also assumed to apply to Urban co-spectra. From the full scale measurements however it can be seen that the possible variation of f_m lies in the range:-

$$-0.05 \leq f_m \leq -0.12$$

Clearly the positioning of the co-spectrum on the frequency scale is dependent on the relative positions, or frequency bands, of the longitudinal and vertical velocity spectra. In this context the work of Panofsky and Mares indicates that the majority of the stress contribution lies in the range,

$$0.01 \leq f \leq 1.0$$

Since the spectra of the vertical fluctuating velocity are height dependent, it can be assumed that the co-spectral measurements will also be a function of the height above ground level. However,

most of the available measurements have been made at heights of less than 50 m. (160 ft.) where variations of the co-spectra due to height would probably not be significant. The slope of the co-spectra at the high frequency end is taken as $-5/3$ when plotted in the $nS_{uw}(n)$ form; this has been adequately verified by the recent measurements of Miyake, Stewart and Burling (1970) and of Sitamaran (1970).

7.5.6 The probability density distribution.

It has been assumed that the probability density distributions of the fluctuating velocities should be Gaussian for near equilibrium conditions. Therefore the probability density,

$$p(x) = \frac{1}{\sigma\sqrt{2\pi}} e^{\frac{-(x-\mu)^2}{2\sigma^2}}$$

which for $\sigma = 1$ and $\mu = 0$ reduces to:-

$$p(x) = \frac{1}{\sqrt{2\pi}} \cdot e^{-\frac{1}{2}x^2}$$

It has been suggested that small variations from this distribution at large values of the standard deviation can be significant with respect to wind loading problems. A review of some of the relevant meteorological papers by Giblett (1932), Shistani (1950), Cramer (1952) and Sutton (1953) suggests that the measured full-scale distributions are Gaussian within the range of $\pm 3\sigma$, but outside this range the measurements show variations from the Gaussian form which do not appear to be insignificant. It is not known how important the simulation of this quantity is in relation to wind tunnel model tests. At present a reliable comparison between model and full-scale data can only be made within the $\pm 3\sigma$ range due to lack of full-scale measurements.

Although the above data are relevant to rural sites, it is again assumed that the comments and conclusions apply equally well in the case of urban terrains.

7.5.7 The Scales of Turbulence.

It has previously been established that the scales of turbulence simulated in the Rural terrain boundary layer were the correct size, relative to the boundary layer height, for compatibility between it and a naturally grown boundary layer (Sect. 5). It now remains to be decided what modifications, if any, could be expected to be imposed on the length scales in flow over an Urban area. The most recent literature [e.g. Teunnisson (1970) and Harris (1970)] suggests that the streamwise length scale of the longitudinal fluctuating velocity is either independent of the roughness of the terrain or that it increases as the terrain gets rougher.

At heights which are relatively free of the effects of building wakes, it is assumed here that there will be no significant change of the scales of turbulence, except perhaps that of the vertical scale. A change of this scale seems possible because of the greater roughness elements, in the form of buildings, producing a greater degree of energy transfer in the vertical direction. At heights which are the same order of magnitude as the buildings, it is assumed that the length scales in the streamwise direction would be reduced due to obstruction and breaking up of the flow by the buildings.

7.5.8 The typical Urban Terrain Boundary Layer.

From the above discussion it can be seen that despite the lack of full-scale data in many areas, some conclusions can be made regarding the flow to be simulated. Since the majority of the available full-scale data are mean velocity profile measurements, then this quantity will be used initially as a guide towards defining the Urban boundary layer.

It is assumed that the velocity profile can be represented by a power law and on the basis of the available data and the arguments put forward, an index of 0.28 is assumed to be the most representative choice - as is the associated value of the mean roughness length of 2.50 m.

However, it should be noted that it has been previously emphasised that the simulation of the large scale turbulence, rather than that of any specific velocity profile, is an essential requirement in this simulation work.

7.6 Discussion.

7.6.1 Effect of increasing the barrier height.

The suggested range of theoretical velocity profiles covering variations in terrain between Rural and Urban is shown in Fig. 96. It was assumed that the applicable velocity profiles could be represented by power laws.

The work on the Rural simulation has shown the effect on the momentum loss due to increase of the barrier height and this is also shown in Fig. 96 and 97. in the development of the Urban simulation. In this case it is assumed that the momentum loss

due to the roughness is considerably greater than in the case of the Rural roughness. Therefore, the roughness is assumed to define the lower section of the velocity profiles, independently of the height of the barrier, to a greater extent than in the case of the Rural simulation.

As a rough guide, an increase of 0.021 y/H in the barrier height will result in a velocity defect of about 0.03 $\bar{u}/\bar{U}_o$. Some of this loss must be attributed to the roughness elements and some allowance made when interpolation of the data is required in the range $0.143 \leq 1/\alpha \leq 0.28$. It can be seen from Fig. 96 that a barrier height of h_1 = 31.75 m.m. (1.25 in.) is adequate for producing a velocity profile with a power index of 0.28.

7.6.2 Mean velocity and turbulence intensity measurements.

The measurements at Station B of the mean velocity and Reynolds stresses are shown in Fig. 98 and 100. It can be seen that the simulated velocity profile approximates fairly closely to a 0.28 power index profile over the majority of the boundary layer height. In addition, the spanwise uniformity of the flow is better than that achieved for the Rural simulated flow. This is attributed to the greater mixing effect of the larger roughness elements. At a height of the order of the roughness height, the ratio of the mean Urban and Rural Reynolds stresses, based on the gradient velocity, is approximately 1.40 compared to the theoretical estimate of 1.50. Similarly, the ratio based on the local velocity is 7, compared to 10 from the full-scale measurements. This degree of agreement is considered to be acceptable when the inherent inaccuracies involved

in full-scale Reynolds stress and mean velocity measurements are considered. More detailed measurements showing the local effects of the roughness elements on the above measurements are shown in Fig. 100. Spanwise variations in the measured quantities are fairly large at heights up to about 1.5 h_R . This again illustrates the difficulty in defining mean values of measurements made in Urban sites.

Similar measurements made at Station A and C are shown in Fig. 102 and 104 respectively. Again these data illustrate the greater degree of spanwise uniformity of the Urban simulated boundary layer.

The measurements of the three components of turbulence intensity are shown in Fig. 99 and 101. The ratios of the lateral to longitudinal and vertical to longitudinal turbulence are 0.75 and 0.59 respectively, in the lower section of the boundary layer, compared to 0.75 and 0.54 for flat-plate data. The results also illustrate a very high degree of spanwise uniformity of the flow. The magnitude of the longitudinal turbulence intensity, near ground level, based on the free-stream velocity is slightly greater than that of the Rural terrain, as anticipated by the Davenport and Harris estimates (see Sect. 7.5.2.). The comparison of the results, based on local velocities, with the full-scale measurements of Helliwell (1971) in the London area is as follows:-

y/H	Simulated Turbulence	Helliwell (1971)
Just above roughness height:	27%	15% to 30%
0.33 :	14%	12%

As indicated previously the full-scale measurements at low heights

generally fall in the range of 20% to 30% (based on the local velocity) and the simulated turbulence intensities are therefore considered to be acceptable. The local effects due to the roughness elements on the above measurements are shown in Fig. 101. These data are significant inasmuch as the spanwise scatter, and its extent in the vertical direction, is of the order expected, whereas the scatter in the case of the lateral and vertical turbulence intensities is relatively insignificant. No explanation of this can be suggested here, but this characteristic may be of some relevance in relation to diffusion problems.

Similar measurements made at Station A and C are shown in Fig. 103 and 105 respectively. In addition to showing the spanwise uniformity of the flow, these data also establish that the above quantities are reasonably invariant in the streamwise direction.

7.6.3 Correlation measurements and Turbulence Scales.

The variations of the correlation coefficients in the simulated boundary layer for vertical separations are shown in Fig. 106 to 109. Similar comments are applicable to these data as were made previously concerning the measurements in the Rural simulated boundary layer. Clearly they follow the same pattern as similar correlation measurements follow in a natural flat-plate boundary layer.

Some of the above data have been compared with the Rural simulated flow data; the comparison is shown in Fig. 110. Generally, at heights comparable to the roughness height, and at

lower heights, the Urban length scales of turbulence in the vertical direction are not significantly different from those measured in the Rural terrain. However at heights greater than the roughness height the vertical scales of turbulence are larger. This is attributed to the greater vertical transfer of energy associated with the large roughness elements which represent the Urban buildings, as suggested in Sect. 7.5.

The variations of the correlation coefficients in the simulated boundary layer for lateral separations are shown in Fig. 111 to 113. The symmetry of the flow for positive or negative correlations is shown in Fig. 111. The remaining data follow similar trends to those previously established in the case of the Rural simulated flow. The only exception occurs in the case of the measurements made at heights of $y/H < 0.06$, that is for heights of the same order, or less than, the roughness element height (Fig. 112). The secondary peaks on the relevant curves are associated with the local turbulence structure of the roughness element wakes.

Some of the above data have been compared with the Rural simulated flow data; this comparison is shown in Fig. 114. Again, at heights comparable to the roughness height, and at lower heights, the Urban and Rural length scales of turbulence are similar. This also applies at heights greater than the roughness element height.

It was assumed in Sect. 7.5 that the length scales of turbulence in the streamwise direction would be reduced in the case of the Urban simulated flow, in the height range influenced by the building wakes. This is shown to be the case in Fig. 115, which shows the variation of the along wind length scales with height for

both the Rural and Urban simulated boundary layers. It can be seen that generally, the length scales of turbulence increase with increase of height up to about $y/H (= y/\delta)$ of about 0.40. Above this height it is assumed that the intermittency in the flow contributes to the reduction in size of turbulence length scales.

As can be seen, very good agreement was obtained between the simulated boundary layer results and the measurements of Antonio and Luxton (1971) in rough and smooth boundary layer flow. Their ratio of roughness height to boundary layer height was similar to that of the Urban simulation and the smooth surface was smoother than the Rural simulation surface which consisted of 'Lego' baseboards. Therefore, the Rural simulation length scales should be, and do so, between the rough and smooth results of Antonio and Luxton. From the above results the length scales of turbulence were considered to be adequately simulated in the Urban boundary layer.

7.6.4 The Power Spectral Densities.

The measurements of the longitudinal velocity power spectra are shown in Fig. 116 to 118. A secondary peak is evident on the measurements made at heights comparable to the roughness height. This can be attributed to vortex shedding from the roughness elements and, as shown in Fig. 118, this can be regarded as a local effect. With the above exception, these spectra can be considered to be comparable to the Rural terrain spectra. The above spectra, measured over a height range of $0.06 \leq y/H \leq 0.50$, have been normalised by the mean squares of the respective fluctuating velocities and have collapsed generally to a single curve, as shown

in Fig. 119, at the high frequency end of the spectrum. At the low frequency end, the collapse is not as good due to the variation of the length scales with height as shown in Sect. 7.6.3.

Typical measurements of the spectra of the lateral and vertical fluctuating velocities are shown in Fig. 120 and 121. For purposes of comparison, a detailed set of vertical velocity spectra from the Rural simulated flow is shown in Fig. 122. At heights of the same order as the roughness element heights, the lateral spectra do not show a peak at any predominent frequency. This is taken to imply that there is a more even distribution of energy through a wider frequency range; this may be associated with the more vigorous mixing produced by the large roughness elements. In addition, it could explain why the data of Fig.101 show very little local scatter due to the presence of the large roughness elements. This effect however is not apparent in the vertical velocity spectra.

Following the analysis of Panofsky (1969), a further check on the similarity of the Urban and Rural spectra with full-scale measurements of this spectrum can be carried out. From the spectra measurements shown in Fig. 121 it can be seen that the peak $nS_v(n)$ value occurs at progressively lower frequencies with increase of height in the boundary layer. In order to determine whether this behaviour is consistent with observations from full-scale data the following table has been derived from Fig. 121:-

y/H :	0.060	0.083	0.167	0.300	0.500
$(y/H).n_p$:	9.00	11.6	18.4	21	27

where n_p is the frequency at which the peak $nS_v(n)$ value occurs.

It can be seen that $(y/H).n_p$ increases with increase of height

in the boundary layer, the rate of increase being greater at heights below about y/δ =0.15. Panofsky's (1969) analysis of many full-scale measurements made over mainly rural terrain, suggests that below y/H of about 0.10 the above product is essentially constant; this implies that the scale of turbulence increases linearly with increase of height. Above this height he found the product $(y/H).n_p$ to increase, which implies that the turbulence scale increases less rapidly with height. Above y/H of 0.15 the simulated flow measurements are consistent with these full-scale observations. Near ground level the vertical scales of turbulence in the Urban simulation increase less rapidly with increase of distance from the ground due to the greater ground roughness, consequently a constant $(y/H).n_p$ is not observed. In the case of the Rural terrain vertical velocity spectra (Fig. 122) measurements at y/H = 0.06 were not made. However it is reasonable to assume that at this height $(y/H)n_p$ will have a value that is not greatly different from 9.00. The corresponding values at y/H of 0.083 and 0.167 are approximately 9.2 and 1.4. Therefore, it is considered that Panofsky's analysis for Rural terrain applies reasonably well in the case of the simulated Rural boundary layer.

Finally, typical spectra of the longitudinal, lateral and vertical fluctuating velocities from the Urban and Rural boundary layer flows are compared in Fig. 123. The longitudinal spectra are seen to be similar in form and have been normalised with respect to the rural terrain longitudinal spectrum to illustrate this. Generally it can be seen that the spectra from both types of flow are similar.

The measurements of the longitudinal scale of turbulence in the streamwise direction have been derived from auto-correlation data and have been shown in Fig. 115. It was shown in Part 1 of this thesis that this length scale can also be derived from power spectral density measurements from,

$$L_{ux} = \frac{1}{2\pi} \times \text{Peak Wavelength}$$

The accuracy of estimating the length scale by this method can now be assessed here by comparing the two sets of data as follows:-

y/H	L_{ux} (m) - Autocorrelations	L_{ux} (m) - Spectra
0.060	110	130
0.083	145	137
0.167	192	180
0.300	220	213

Clearly the two sets of data agree very well. However, estimates from power spectra rely to a major extent on having sufficient measurements available to define a definite peak wavelength. If a peak is defined then the above expression can be confidently used.

7.6.5 The Co-spectra of the Reynolds Stresses.

The measured co-spectra of the Reynolds stresses are shown in Fig. 124 and are compared with the rural terrain co-spectra and the semi-empirical form suggested by Panofsky and Mares (1968). As can be seen, the major part of the energy contribution lies between $0.01 \leq f \leq 1.0$ as previously suggested.

The forms of the semi-empirical curve and the Rural terrain measurements at $y/H = 0.083$ are very similar. This is to be

expected since the curve of Panofsky and Mares was derived from data mainly obtained near ground level.

The co-spectral measurements in the Urban terrain at various heights generally agree with those made in the simulated Rural terrain, apart from one inconsistency, which can only be attributed to some local effect associated with the large roughness elements. However, since the forms of the longitudinal and vertical spectra and their variations with height, in the height range considered, were considered acceptable, it follows that this variation of the co-spectra with height is also acceptable.

7.6.6. The Probability Density Distributions.

Typical measurements of the probability density distributions of the longitudinal fluctuating velocity in the simulated Urban and Rural boundary layers are shown in Fig. 125. Both sets of measurements cover a range of ± 3 standard deviations and are compared with a Gaussian distribution over the same range. Within the limits of accuracy to which full-scale measurements are termed Gaussian, these distributions can also be considered as Gaussian. However, they do show variations from the theoretical distribution at high values of the standard deviation which can be significant in relation to wind loading problems. More full-scale data over a wider standard deviation range are needed to check this point. Similar distributions were obtained in the case of both the lateral and vertical fluctuating velocities.

7.6.7 Variation of the power-index with the Roughness Length.

It can now be assumed that a satisfactory simulation has been

obtained of boundary layer flow over both Rural and Urban terrain types. However, it is also probable that the flow over suburban terrain will need to be simulated, hence its typical characteristics need to be defined. These conditions can be interpolated from the available meteorological data (see Part 1 of thesis) and from the boundary layer simulation work. Hence the three main types of terrain can be defined generally as follows:-

Terrain		Rural	Suburban	Urban
$1/\alpha$	:	0.143	0.21-0.22	0.28
y_o(m)	:	0.10	1.00	2 - 3
h_1/H	:	0.146	0.175	0.208

(h_1 = barrier height to base of castellations)

For the above simulations, the full-scale mean boundary layer depth has been assumed in all cases to be of the order of 600 m. (2000 ft.). Hence if the roughness length of a particular site can be defined, then the boundary layer structure can be derived from Part 1 of this thesis and the relevant adiabatic atmospheric boundary layer flow can be modelled in a wind tunnel, within the range of terrain types considered.

7.6.8 Wind Tunnel Axial Static Pressure Gradient.

In order to determine whether any adverse pressure gradients were introduced into the wind tunnel flow by the boundary layer simulation equipment, the static pressure gradient was measured along the tunnel axis. This was measured in the presence of both the Rural and Urban boundary layer flows and the results are presented in Fig. 126. Downstream of a position which corresponds

to about 3 to $3\frac{1}{2}$ boundary layer heights from the generator trailing edges there are no unacceptable pressure gradients.

8. GENERAL COMPARISON OF THE SIMULATED AND FULL-SCALE ADIABATIC BOUNDARY LAYERS.

Generally, the comparisons between the simulated and full-scale flows have to date been based on the comparison of just specific data related to either Rural or Urban boundary layer flows. However, it is also considered essential, as a final check on the overall accuracy, to see how measurements made in these simulated flows fit in with the final analysis of the data of Part 1 of this thesis. These comparisons are shown in the final figures of this part of the thesis, that is in Fig. 127 to 130.

The variation of the power index with roughness length for the various terrain types is shown in Fig. 127. Clearly the values of these quantities represented in the simulated flows for typical Rural and Urban conditions fall well within the acceptable limits of scatter of the data. The variations of the turbulence intensity, based on local velocity and at the reference height of 30 m, with the roughness length is shown in Fig. 128. The points plotted from the simulated flows again fall within acceptable limits on the proposed curve. Similar comments apply to the data of Fig. 129 which shows the simulated flow results plotted on the proposed variation of the ground level Reynolds stresses with roughness length. In this case however, there is obviously a need for more full-scale measurements of this quantity. Finally, the variation of the length scale of turbulence in the longitudinal direction with both height in the boundary layer and roughness length is shown in Fig. 130. Again the agreement is very good between the simulated and atmospheric boundary layers. Therefore it is considered that

the simulated Rural and Urban boundary layer structures agree very well with the overall structure proposed for atmospheric adiabatic boundary layers.

9. APPLICATION OF THESE SIMULATED BOUNDARY LAYERS IN INDUSTRIAL AERODYNAMICS.

Using this boundary layer simulation technique the following range of problems in industrial aerodynamics have been studied or are currently being studied:-

(a) Static and dynamic wind loads on cooling towers.

(b) Static and dynamic wind loads on buildings.

(c) Wind loads on and vibration of chimneys.

(d) Investigation of wake flows of two and three dimensional buildings.

(e) Wind loads on overhead lines in relation to the local gust structure.

(f) Flow over sinusoidal hills and ramps.

(g) Plume dispersion studies.

A reliable study of the above topics is mainly dependent on correct modelling of the atmospheric boundary layer. In the case of (a), (d) and (f) of the above subjects some full-scale data have also been available for comparison with the model measurements made in the simulated boundary layers. The degree of agreement between model and full-scale data have generally shown the validity of the flow modelling technique. In relation to the terrain model being investigated, it has been shown that some tests need more detailed local topographical modelling than others.

The above problems have been studied in the Central Electricity Generating Board industrial aerodynamics wind tunnels at Leatherhead and Marshwood Research Laboratories using this simulation technique. In addition, interest in this work has been shown to be widespread, based on the number of requests received for details of the system

used to generate the simulated boundary layer flows. The number of requests received is about eighty from seventeen different countries. Hence the development of this technique can be considered to have made some advance in the field of Technology.

10. CONCLUSIONS.

The following conclusions can be made

(a) The system developed produces an adequate simulation of boundary layer flows in the required distance.

(b) The simulated Rural and Urban boundary layers have been shown to be representative of such full-scale flows.

(c) Model tests carried out in the simulated boundary layers have been shown to produce realistic results.

11. ACKNOWLEDGEMENTS.

The experimental work was carried out at the Central Electricity Research Laboratories, Leatherhead, and the experimental data are presented in this thesis by permission of the Central Electricity Generating Board. Acknowledgements are due to supervisors Prof. R. N. Cox and Mr. D. J. W. Richards for their continued interest and discussions on various aspects of the project; also to many colleagues at C.E.R.L. (Leatherhead) for discussions on various aspects of boundary layer flows.

12. REFERENCES.

1. Antonia, R.A. and Luxton, R.E. 1971 "The response of a turbulent boundary layer to an upstanding step change in surface roughness." Trans. A.S.M.E. - March

2. Arie, M and Rouse, H. 1956 "Experiments on two-dimensional flow over a normal wall". J.F.M. 1, P.129.

3. Armitt, J. 1966 "The simulation of the atmospheric boundary layer in a wind tunnel". C.E.R.L. Note RD/L/N 83/66.

4. Armitt, J and Counihan, J. 1968 "The simulation of the atmospheric boundary layer in a wind tunnel." Atmos. Environ. Vol. 2.

5. Baines, W.D. 1963 "Effect of velocity distribution on wind loads and flow patterns on Buildings". Symp. on Wind Effects on Buildings and Strucs. N.P.L.

6. Baines, W.D. and Peterson, E.G. 1951 "An investigation of flow through screens". Trans. A.S.M.E. Vol. 73, P. 467.

7. Busch, N.E. and Panofsky, H.A. 1968 "Recent spectra of atmospheric turbulence". Q.J.R.M.S. 94, P. 132 - 148.

8. Campbell, G.S. and Standen, N.M. 1969 "Progress report 2 on simulation of the Earths surface winds by artificially thickened wind tunnel boundary layers". N.R.C. Canada, LTR - LA - 37.

12. REFERENCES. (cont.)

9. Cermak, J.E. 1966 "Laboratory simulation of atmospheric motions in the lowest 100 m". Meeting on Ground Wind Load Problems in relation to Launch Vehicles, Langley Res. Centre, Hampton, Virginia.

10. Cermak, J.E. 1966 "Wind tunnel simulation of atmospheric phenomena". Symp. on Atmos. Simulation - Ed. G.M. Hidy, N.C.A.R. Tech. Note TN.22

11. Cermak, J.E. 1971 "Laboratory simulation of the Earths Boundary Layer". A.I.A.A. Paper No. 70 - 751.

12. Cermak, J.E. et al. 1965 "Simulation of atmospheric motions by wind tunnel flows". Tech. Rep. CER66J.E.C. - V.A.S.- E.J.P. - G.J.B. - H.C. - R.M.M. - S117.

13. Chandler, A.G. 1968 World Met. Organisation. Symp. on Urban Climates, Brussels.

14. Collar, A.R. 1939 "The effect of a gauze on the velocity distribution in a uniform duct". R. and M. 1867.

15. Cook, N.J. 1972 "Wind tunnel simulation of the atmospheric boundary layer - methods in current use at Bristol Univ.". Symp. on External Flows - Bristol Univ.

16. Cook, N.J. 1973 "On simulating the lower third of the urban adiabatic boundary layer in a wind tunnel". Atmos. Envir. Vol. 7., p. 691 - 705.

17. Corrsin, S. and Kistler A.L. 1954 N.A.C.A., T.N. 3133.

12. REFERENCES (cont.)

18. Counihan, J. 1967 "Simulation of the atmospheric boundary layer in a low-speed wind tunnel". C.E.R.L. RD/L/N 76/67.

19. Cowdrey, C.F. 1967 "A simple method for the design of wind tunnel velocity profile grids". N.P.L. Aero. Note 1055.

20. Cramer, H.E. 1952 "Preliminary results of a program for measuring the structure of turbulent flow near the ground". Geophys. Res. Paper, (19) A.F.C.R.L.

21. Davis M.L. 1970 "Modelling Urban Atmospheric Temperature Profiles". Atmos. Envir. Vol. 4.

22. Davenport, A.G. 1960a "Application of statistical concepts to the wind loading of structures". Proc. Inst. Civ. Engrs. - August.

23. Davenport A.G. 1960b "A rationale for the determination of design wind velocities". Proc. A.S.C.E., Jour. Struc. Div. 86, 39.

24. Davenport, A.G. 1961 "The spectrum of horizontal gustiness near the ground in high winds". Q.J.R.M.S. 87 p. 194 - 211

25. Davenport, A.G. 1963a "The relationship of wind structure to wind loading". Symp. - Wind Effects on Buildings and Structures - N.P.L.

26. Davenport, A.G. 1963b "The buffeting of structures by gusts". Symp. - Wind Effects on Buildings and Structures - N.P.L.

12. REFERENCES (cont.)

27. Davenport, A.G. 1966 "An approach to the wind tunnel modelling of the response of structures to the natural wind". Proc. - Ground Wind Load Problems in relation to Launch Vehicles, N.A.S.A. Res. Centre, Hampton, Virginia.

28. Davenport, A.G. 1967 "The dependence of wind loads on meteorological parameters". Wind Effects on Buildings and Structures. N.R.C. Canada.

29. Davenport, A.G. and Isyumov. 1967 "The application of the boundary layer wind tunnel to the prediction of wind loading". Wind Effects on Buildings and Structures, N.R.C. Canada.

30. Deland, R. and Panofsky, H.A. 1957 "Structure of turbulence at O'Neill, Nebraska, and its relation to the structure at "Brookhaven". Sci. Rep. 2, Contract No. AF.19 (604) - 1027 Penn. State Univ.

31. Elder, J.W. 1959 "Steady flow through non-uniform gauzes of arbitrary shape". J.F.M. 5, p. 355 - 368.

32. Fekete, G.I. 1967 Symp. - Wind Effects on Buildings and Structures - N.R.C. Canada: Discussion of Paper 19.

33. Gandemer, J. 1973 "La soufflerie a couche limite Du C.S.T.B. : etude preliminaire". C.S.T.B. Nantes - ADYM1 - 73.

12. REFERENCES. (cont.)

34. Giblett, F. 1932 "Structure of wind over level country". Geophys. Mem. No. 54.

35. Grant, H.L. 1958 "The large eddies of turbulent motion". J.F.M. 4, 2 p149.

36. Harris, R.I. 1963 E.R.A. Report SP1/T14.

37. Harris, R.I. 1968 "Measurements of wind structure at heights up to 598 ft. above ground level". Wind Effects on Buildings and Structures - Loughborough Univ.

38. Harris, R.I. 1970 "The nature of the wind". Mod. Design of wind sensitive structures - C.I.R.I.A. Symp.

39. Helliwell, N.C. 1971 "Wind over London". Unpublished note - Met. Office.

40. Hinze, 1959 "Turbulence - an introduction to its mechanism and theory". Mc Graw-Hill, New York.

41. Holmes, J.D. 1970 "Full and model scale cross-spectral density measurements of fluctuating wind pressures on the face of a large building". C.A.A.R.C. Symp. on Sep. Wakes, Melbourne Univ.

42. Holmes, J.D. 1971 "Turbulent pressure fluctuations on the fact of a low aspect ratio, rectangular prismatic building". IV Australasian Conf. on Hydr. and Fluid Mech., Monash Univ.

43. Jensen, M. 1958 "The model-law for phenomena in natural wind". Ingenioren, Int. Edition. Vol. 2. No. 4.

12 REFERENCES (cont.)

44. Jensen, M. and Franck, N. 1963 "Model scale tests in turbulent wind". Part 1. Danish Tech. Press, Copenhagen.

45. Jones, P.M. et al. 1971 "The urban wind velocity profile". Atmos. Envir. Vol. 5, p. 89-102.

46. Kamei, I. 1955 "Studies on natural wind pressure on buildings and other structures". Report No. 16, Buildings Res. Inst., Ministry of Construction, Japan.

47. Klebanoff, P.S. and Diehl, Z.W. 1952 "Some features of artificially thickened fully developed turbulent boundary layers with zero pressure gradient". N.A.C.A. Rep. 1110.

48. Kline, S.J. et al. 1967 "The structure of turbulent boundary layers". J.F.M. 30, 4, p.741-773.

49. Kolmogoroff, A.N 1941 "The local structure of turbulence in incompressible viscous fluid for very large Reynolds numbers". Trans. Friedlander and Topper, 1961.

50. Lawson, T.V. 1968 "Methods of producing velocity profiles in wind tunnels". Atmos. Envir. 2, 1.

51. Livesey, J.L. and Turner J.T. 1964 "The generation of symmetrical duct velocity profiles of high uniform shear". J.F.M. 20, p.201-208.

52. Lloyd, A. 1967 "The generation of shear flow in a wind tunnel". Q.J.R.M.S. 93, p. 79-96.

53. Ludwig, C.R. and Sundaram, T.R. 1969 "On the laboratory simulation of small-scale atmospheric turbulence". C.A.L. Rep. No. VC - 2740 - S - 1.

12 REFERENCES (cont.)

54. Ludwig, G.R. et al. 1971 "Laboratory modelling of the atmospheric surface layer with emphasis on diffusion". C.A.L. Rep. No. VC - 2740 - S - 2.

55. McVehil, G.E. et al. 1967 "On the feasibility of modelling small scale atmospheric motions". C.A.L. Rep. No. ZB - 2328 - P - 1.

56. Melbourne, W.H. 1971 "Comparison of pressure measurements made on a large isolated building in full and model scale". Rep. Dept. of Mech. Eng., Monash Univ.

57. Miyake, M. et al. 1970 "Spectra and co-spectra of turbulence over water". Q.J.R.M.S. Vol. 96. No. 407.

58. Morkovin, M.V. 1972 "On modelling of atmospheric surface layers by the counter-jet technique - preliminary results". Illinois Inst. Tech., Themis Tech. Rep. R72 - 7.

59. Owen, P.R. and Zienkiewicz,H.K 1957 "The production of uniform shear flow in a wind tunnel". J.F.M. 2 p. 521-531.

60. Paeschke, W. 1937 Beitr Phys. fr. Atmos. 24, P. 163-189.

61. Panofsky, H.A. 1969 "The structure of atmospheric shear flows". Aero. of Atmos. Shear Flows - A.G.A.R.D. C.P.48.

62. Panofsky, H.A. and Mares, E. 1968 "Recent measurements of co-spectra for heat flux and stress". Q.J.R.M.S. Vol. 94. p.581 - 585.

63. Panofsky H.A. and McCormick, R.A. 1954 "Properties of the spectra of atmospheric turbulence at 100 m." Q.J.R.H.S. 80, p.557-558.

12 REFERENCES (cont.)

64. Pasquill, F. 1950 "The aerodynamic drag of grassland". Proc. Roy. Soc. A, 202, p. 143-153

65. Pasquill, F. 1970 "Wind structure in the atmospheric boundary layer". Phil. Trans. Roy. Soc. A 269, p. 321-554.

66. Perry, A.E. and Joubert, P.N. 1963 "Rough wall boundary layers in adverse pressure gradients". J.F.M. 17, p. 193-211.

67. Perry, A.E. et al. 1969 "Rough wall turbulent boundary layer". J.F.M., 37, p. 383-413.

68. Plate, E.J. and Cermak, J.E. 1963 "Micrometeorological wind tunnel facility - description and characteristics". C.S.U. Fluid Dyn. and Diff. Lab. T.R. C.E.R.63. E.J.P. - J.E.C.9.

69. Roberson, J.A. and Chen, C.K. 1970 "Flow in conduits with low roughness concentration." A.S.C.E. Jour. Hyd. Div. HY4, 96, April

70. Rose, W.G. 1966 "Results of an attempt to generate a homogeneous turbulent shear flow". J.F.M. 25 p. 97-120.

71. Sandborn, V.A. and Marshall, R.D. 1965 "Local isotropy in wind tunnel turbulence". Fluid Dyn. and Diff. Lab., C.S.U.

72. Schlichting, H. 1960 "Boundary layer theory". McGraw-Hill, New York.

73. Scriven, R.A. 1969 "Assessment of E.R.A. Gust Analysis". C.E.R.L. Note (Unpublished).

12 REFERENCES (cont.)

74. Schon, J.P. and Mery, P. 1971 "A preliminary study of the simulation of a neutral atmospheric boundary layer using air injection in a wind tunnel". Atmos. Envir. Vol. 5 p. 299-311.

75. Shellard, H.C. 1963 "The estimation of design wind speeds". Wind Effects and Buildings and Structures. N.P.L.

76. Shiotani, M. 1950 "Turbulence in the lowest layers of the atmosphere". Sci. Pap. Tohuku Univ. 5th series, Vol. 2, No. 3.

77. Shiotani, M. 1962 "The relation between wind profiles and stability of the air layer in the outskirts of the City". J. Met. Soc. Japan. Sec. II, 40, (6) p.315.

78. Shiotani, M. and Yamamoto, G. 1948 "Atmospheric turbulence over a large city, turbulence in the free atmosphere". Geophys. Mag. 21, 2.

79. Singer, I. 1960 "A study of the wind profile in the lowest 400 ft. of the atmosphere". Prog. Rep. 5 - Brookhaven.

80. Sitaraman, V. 1970 "Spectra and co-spectra of turbulence in the atmospheric surface layer". Q.J.R.M.S. 96, No. 410.

81. Slade, D.H. 1969 "Wind measurements on a tall tower in rough and inhomogeneous terrain". J. Appl. Met. 8, No. 2.

12. REFERENCES (cont.)

82. Smith, F.B. 1971 "The profile of shearing stress in the boundary layer of the atmosphere". (unpublished note - Met. Office)

83. Standen, N.M. 1972 "A spire array for generating thick turbulent shear layers for natural wind simulation in wind tunnels". N.R.C. Canada, LTR - LA - 94.

84. Standen, N.M. et al. 1971 "A wind tunnel and full-scale study of turbulent wind pressures on a tall building". Wind effects on buildings and structures. Tokio.

85. Strom, G.H. and Kaplin, E.J. 1960 "Convective turbulence wind tunnel project". Arg. Nat. Lab., A.N.L. 6199.

86. Sundaram, T.R. et al. 1971 "Modelling of the turbulent structure of the atmospheric surface layer". A.I.A.A. Paper No. 71-136.

87. Sutton, O.G. 1953 "Micrometeorology". 1st. ed. McGraw-Hill, Book Co., N.Y.

88. Taylor, G.I. 1935 "Statistical theory of turbulence". Proc. Roy. Soc. A., 151 p. 430-454.

89. Taylor, H.D. 1950 "U.A.C. Research Dept. - Summary Report on vortex generators". U.A.C. Res. Dept., East Hartford, Conn., Rep. R - 05280-9.

90. Templin, R.J. 1969 "Interim progress note on simulation of Earth's surface winds by artificially thickened wind tunnel boundary layers". N.R.C. Canada, LTR - LA - 22.

12 REFERENCES (cont.)

91. Teunisson, H.W. 1970 "Characteristics of the mean wind and turbulence in the planetary boundary layer". U.T.I.A.S. Rev. No. 32.

92. Teunisson, H.W. 1972 "Simulation of the planetary boundary layer in a multiple jet wind tunnel". U.T.I.A.S. Rep. No. 182.

93. Townsend, A.A. 1958 "The turbulent boundary layer". Proc. I.U.T.A.M. Symp. on Boundary Layer Res., Springer, Berlin.

94. Tritton, D.J. 1967 "Some new correlation measurements in a turbulent boundary layer". J.F.M., 28, Part 3, p. 439-462.

95. Vickery, B.J. 1965 "On the flow behind a coarse grid and its use as a model of atmospheric turbulence in studies related to wind loads on buildings". N.P.L. Aero. Rep. 1143.

96. Wardlaw, R.L. 1970 "A standard tall building model for the comparison of simulated natural winds in wind tunnels". C.A.A.R.C., C.C.666 Tech. 25.

97. Whitbread, R.E. 1968 "On the introduction of turbulence into wind tunnel investigations for the determination of wind-induced amplitudes of oscillation". Wind effects on buildings and structures, Loughborough Univ.

12 REFERENCES (cont.)

98. Weighardt, K.E.G. "On the resistance of screens".
1953 Aero. Quarterly, 4, p. 186-192.

99. Wills, J.A.B. "Simulation of the natural wind".
1972 (preliminary data - presented at N.P.L. Open Day)

100. Wilson, D.J. "Turbulent dispersion in atmospheric shear flow
1971 and its wind tunnel simulation".
V.K.I. Tech. Note 76.

101. Winternitz, "Effects of inlets on conical diffusers".
F.A.L. and 1957 Jour. Roy. Aero. Soc. 61, p. 116-124.
Ramsey, W.J.

102 Wooding, R.E. "Drag due to regular arrays of roughness
1969 elements of varying geometry".
C.S.I.R.O. Plant Industry Note.

APPENDIX I

The velocity defect law for a flat plate equilibrium boundary layer is as follows:

$$\frac{\bar{U}_{max} - \bar{u}}{U_*} = A + B \log_{10} (\delta/y)$$

where constants A and B are taken as 2.80 and 5.60 respectively.

When $\bar{u} = 0$, $y = y_o$

$$\therefore \quad \frac{\bar{U}_{max}}{U_*} = A + B \log_{10} (\delta/y_o) \qquad \ldots \ldots \quad (A1)$$

The theoretical wall shear stress of a natural rough-wall boundary layer 152.4 mm (6 in.) thick, knowing the properties of this boundary layer when it is 24.13 mm (0.95 in.) thick (Fig.27.), can be calculated using equation (A1).

Denoting the properties of the 152.4 mm (6 in.) boundary layer by suffix (1), and those of the 24.13 mm (0.95 in.) boundary layer by (2):

$$\frac{\bar{U}_{max}}{U_{*_1}} - \frac{\bar{U}_{max}}{U_{*_2}} = B(\log_{10}[\delta_1/y_{o_1}] - \log_{10}[\delta_2/y_{o_2}])$$

Since $y_{o_1} = y_{o_2}$ it follows that:

$$\frac{\bar{U}_{max}}{U_{*_1}} - \frac{\bar{U}_{max}}{U_{*_2}} = B \log (\delta_1/\delta_2)$$

Knowing that

$$\delta_1 = 152.4 \text{ mm (6 in.)}$$

and

$$\delta_2 = 23.13 \text{ mm (0.95 in.)}$$

gives

$$\frac{\bar{U}_{max}}{U_{*_1}} - \frac{\bar{U}_{max}}{U_{*_2}} = 4.490$$

Since

$$(U_{*_2}/\bar{U}_{max})^2 = (\overline{u'v'}/\bar{U}^2_{max})_2 = 0.004 \qquad \text{(Fig.27.)}$$

$$\therefore \quad (\bar{U}_{max}/U_{*_1}) = 4.49 + (1/\sqrt{0.004}) = 20.30$$

$$\therefore \quad (\overline{u'v'}/\bar{U}^2_{max})_1 = 0.0024 \text{ cf: } \underline{0.0024 \text{ Fig. 39 and}} \; \underline{\sim 0.0020 \text{ Fig. 44}}$$

for the simulated boundary layer.

ESTIMATION OF THE CORRESPONDING THEORETICAL VELOCITY RATIOS

From the above calculations,

$$(U_{*_2}/U_{*_1}) = 1.284$$

Denoting the 152.4 mm (6 in.) boundary layer by suffix (1) and the 24.13 mm (0.95 in.) thick boundary layer by suffix (2), the velocity defect law gives:

$$\frac{\bar{U}_{max}}{U_{*_1}}\left(1 - \frac{\bar{u}_1}{\bar{U}_{max}}\right) - \frac{\bar{U}_{max}}{U_{*_2}}\left(1 - \frac{\bar{u}_2}{\bar{U}_{max}}\right) = B\left(\log_{10}[\delta_1/y_1] - \log_{10}[\delta_2/y_2]\right)$$

Since the velocity ratios will be compared at conditions of

$$\frac{\delta_1}{y_1} = \frac{\delta_2}{y_2} \quad ,$$

it follows that

$$\frac{1 - \dfrac{\bar{u}_1}{\bar{U}_{max}}}{1 - \dfrac{\bar{u}_2}{\bar{U}_{max}}} = \frac{U_{*_1}}{U_{*_2}} \quad \text{at any } \left(\frac{y}{\delta}\right) \quad .$$

The theoretical velocity ratios can be evaluated for the 152.4 mm (6 in.) thick boundary layer using the data from the 24.13 mm (0.95 in.) thick natural rough-wall boundary layer:

y/δ	Natural 24.13 mm thick boundary layer	Theoretical 152.4 mm thick boundary layer	Simulated 152.4 mm thick boundary layer
0.40	0.815	0.860	0.875
0.30	0.740	0.800	0.840
0.20	0.650	0.730	0.805
0.10	0.515	0.620	0.730

Atmospheric Boundary Layer Simulation.

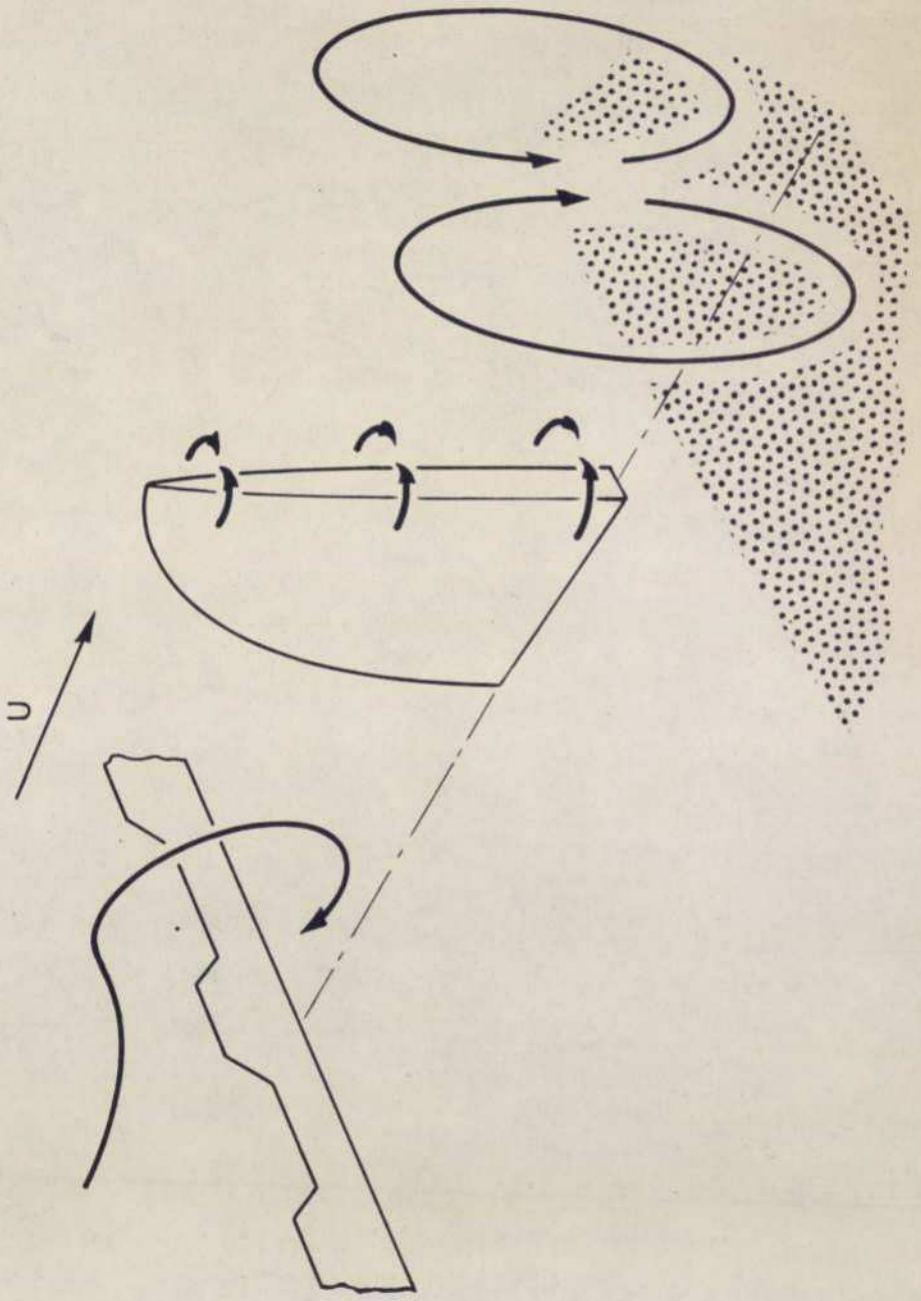
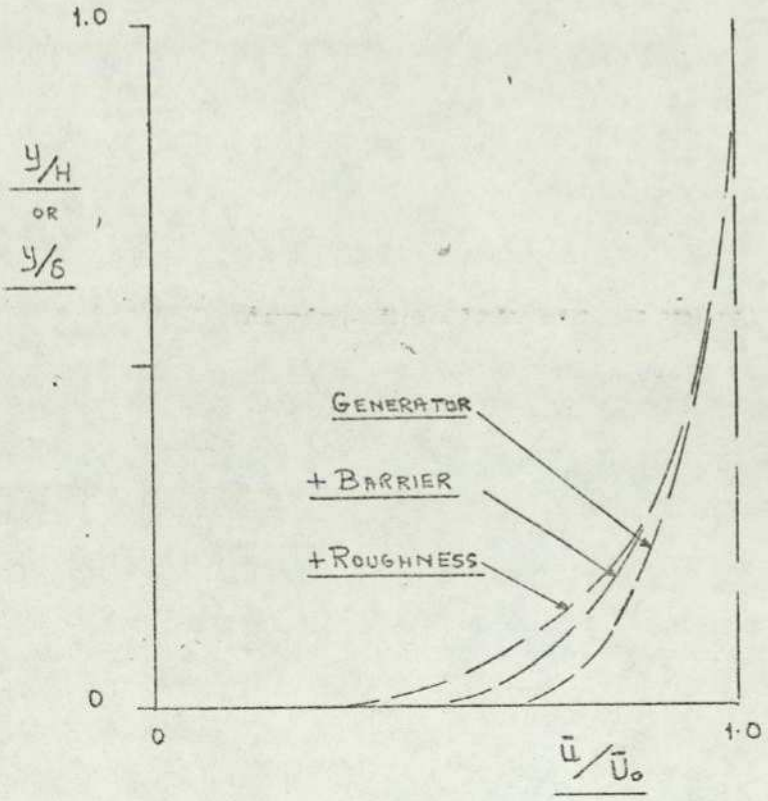


Fig. 1. Anticipated Vortex Production in Boundary Layer Simulation



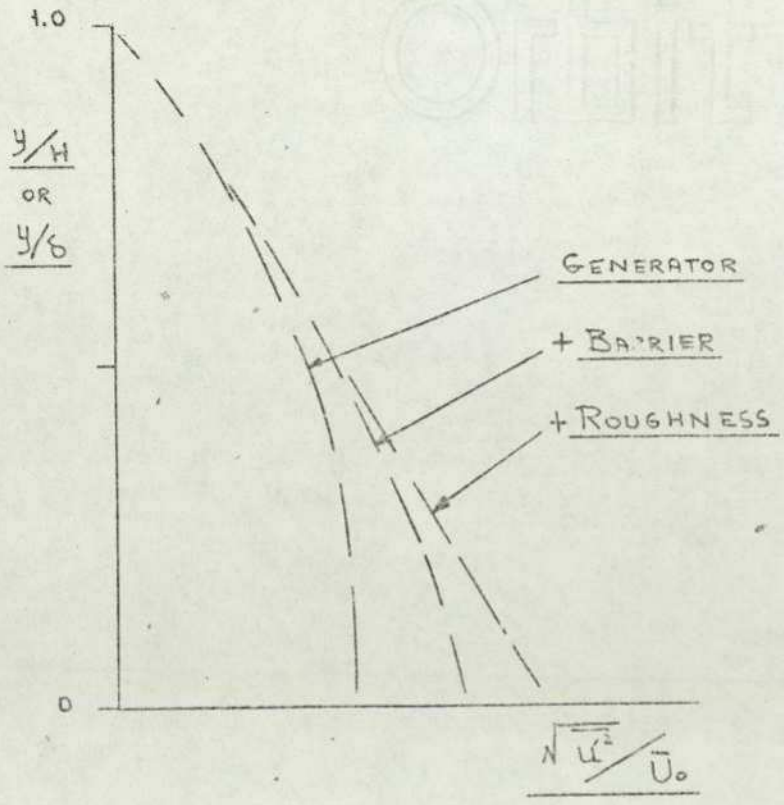


FIG. 2 ANTICIPATED MOMENTUM LOSS AND TURBULENCE PRODUCTION BY THE BOUNDARY LAYER SIMULATION COMPONENTS

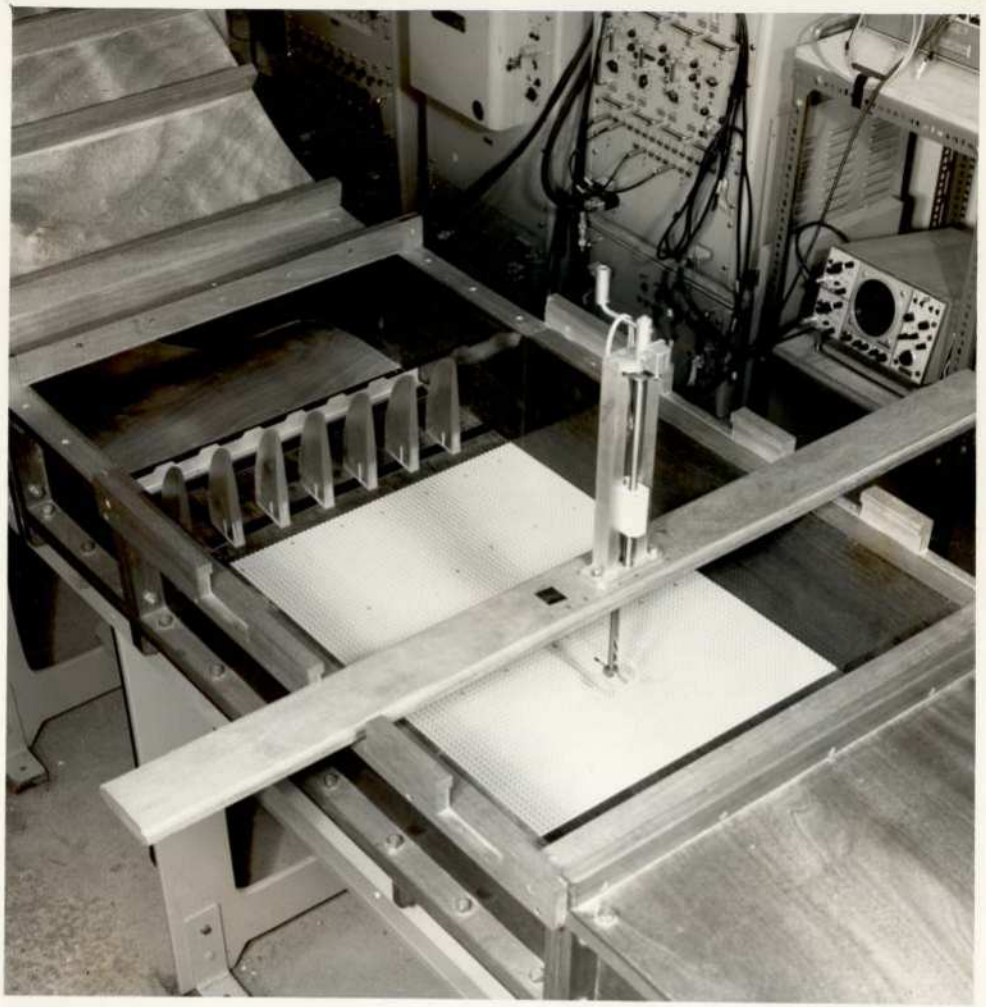


FIG. 3. ATMOSPHERIC BOUNDARY LAYER SIMULATION TESTS

FINAL ARRANGEMENT OF ELLIPTIC WEDGE GENERATORS, MODIFIED BARRIER WALL AND THE SURFACE ROUGHNESS IN THE LOW SPEED WORKING SECTION OF THE BOUNDARY LAYER WIND TUNNEL

THE SLIDING ROOF SECTION WHICH IS USED FOR LATERAL TRAVERSING, AND WHICH CARRIES THE VERTICAL TRAVERSING GEAR, IS SHOWN POSITIONED SUCH THAT THE TIP OF THE HOT WIRE PROBE IS 457.2 mm (18in) FROM THE GENERATOR TRAILING EDGE

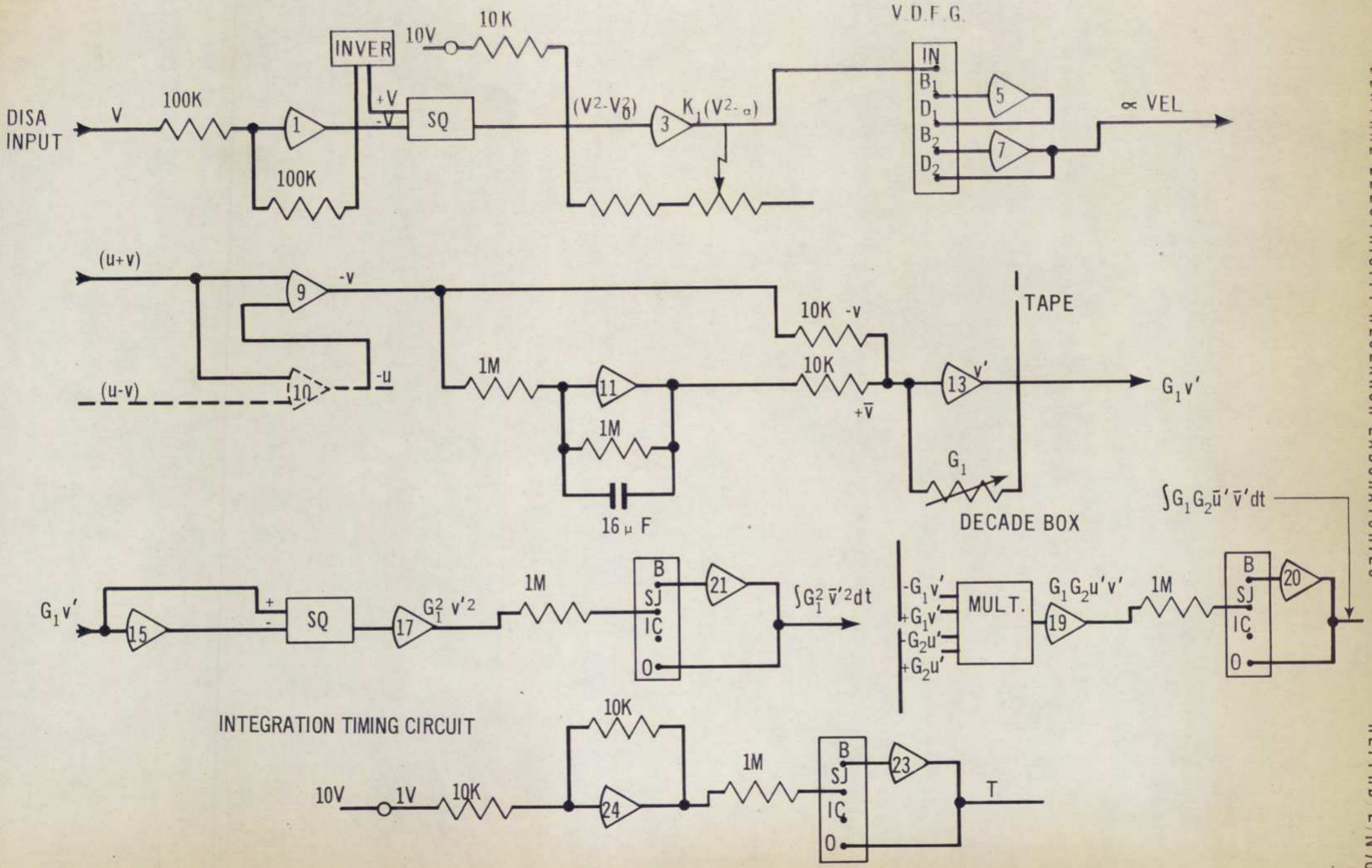


FIG. 4 ATMOSPHERIC BOUNDARY LAYER SIMULATION TESTS

ATMOSPHERIC BOUNDARY LAYER SIMULATION

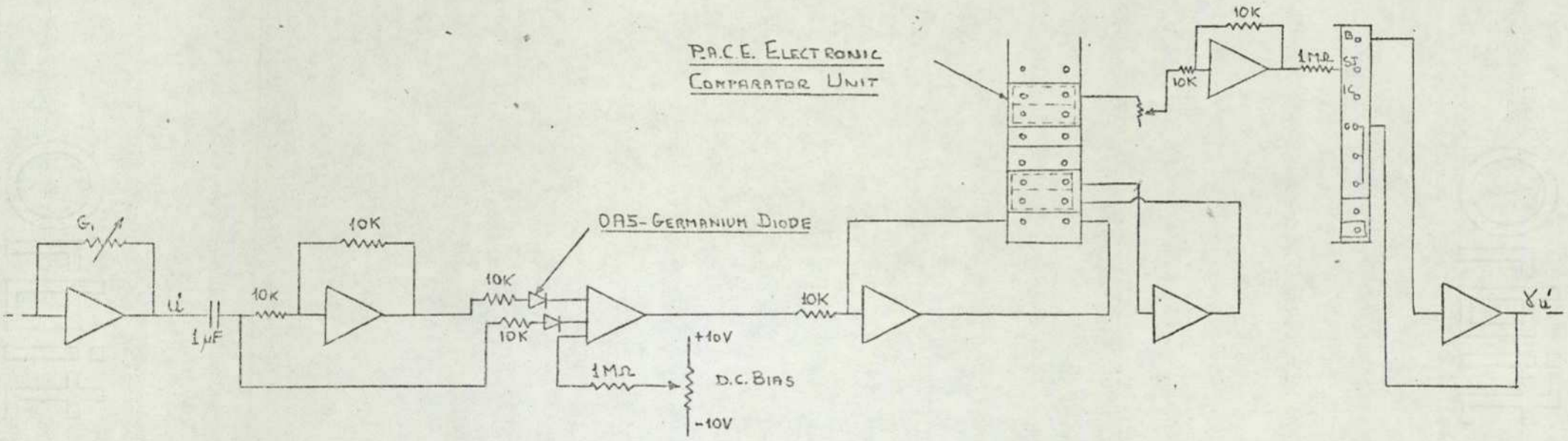
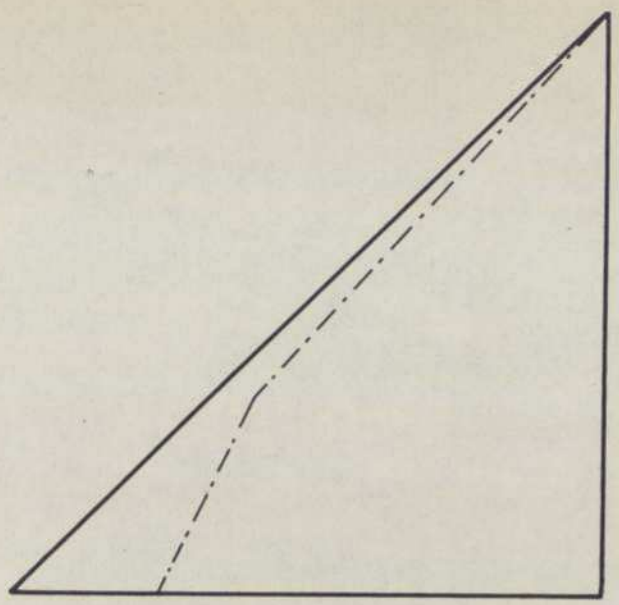
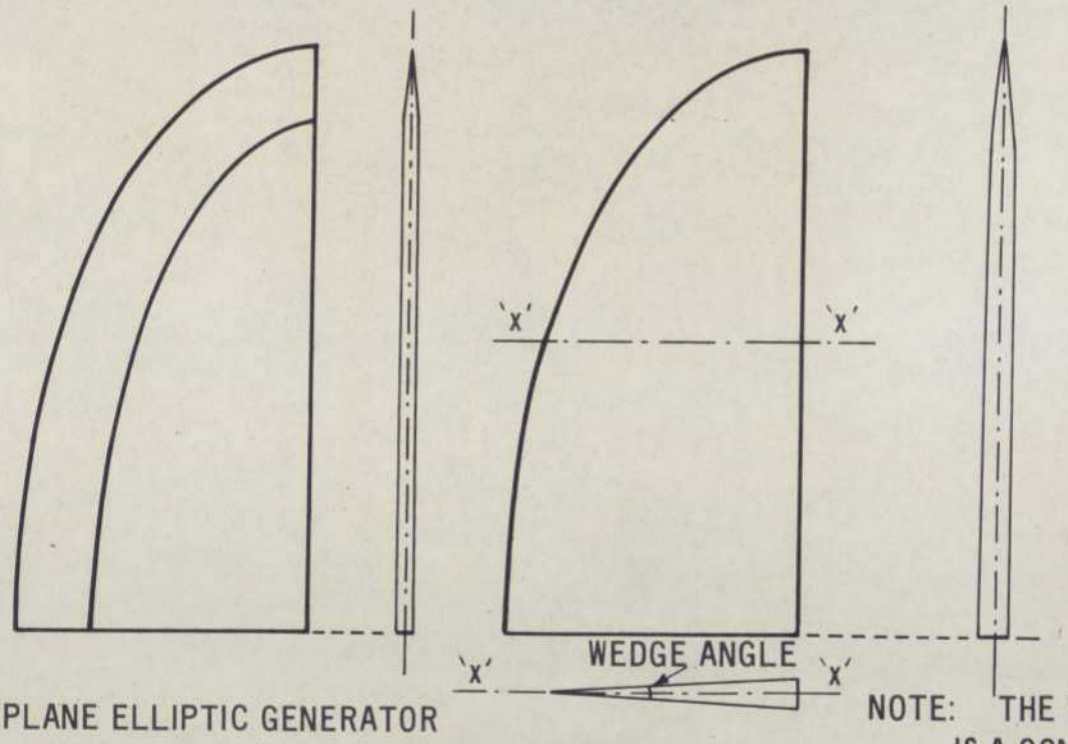


FIG. 5 MEASUREMENT OF INTERMITTENCY FACTORS

TYPES OF GENERATORS WHOSE WAKE CHARACTERISTICS WERE INVESTIGATED



SIDE VIEW OF TRIANGULAR AND CRANKED GENERATORS



PLANE ELLIPTIC GENERATOR

ELLIPTIC WEDGE GENERATOR

NOTE: THE WEDGE ANGLE IS A CONSTANT AT ANY HORIZONTAL SECTION 'x-x'

SCALE: ½

FIG. 6 ATMOSPHERIC BOUNDARY LAYER SIMULATION TESTS

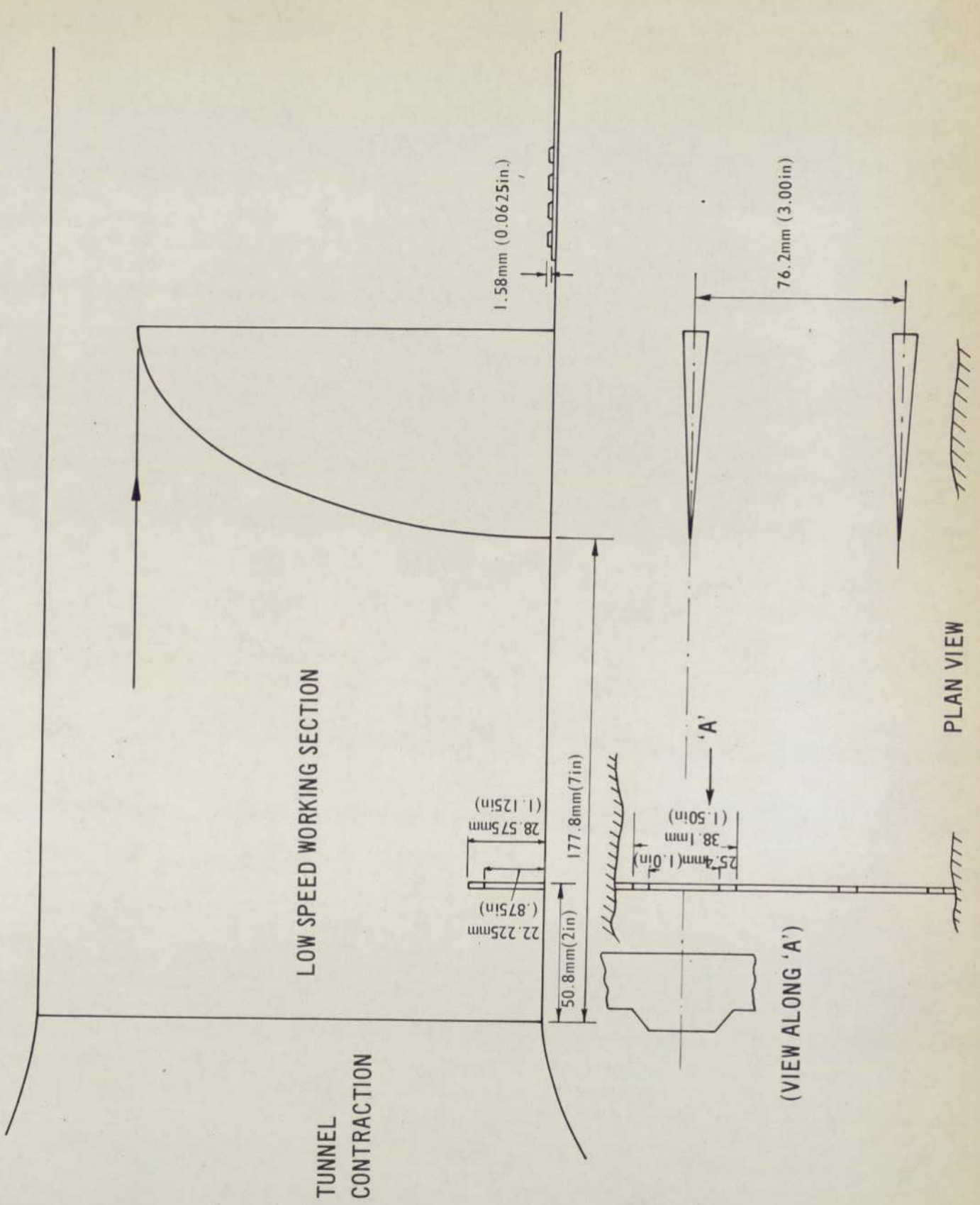
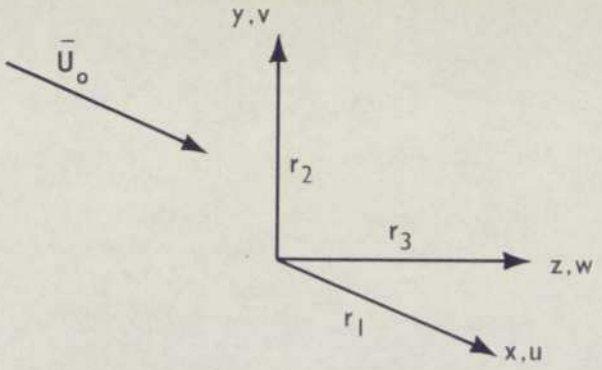


FIG. 7. FINAL LAYOUT OF SIMULATION SYSTEM

JC/GH(CON.)(14.8.68.)RL.3.3.1526



Ruu (0, r, 0) MEASUREMENTS

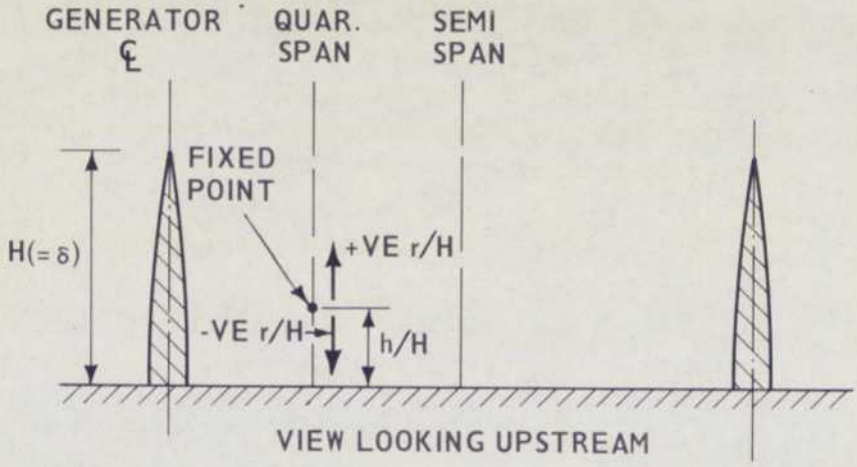


ILLUSTRATION OF A TRAVERSE RELATIVE TO A FIXED POINT (i.e. PROBE)

Ruu (0, 0, r) MEASUREMENTS

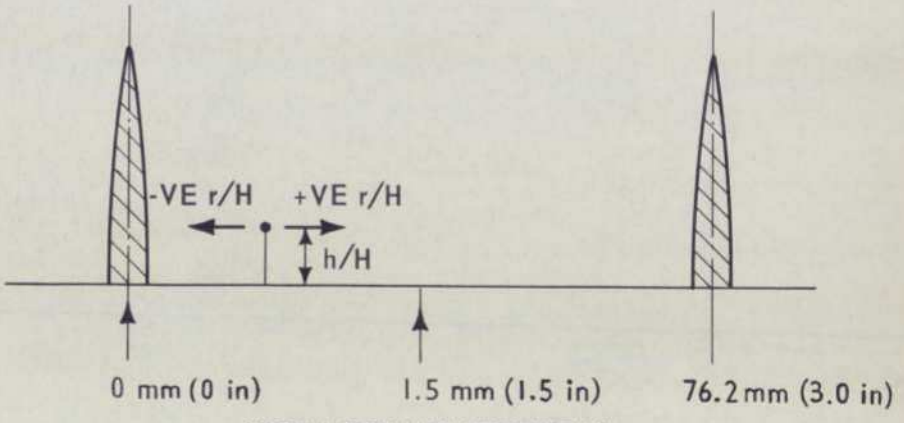


FIG. 8 SIGN CONVENTION FOR MEASUREMENTS OF CORRELATION COEFFICIENTS

CALIBRATION OF LOW SPEED WORKING SECTION OF THE BOUNDARY LAYER WIND TUNNEL
SPANWISE VELOCITY DISTRIBUTIONS q_{REF} = 4.50 mm OF WATER

UPSTREAM AXIAL STATION v = 28.29 ft/sec 8.62 m/sec

+ 0	+ 0	+ 0	+ +0.2	+ +0.2	+ 0	+ 0	+ -0.1	+ -0.2	+ -0.2	+ -0.2	+ -0.2	+ -0.2
+ -4.4	+ +.4	+ +0.2	+ +0.2	+ +0.2	+ +0.2	+ +0.2	+ +0.2	+ +0.2	+ +0.2	+ +0.2	+ +0.2	+ -0.23
+ +0.2	+ +0.4	+ +0.4	+ +0.5	+ +0.5	+ +0.4	+ +0.4	+ +0.4	+ +0.4	+ +0.4	+ +0.2	+ +0.2	+ +0.2

FIGURES INDICATE: $\Delta u/u$ %

CENTRAL AXIAL STATION u = 28.49 ft/sec 8.68 m/sec

+ +0.4	+ +0.3	+ +0.3	+ +0.3	+ 0	+ +0.4	+ +0.6	+ +0.6	+ +0.4	+ +0.3	+ +0.2	+ +0.2	+ +0.2
+ -8.2	+ +0.6	+ +0.4	+ +0.4	+ +0.4	+ +0.4	+ +0.4	+ +0.4	+ +0.4	+ +0.4	+ +0.4	+ +0.3	+ -5.6
+ +0.4	+ +0.6	+ +0.4	+ +0.4	+ +0.4	+ +0.4	+ +0.4	+ +0.6	+ +0.6	+ +0.6	+ +0.4	+ +0.4	+ +0.3

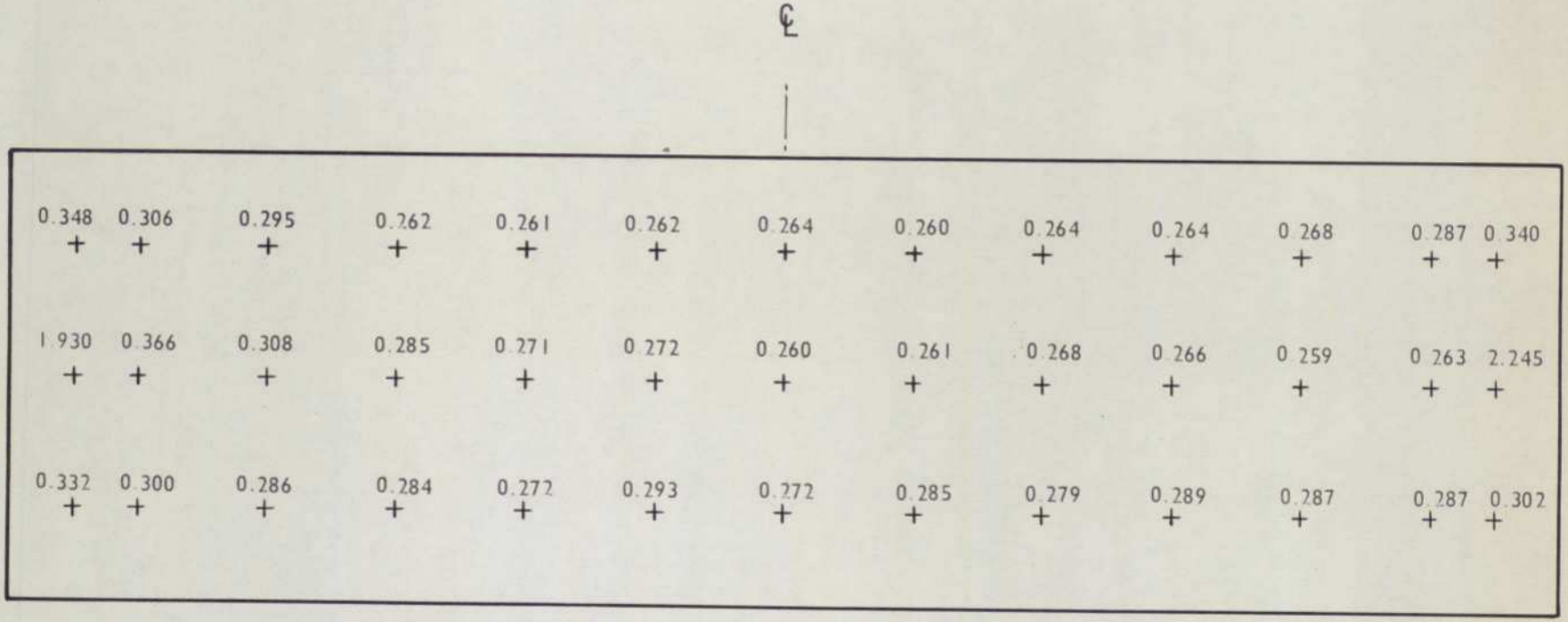
DOWNSTREAM AXIAL STATION u = 28.62 ft/sec 8.72 m/sec

+ +0.3	+ +0.3	+ +0.2	+ +0.6	+ +0.4	+ +0.3	+ +0.4	+ +0.4	+ +0.4	+ +0.4	+ +0.3	+ +0.2	+ +0.2
+ -9.3	+ +0.6	+ +0.5	+ +0.5	+ +0.4	+ +0.4	+ +0.4	+ +0.4	+ +0.3	+ +0.3	+ +0.3	+ +0.3	+ -5.1
+ +0.6	+ +0.6	+ +0.6	+ +0.6	+ +0.6	+ +0.6	+ +0.6	+ +0.5	+ +0.6	+ +0.4	+ +0.4	+ +0.3	+ +0.2

FIG. 9 ATMOSPHERIC BOUNDARY LAYER SIMULATION TESTS

JC/GH(CON.)(19.8.68.)RL.3.3.1527

VIEW UPSTREAM OF LOW SPEED WORKING SECTION
PLANE OF TRAVERSE CORRESPONDS TO PLANE 457.2 mm (18 in)
AFT OF V.G. TRAILING EDGE



FIGURES GIVE LONGITUDINAL TURBULENCE %, $(\sqrt{u^{-2}}/U_{MAX})$

FIG. 10 ATMOSPHERIC BOUNDARY LAYER SIMULATION TESTS
CALIBRATION OF LOW SPEED WORKING SECTION OF THE BOUNDARY LAYER WIND TUNNEL

JC/LRC (29.10.68) RL 3.3.1630

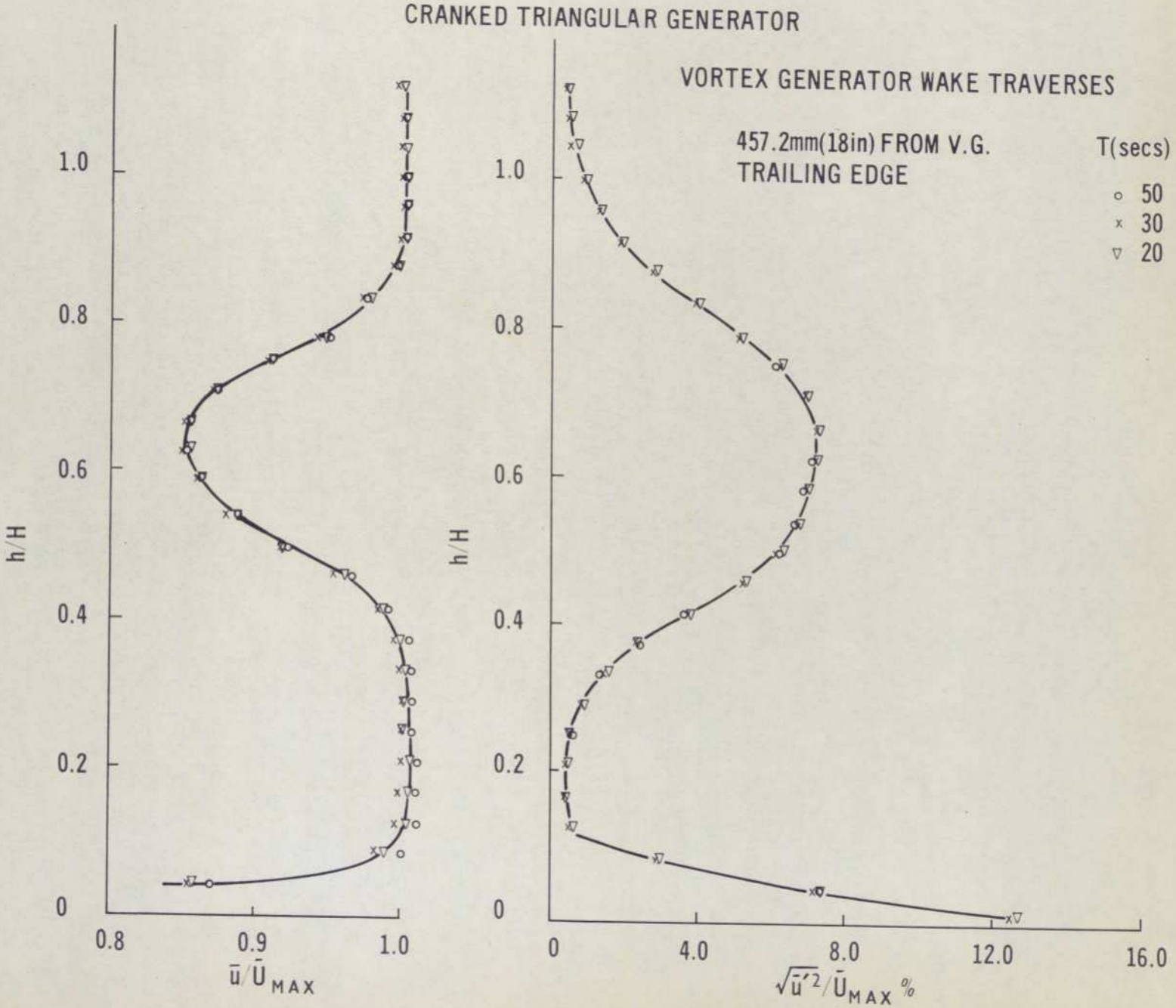


FIG.11 ATMOSPHERIC BOUNDARY LAYER SIMULATION TESTS

JC/GH(CON.)(14.8.68.)RL.3.3.1529

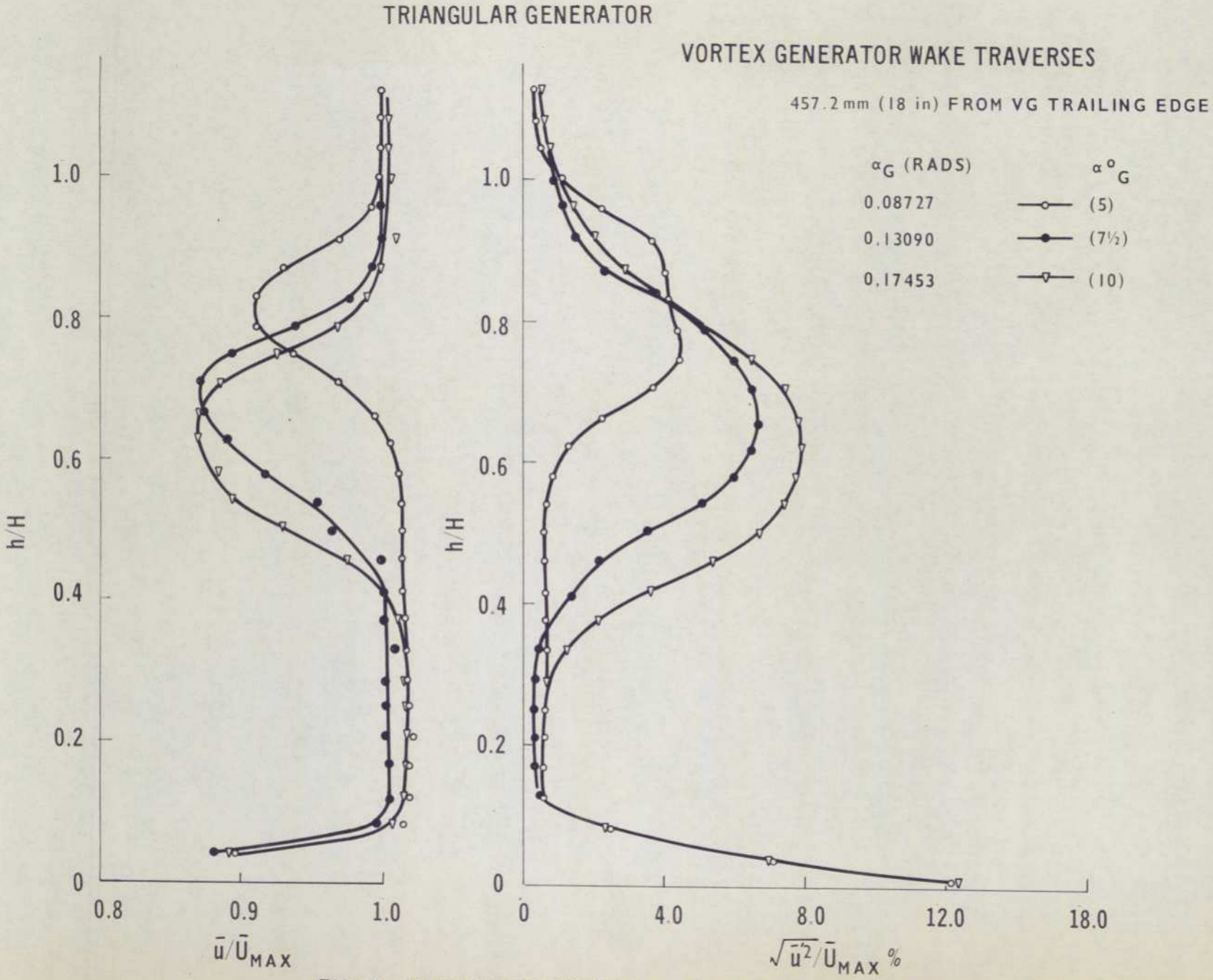


FIG.12 ATMOSPHERIC BOUNDARY LAYER SIMULATION TESTS

JC/GH(CON)(30.9.68)RL.3.3.1532

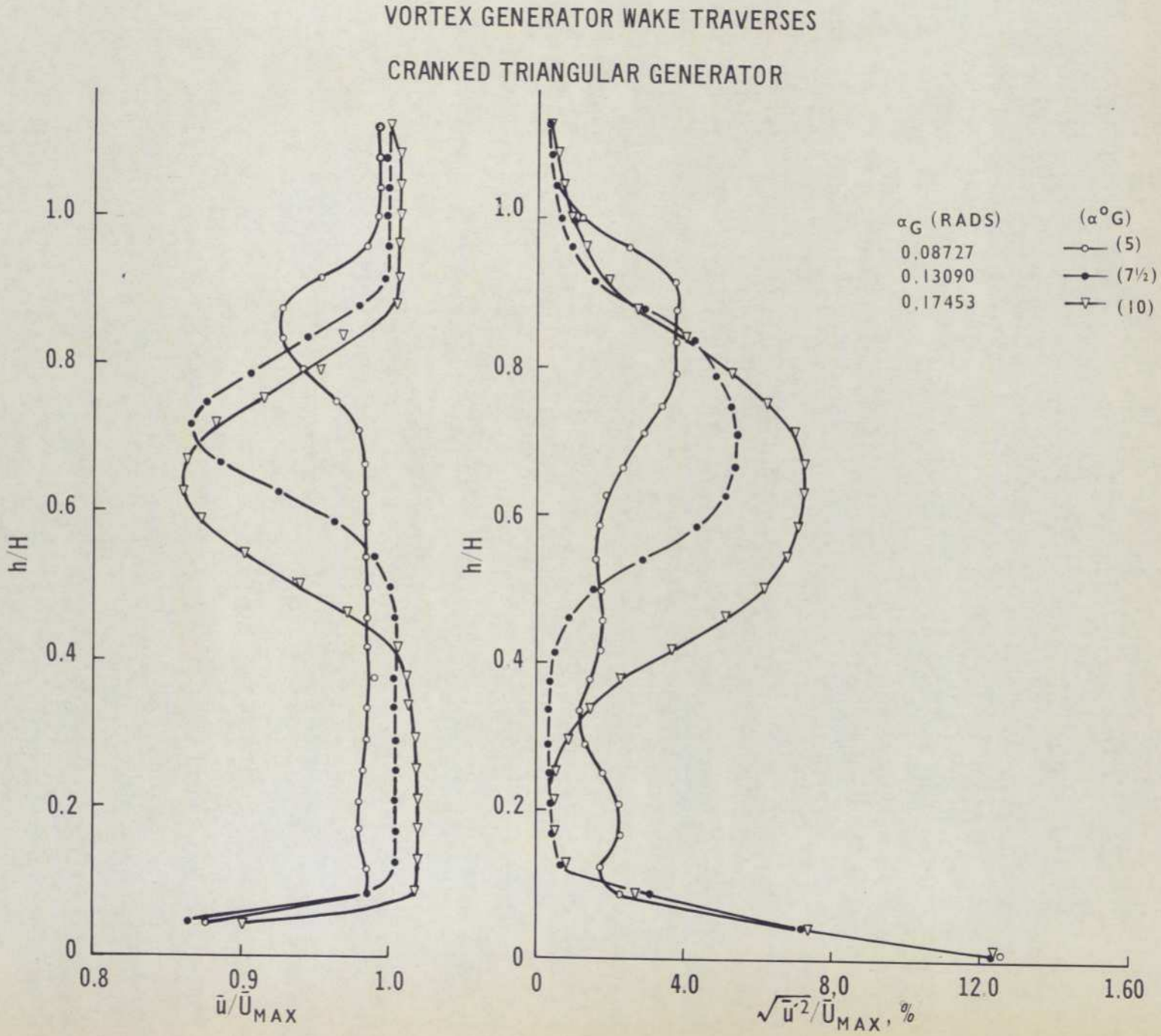


FIG. 13 ATMOSPHERIC BOUNDARY LAYER SIMULATION TESTS

JC/GH(CON.)(16.8.68.)RL.3.3.1533

PLANE ELLIPTICAL GENERATORS

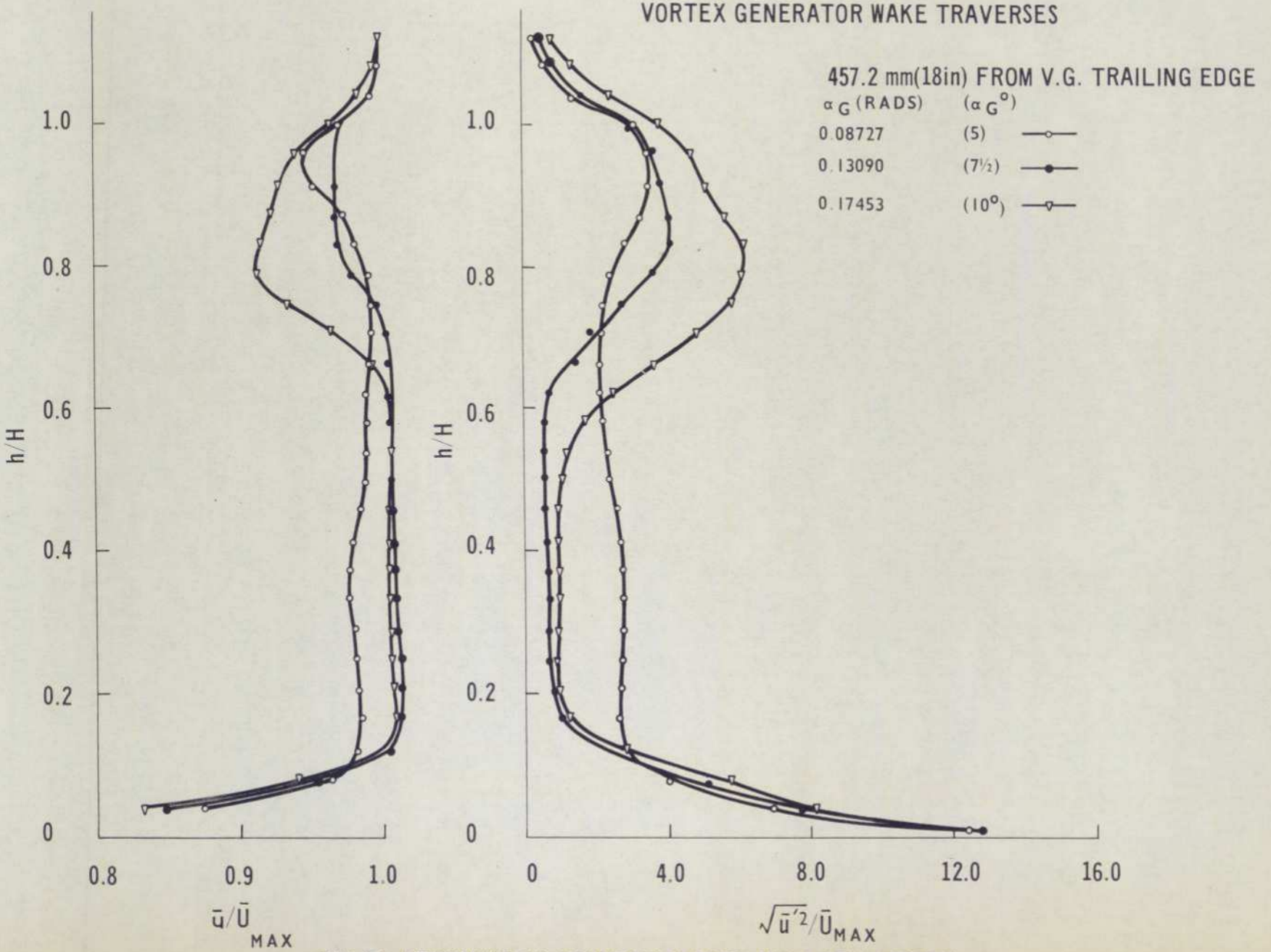


FIG.14. ATMOSPHERIC BOUNDARY LAYER SIMULATION TESTS

JC/GH(CON)(30.9.68.)RL.3.3.1534

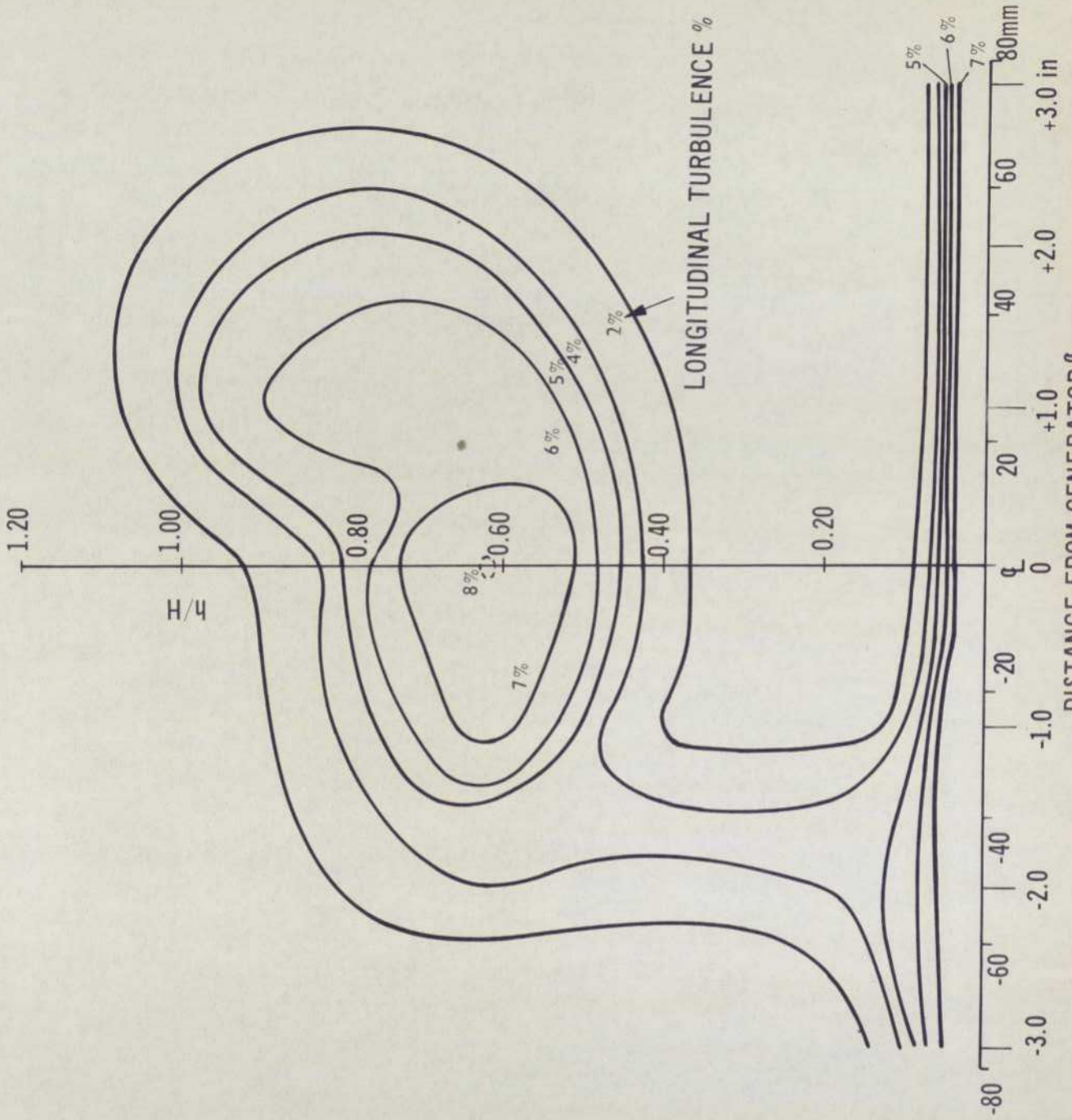


FIG.15. ATMOSPHERIC BOUNDARY LAYER SIMULATION TESTS

CONTOURS OF CONSTANT LONGITUDINAL TURBULENCE IN THE WAKE OF A TRIANGULAR GENERATOR AT AN INCIDENCE OF 0.17493 RAD (10^0)

AXIAL STN. 457.2mm (18in) AFT OF GENERATOR TRAILING EDGE VIEW UPSTREAM WITH T.E. DEFLECTED TO LEFT OF ℄

JC/GH(CON.)(16.8.68.)RL.3.3.1535

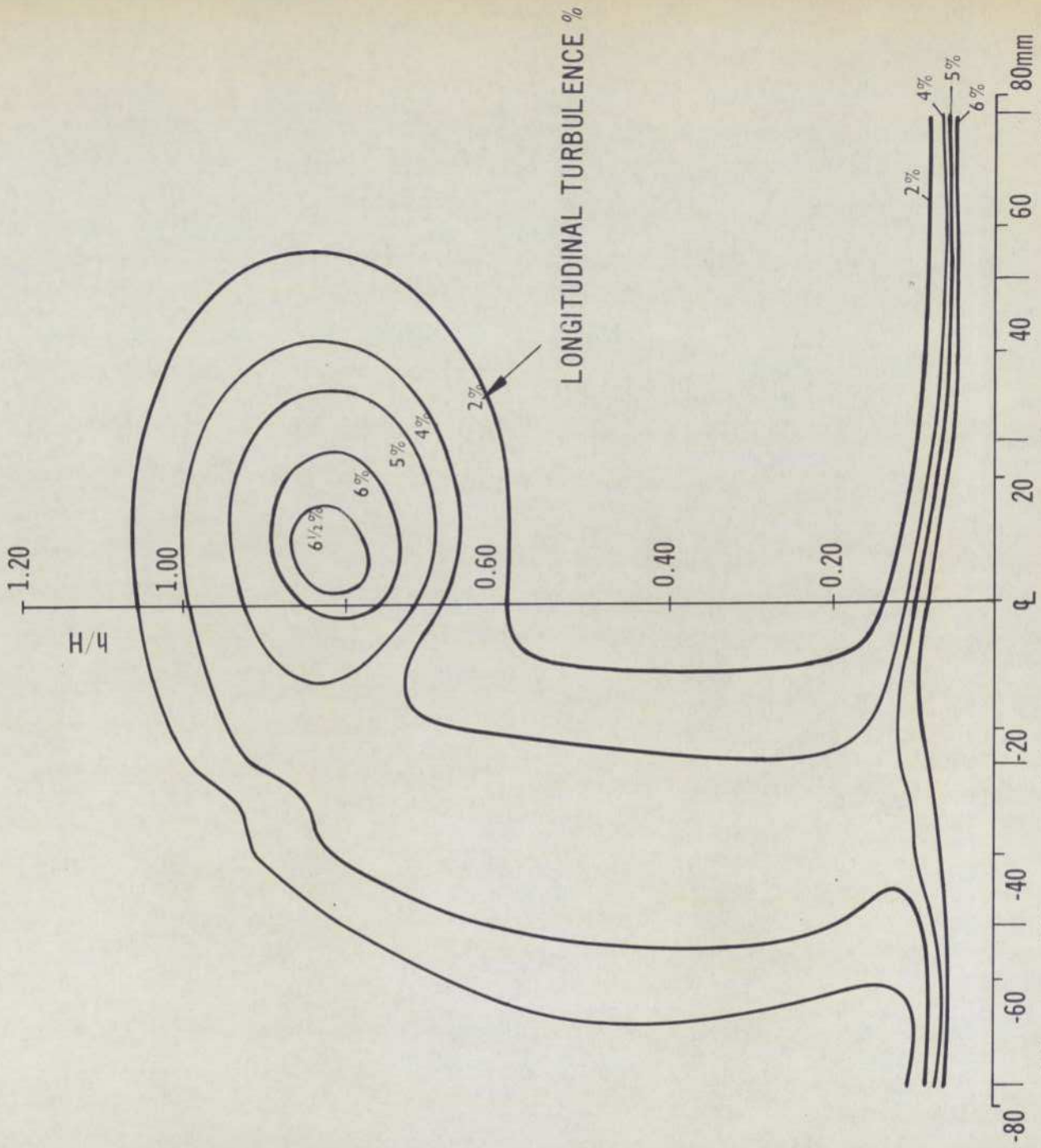


FIG.16. ATMOSPHERIC BOUNDARY LAYER SIMULATION TESTS

CONTOURS OF CONSTANT LONGITUDINAL TURBULENCE IN THE WAKE OF A PLANE ELLIPTIC GENERATOR AT AN INCIDENCE OF 0.17453 RADS (10^0)

AXIAL STN. 457.2 (18in) AFT OF GENERATOR TRAILING EDGE
VIEW UPSTREAM WITH T.E. DEFLECTED TO LEFT OF ℄

JC/GH(CON.)(16.8.68.)RL.3.3.1536

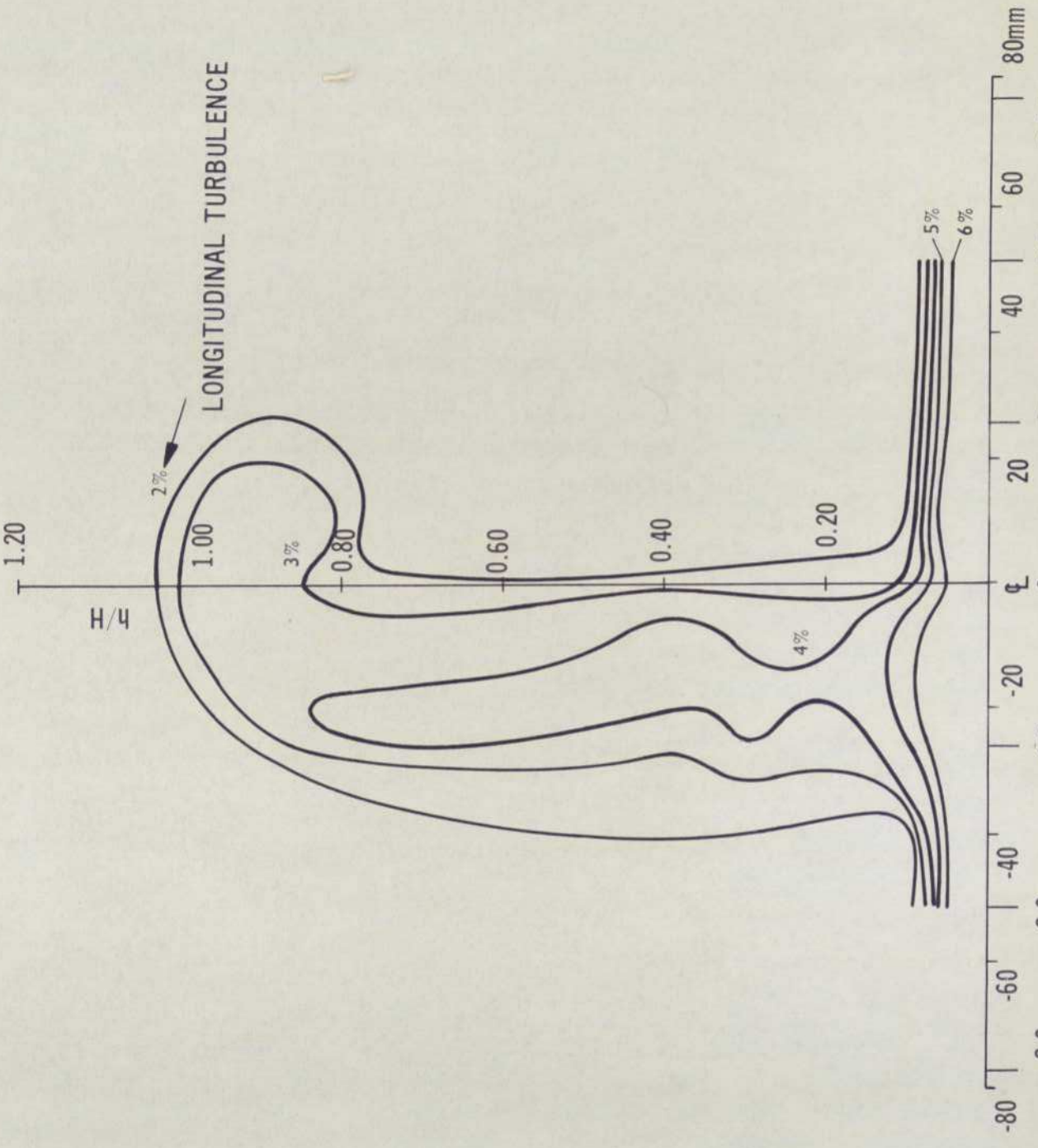


FIG. 17. ATMOSPHERIC BOUNDARY LAYER SIMULATION TESTS

CONTOURS OF CONSTANT LONGITUDINAL TURBULENCE IN THE WAKE OF A PLANE ELLIPTIC GENERATOR AT AN INCIDENCE OF 10.08727 RADS (5^0)

AXIAL STN. 457.2mm (18in) AFT OF GENERATOR TRAILING EDGE

VIEW UPSTREAM WITH T.E. DEFLECTED LEFT OF ℄

JC/GH(CON.)(16.8.68.)RL.3.3.1537

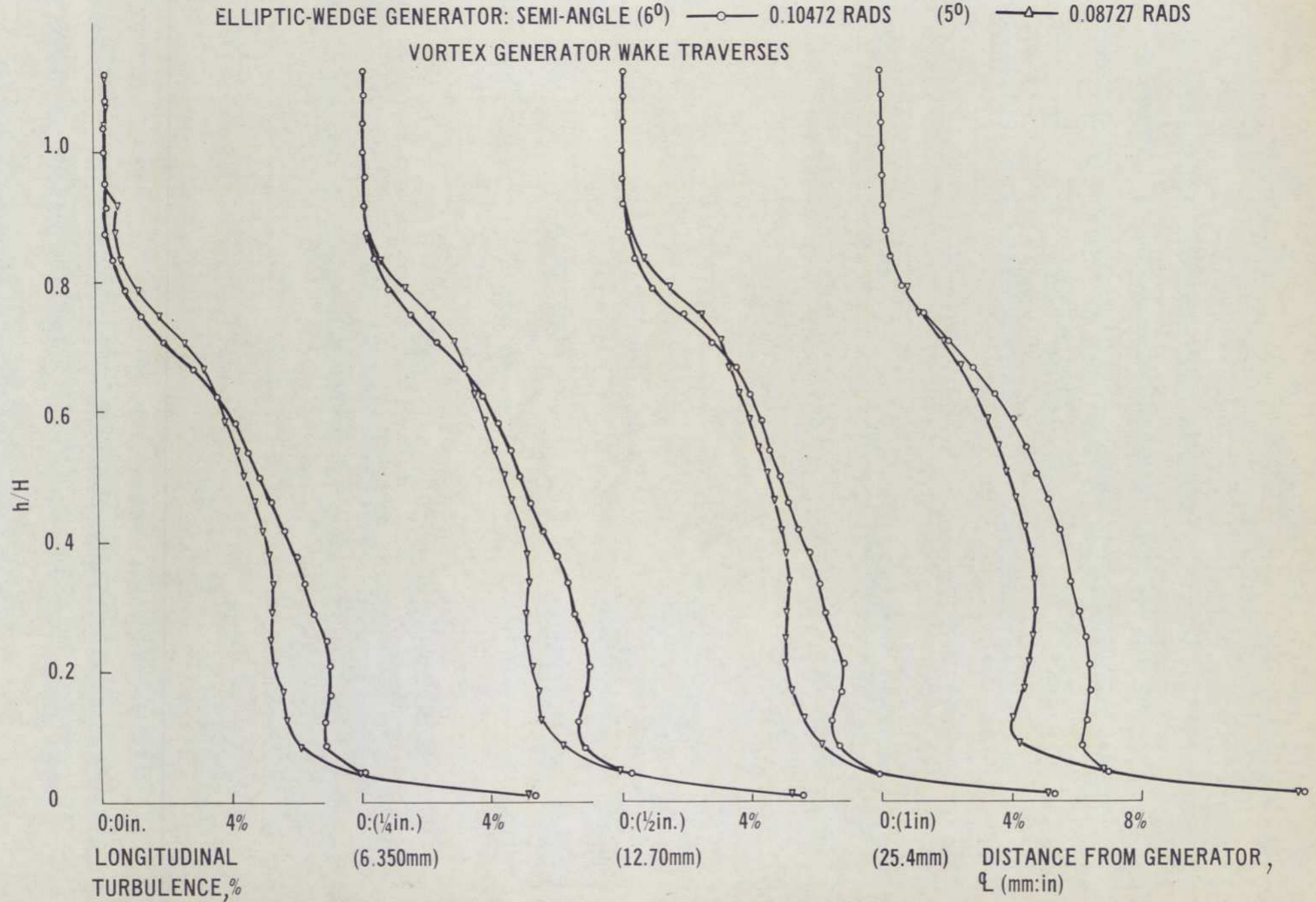


FIG. 18 ATMOSPHERIC BOUNDARY LAYER SIMULATION TESTS

CENTRAL ELECTRICITY RESEARCH LABORATORIES

REF. RD/L/R 1540

JC/GH(CON)(30.9.68.)RL.3.3.1538

CONTOURS OF CONSTANT LONGITUDINAL TURBULENCE IN THE WAKE OF AN ELLIPTIC WEDGE GENERATOR

AXIAL STN. 457.2mm (18in) AFT OF GENERATOR TRAILING EDGE VIEW UPSTREAM

FIG. 19 ATMOSPHERIC BOUNDARY LAYER SIMULATION TESTS

BARRIER WAKE TRAVERSES

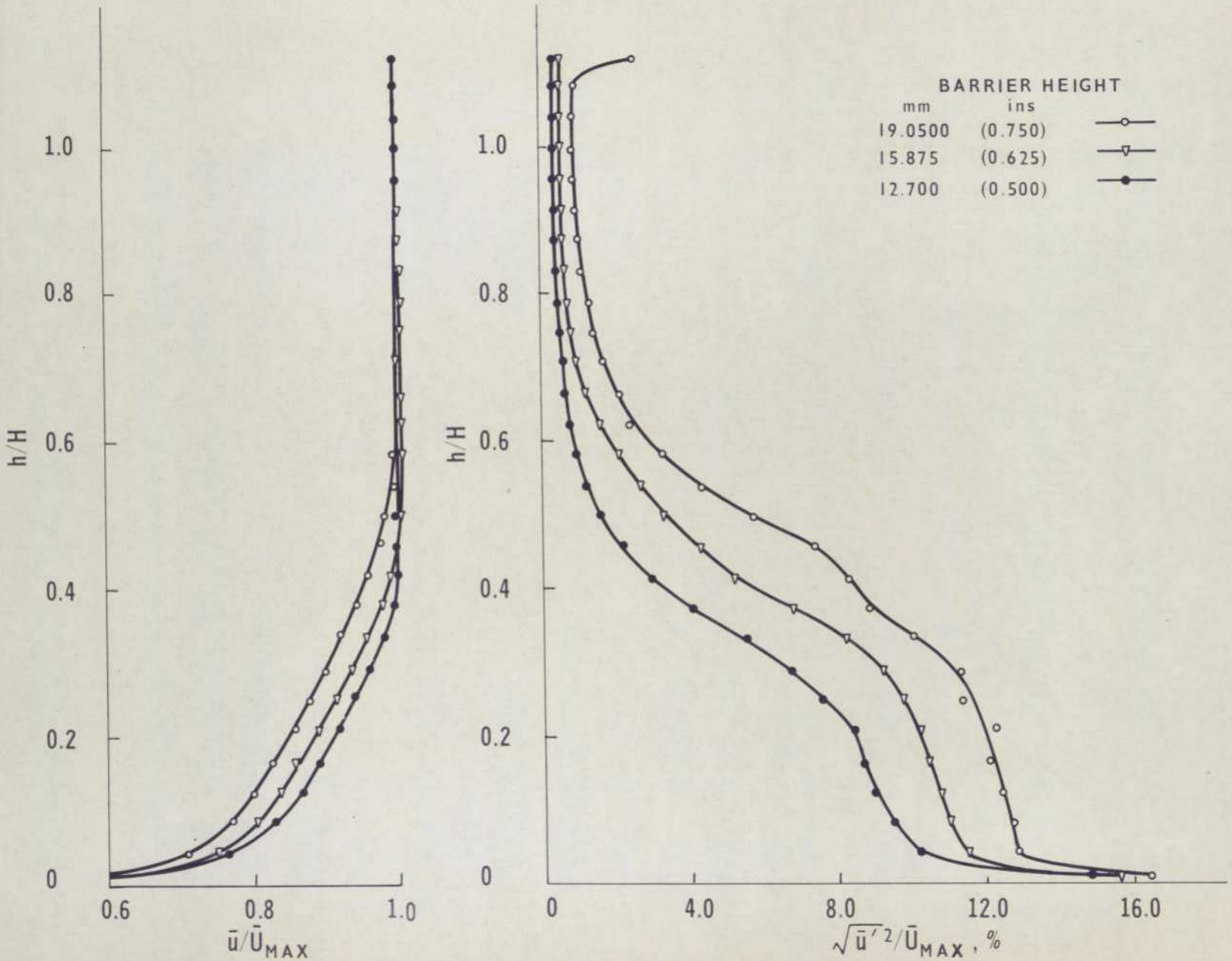


FIG.20 ATMOSPHERIC BOUNDARY LAYER SIMULATION TESTS

JC/GH(CON)(30.9.68.)RL.3.3.1540

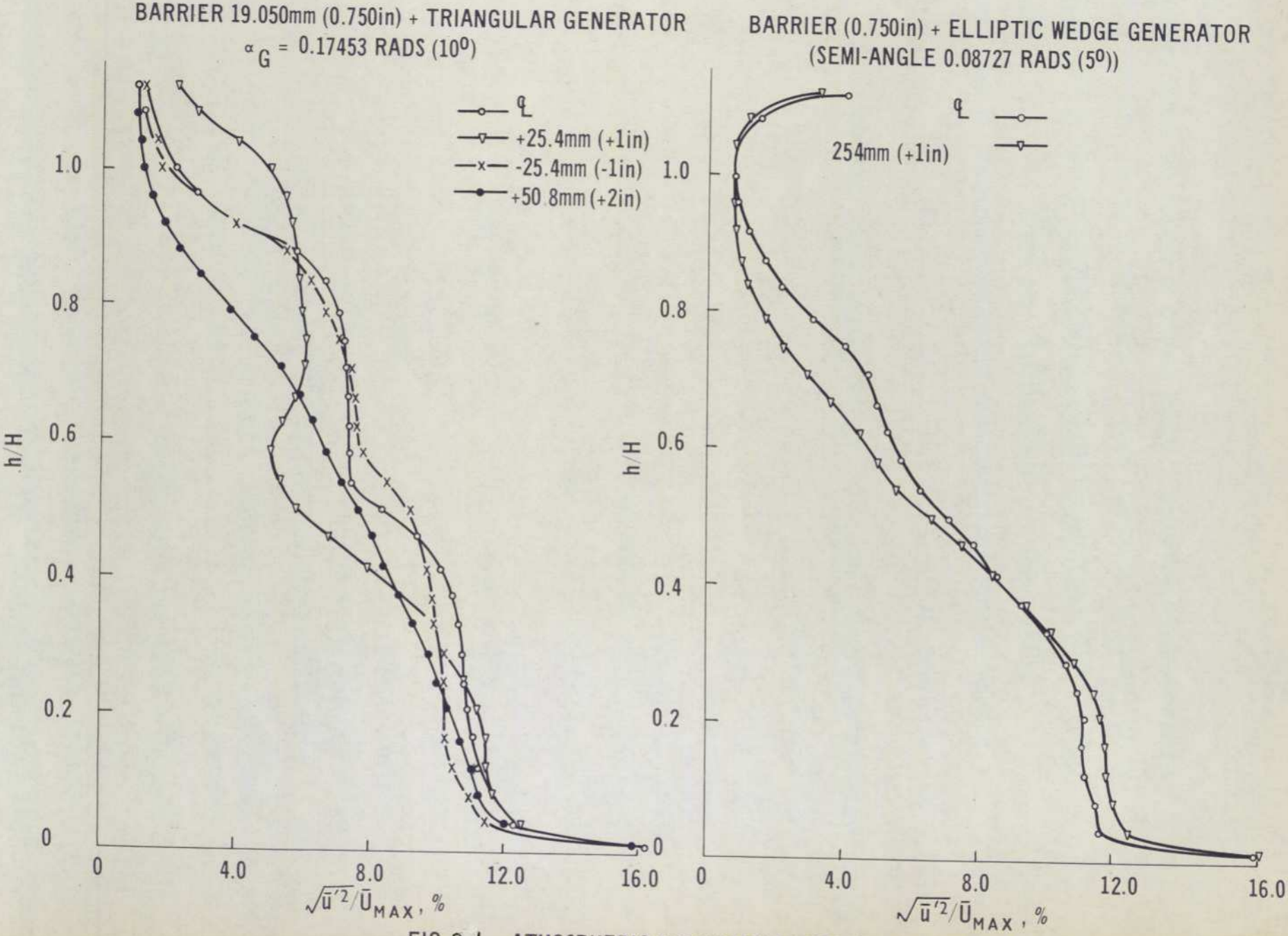


FIG. 2.1. ATMOSPHERIC BOUNDARY LAYER SIMULATION TESTS

BARRIER + ONE VORTEX GENERATOR TRAVERSES

JC/GH(CON)(30.9.68.)RL.3.3.1541

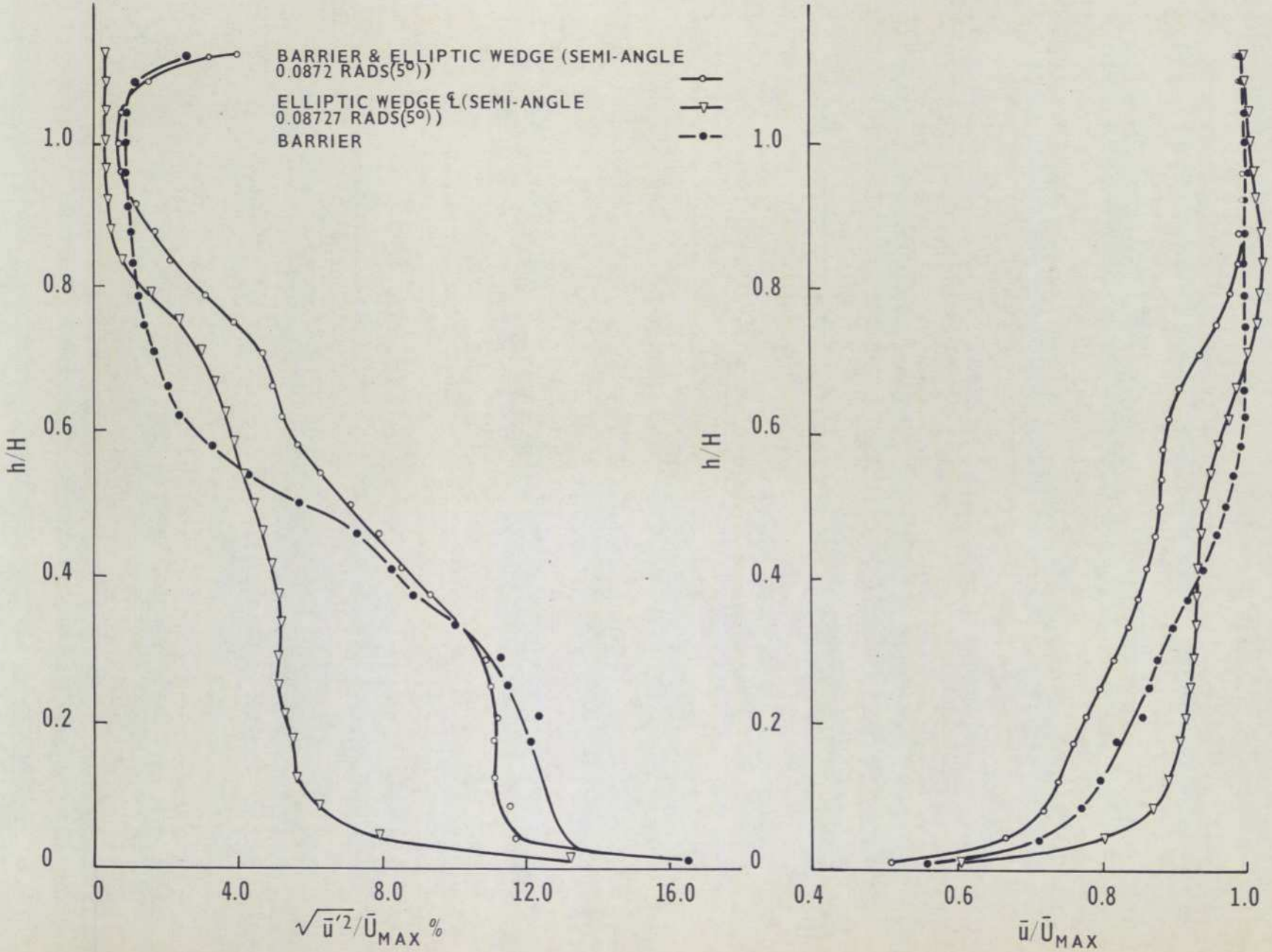


FIG. 22 ATMOSPHERIC BOUNDARY LAYER SIMULATION TESTS

BARRIER AND VORTEX GENERATOR TRAVERSES

JC/GH(CON.)(19.8.68)RL.3.3.1542

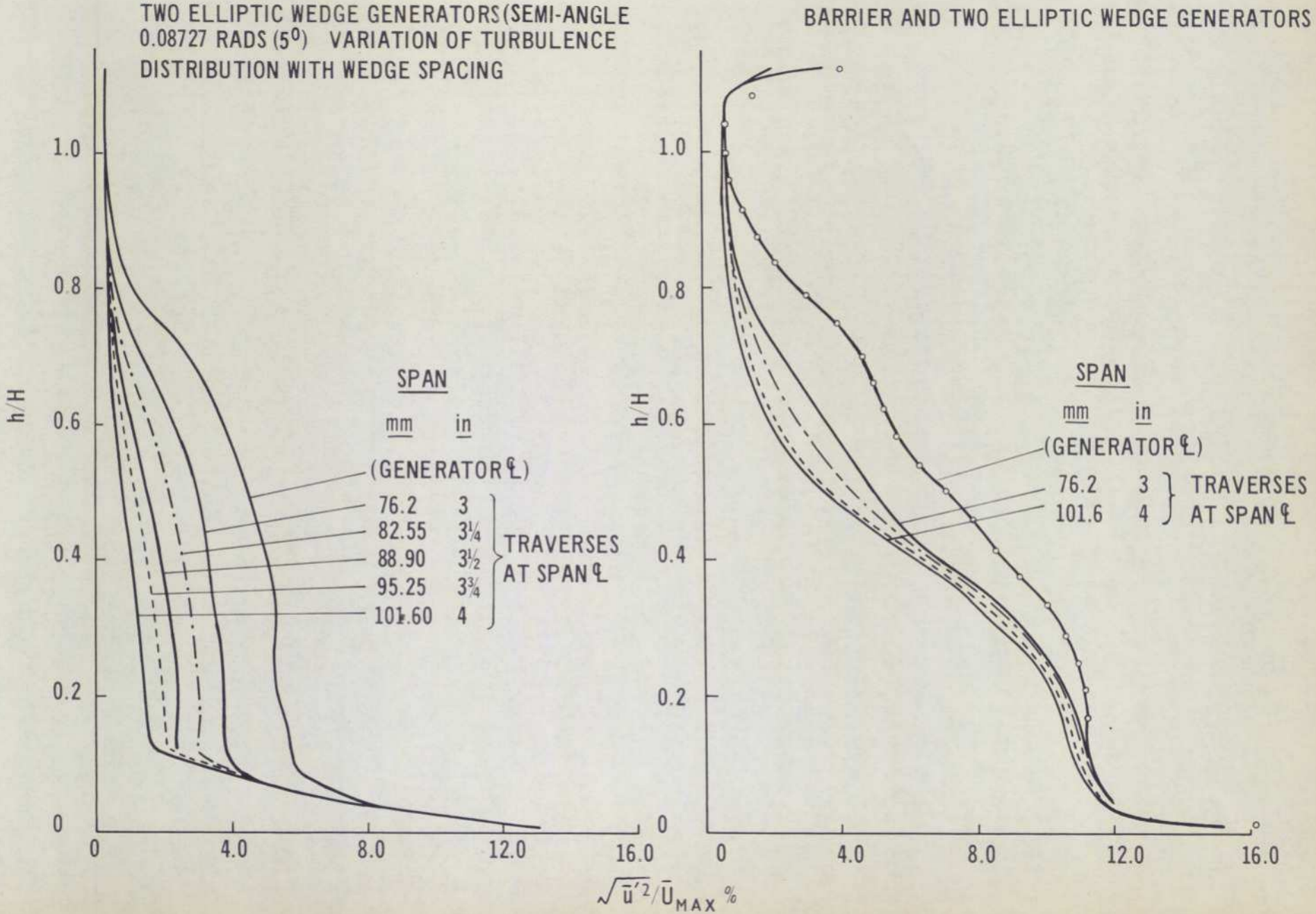
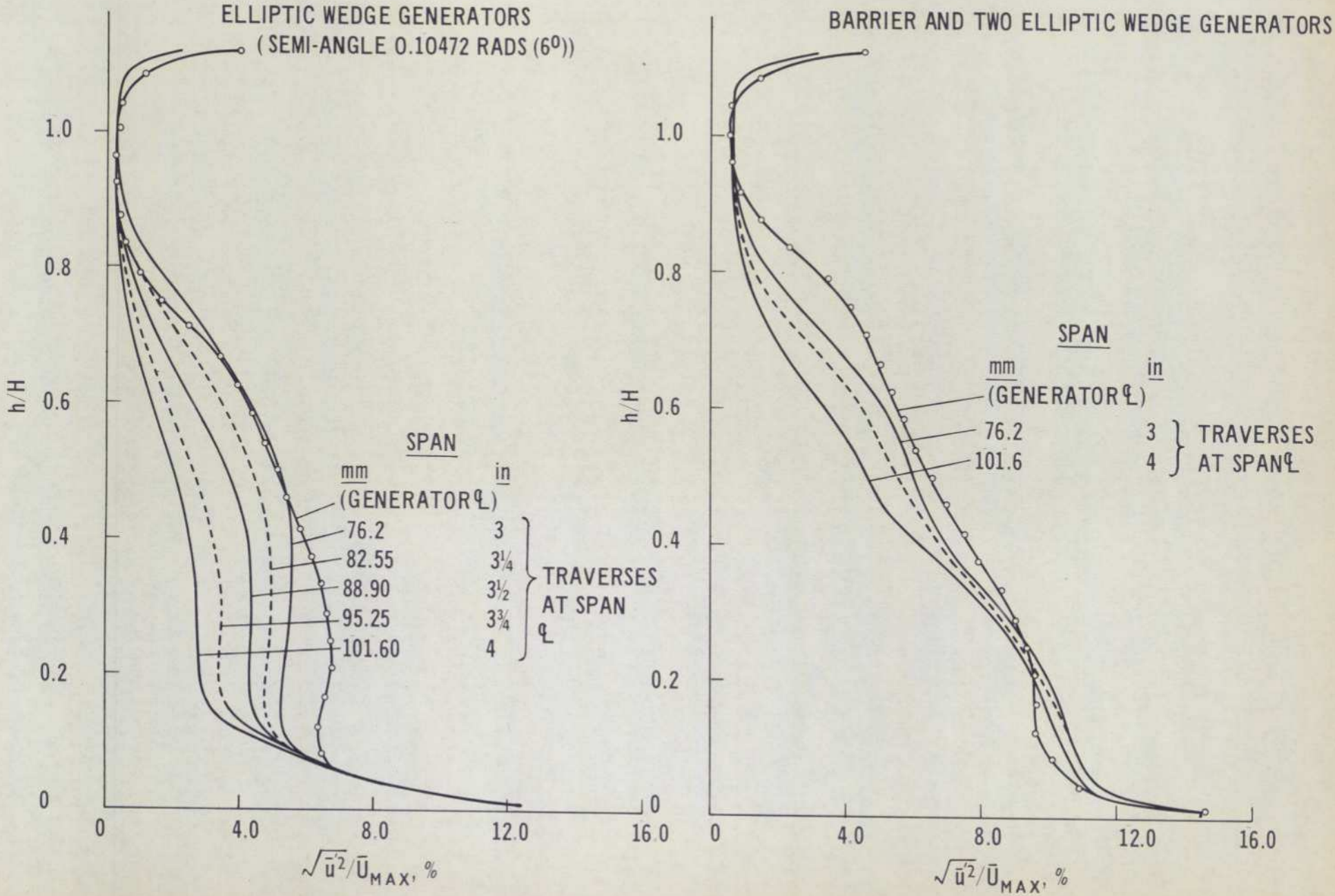


FIG. 23. ATMOSPHERIC BOUNDARY LAYER SIMULATION TESTS

VARIATION OF TURBULENCE DISTRIBUTION WITH WEDGE SPACING
BARRIER AND VORTEX GENERATOR TRAVERSES



JC/GH(CON)(30.9.68.)RL.3.3.1544

FIG. 24. ATMOSPHERIC BOUNDARY LAYER SIMULATION TESTS

VARIATION OF LONGITUDINAL TURBULENCE WITH HEIGHT FOR VARIOUS GENERATOR/BARRIER SPACINGS

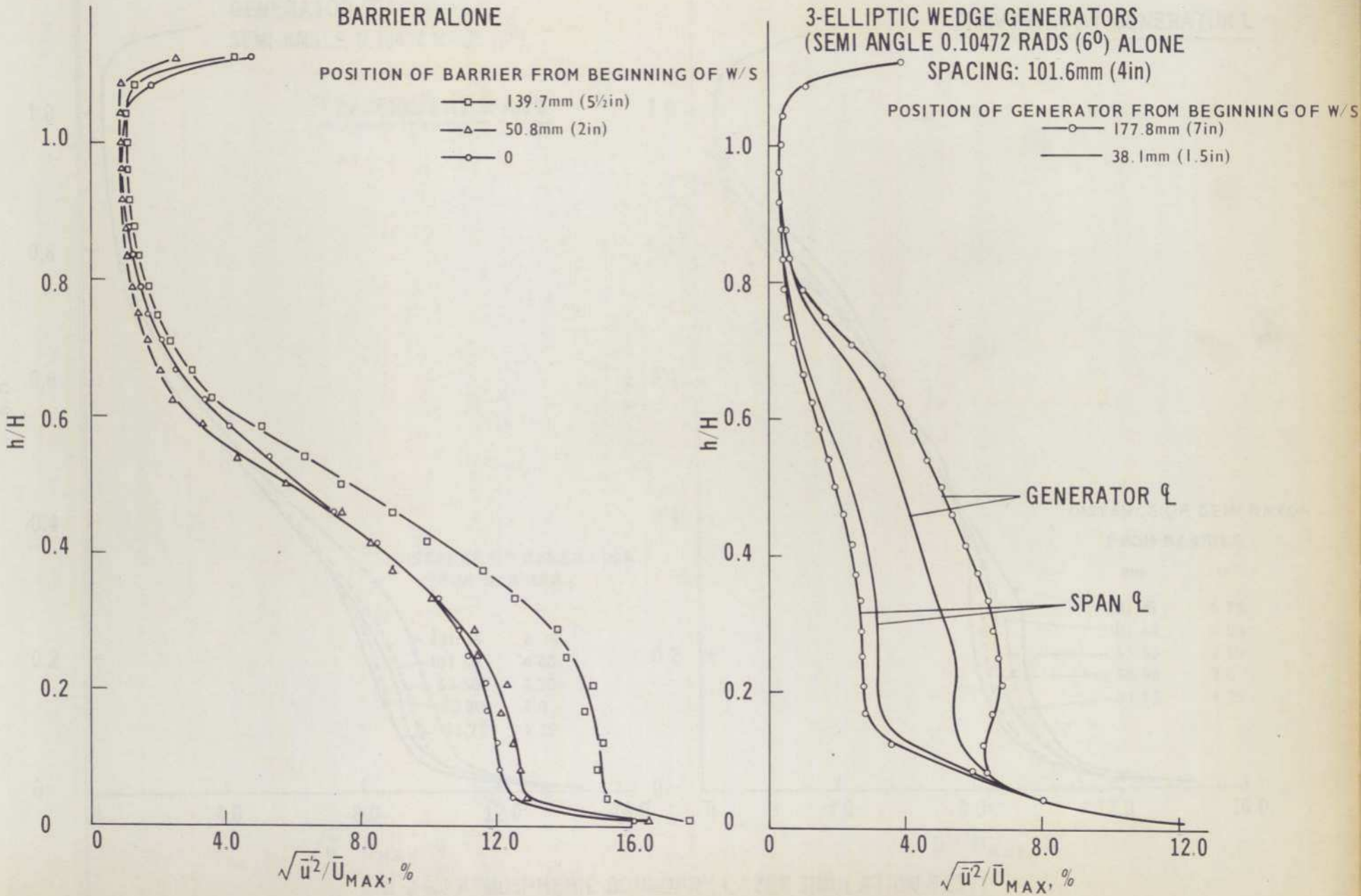


FIG. 25. ATMOSPHERIC BOUNDARY LAYER SIMULATION TESTS

JC/GH(CON)(30.9.68.)RL.3.3.1545

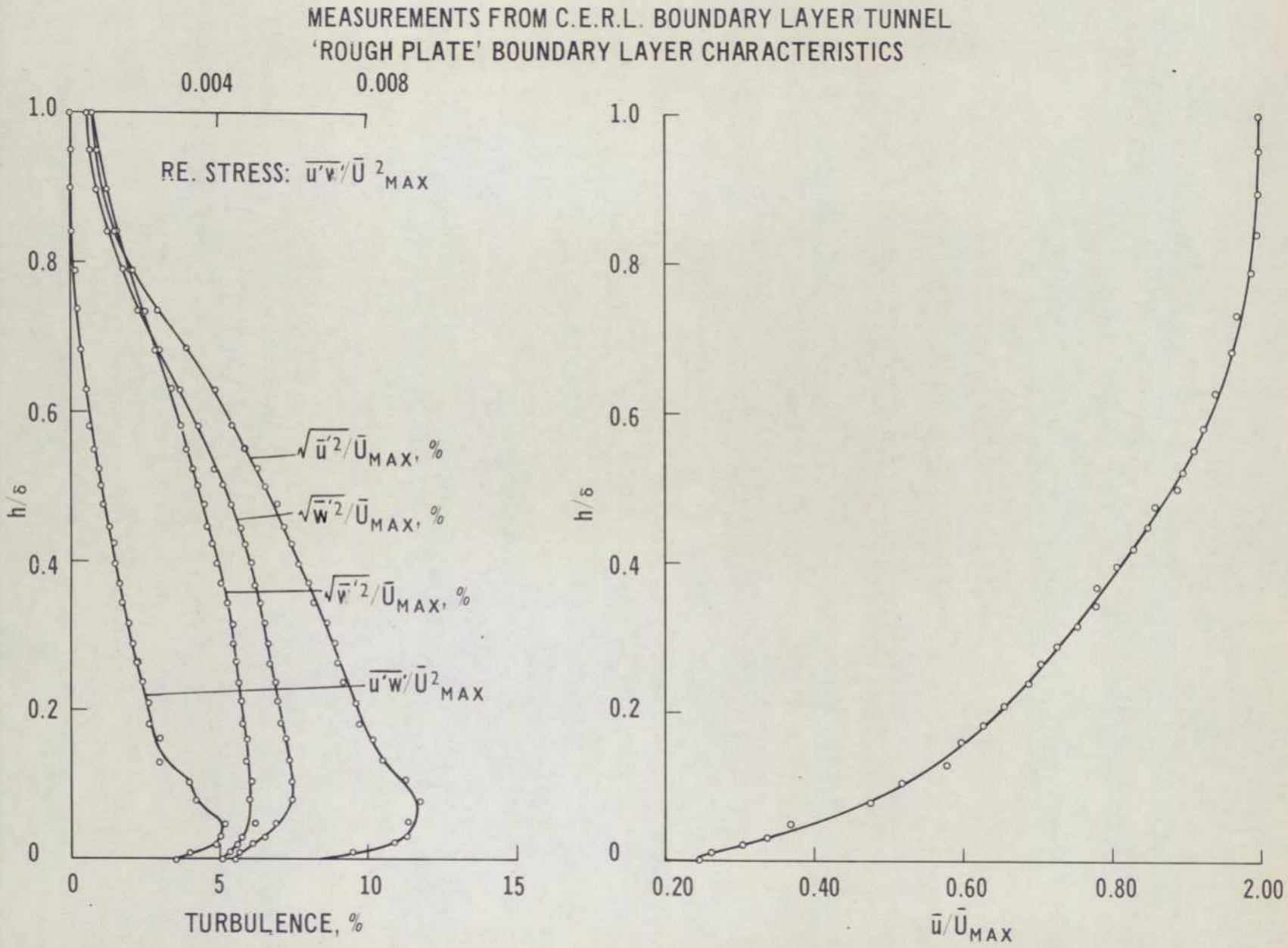


FIG 27 ATMOSPHERIC BOUNDARY LAYER SIMULATION TESTS

JC/GH(CON)(30.9.68.)RL.3.3.1547

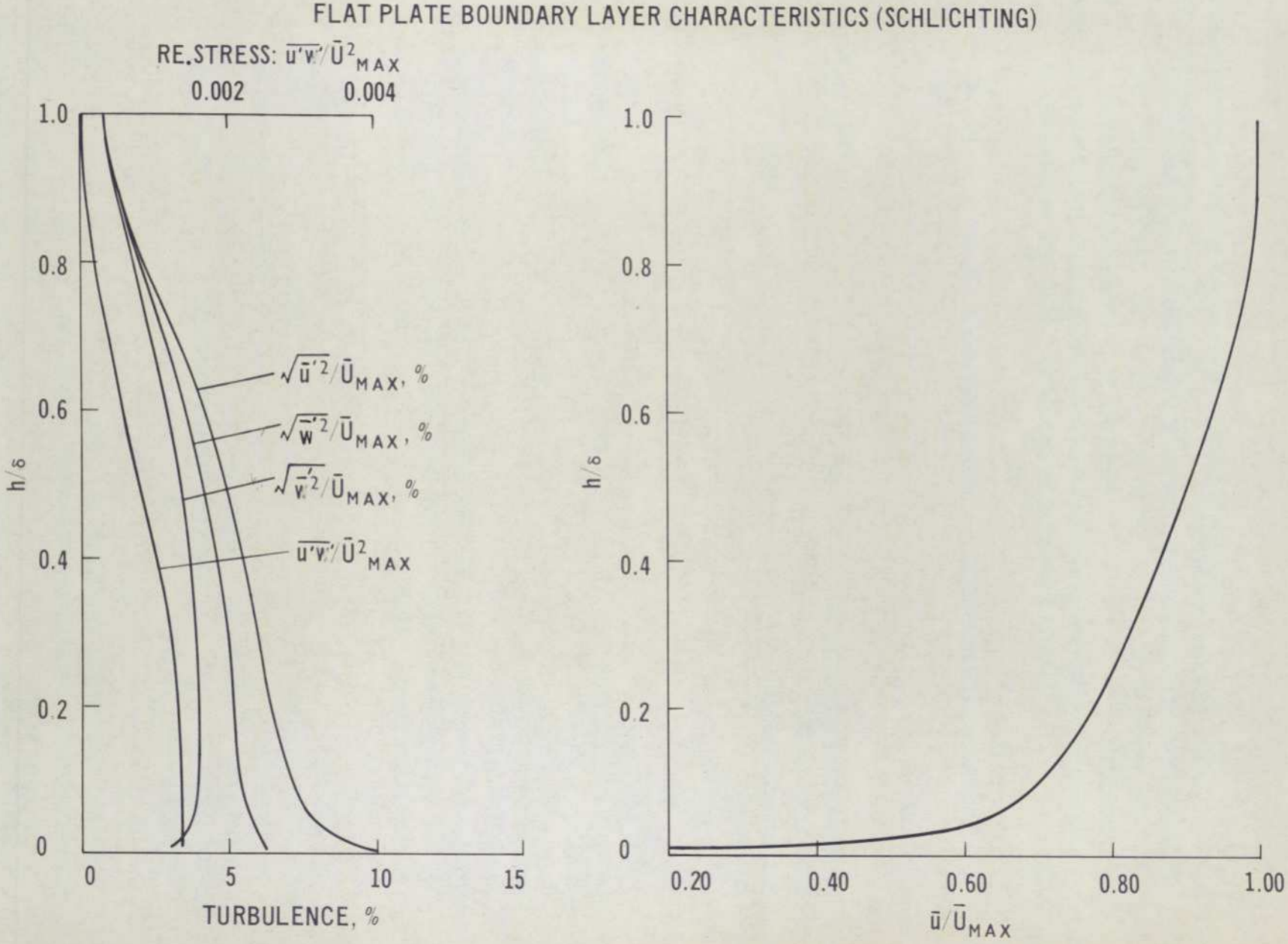


FIG. 28. ATMOSPHERIC BOUNDARY LAYER SIMULATION TESTS

JC/GH(CON)30.9.68.)RL.3.3.1548

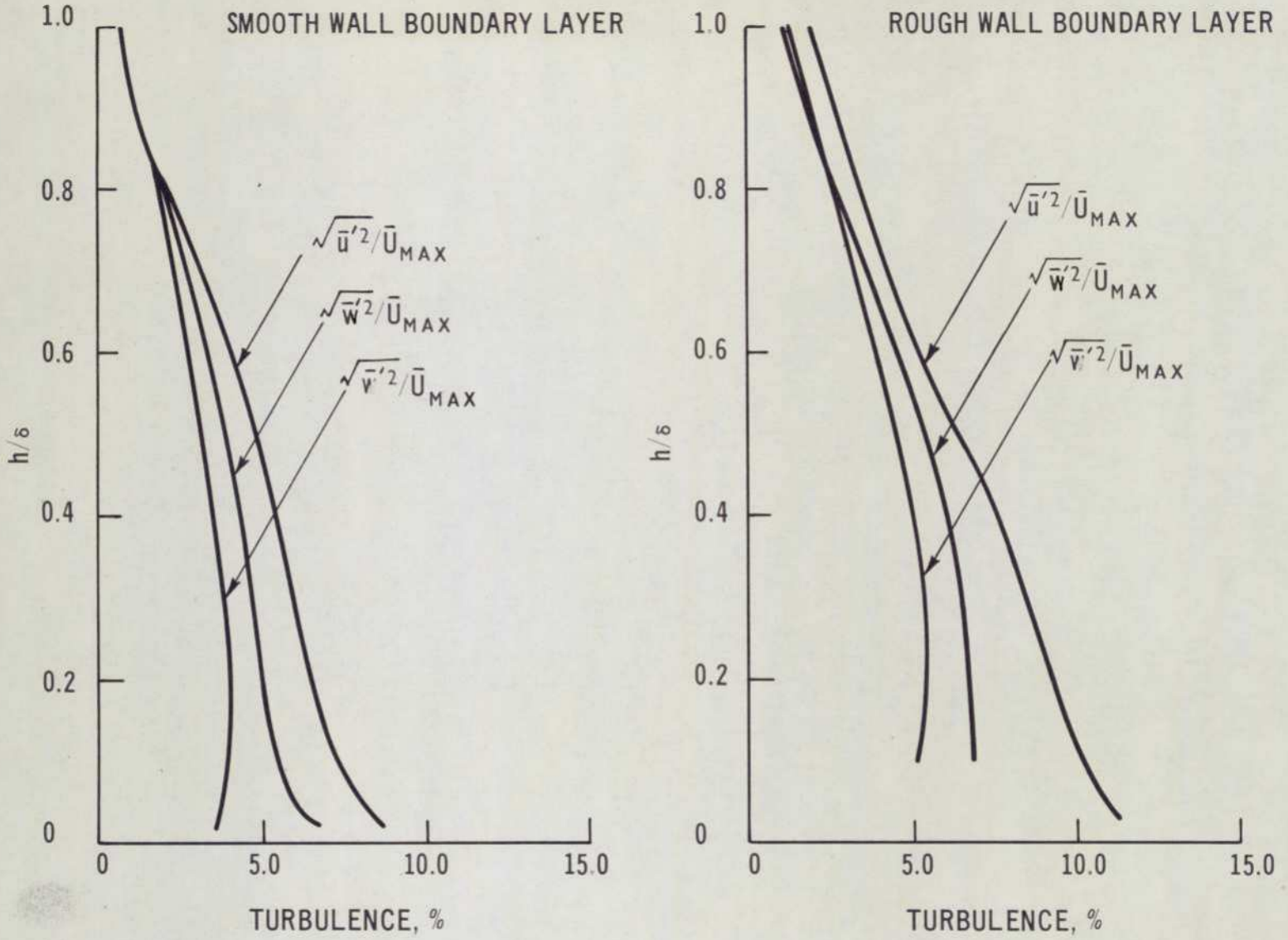


FIG. 29. ATMOSPHERIC BOUNDARY LAYER SIMULATION TESTS: ROUGH AND SMOOTH WALL BOUNDARY LAYER CHARACTERISTICS (HINZE)

JC/GH(CON.)(14.8.68.)RL.3.3.1624

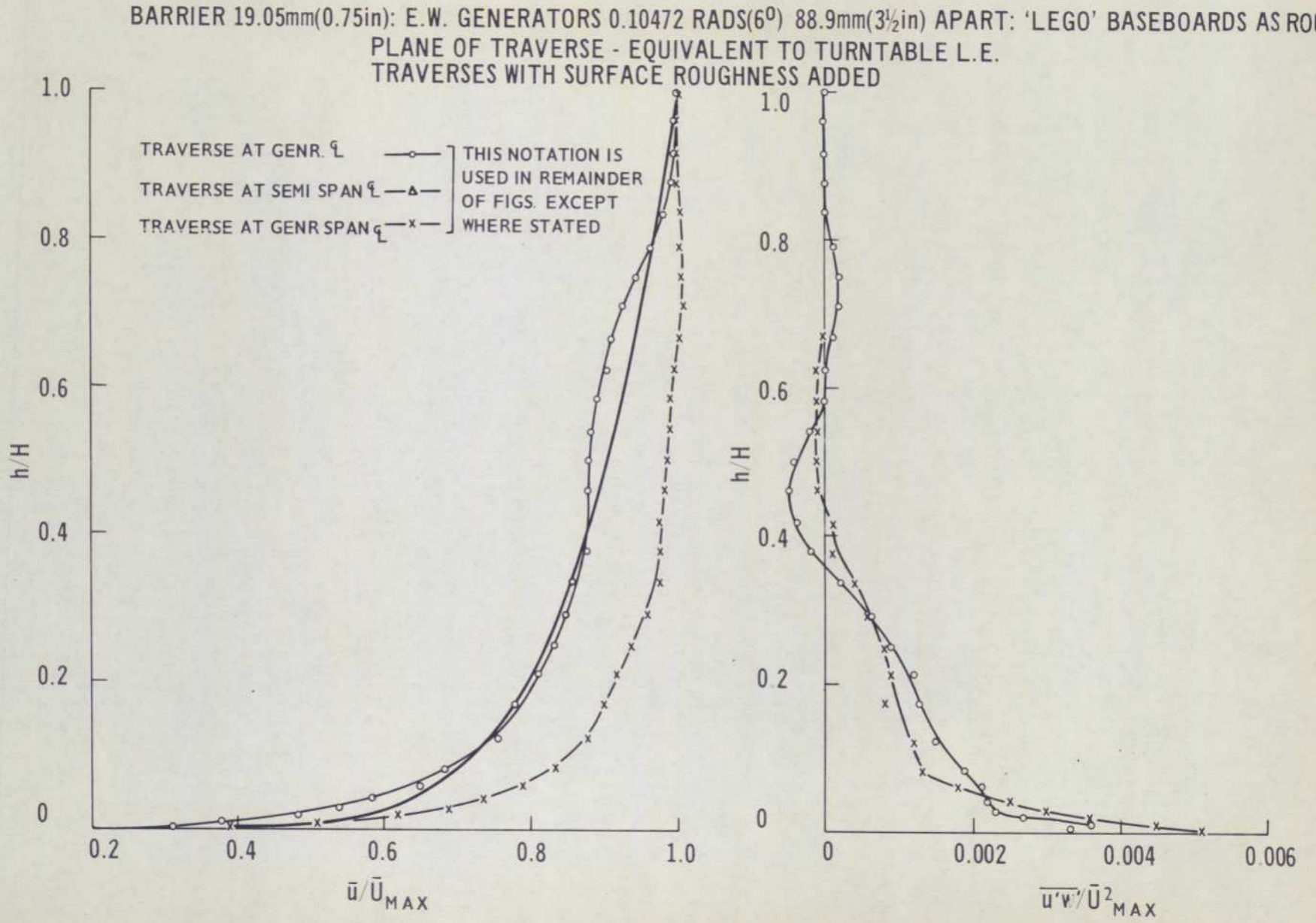


FIG. 30 TRAVERSES WITH SURFACE ROUGHNESS ADDED

JC/GH(CON)(30.9.68.)RL.3.3.1549

BARRIER 19.05mm(0.75in): E.W. GENERATORS 0.10472 RADS(6°)88.9 mm (3½in) APART: 'LEGO' BASEBOARDS AS ROUGHNESS
PLANE OF TRAVERSE - EQUIVALENT TO TURNTABLE L.E.
TRAVERSES WITH SURFACE ROUGHNESS ADDED

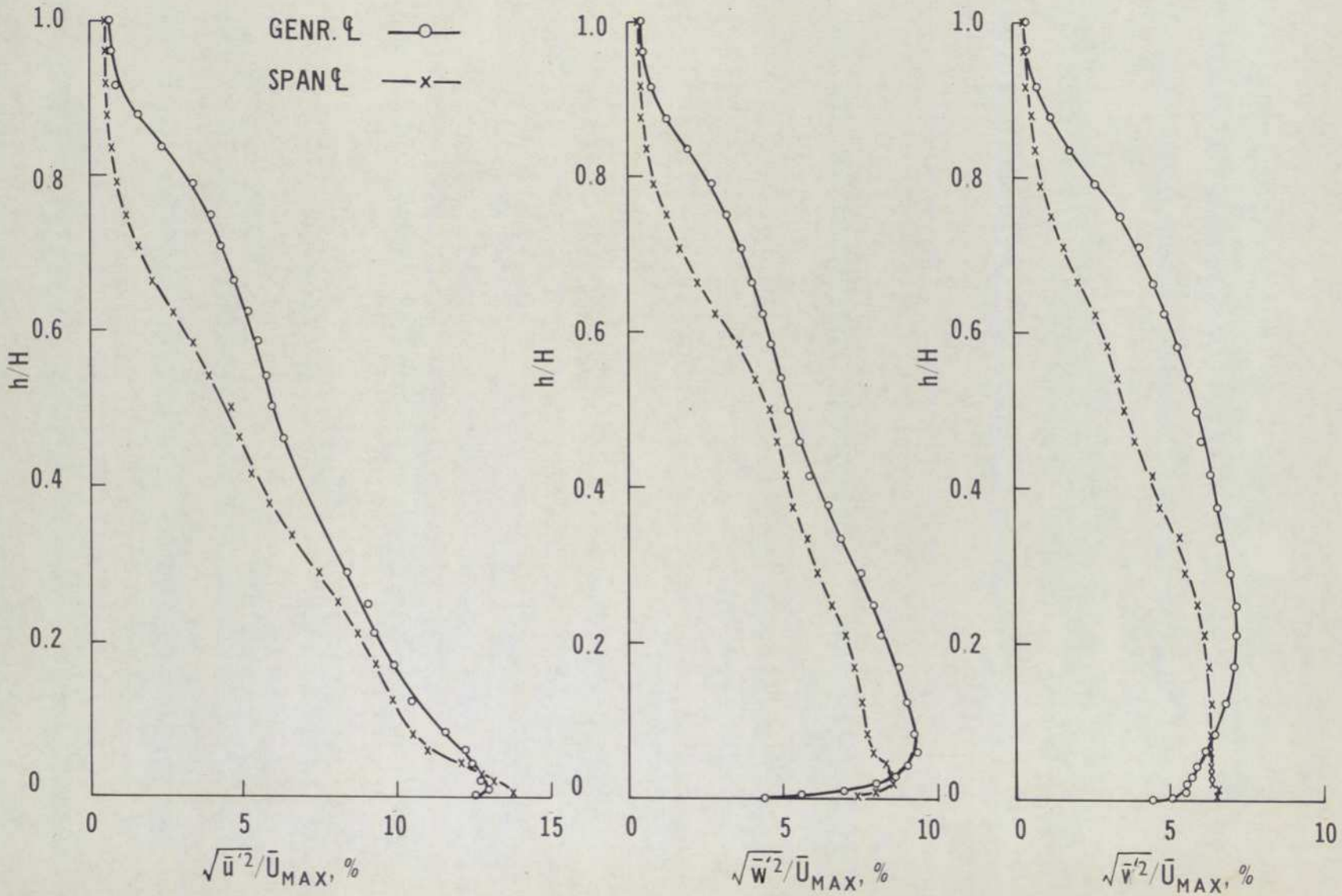


FIG.31. ATMOSPHERIC BOUNDARY LAYER SIMULATION TESTS

JC/GH(CON)(30.9.68.) RL.3.3.1550

BARRIER 19.05mm (0.75in): E.W. GENERATORS 0.10472 RADS (6^0) 76.2mm (3 in) APART: 'LEGO' BASEBOARDS AS ROUGHNESS
PLANE OF TRAVERSE - EQUIVALENT TO TURNTABLE L.E.
TRAVERSES WITH SURFACE ROUGHNESS ADDED

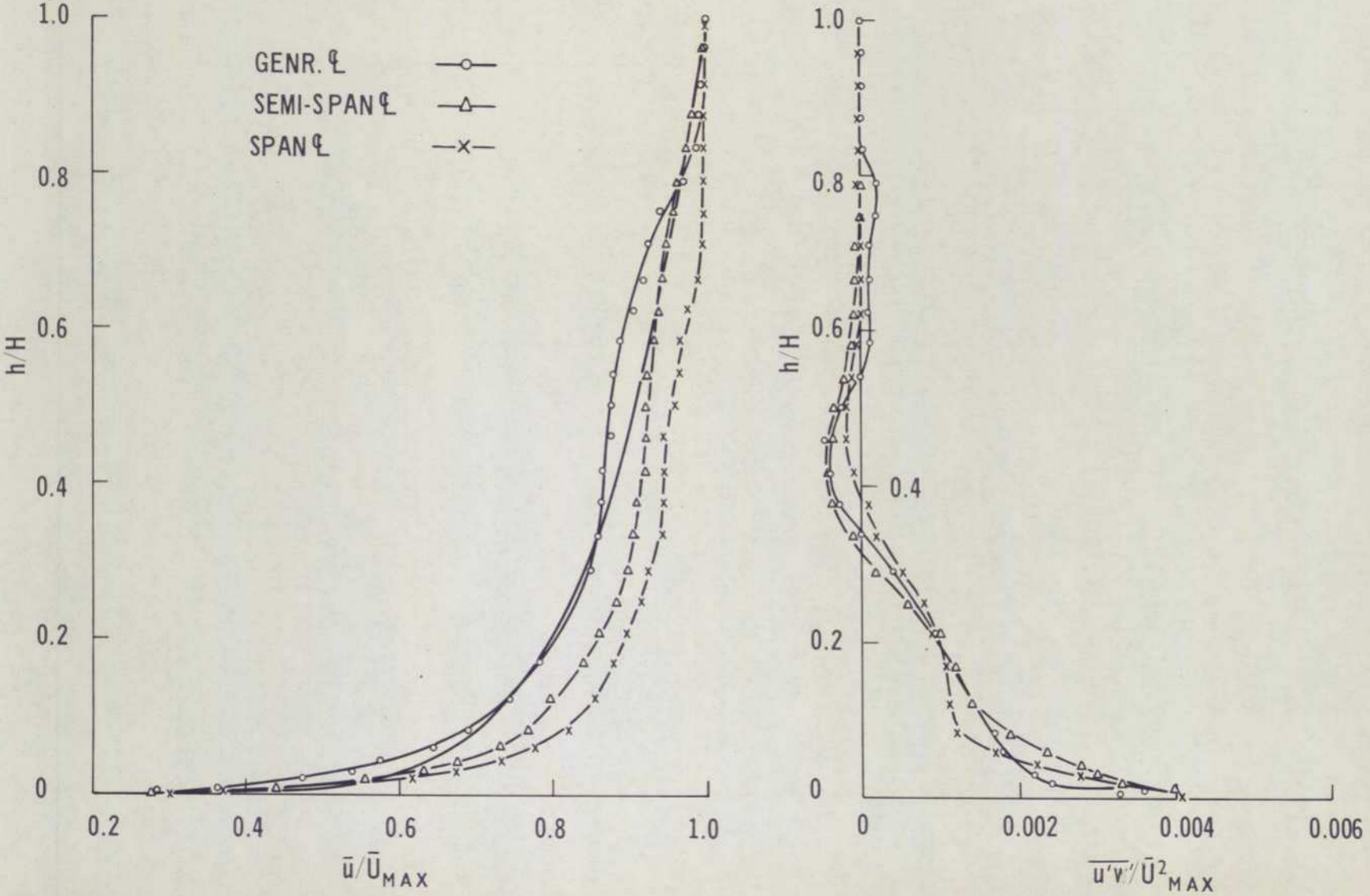


FIG. 32 ATMOSPHERIC BOUNDARY LAYER SIMULATION TESTS

JC/GH(CON)(30.9.68.)RL.3.3.1551

BARRIER 19.05mm (0.75in): E.W. GENERATORS 0.10472RADS (6^0)76.2mm (3in) APART: 'LEGO' BASEBOARDS AS ROUGHNESS

PLANE OF TRAVERSE - EQUIVALENT TO TURNTABLE L.E.

TRAVERSES WITH SURFACE ROUGHNESS ADDED

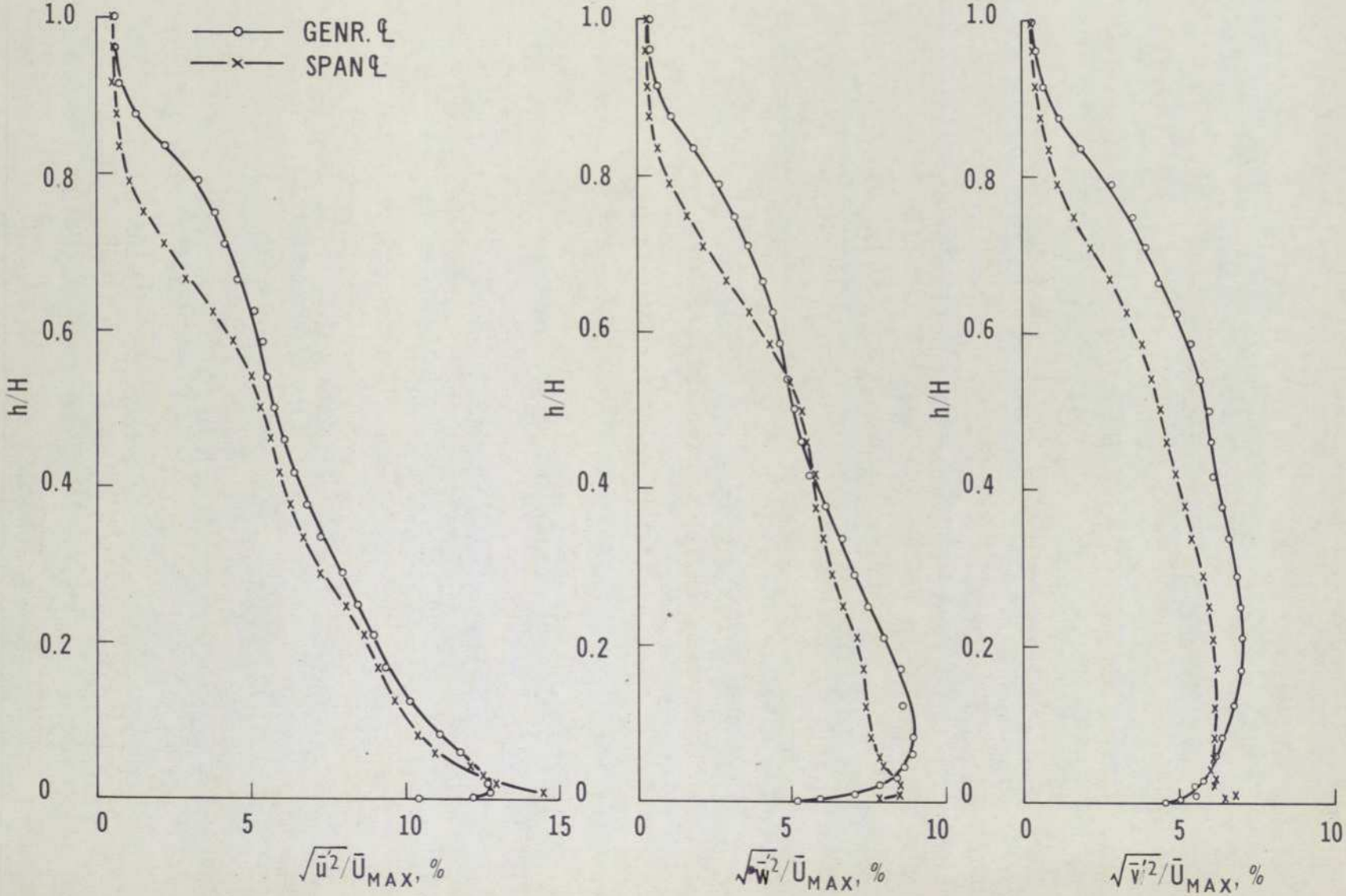


FIG.33. ATMOSPHERIC BOUNDARY LAYER SIMULATION TESTS

JC/GH(CON)(30.9.68.)RL.3.3.1552

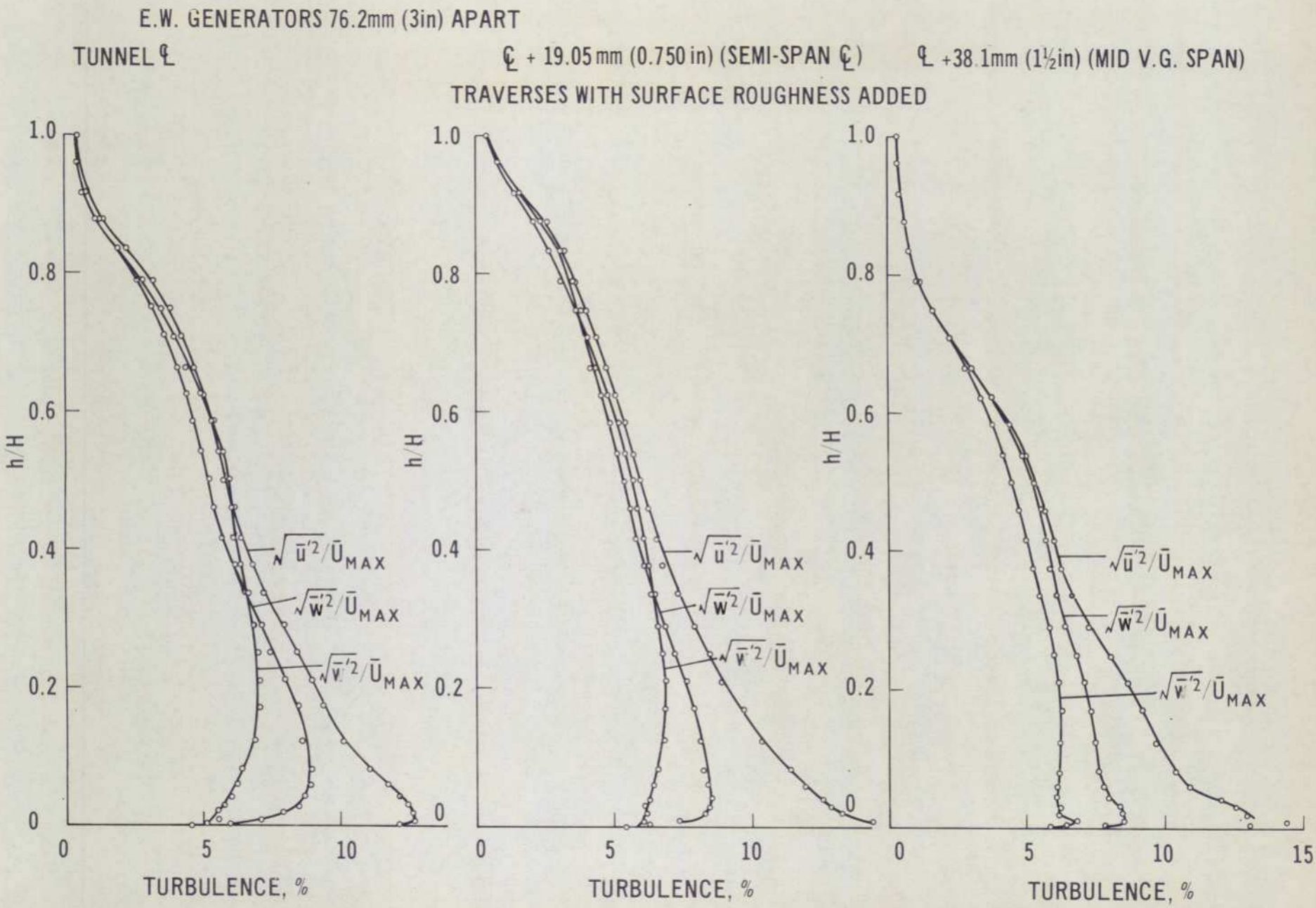


FIG. 34. ATMOSPHERIC BOUNDARY LAYER SIMULATION TESTS

JC/GH(CON)(30.9.68.)RL.3.3.1553

BARRIER 22.225mm (0.875in): E.W. GENERATORS (0.10472 RADS (6^0)) 88.9m (3.50in) APART
PLANE OF TRAVERSE EQUIVALENT TO TURNTABLE L.E.
TRAVERSES WITH SURFACE ROUGHNESS ADDED

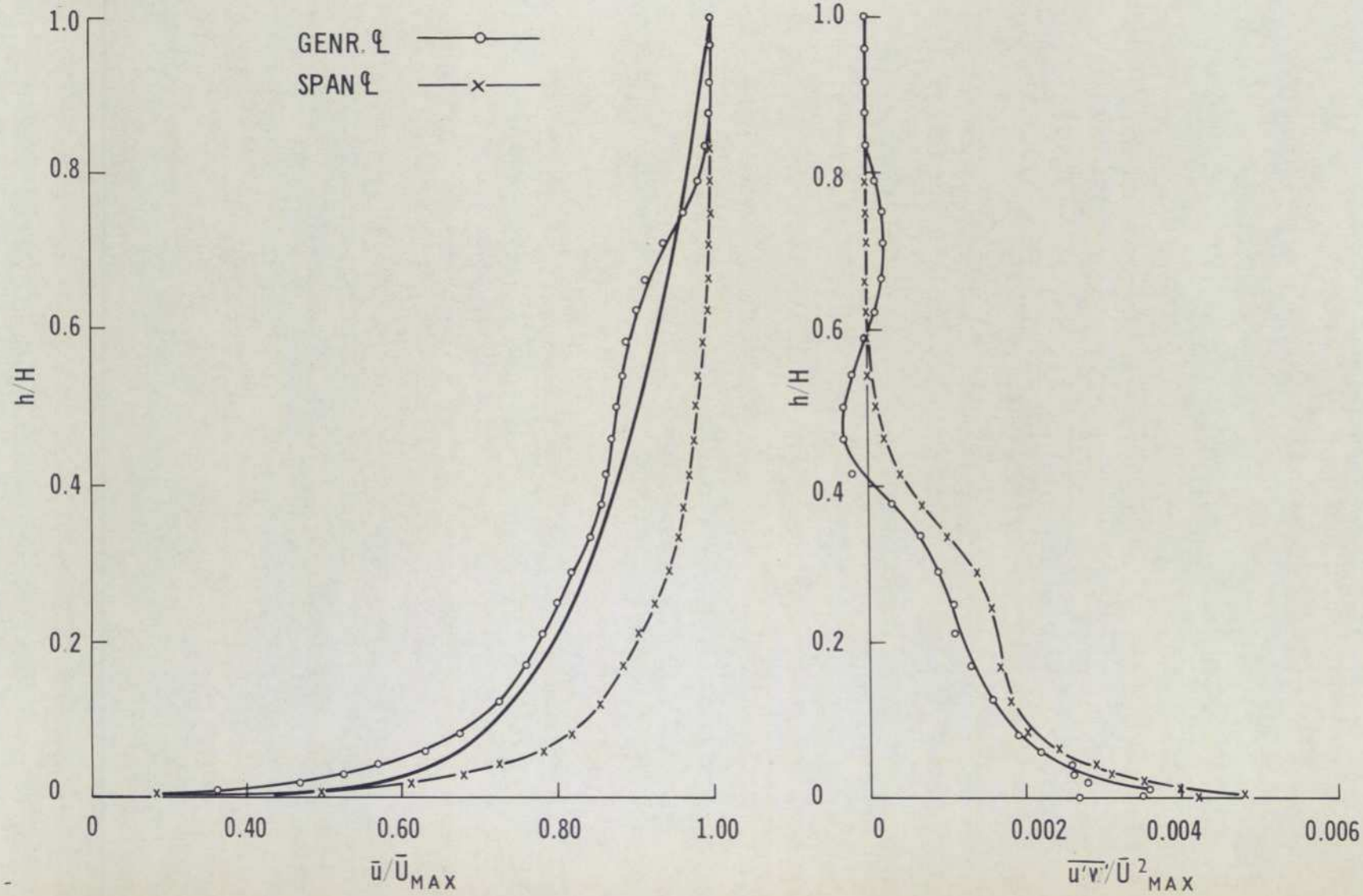


FIG. 35. ATMOSPHERIC BOUNDARY LAYER SIMULATION TESTS

JC/GH(CON)(30.9.68.)RL.3.3.1554

BARRIER, 22.225mm (0.875in): E.W. GENERATORS (0.10472RADS (6^0)) 88.90mm ($3\frac{1}{2}$in) APART
PLANE OF TRAVERSE EQUIVALENT TO TURNTABLE L.E.
TRAVERSES WITH SURFACE ROUGHNESS ADDED

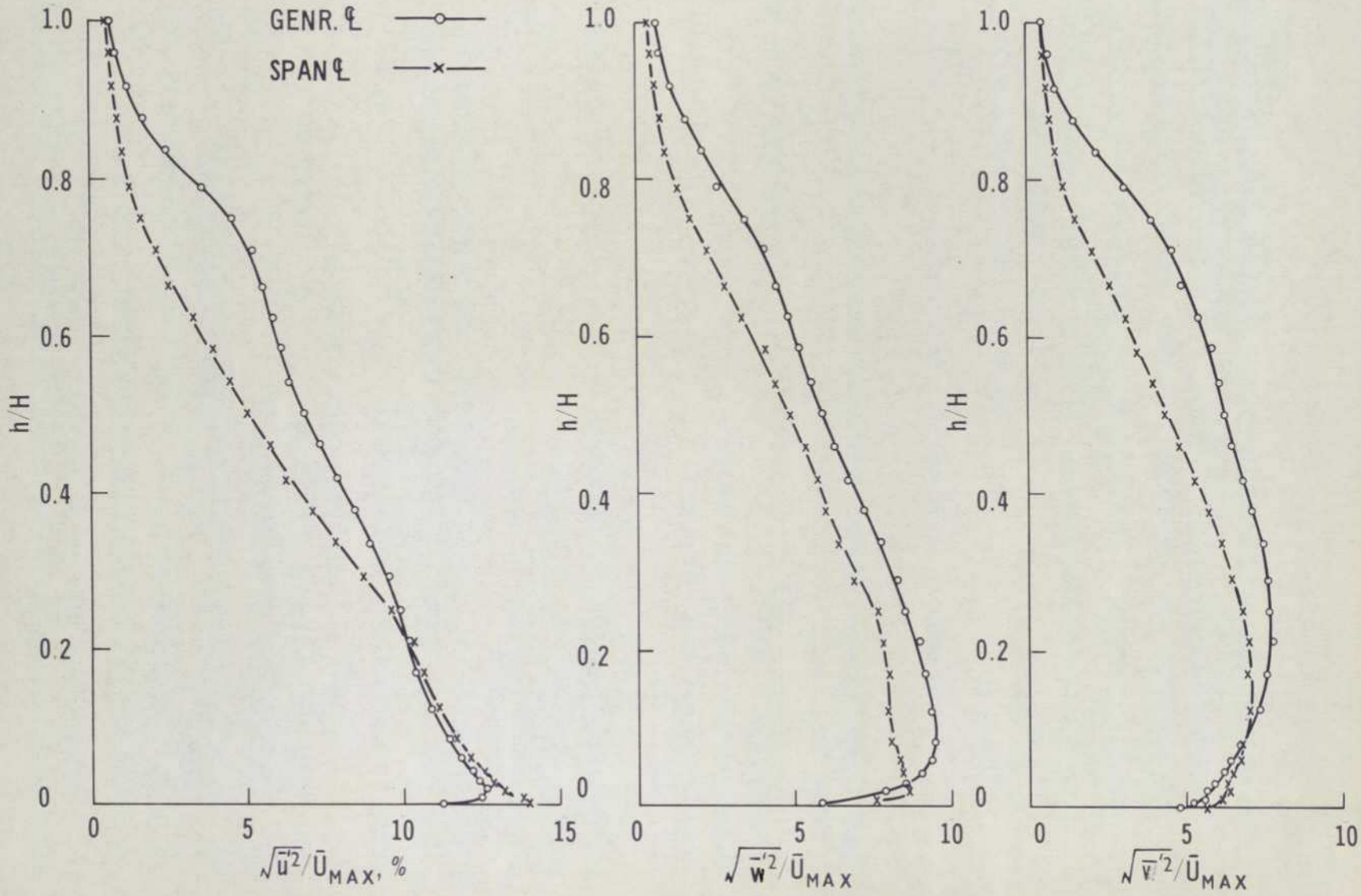
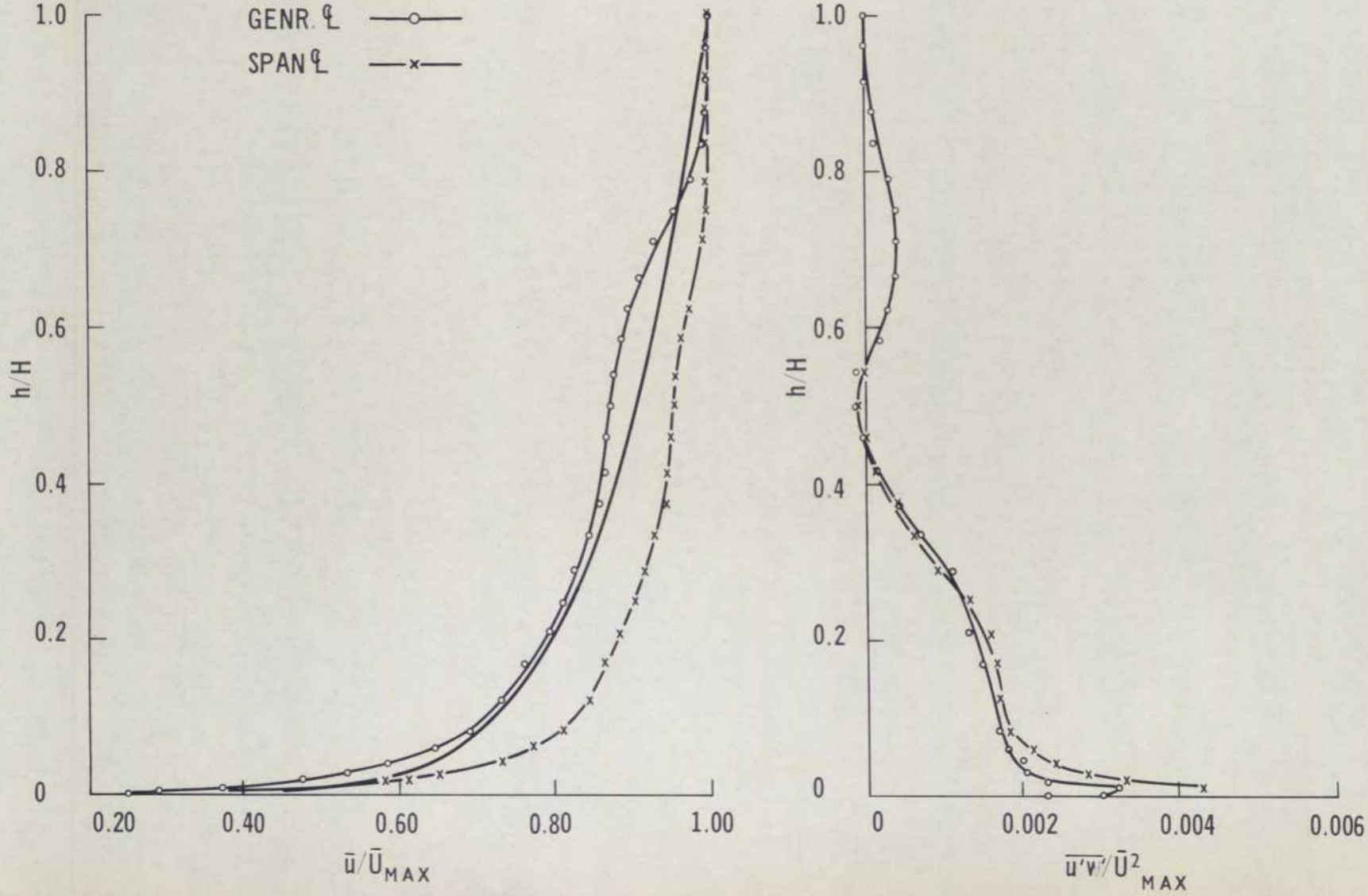


FIG. 36. ATMOSPHERIC BOUNDARY LAYER SIMULATION TESTS

JC/GH(CON)(30.9.68.)RL.3.3.1555

BARRIER 22.225mm (0.875in): E.W. GENERATORS (0.10472 RADS (6^0)) 76.2mm (3in) APART
PLANE OF TRAVERSE EQUIVALENT TO TURNTABLE L.E.
TRAVERSES WITH SURFACE ROUGHNESS ADDED



JC/GH(CON)(30.9.68)RL.3.3.1556

FIG. 37. ATMOSPHERIC BOUNDARY LAYER SIMULATION TESTS

BARRIER 22.225mm (0.875in): E.W. GENERATORS (0.10472 RADS (6^0)) 76.2mm (3in) APART
PLANE OF TRAVERSE EQUIVALENT TO TURNTABLE L.E.
TRAVERSES WITH SURFACE ROUGHNESS ADDED

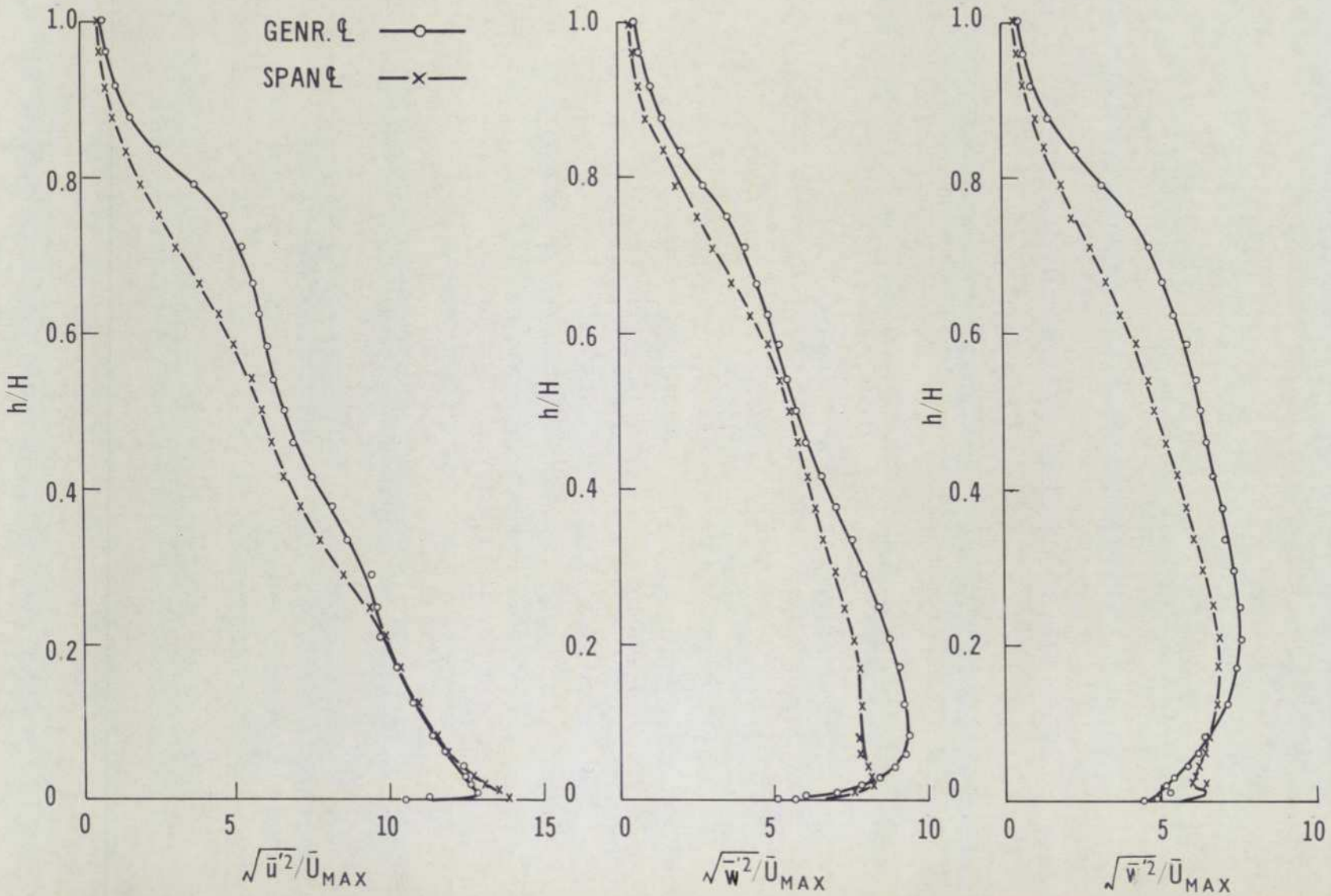


FIG. 3 8. ATMOSPHERIC BOUNDARY LAYER SIMULATION TESTS

JC/GH(CON)(30.9.68.)RL.3.3.1557

ELLIPTIC WEDGE 0.10472 RADS (6^0) V.G. SPACING 76.2mm (3in): BARRIER HEIGHT 22.225mm (0.875in) + MOD. A.
TRAVERSE AT 457.2mm (18in) FROM V.G. TRAILING EDGE
TRAVERSES WITH SURFACE ROUGHNESS ADDED

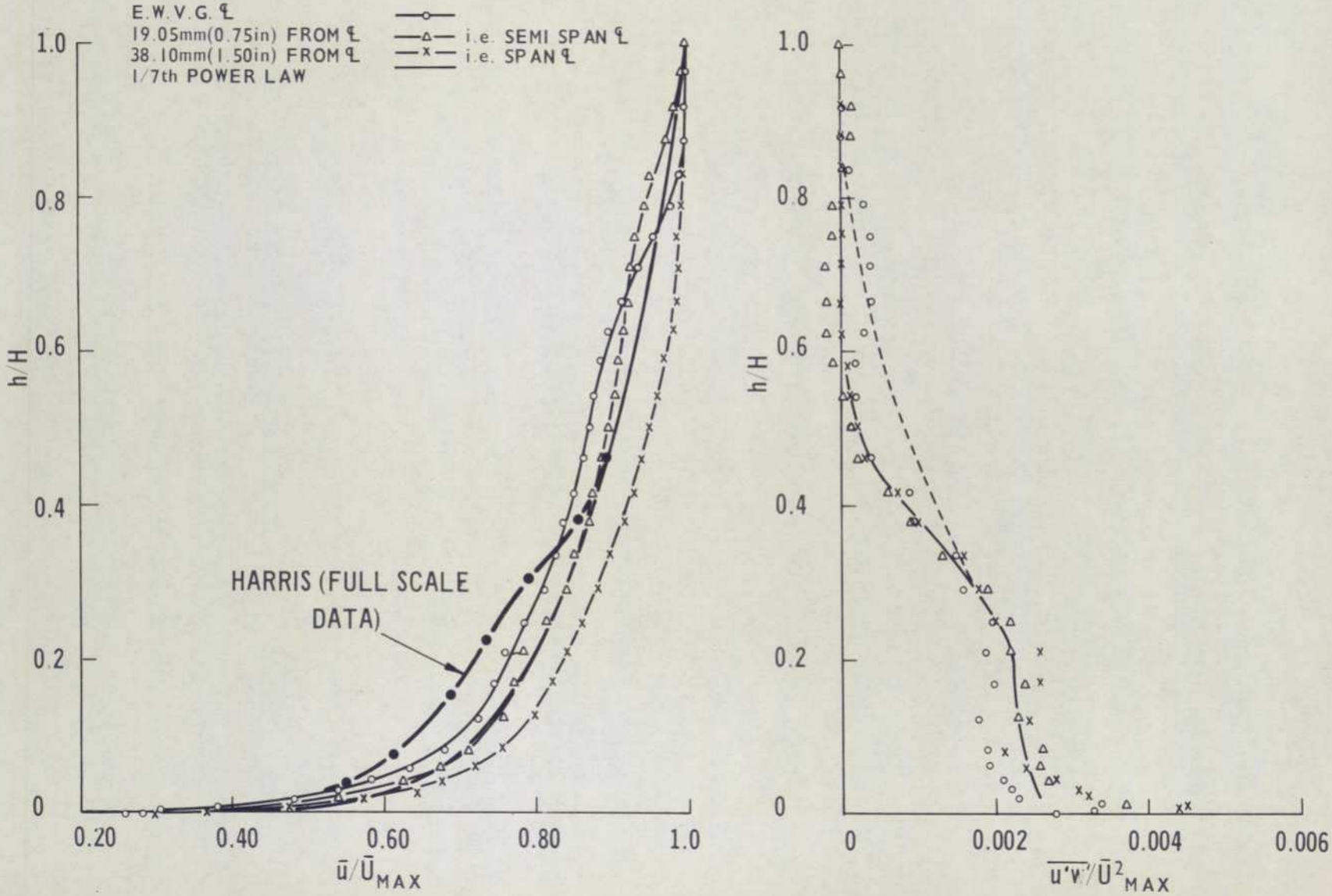


FIG. 39. ATMOSPHERIC BOUNDARY LAYER SIMULATION TESTS

JC/GH(CON)(30.9.68.)RL.3.3.1558

ELLIPTIC WEDGE 0.10472 RADS(6^0) V.G. SPACING 76.2mm(3in): BARRIER HEIGHT 22.225mm (0.875in)+MOD. A
TRAVERSE AT 457.2mm (18in) FROM V.G. TRAILING EDGE
TRAVERSES WITH SURFACE ROUGHNESS ADDED

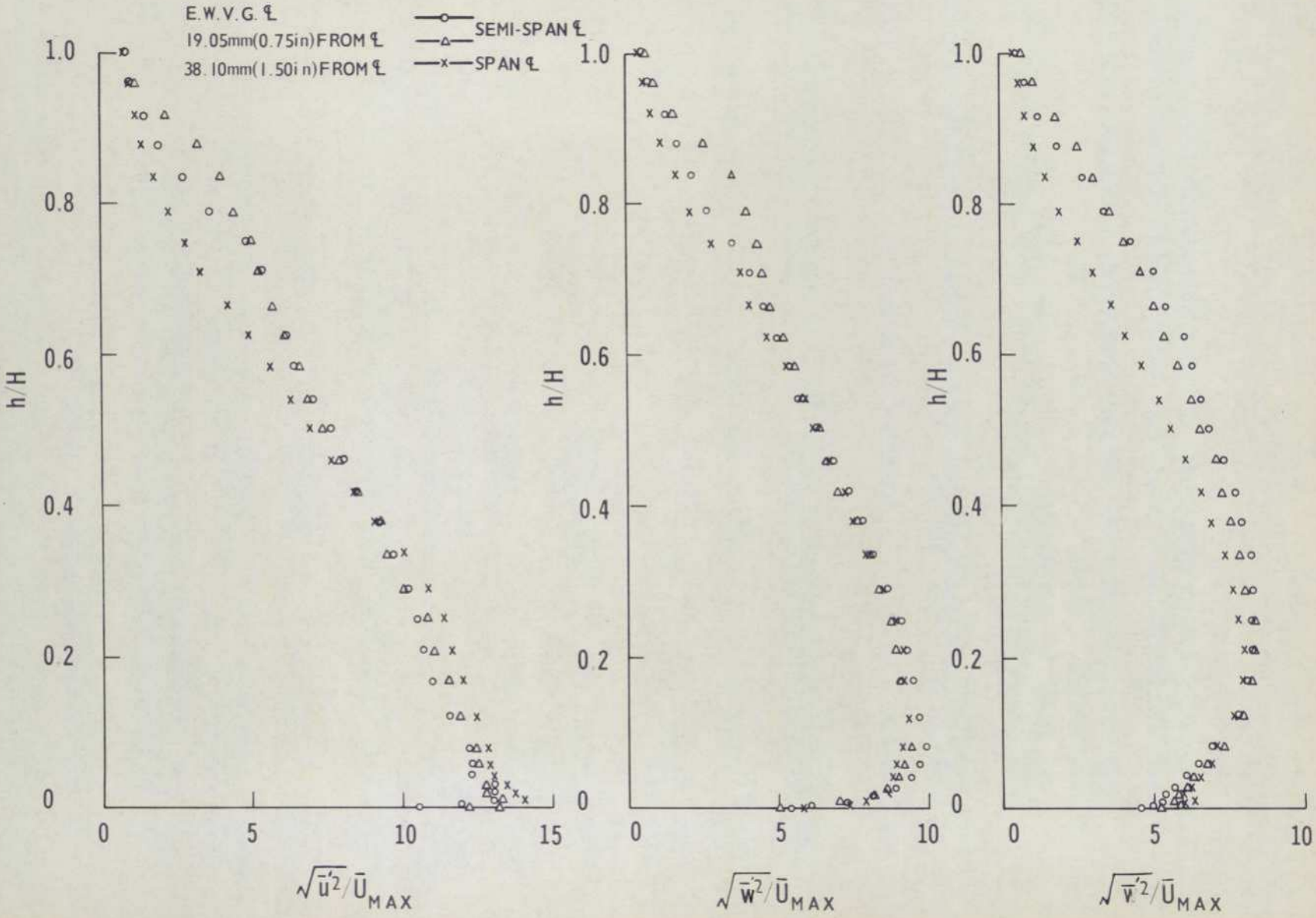
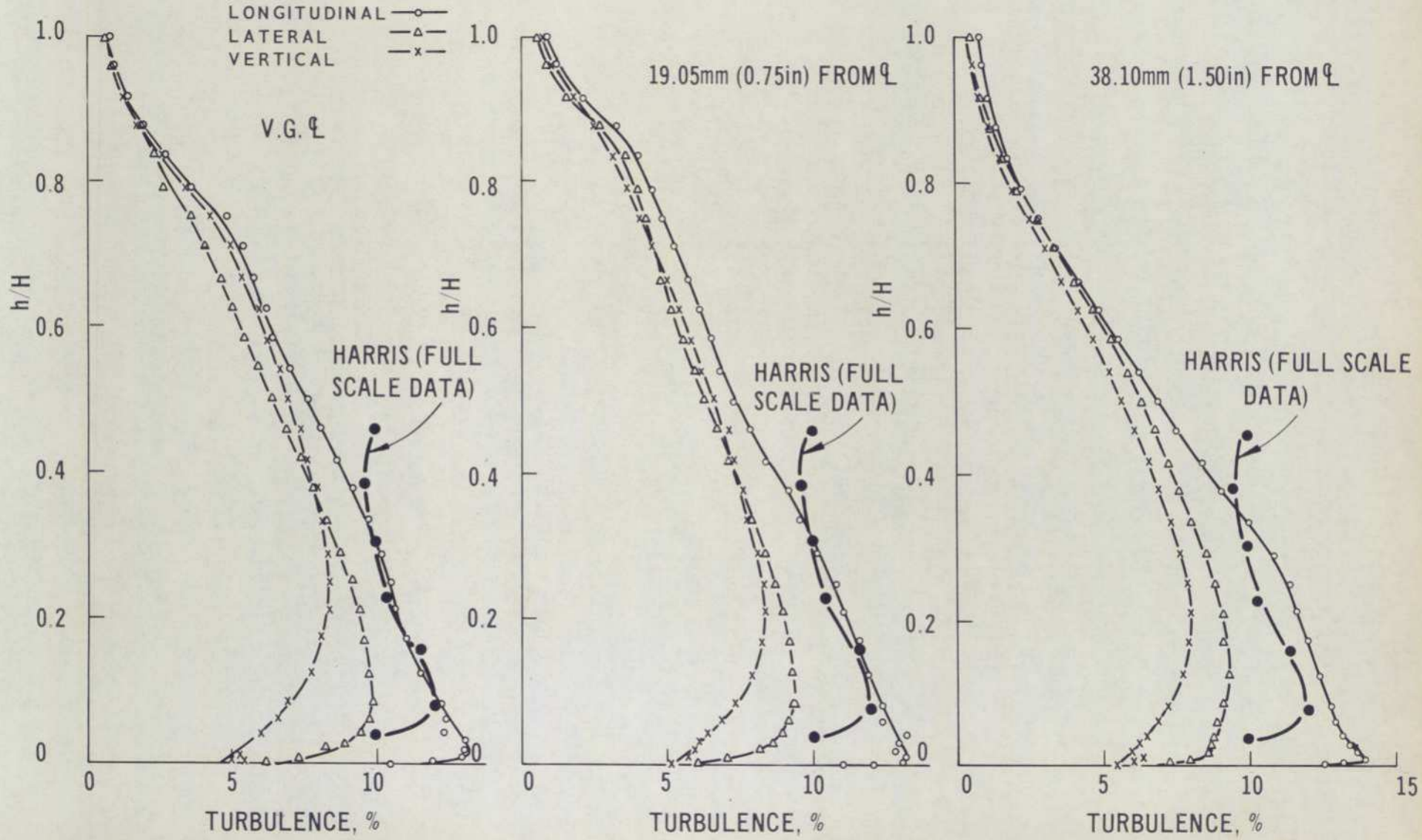


FIG. 40. ATMOSPHERIC BOUNDARY LAYER SIMULATION TESTS

JC/GH(CON)(30.9.68.)RL.3.3.1559

ELLIPTIC WEDGE 0.10472 RADS (6^0) V.G. SPACING 76.2mm (3in): BARRIER HEIGHT 22.225mm (0.875in)+MOD. A
TRAVERSES AT 457.2mm (18in) FROM V.G. TRAILING EDGE
TRAVERSES WITH SURFACE ROUGHNESS ADDED



JC/GH(CON)(30.9.68)RL.3.3.1560

FIG.41 ATMOSPHERIC BOUNDARY LAYER SIMULATION TESTS

ELLIPTIC WEDGE 0.10472 RADS (6^0) V.G. SPACING 76.2mm (3in): BARRIER HEIGHT 22.225mm (0.875in)+MOD. A
TRAVERSE 228.6mm (9in) FROM V.G. TRAILING EDGE
TRAVERSES WITH SURFACE ROUGHNESS ADDED

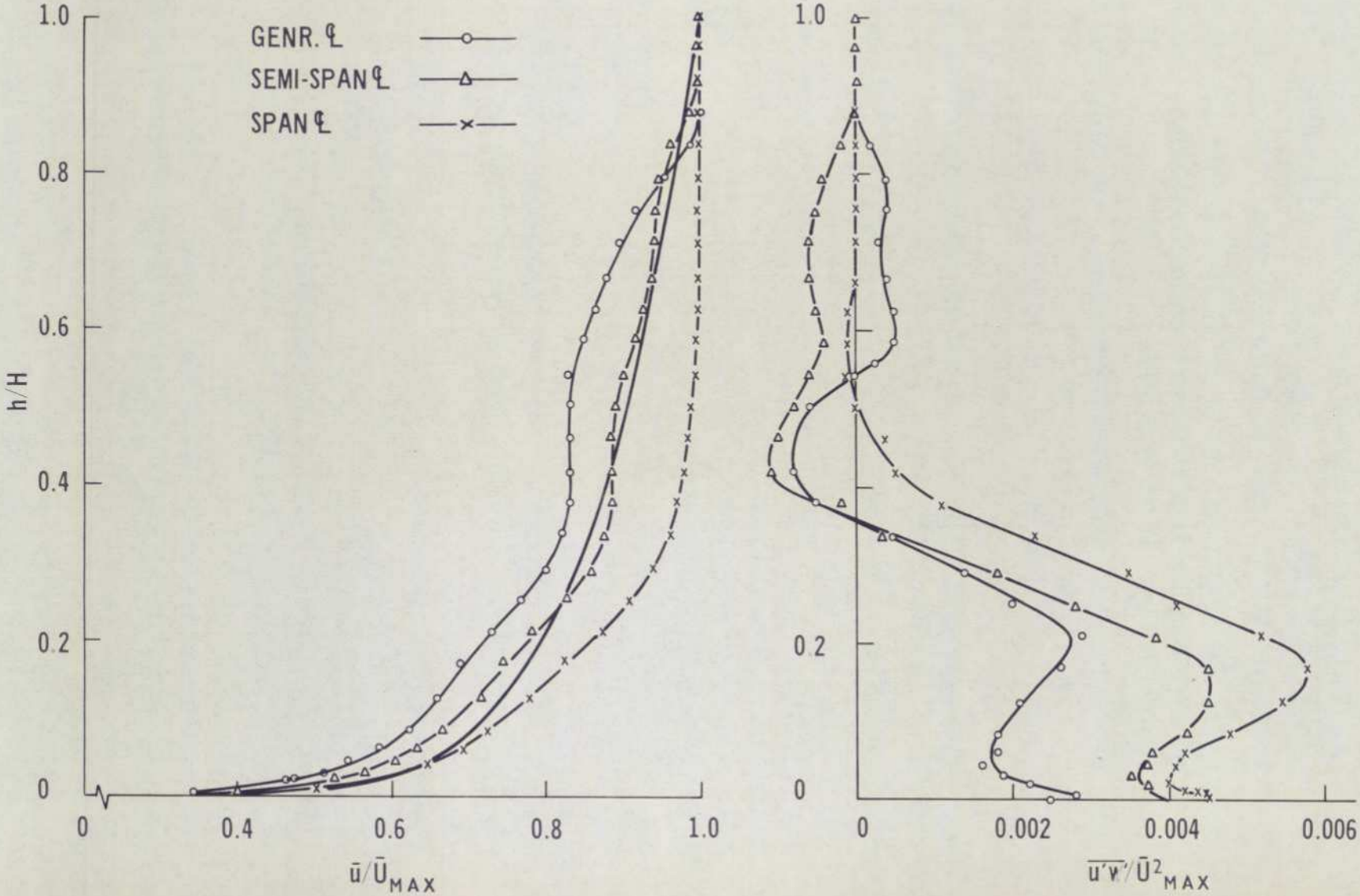


FIG.42 ATMOSPHERIC BOUNDARY LAYER SIMULATION TESTS

JC/GH(CON)(30.9.68.)RL.3.3.1561

ELLIPTIC WEDGE 0.10472 RADS (6°) V.G. SPACING 76.2mm (3in): BARRIER HEIGHT 22.225mm (0.875in)+MOD. A
TRAVERSE 228.6mm (9in) FROM V.G. TRAILING EDGE
TRAVERSES WITH SURFACE ROUGHNESS ADDED

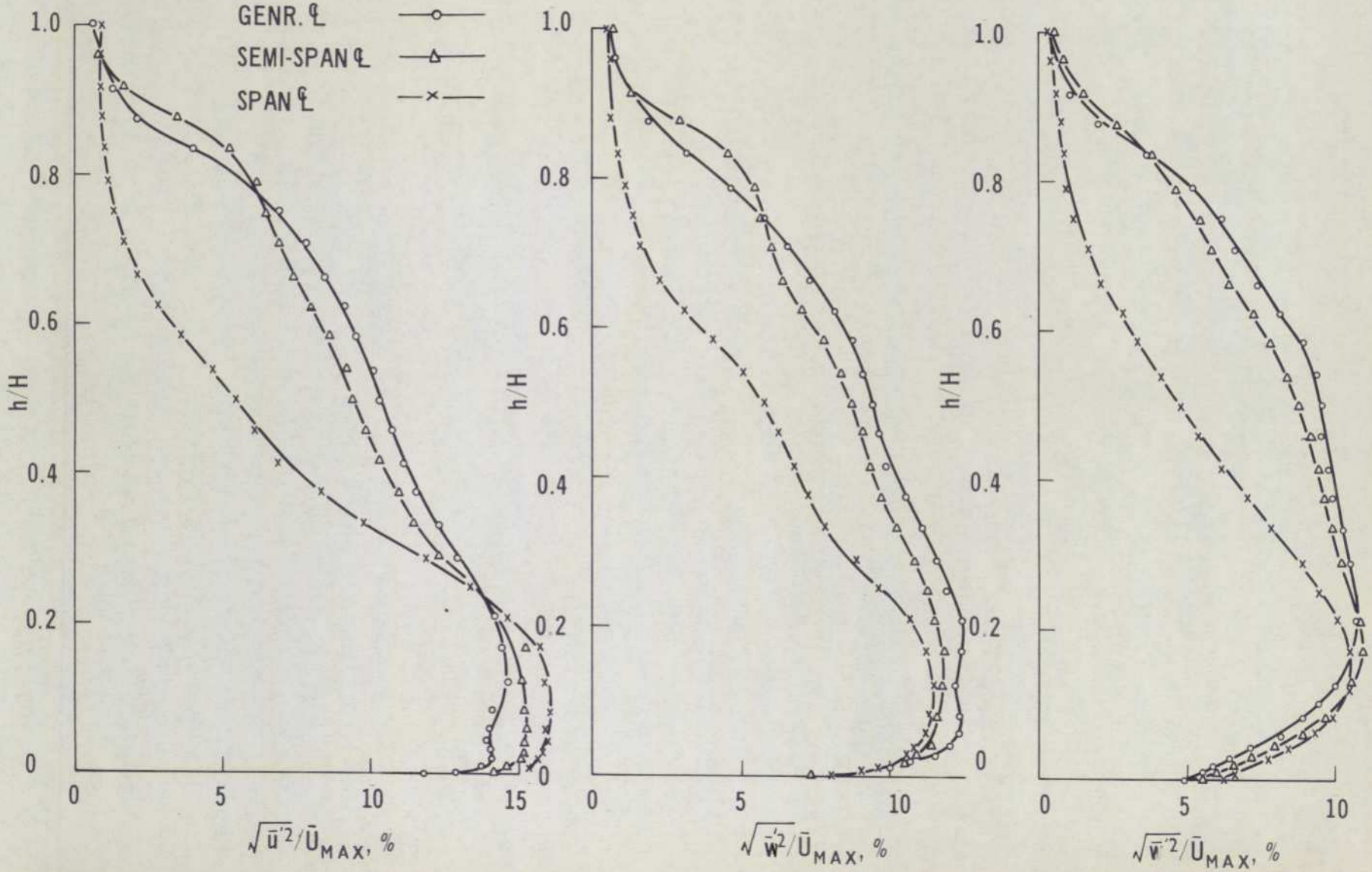


FIG. 43. ATMOSPHERIC BOUNDARY LAYER SIMULATION TESTS

JC/GH(CON)(30.9.68.)RL.3.3.1562

ELLIPTIC WEDGE 0.10472 RADS (6^0) V.G. SPACING 76.2mm (3in): BARRIER HEIGHT 22.225mm (0.875in)+MOD. A
TRAVERSE 685.8mm (27in) FROM V.G. TRAILING EDGE
TRAVERSES WITH SURFACE ROUGHNESS ADDED

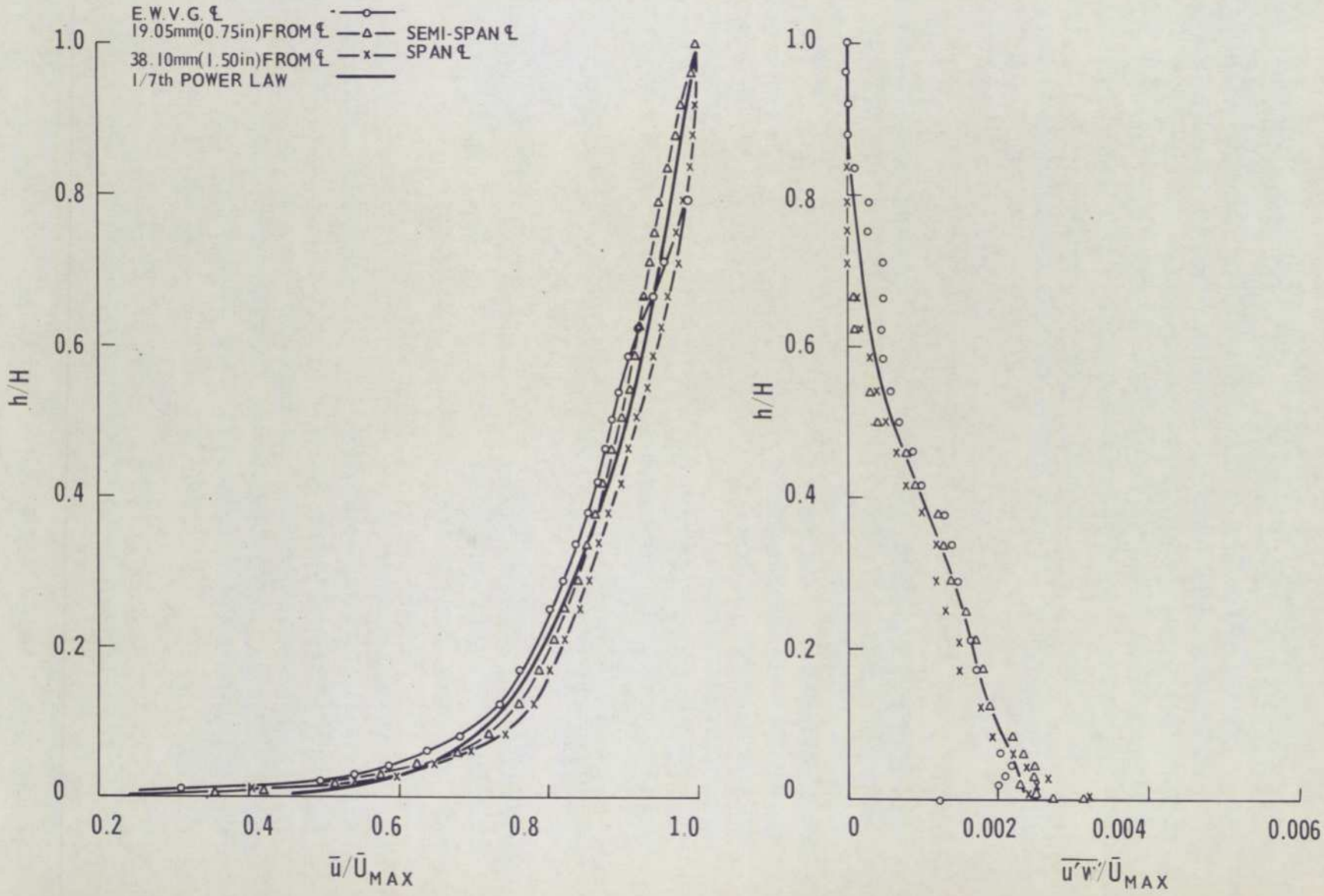


FIG. 44. ATMOSPHERIC BOUNDARY LAYER SIMULATION TESTS

JC/GH(CON)(30.9.68.)RL.3.3.1563

ELLIPTIC WEDGE 0.10472 RADS. (6°) _ V.G. SPACING 76.2mm (3IN) _ BARRIER HEIGHT 22.225mm (.875IN) + MODA

TRAVERSE 685.8mm (27IN) FROM V.G. TRAILING EDGE

TRAVERSES WITH SURFACE ROUGHNESS ADDED.

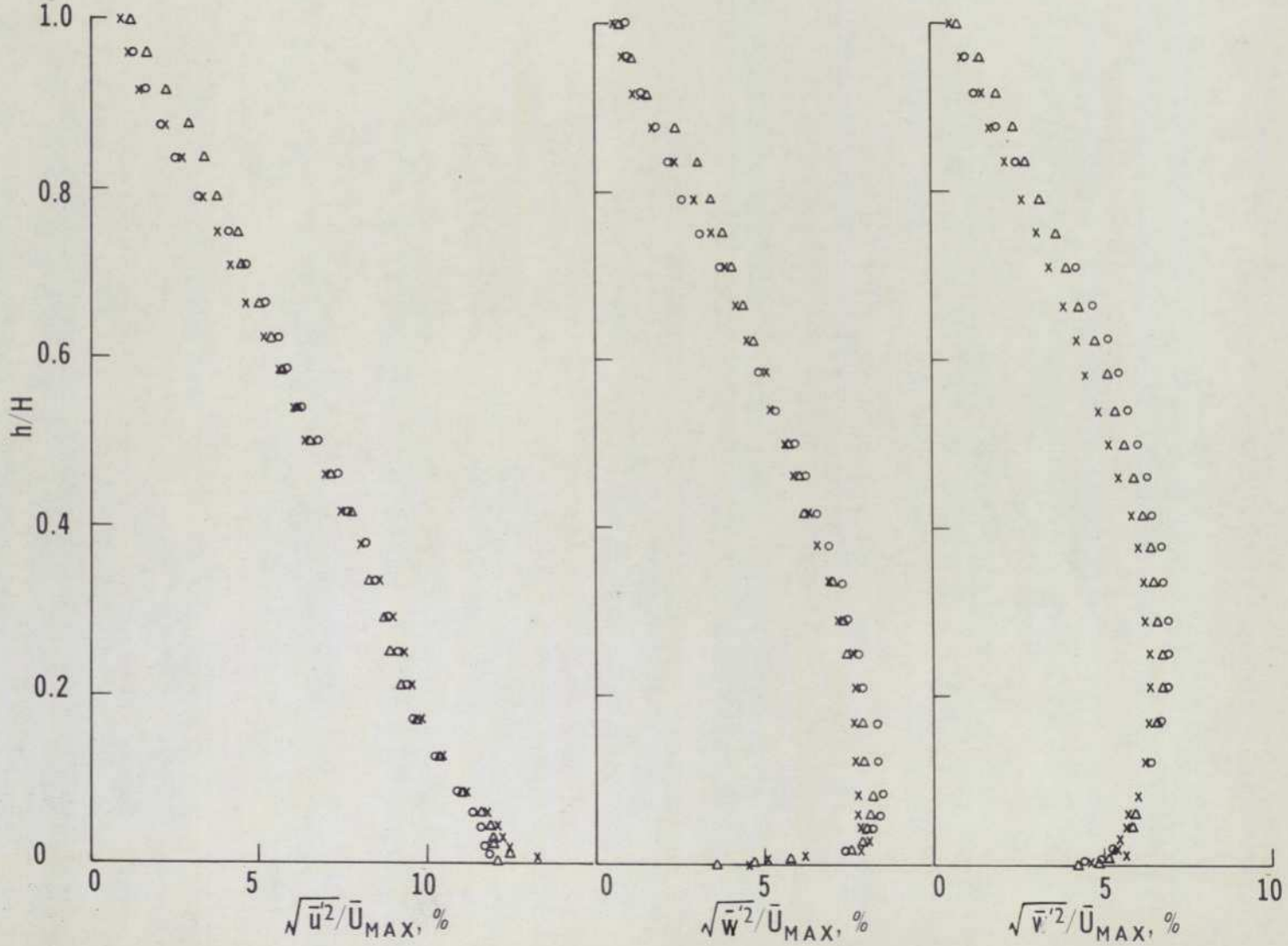
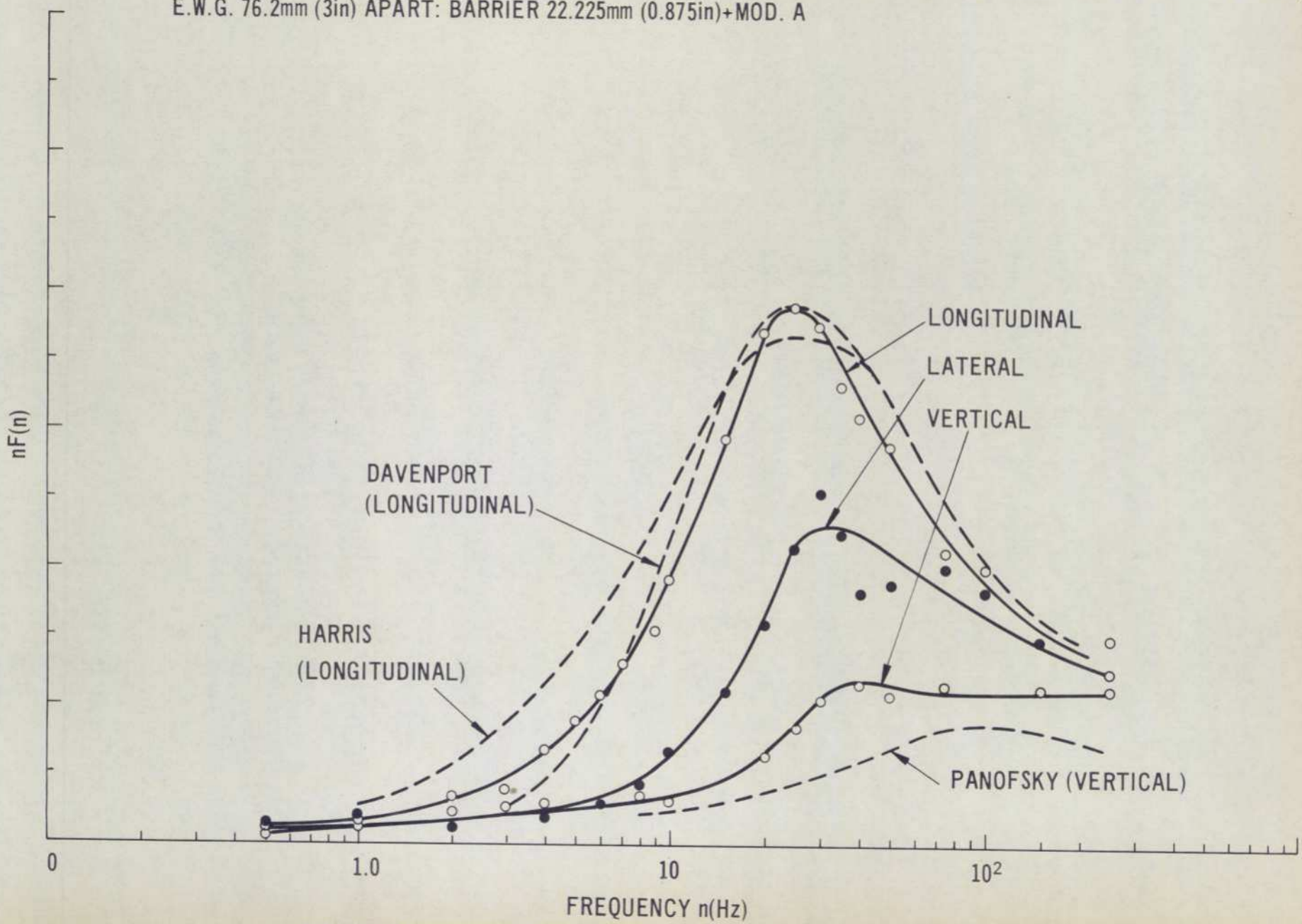


FIG. 45. ATMOSPHERIC BOUNDARY LAYER SIMULATION TESTS

D8677

JC/GH(CON)(30.9.68.)RL.3.3.1564



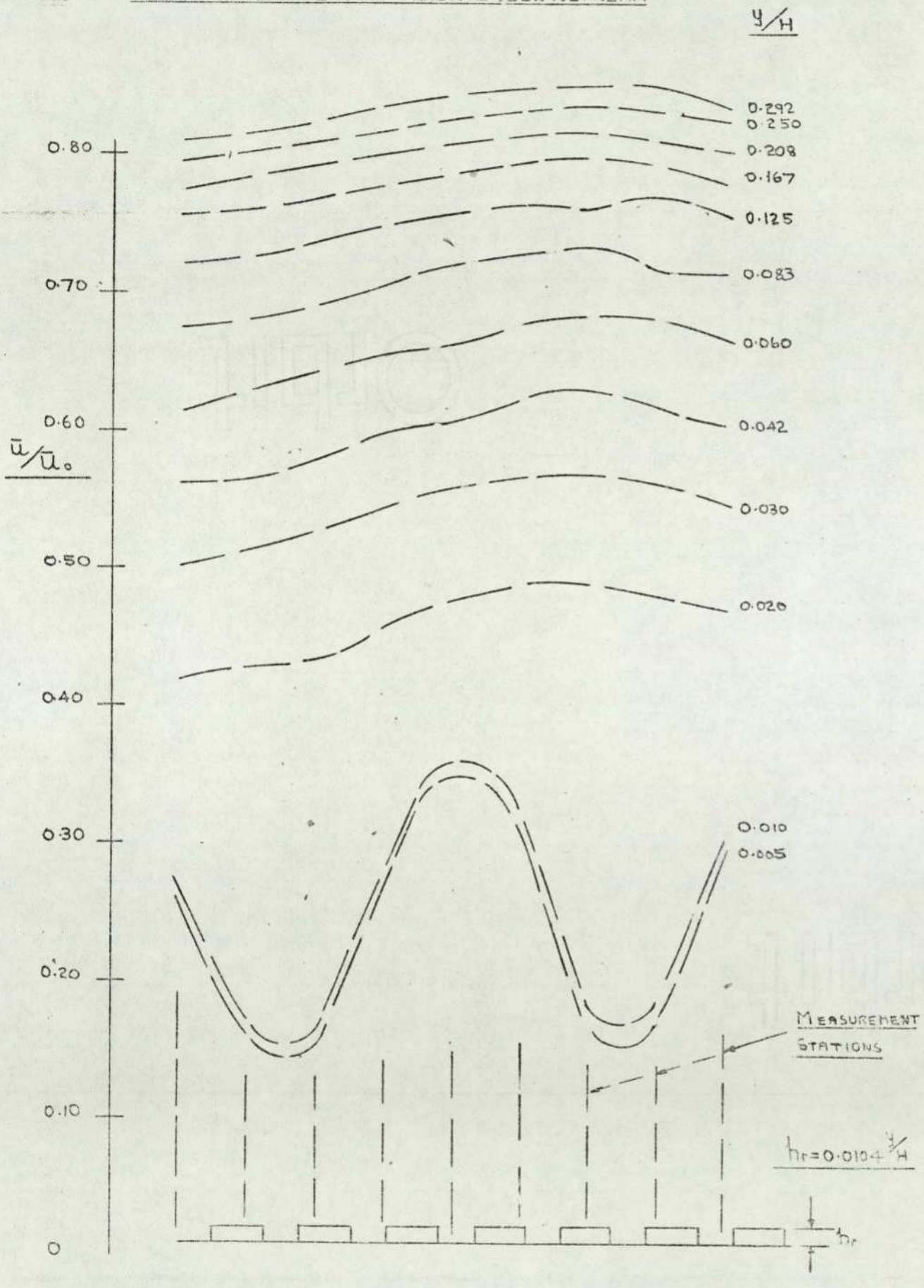
JC/GH(CON)(30.9.68)RL.3.3.1565

FIG.46 ATMOSPHERIC BOUNDARY LAYER SIMULATION TESTS

ATMOSPHERIC BOUNDARY LAYER SIMULATION.

FIG. 47 SPANWISE VARIATION OF MEAN VELOCITY

4½ BOUNDARY LAYER HEIGHTS DOWNSTREAM



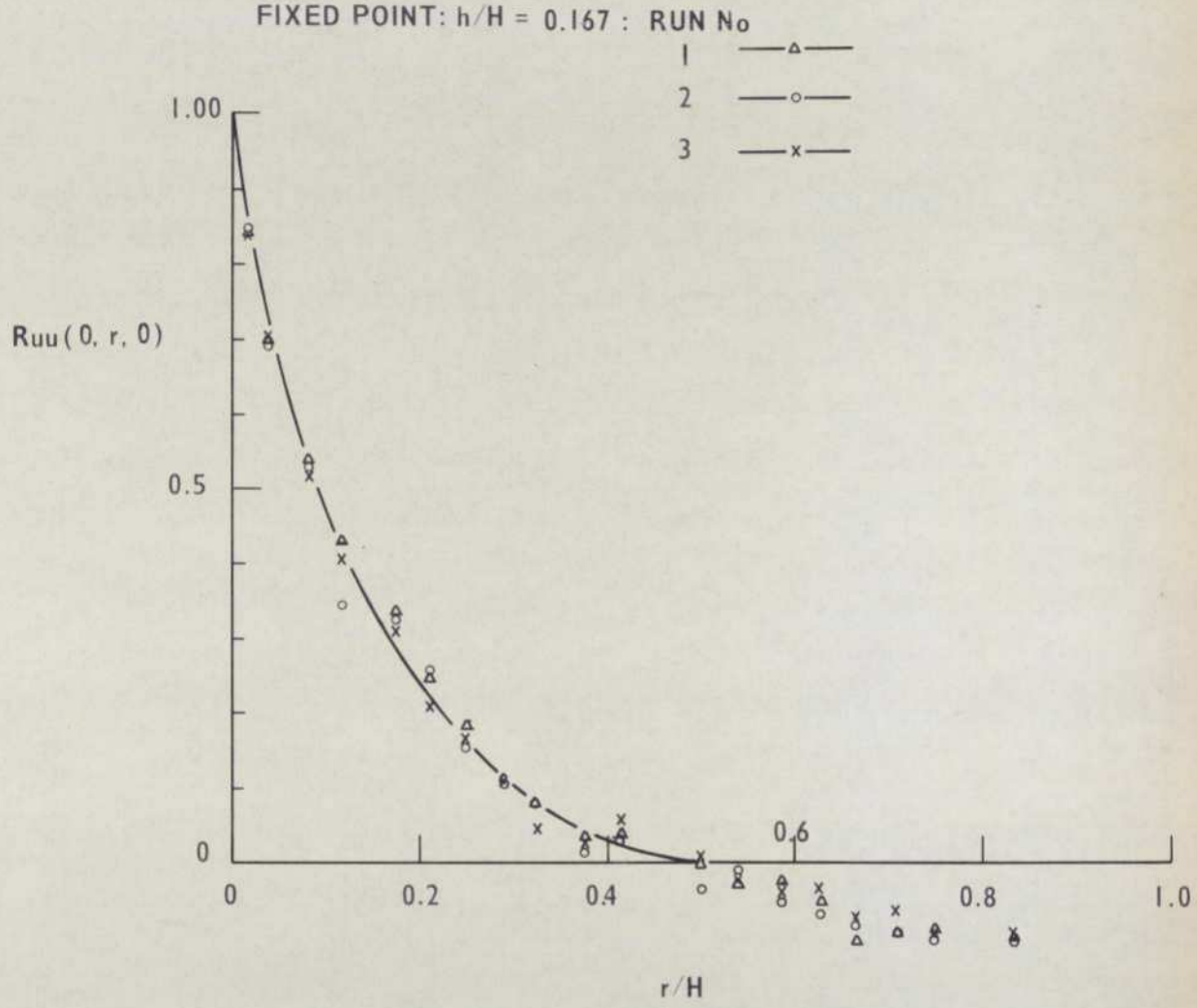


FIG.48 REPEATIBILITY OF CORRELATION COEFFICIENT MEASUREMENTS IN A SIMULATED BOUNDARY LAYER. 457mm (18in) AFT OF GENERATOR T.E. MID SPAN OF GENERATORS

VERTICAL CORRELATION OF LONGITUDINAL VELOCITY COMPONENT

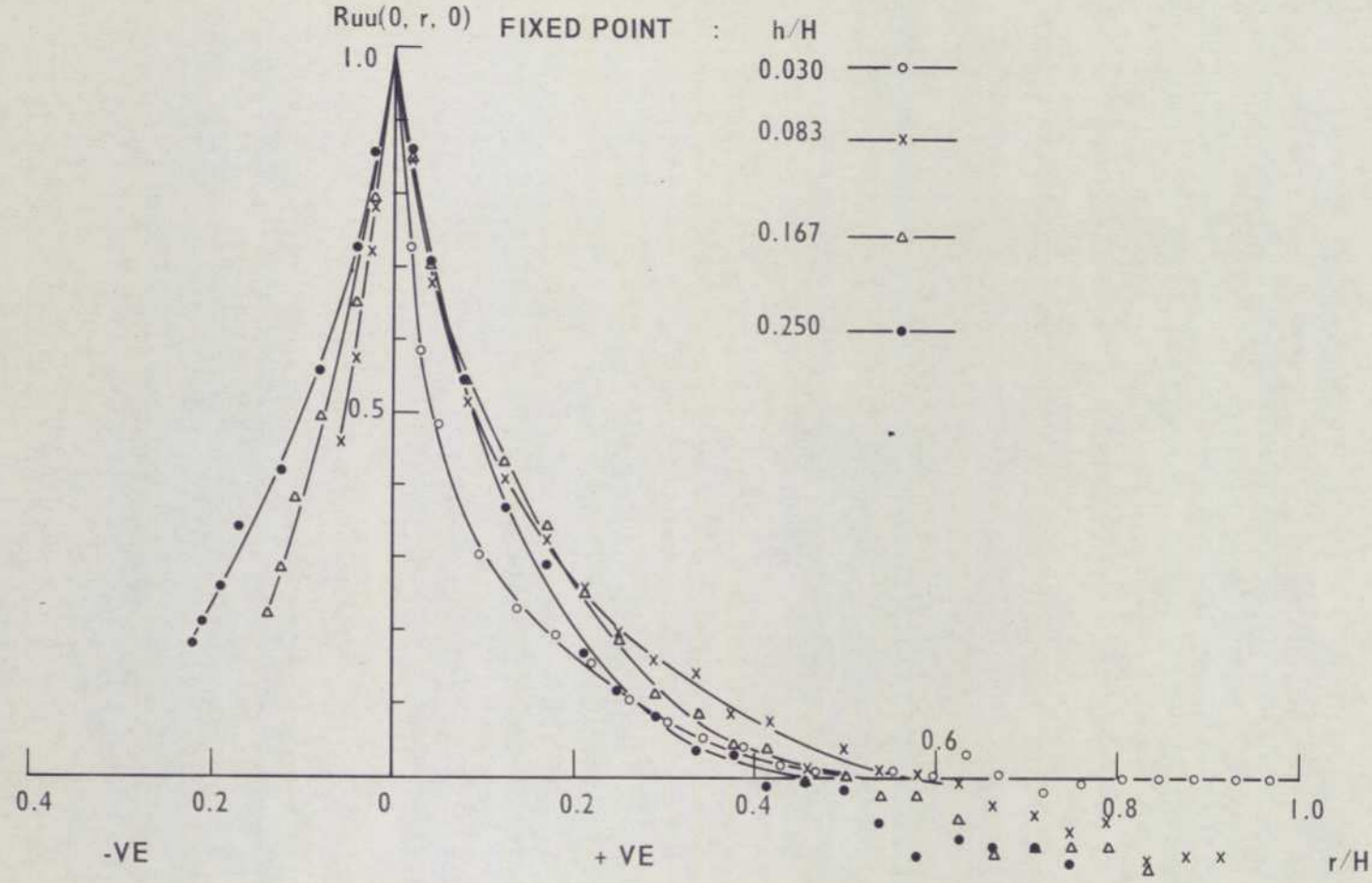


FIG.49 CORRELATION COEFFICIENT DISTRIBUTION IN A SIMULATED BOUNDARY LAYER 457mm(18in) AFT OF VORTICITY GENERATOR TRAILING EDGES.SPANWISE POSITION - GENERATOR MID-SPAN

JC/G.H.LTD.(CON)(22.5.69) RL3.3.1862

VERTICAL CORRELATION OF LONGITUDINAL VELOCITY COMPONENT

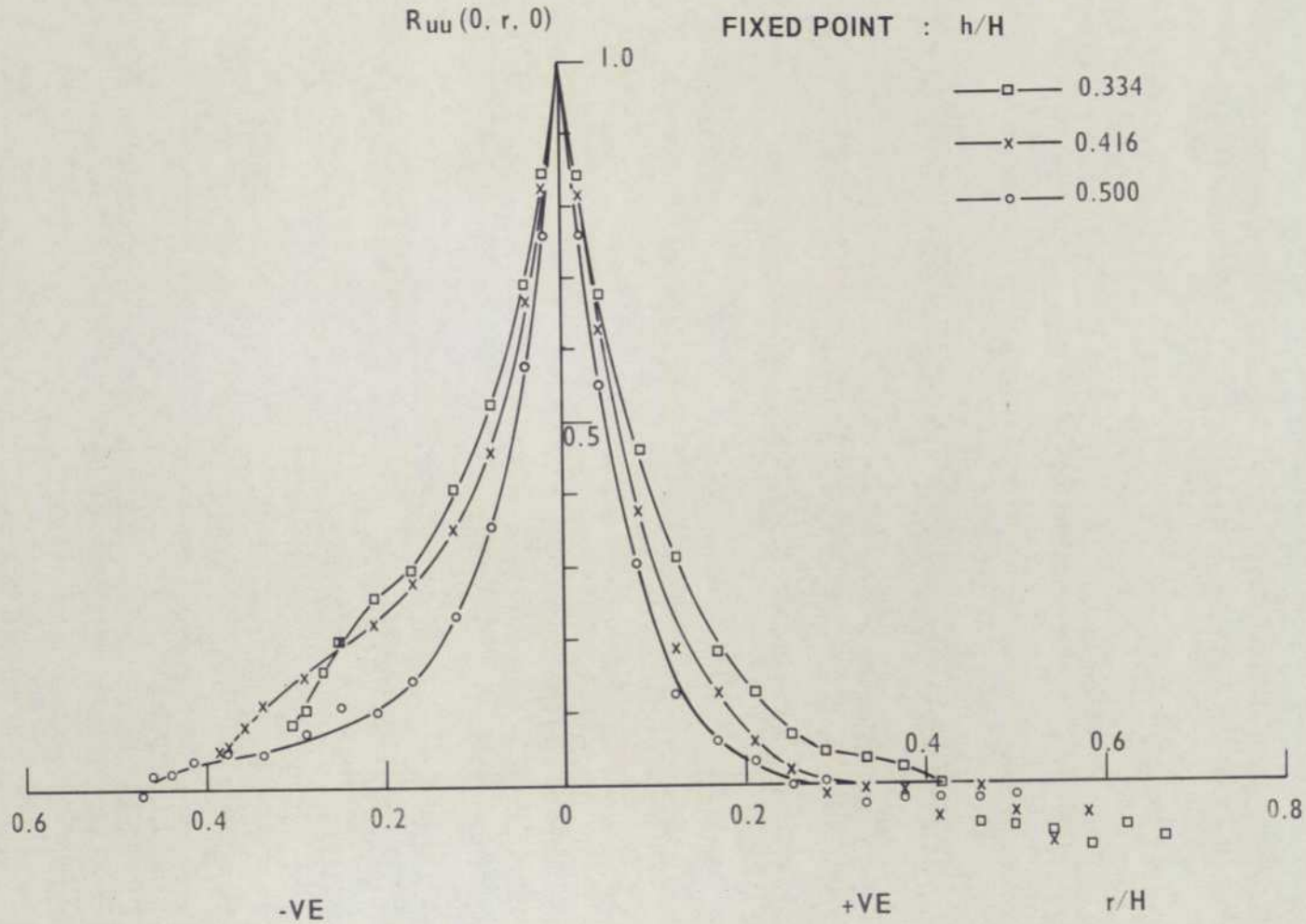


FIG.50. CORRELATION COEFFICIENT DISTRIBUTION IN A SIMULATED BOUNDARY LAYER 457mm (18 in) AFT OF VORTICITY GENERATOR TRAILING EDGES.SPANWISE POSITION - GENERATOR MID-SPAN

JC/G.H.Ltd.(CON)(22.5.69)RL.3.3.1863

VERTICAL CORRELATION OF LONGITUDINAL VELOCITY COMPONENT

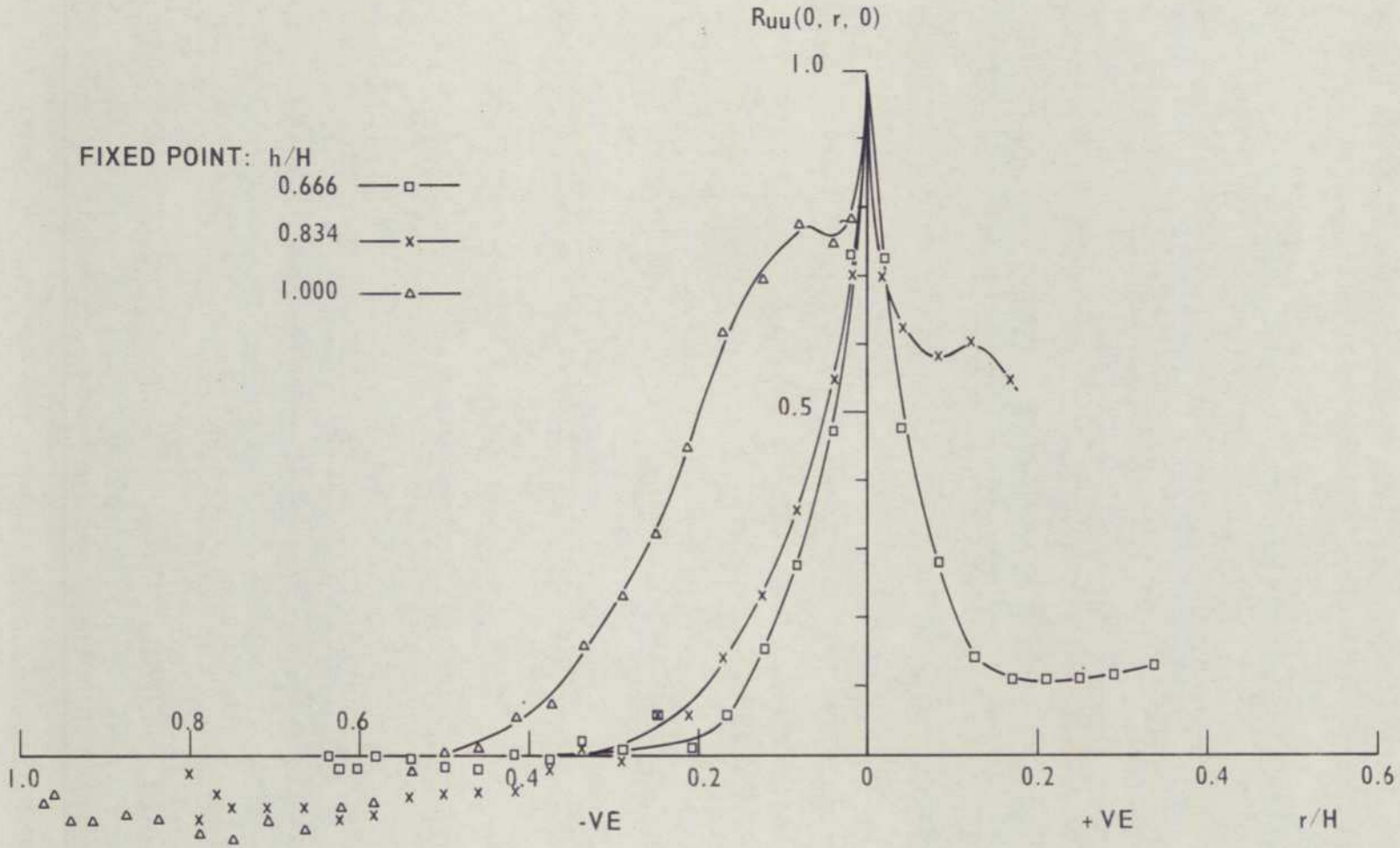


FIG. 51. CORRELATION COEFFICIENT DISTRIBUTION IN A SIMULATED BOUNDARY LAYER 457mm(18in) AFT OF VORTICITY GENERATOR TRAILING EDGES. SPANWISE POSITION - GENERATOR MID-SPAN

JC/G.H.LTD.(CON)(22.5.69) RL 3.3.1864

VERTICAL CORRELATION OF LONGITUDINAL VELOCITY COMPONENT

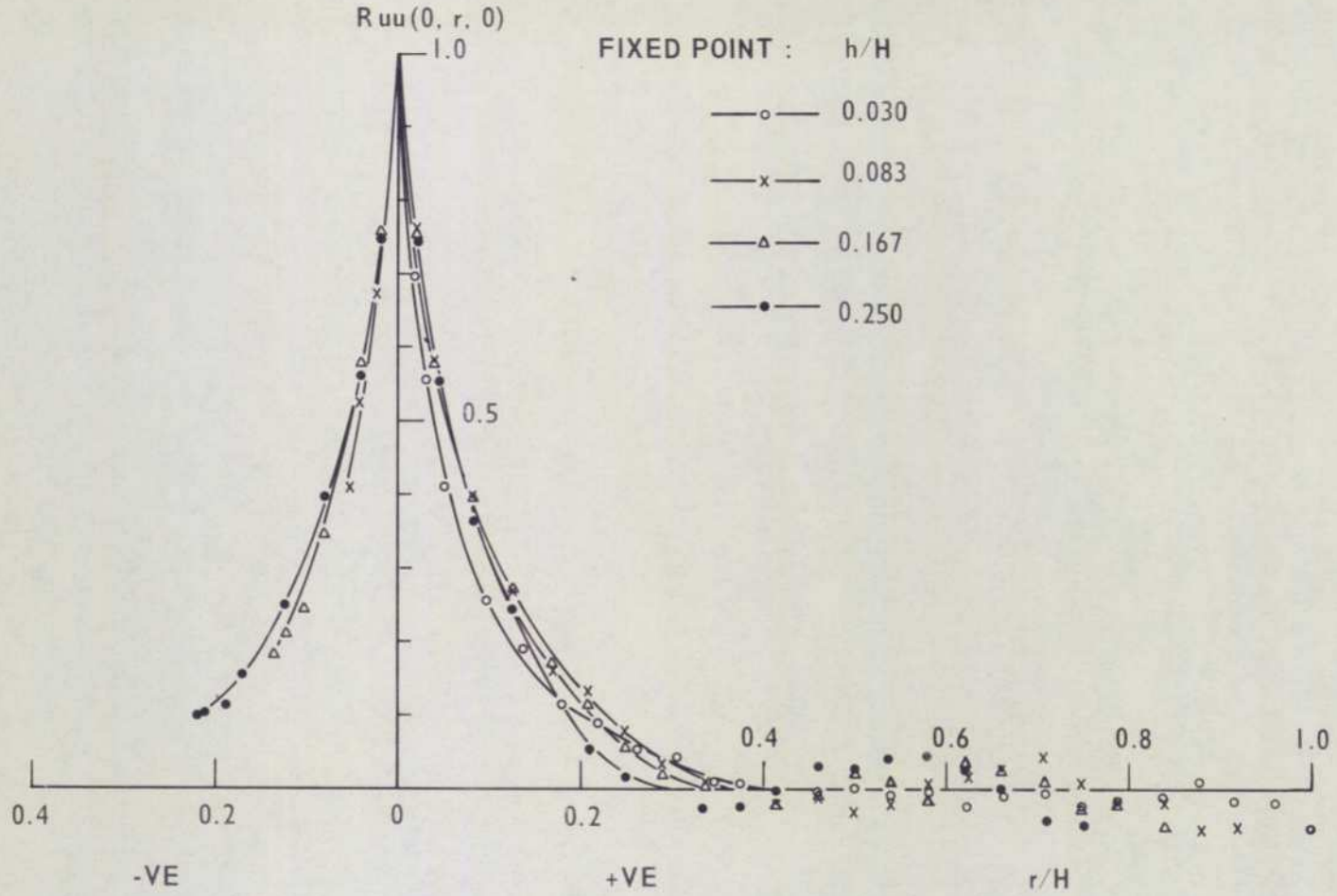


FIG. 52. CORRELATION COEFFICIENT DISTRIBUTIONS IN A SIMULATED BOUNDARY LAYER 457mm (18 in) AFT OF VORTICITY GENERATOR TRAILING EDGES. SPANWISE POSITION - GENERATOR ℄

JC/G.H.Ltd.(CON)(22.5.69)RL.3.3.1865

VERTICAL CORRELATION OF LONGITUDINAL VELOCITY COMPONENT

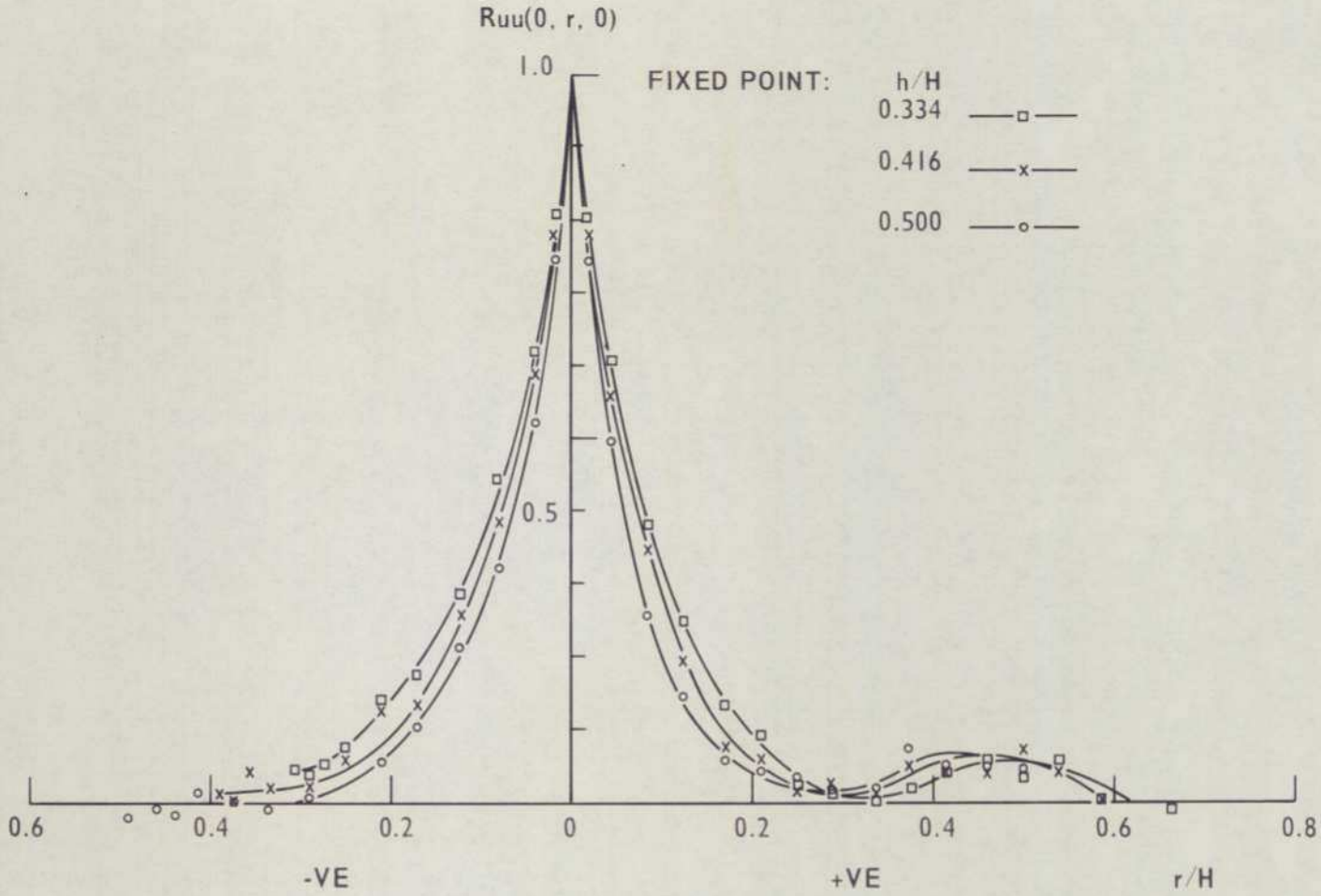


FIG.53. CORRELATION COEFFICIENT DISTRIBUTION IN A SIMULATED BOUNDARY LAYER 457mm (18in) AFT OF VORTICITY GENERATOR TRAILING EDGES. SPANWISE POSITION- GENERATOR ℄

JC/G.H.LTD.(CON)(22.5.69) R L 3.3.1866

VERTICAL CORRELATION OF LONGITUDINAL VELOCITY COMPONENT

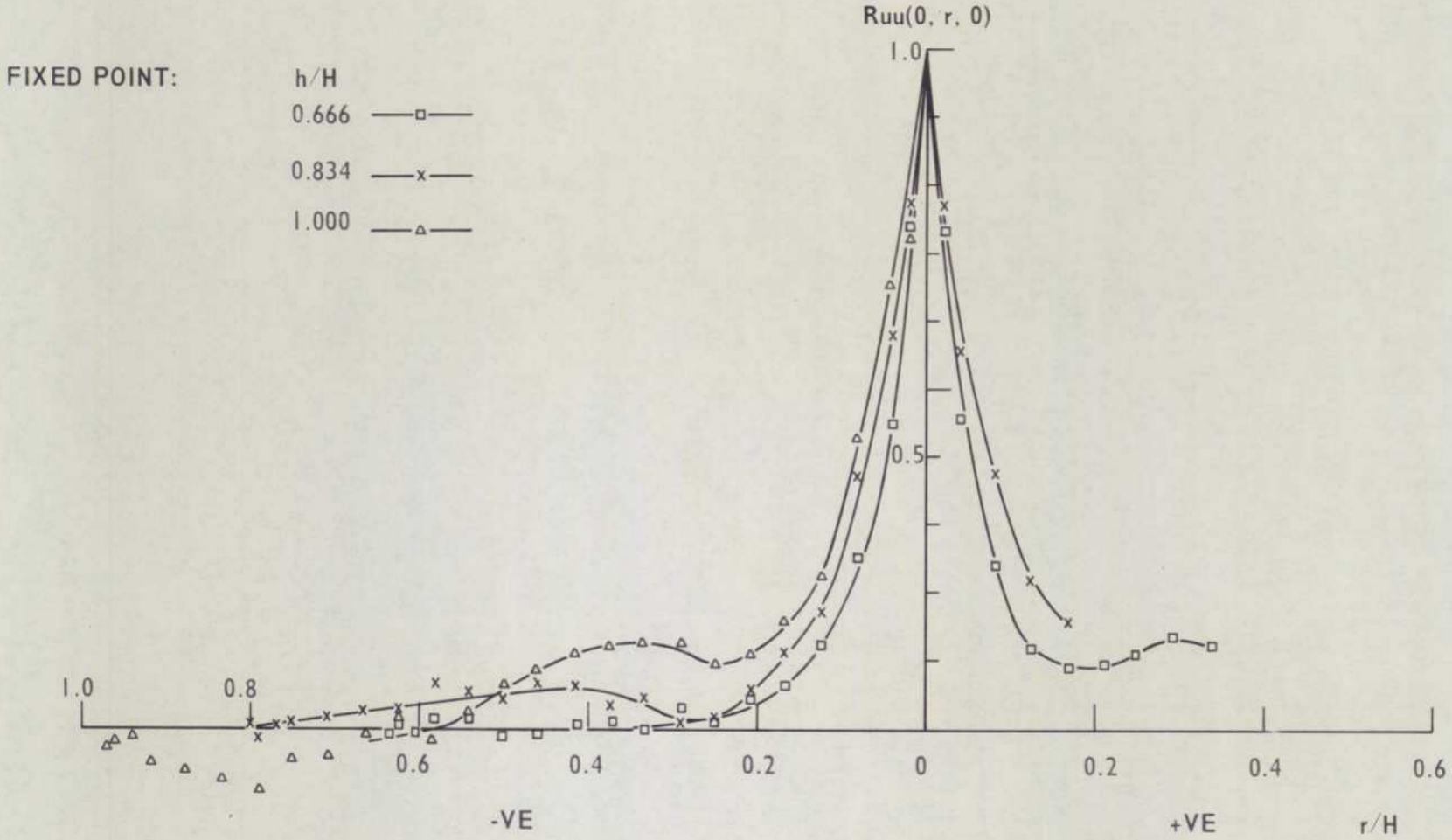


FIG. 54. CORRELATION COEFFICIENT DISTRIBUTION IN A SIMULATED BOUNDARY LAYER 457mm (18in) AFT OF VORTICITY GENERATOR TRAILING EDGES. SPANWISE POSITION - GENERATOR ℄

JC/G.H.LTD.(CON)(22.5.69) RL 3.3.1867

VERTICAL CORRELATION OF LONGITUDINAL VELOCITY COMPONENT

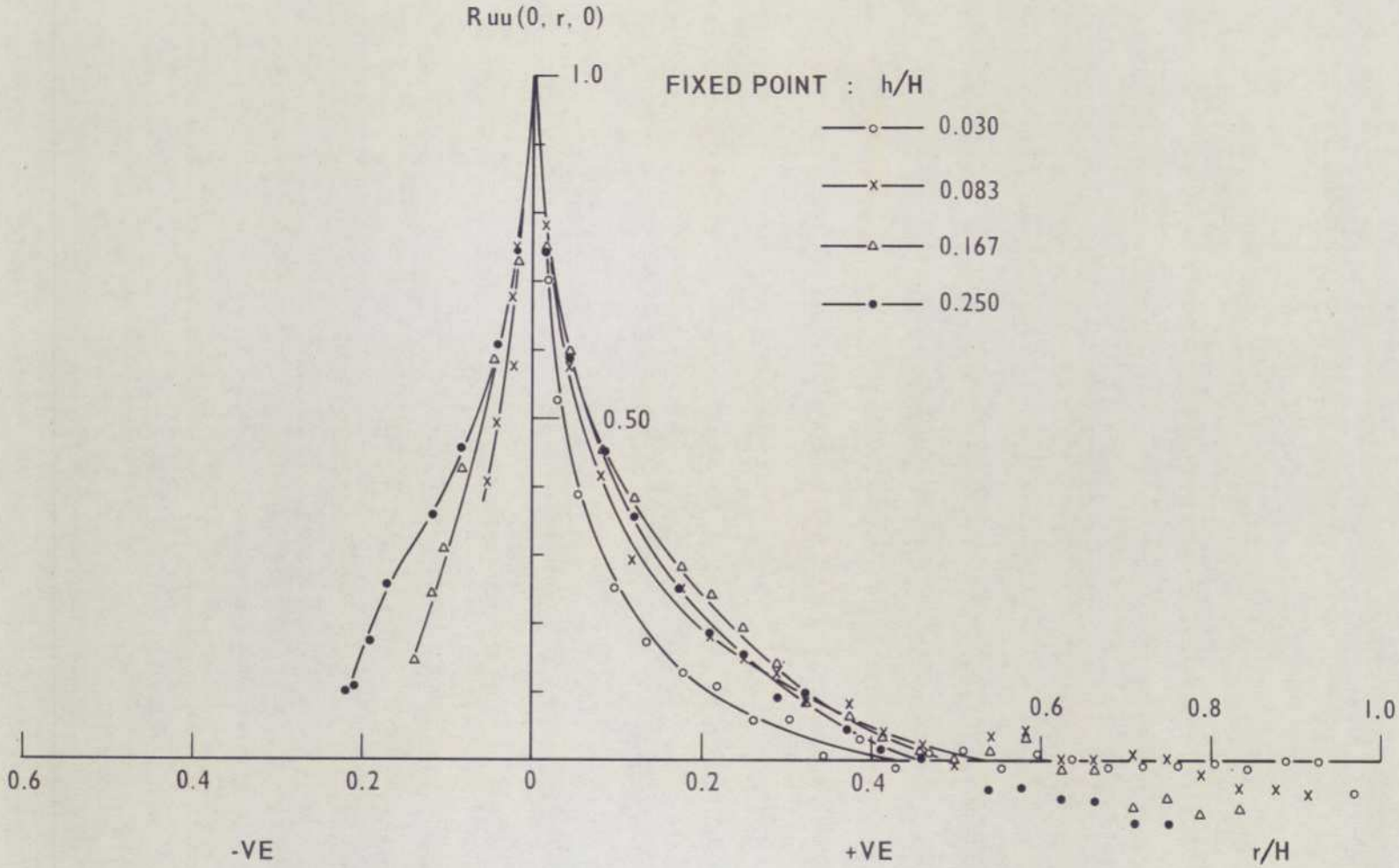


FIG.55 CORRELATION COEFFICIENT DISTRIBUTIONS IN A SIMULATED BOUNDARY LAYER 685 mm(27 in) AFT OF VORTICITY GENERATOR TRAILING EDGES-SPANWISE POSITION - GENERATOR MID-SPAN

JC/G.H.LTD (CON)(11.9.69) RL 3.3.1868

VERTICAL CORRELATION OF LONGITUDINAL VELOCITY COMPONENT

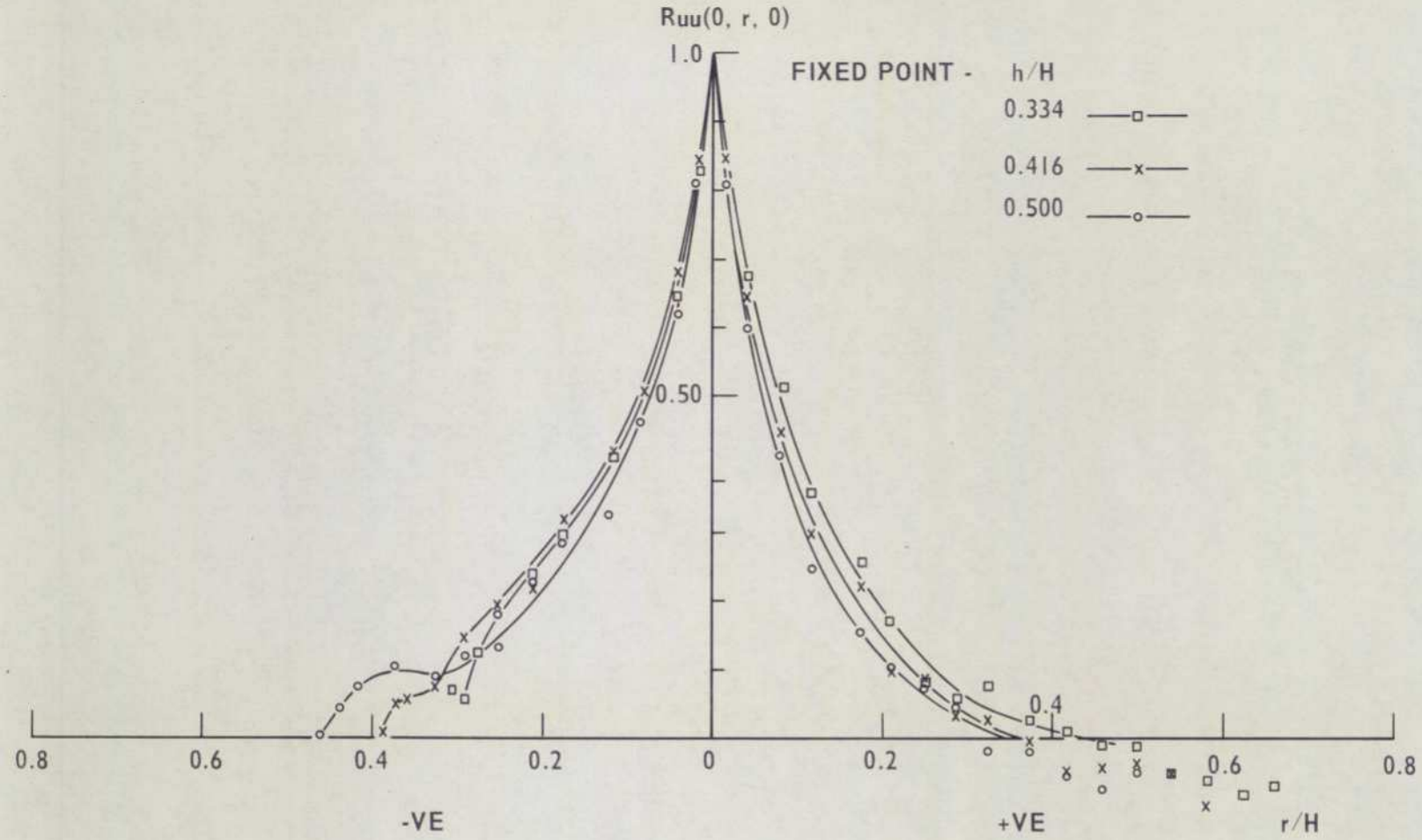


FIG.56. CORRELATION COEFFICIENT DISTRIBUTION IN A SIMULATED BOUNDARY LAYER 685mm (27in) AFT OF VORTICITY GENERATOR TRAILING EDGES SPANWISE POSITION - GENERATOR MID-SPAN

JC/G.H.LTD.(CON)(22.5.69) RL 3.3.1869

VERTICAL CORRELATION OF LONGITUDINAL VELOCITY COMPONENT

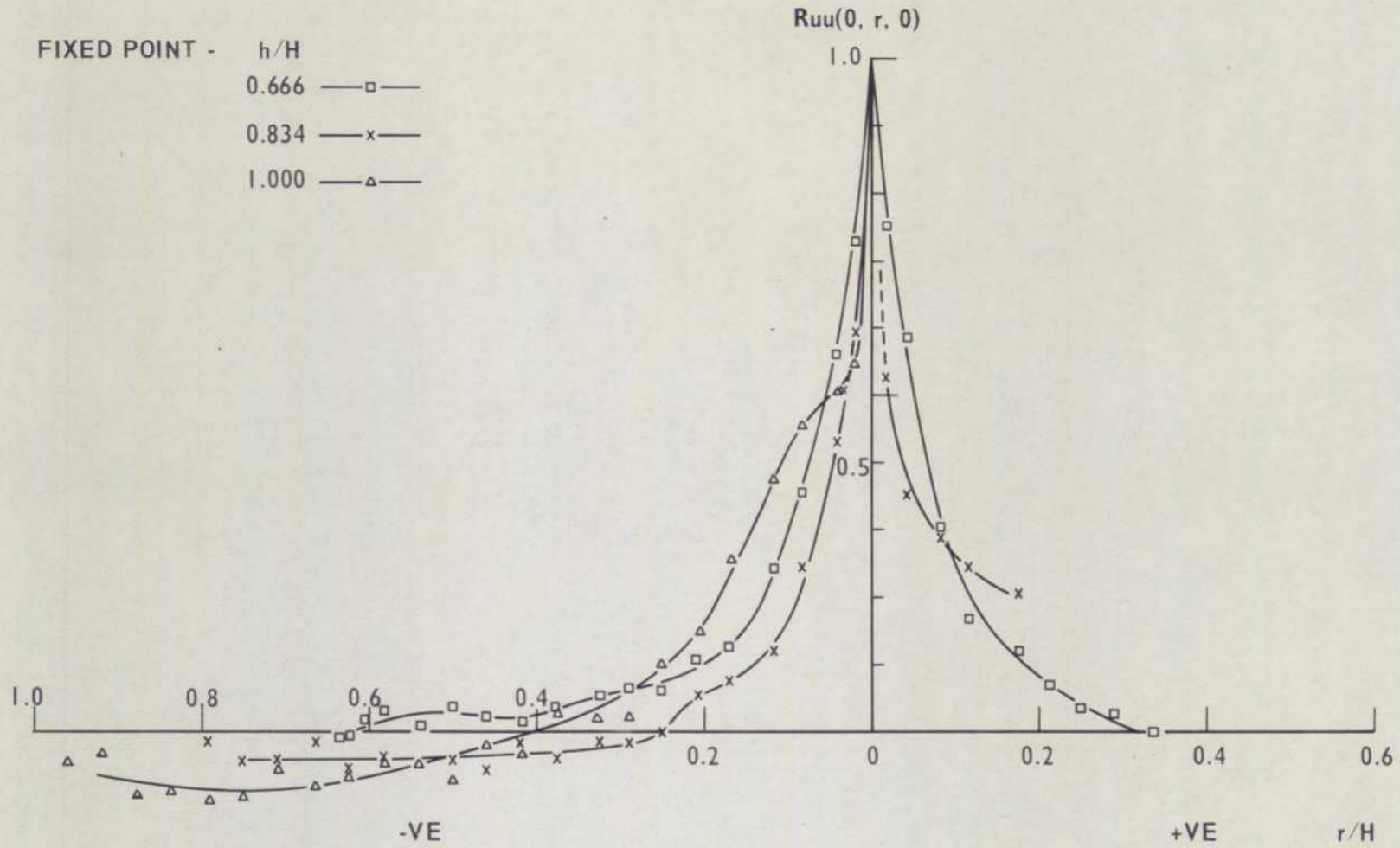


FIG.57. CORRELATION COEFFICIENT DISTRIBUTION IN A SIMULATED BOUNDARY LAYER 685mm (27in) AFT OF VORTICITY GENERATOR TRAILING EDGES·SPANWISE POSITION - GENERATOR MID-SPAN

JC/G.H.LTD.(CON)(22.5.69) RL 3.3.1870

VERTICAL CORRELATION OF LONGITUDINAL VELOCITY COMPONENT

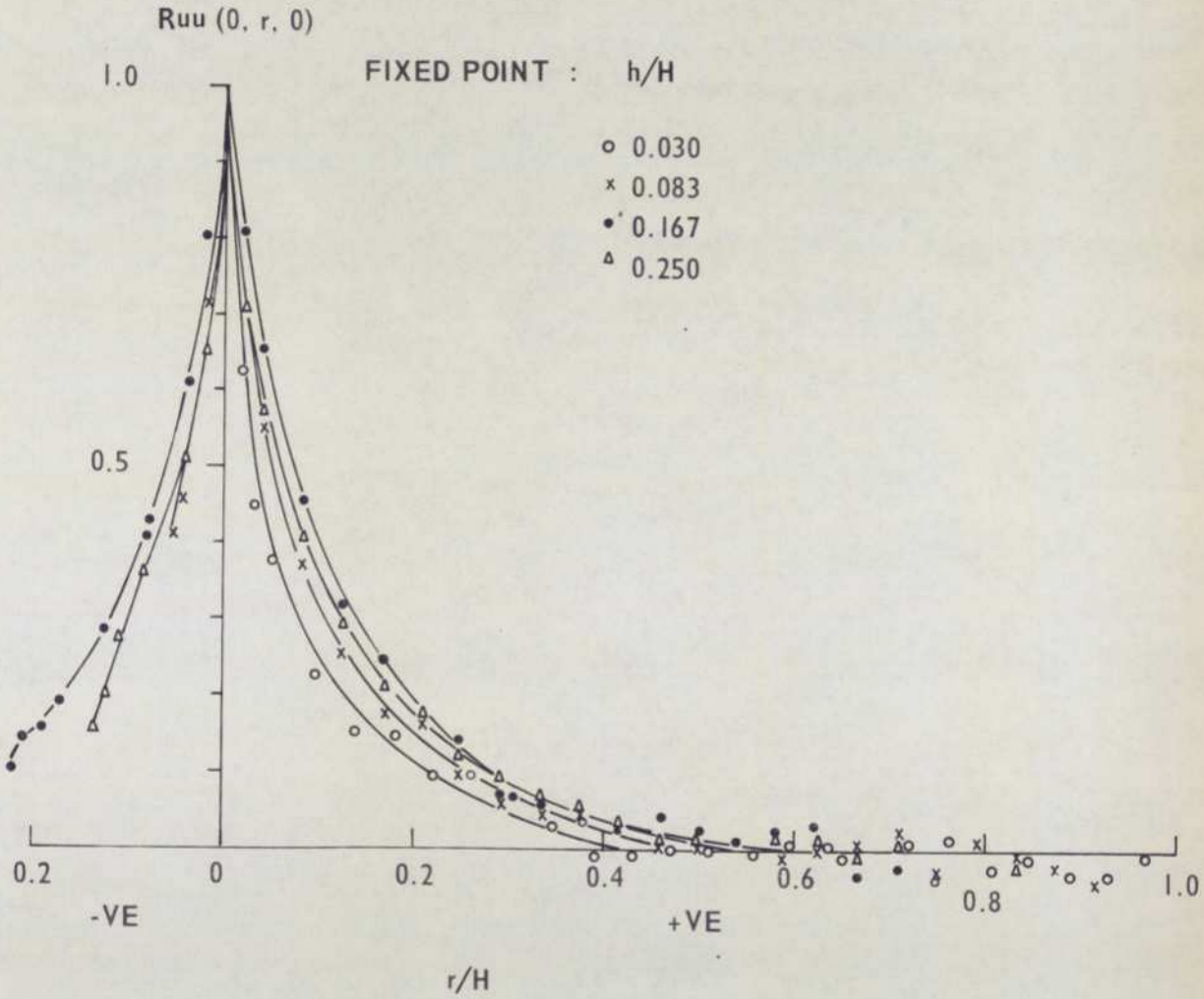


FIG. 58. CORRELATION COEFFICIENT DISTRIBUTIONS IN A SIMULATED BOUNDARY LAYER 685 mm(27 in) AFT OF VORTICITY GENERATOR TRAILING EDGES SPANWISE POSITION - GENERATOR ℄

VERTICAL CORRELATION OF LONGITUDINAL VELOCITY COMPONENT

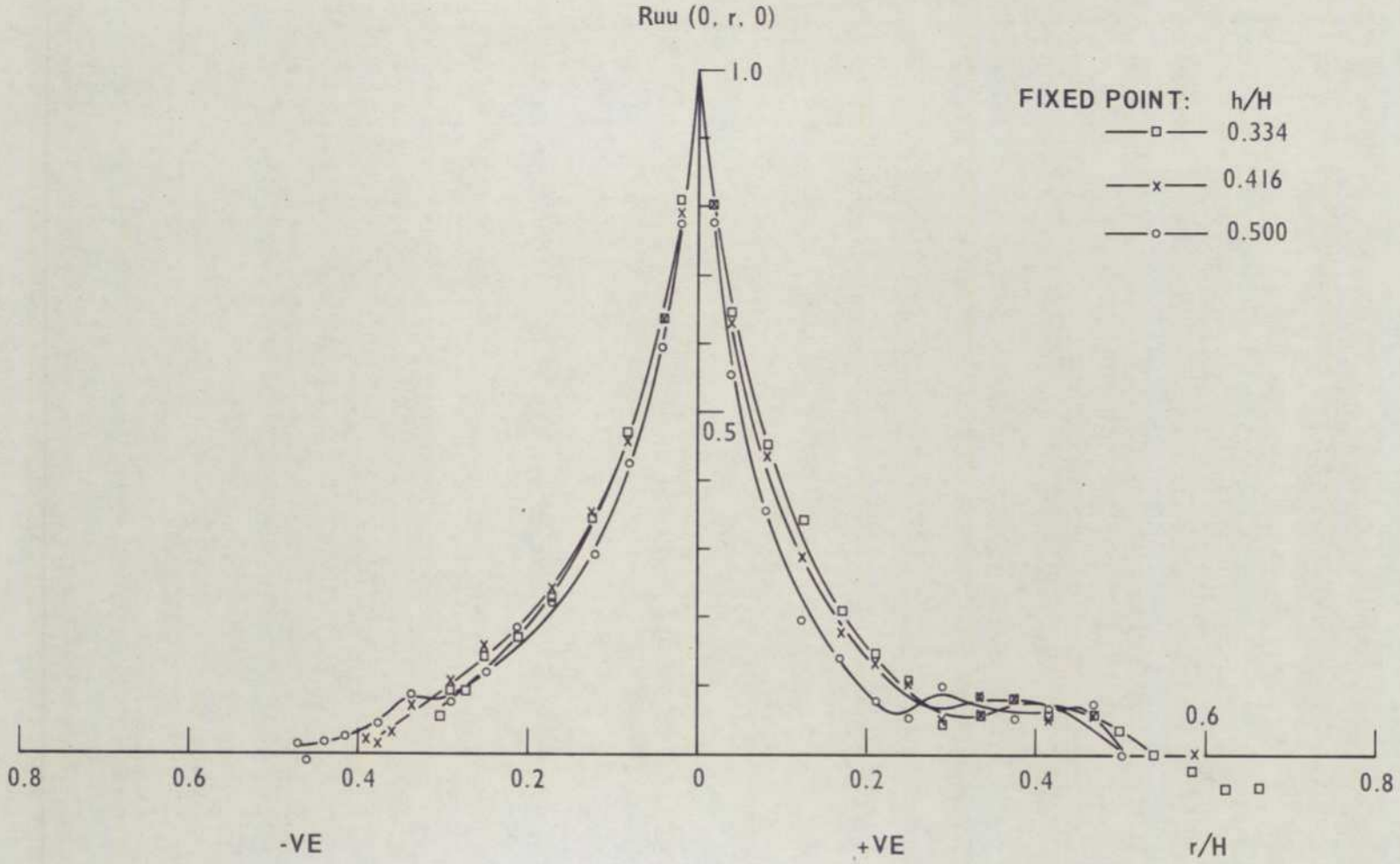


FIG.59. CORRELATION COEFFICIENT DISTRIBUTION IN A SIMULATED BOUNDARY LAYER 685.mm(27 in) AFT OF VORTICITY GENERATOR TRAILING EDGES. SPANWISE POSITION - GENERATOR ℄

JC/G.H.LTD (CON)(11.9.69) RL 3.3.1872

VERTICAL CORRELATION OF LONGITUDINAL VELOCITY COMPONENT

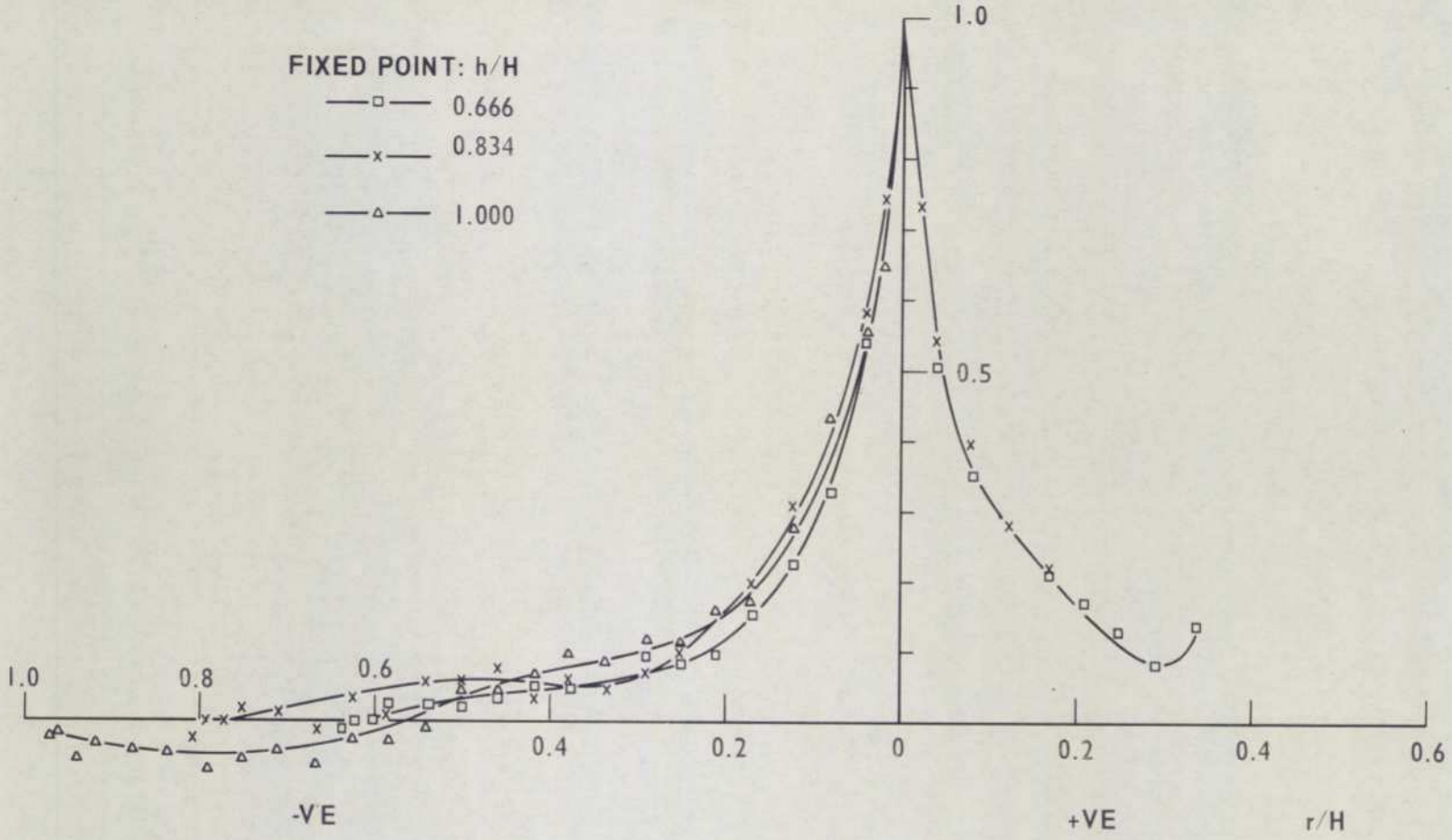


FIG. 60. CORRELATION COEFFICIENT DISTRIBUTION IN A SIMULATED BOUNDARY LAYER 685mm (27 in) AFT OF VORTICITY GENERATOR TRAILING EDGES. SPANWISE POSITION - GENERATOR ℄

JC/G.H.Ltd.(CON)(22.5.69)RL.3.3.1873

LATERAL CORRELATION OF LONGITUDINAL VELOCITY COMPONENT

(TRAVERSE FROM FIXED POINT:)

+VE —o—

-VE —x—

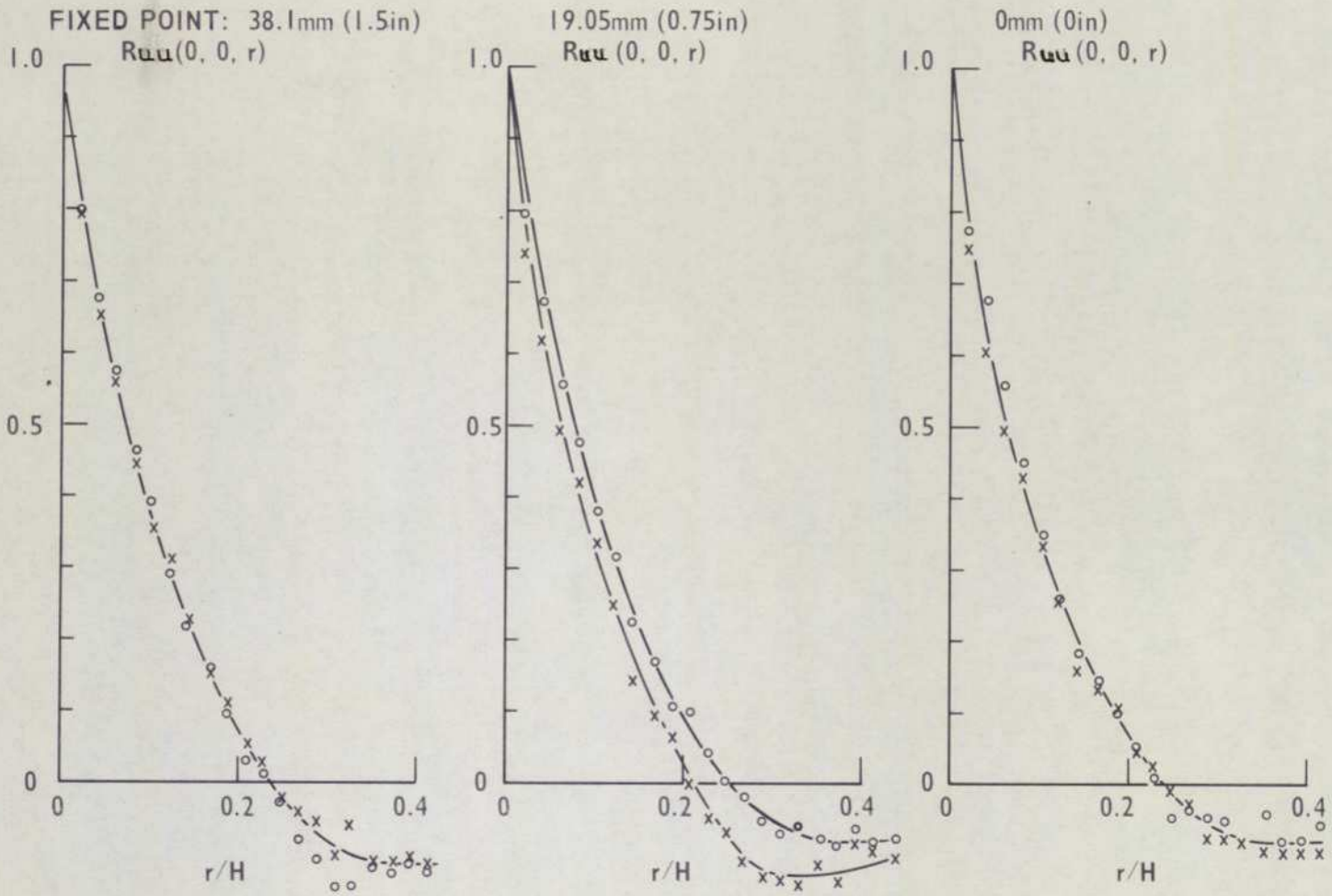


FIG. 61. SYMMETRY OF CORRELATION COEFFICIENT DISTRIBUTIONS PLANE OF TRAVERSE: 457mm (18in) AFT OF GENERATORS

h/H = 0.20

JC/G.H.LTD.(CON)(22.5.69) R L 3.3.1874

LATERAL CORRELATION OF LONGITUDINAL VELOCITY COMPONENT

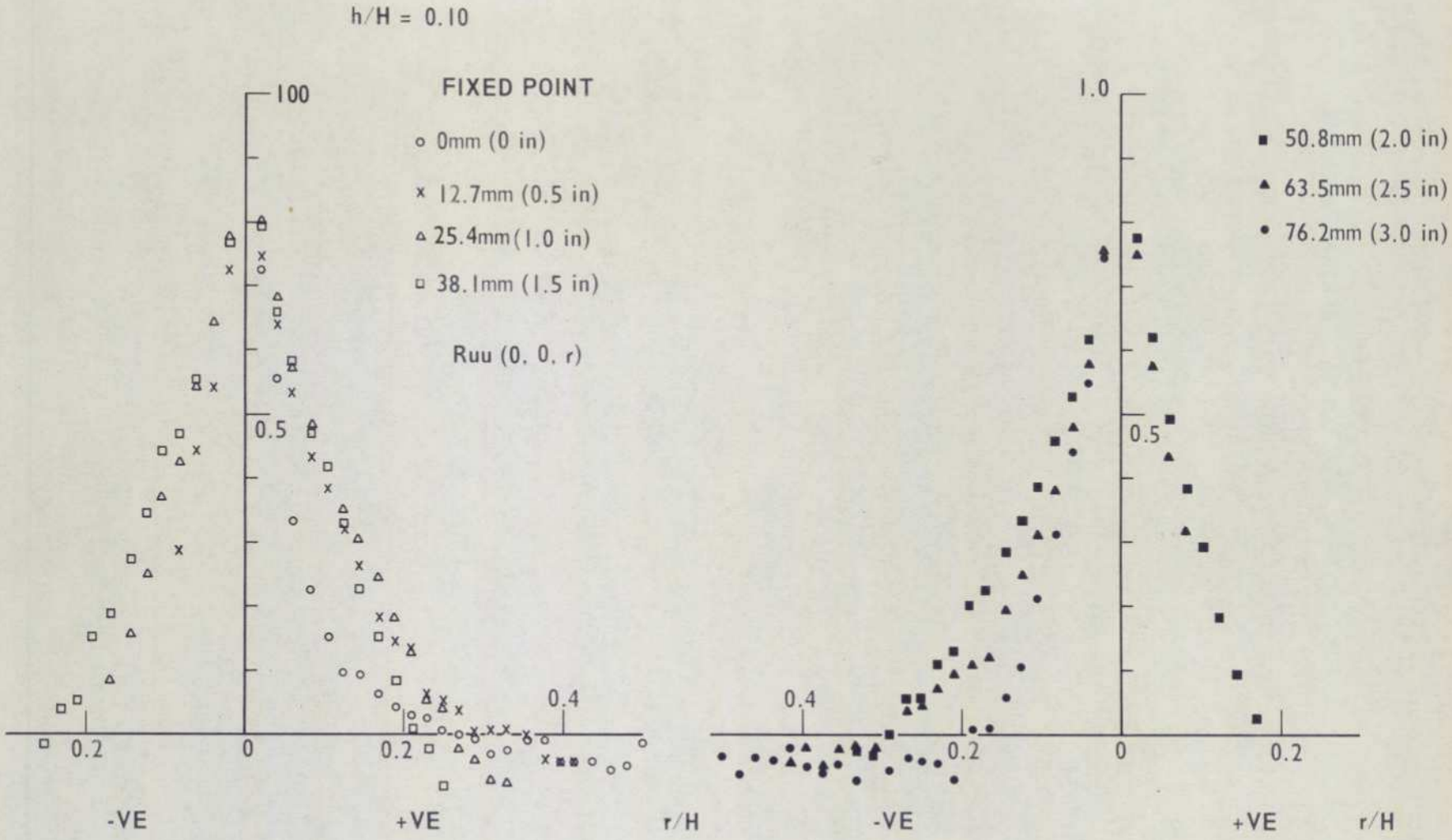


FIG. 62. CORRELATION COEFFICIENT MEASUREMENTS AT VARIOUS FIXED SPANWISE POSITIONS. PLANE OF TRAVERSE: 475mm (18 in) AFT OF GENERATOR

JC/G.H.Ltd.(CON)(22.5.69)RL.3.3.1875

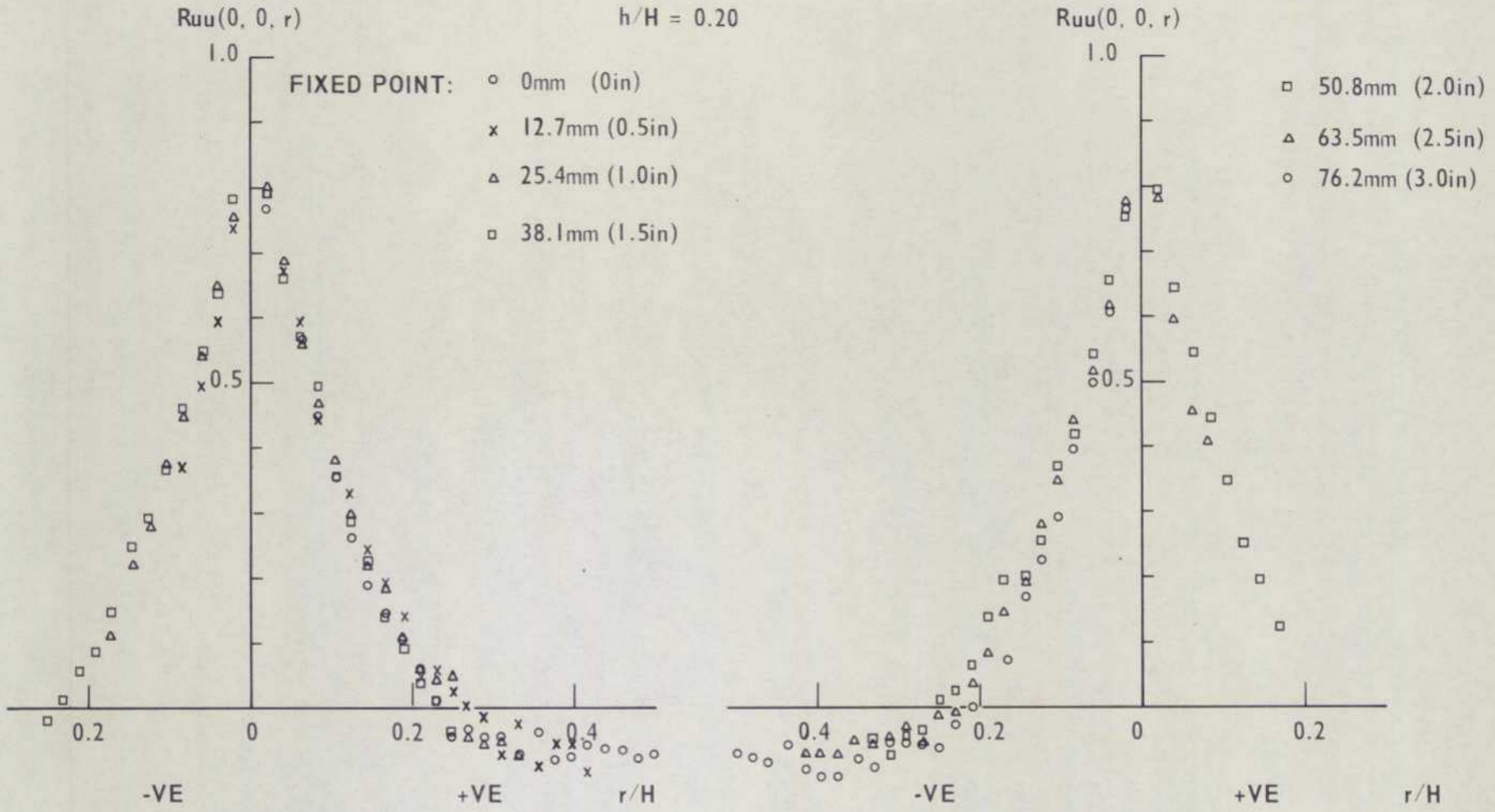


FIG. 63. CORRELATION COEFFICIENT MEASUREMENTS AT VARIOUS FIXED SPANWISE POSITIONS. PLANE OF TRAVERSE: 457mm (18in) AFT OF GENERATORS

LATERAL CORRELATION OF LONGITUDINAL VELOCITY COMPONENT
FIXED POINT, (0in)

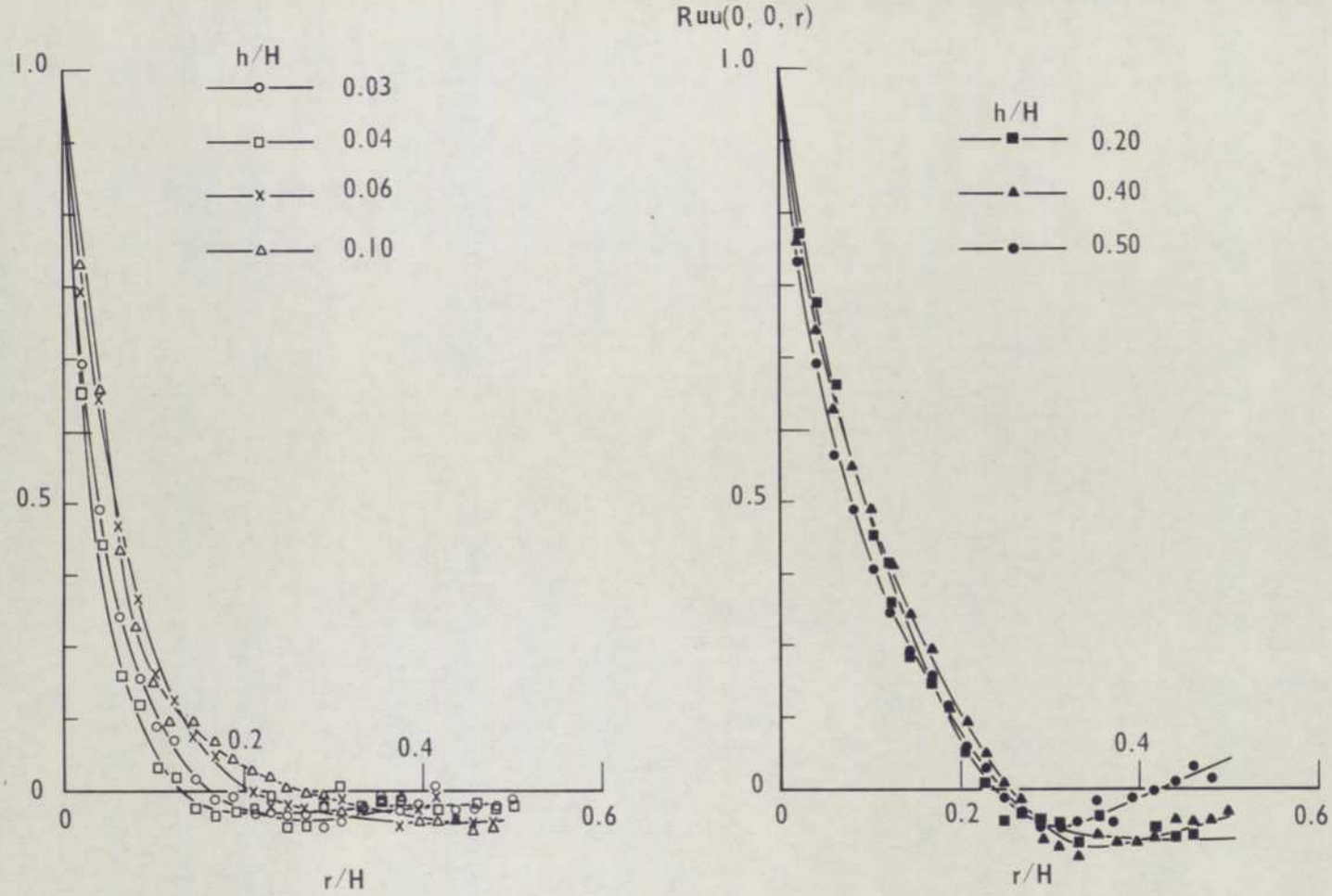


FIG. 64. CORRELATION COEFFICIENT MEASUREMENTS AT VARIOUS HEIGHTS. PLANE OF TRAVERSE: 457mm (18in) AFT OF GENERATORS. FIXED POINT: 0mm (0in)

JC/G.H.LTD.(CON)(23.5.69) RL 3.3.1877

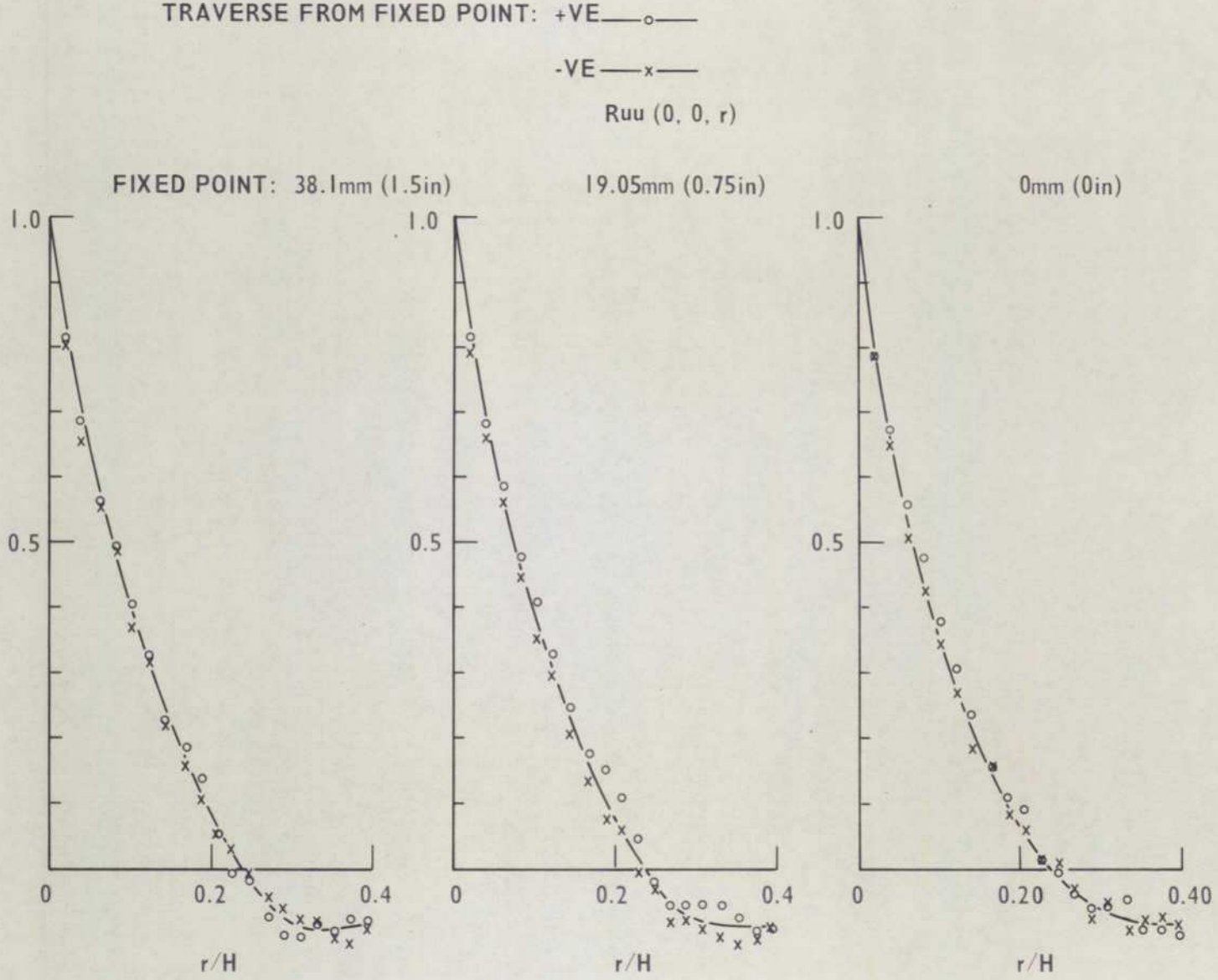


FIG. 65. SYMMETRY OF CORRELATION COEFFICIENT DISTRIBUTIONS PLANE OF TRAVERSE: 685 (27in) AFT OF GENERATORS

h/H = 0.20

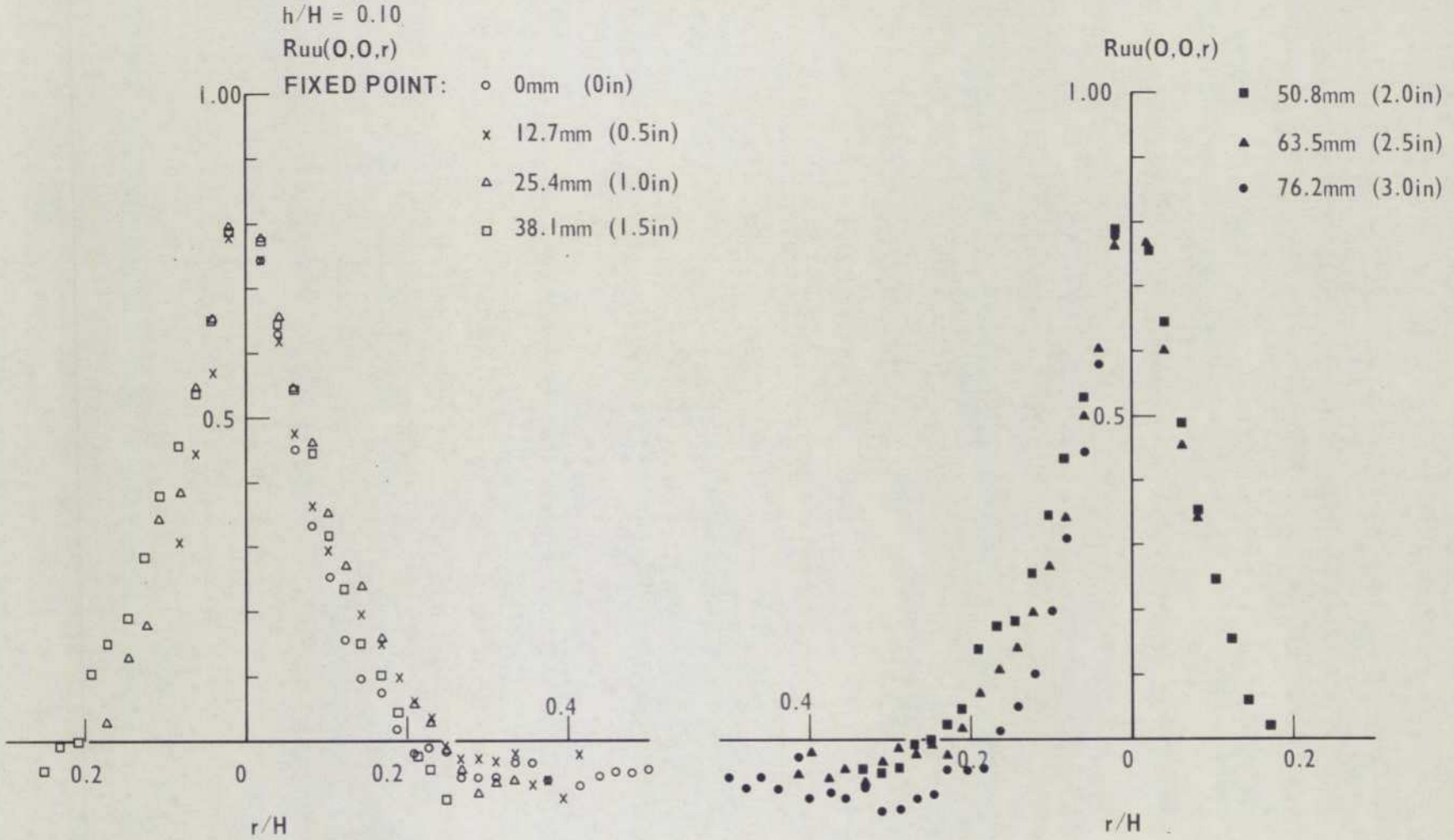


FIG. 66 CORRELATION COEFFICIENT MEASUREMENTS AT VARIOUS FIXED SPANWISE POSITIONS. PLANE OF TRAVERSE: 685mm (27in) AFT OF GENERATORS

JC/G.H.LTD.(CON)(23.5.69) RL 3.3.1879

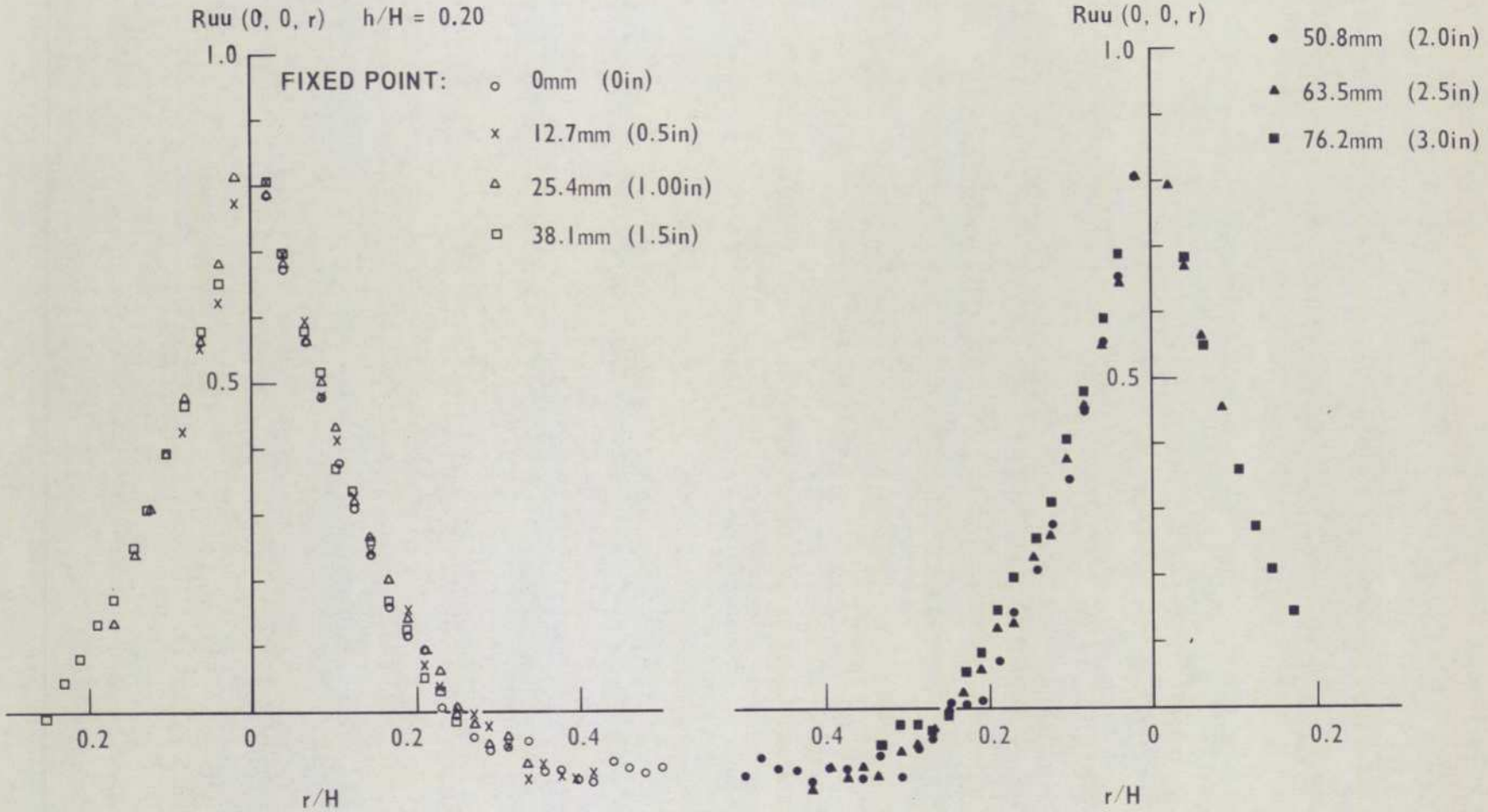


FIG. 67. CORRELATION COEFFICIENT MEASUREMENTS AT VARIOUS FIXED SPANWISE POSITIONS. PLANE OF TRAVERSE: 685mm (27in) AFT OF GENERATORS

JC/G.H.LTD.(CON) (23.5.69) RL 3.3.1880

FIG. 6.8. CORRELATION COEFFICIENT MEASUREMENTS AT VARIOUS HEIGHTS
PLANE OF TRAVERSE: 685 mm(27 in) AFT OF GENERATORS, FIXED POINT: 0 mm (0 in)

VERTICAL CORRELATION OF LONGITUDINAL VELOCITY COMPONENT
COMPARISON WITH MEASUREMENTS FROM A NATURALLY GROWN
BOUNDARY LAYER

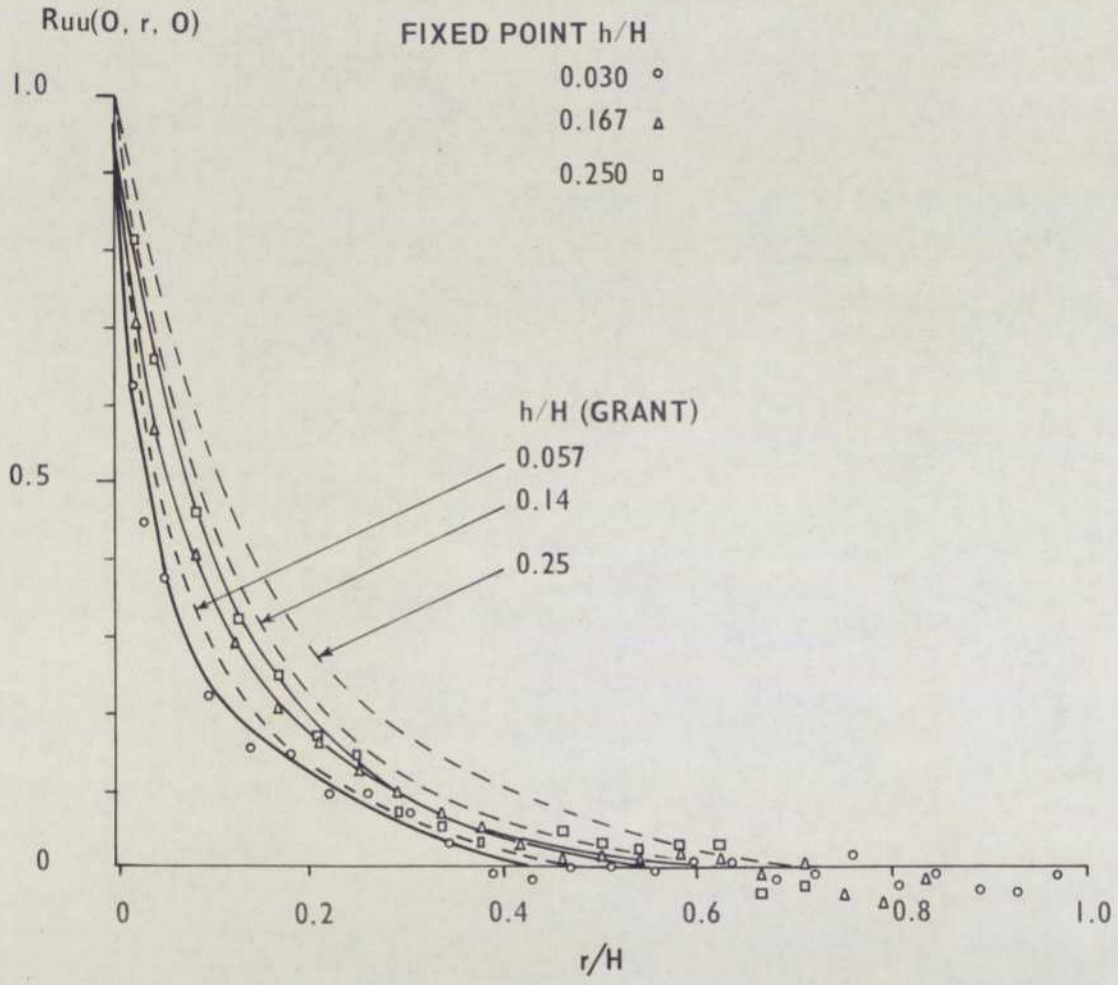


FIG. 69. COMPARISON OF CORRELATION COEFFICIENT DISTRIBUTIONS. SIMULATED BOUNDARY LAYER PLANE OF TRAVERSE 685 mm(27in.) AFT OF GENERATORS. SPANWISE POSITION - GENERATOR ℄

LATERAL CORRELATION OF LONGITUDINAL VELOCITY COMPONENT
COMPARISON WITH MEASUREMENTS FROM A NATURALLY GROWN
BOUNDARY LAYER

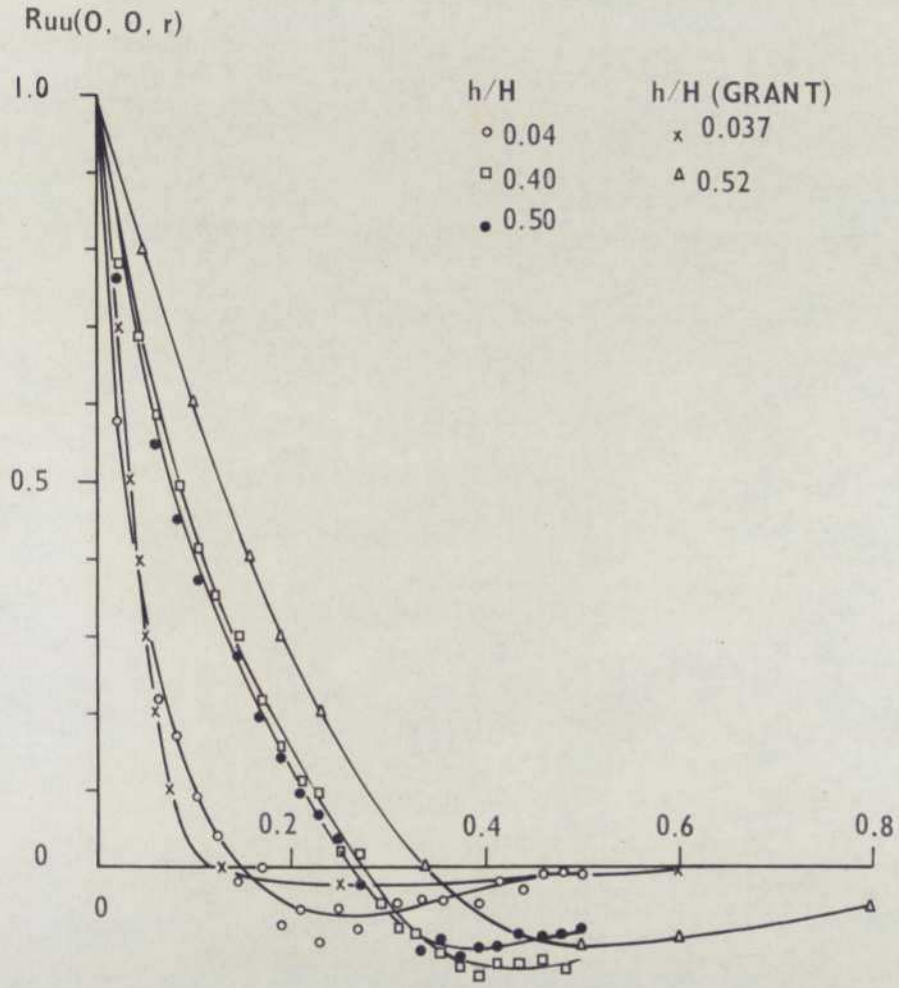


FIG. 70. COMPARISON OF CORRELATION COEFFICIENT DISTRIBUTIONS. SIMULATED BOUNDARY PLANE OF TRAVERSE: 685 mm(27in.) AFT OF GENERATORS
FIXED POINT: 0 mm(0in.)

VERTICAL CORRELATION OF LONGITUDINAL VELOCITY COMPONENT

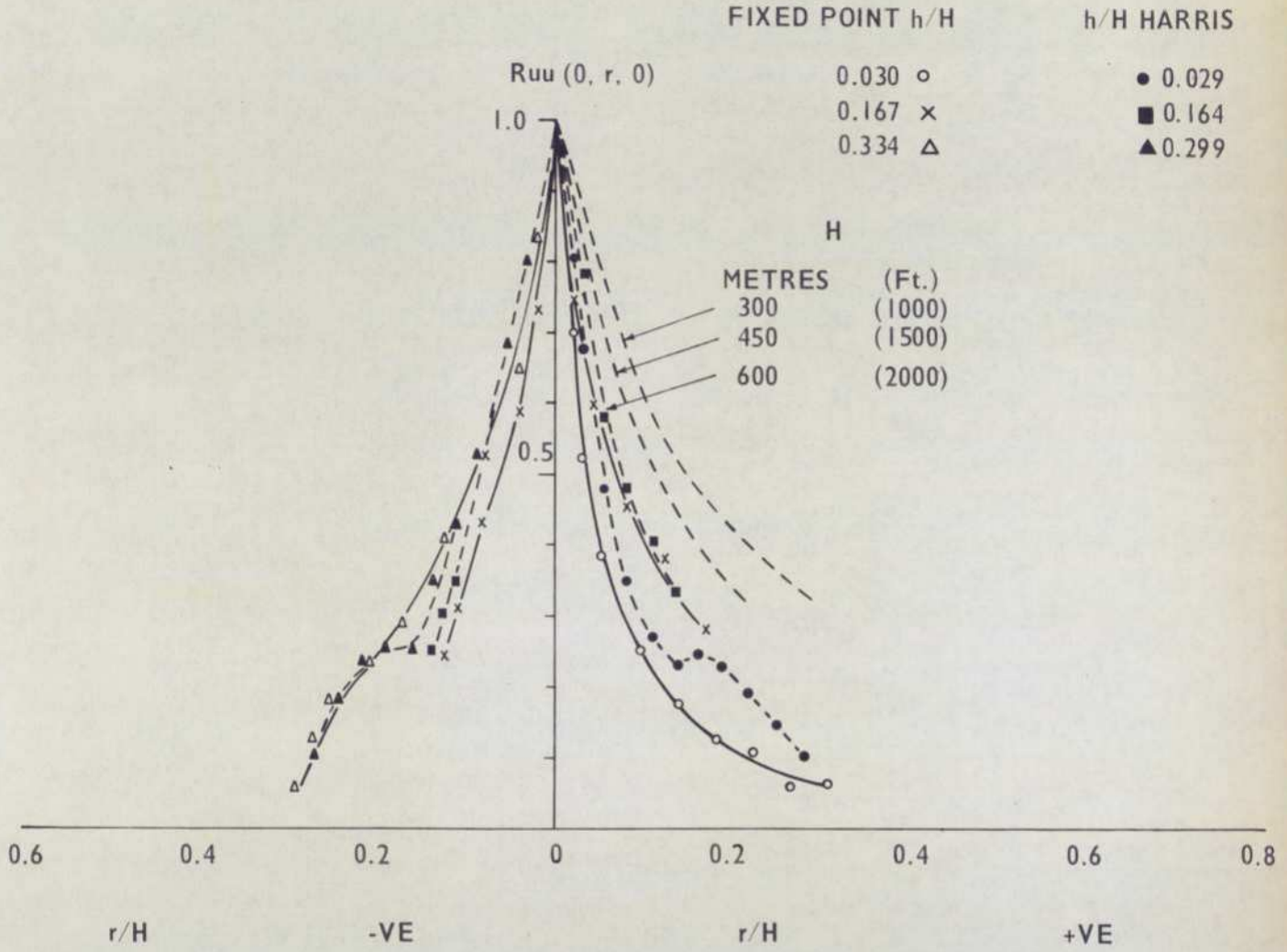


FIG. 71. COMPARISON OF CORRELATION COEFFICIENT DISTRIBUTIONS. SIMULATED BOUNDARY LAYER PLANE OF TRAVERSE: 685 mm(27in.) AFT OF GENERATORS. SPANWISE POSITION GENERATOR MID-SPAN

VERTICAL CORRELATION OF LONGITUDINAL VELOCITY COMPONENT

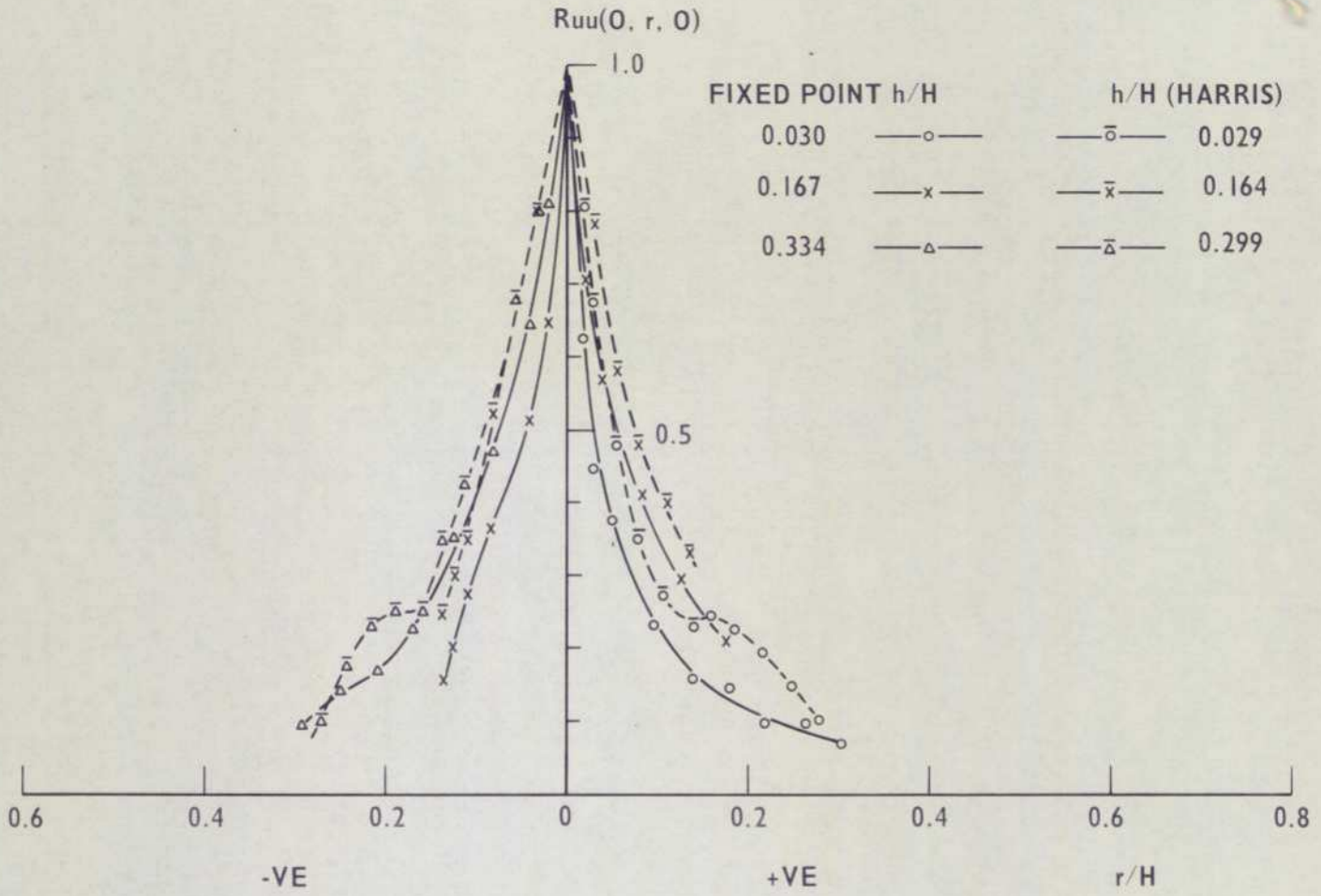


FIG. 72. COMPARISON OF CORRELATION COEFFICIENT DISTRIBUTIONS. SIMULATED BOUNDARY LAYER PLANE OF TRAVERSE: 685mm (27 in) AFT OF GENERATORS. SPANWISE POSITION - GENERATOR ℄

JC/G:H.Ltd.(CON)(23.5.69)RL.3.3.1885

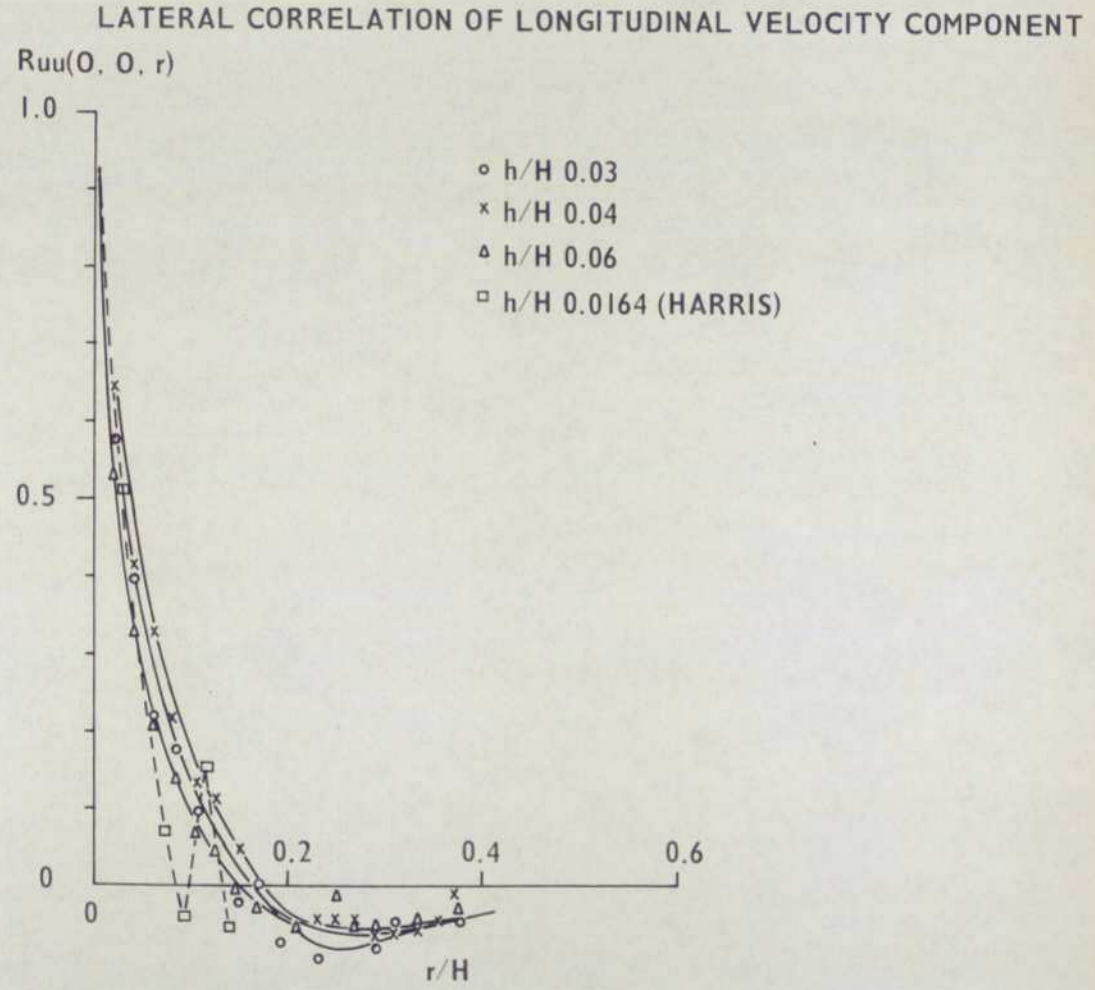


FIG. 73. COMPARISON OF CORRELATION COEFFICIENT DISTRIBUTIONS
SIMULATED BOUNDARY LAYER PLANE OF TRAVERSE: 685mm (27 in) AFT OF GENERATORS
FIXED POINT: 0mm (0 in)

MEASUREMENTS CORRECTED FOR EFFECTS OF POSSIBLE SPURIOUS INPUTS

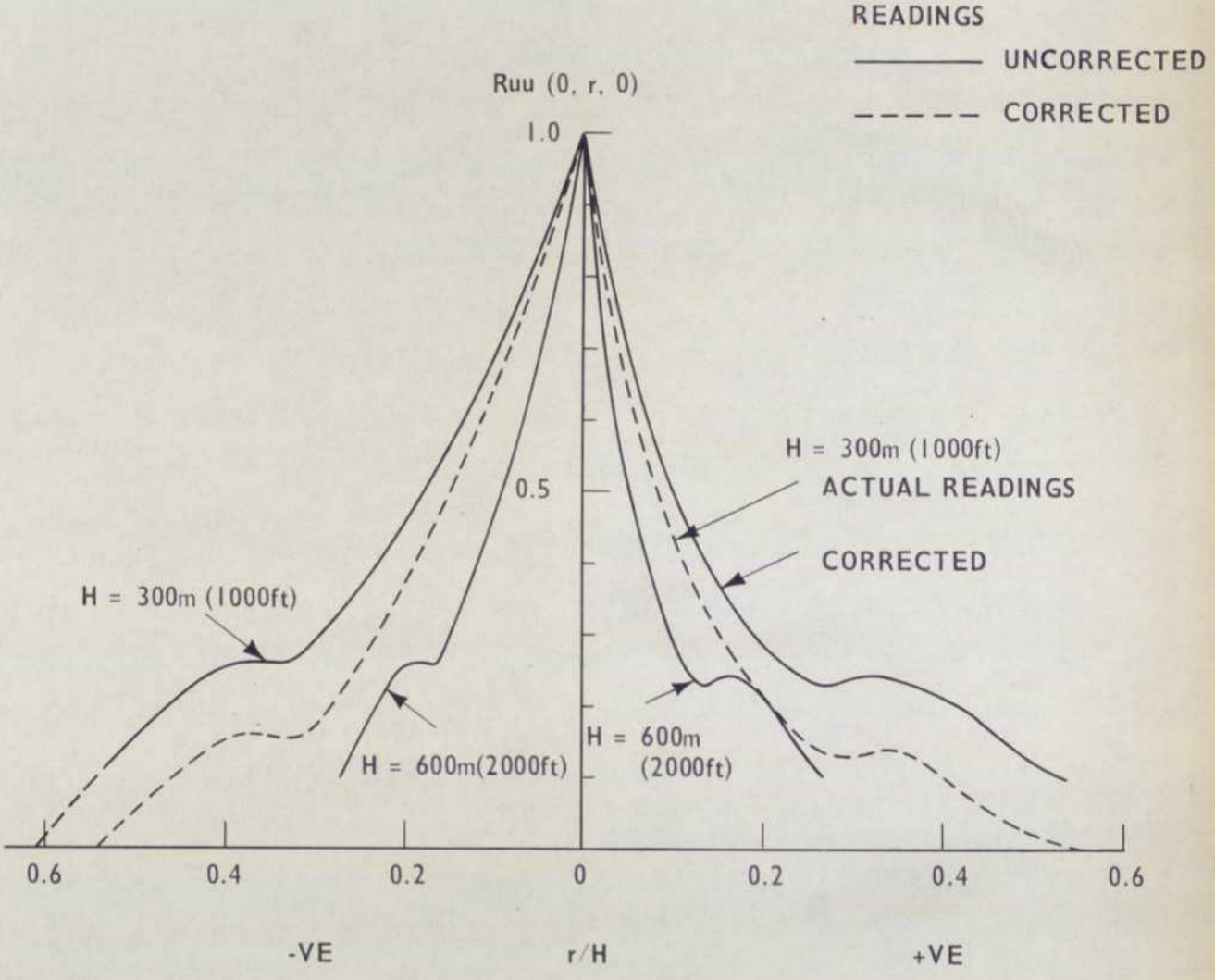


FIG. 74. MEASUREMENTS OF THE VERTICAL CORRELATION OF THE LONGITUDINAL VELOCITY COMPONENT IN AN ATMOSPHERIC BOUNDARY LAYER (HARRIS)

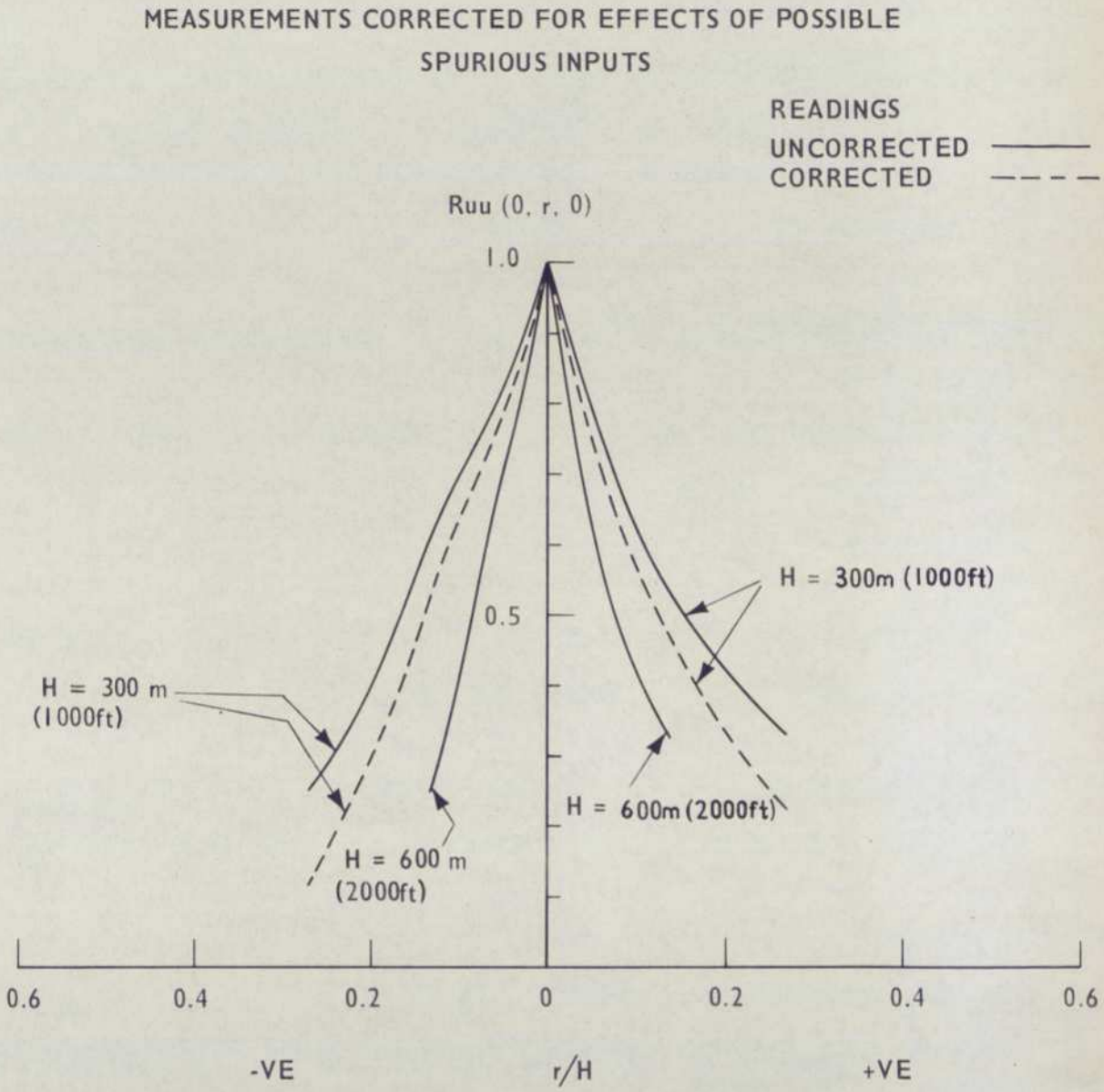


FIG. 75. MEASUREMENTS OF THE VERTICAL CORRELATION OF THE LONGITUDINAL VELOCITY COMPONENT IN AN ATMOSPHERIC BOUNDARY LAYER (HARRIS)

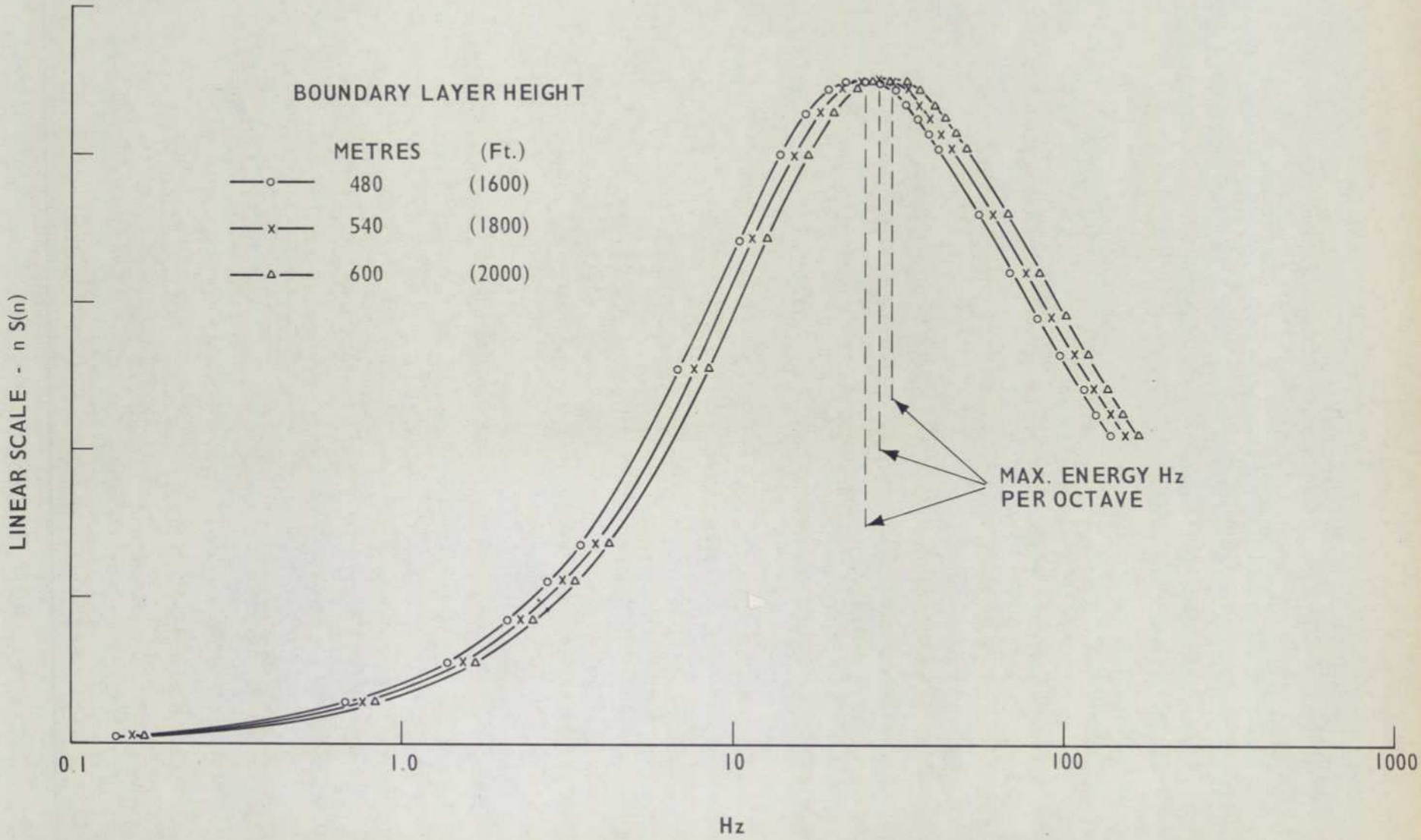


FIG. 76. HARRIS'S THEORETICAL LONGITUDINAL POWER SPECTRA. EFFECTS OF VARYING B.L. HEIGHT

JC/G.H.Ltd.(CON)(23.5.69)RL.3.3.1889

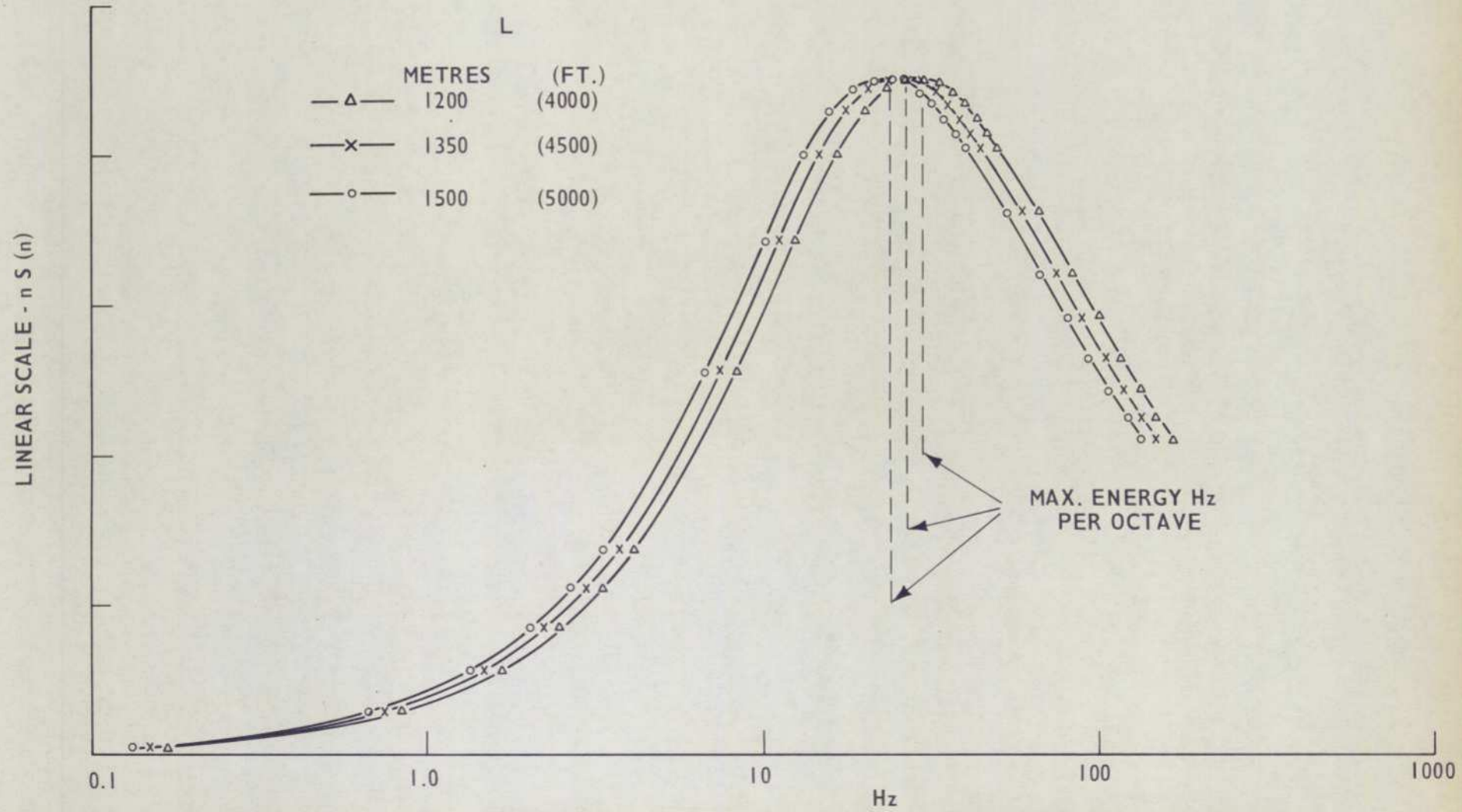


FIG. 77. HARRIS'S THEORETICAL LONGITUDINAL POWER SPECTRA. EFFECTS OF VARYING PARAMETER L.B.L. HEIGHT - 600m (2000ft)

JC/G.H.LTD.(CON)(23.5.69) RL 3.3.1890

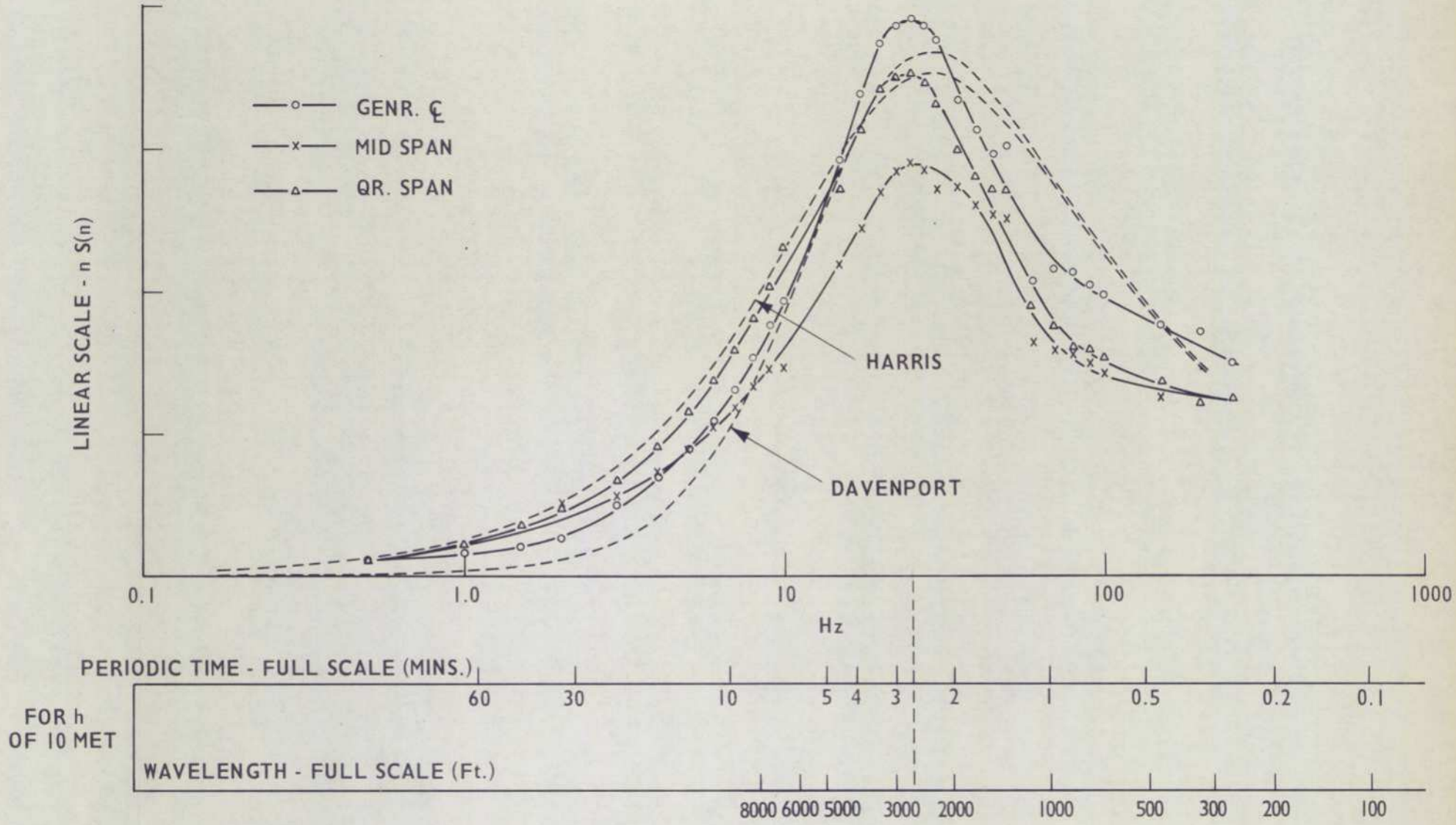


FIG. 78. LONGITUDINAL POWER SPECTRA AT h/H = 0.167 AND PROPOSED SPECTRA OF HARRIS AND DAVENPORT 457mm (18 in) AFT OF V.G. TRAILING EDGE

JC/G.H.LTD (CON)(11.9.69) RL 3.3.1891

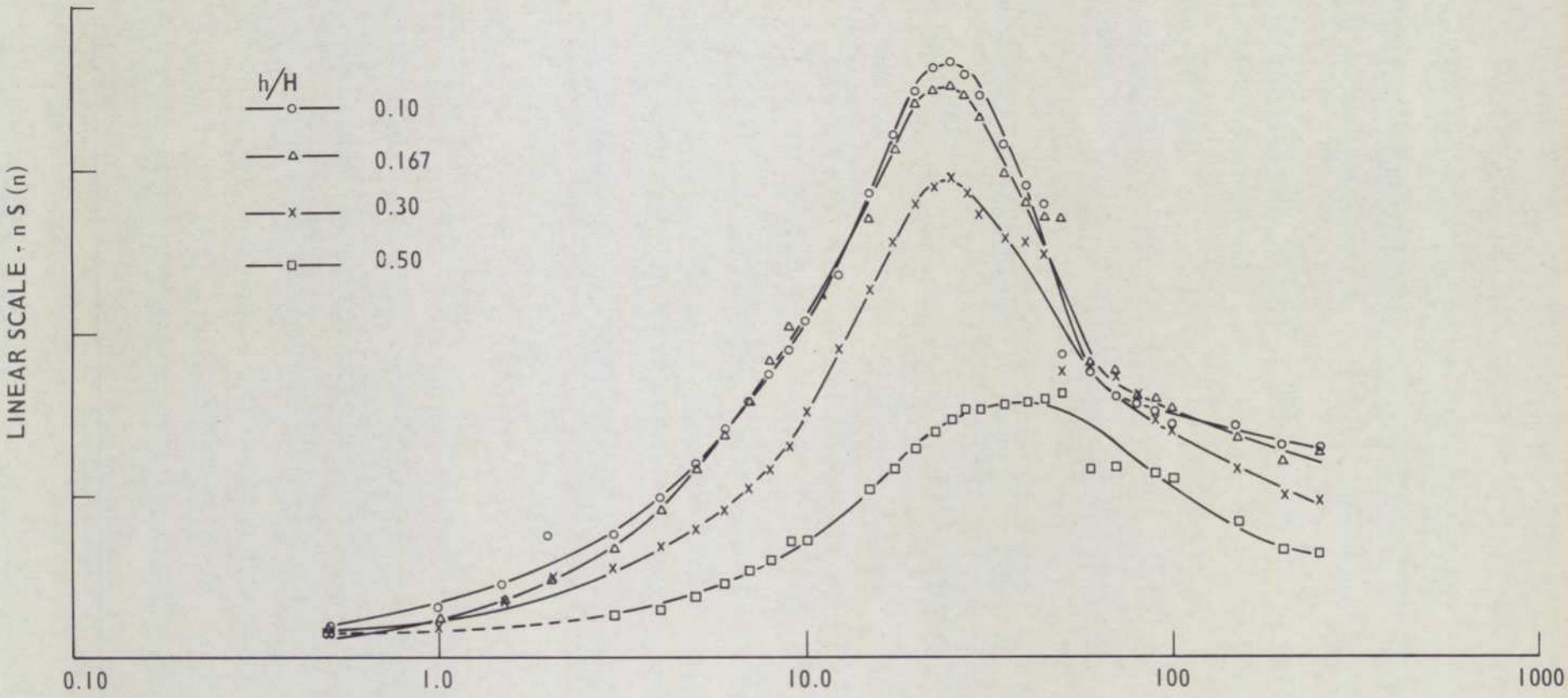


FIG.79. LONGITUDINAL POWER SPECTRA - VARIATION WITH HEIGHT. 457.0 mm(18in) AFT OF V.G. TRAILING EDGE. SEMI-SPAN ℄

JC/G.H.LTD (CON)(11.9.69) RL 3.3.1892

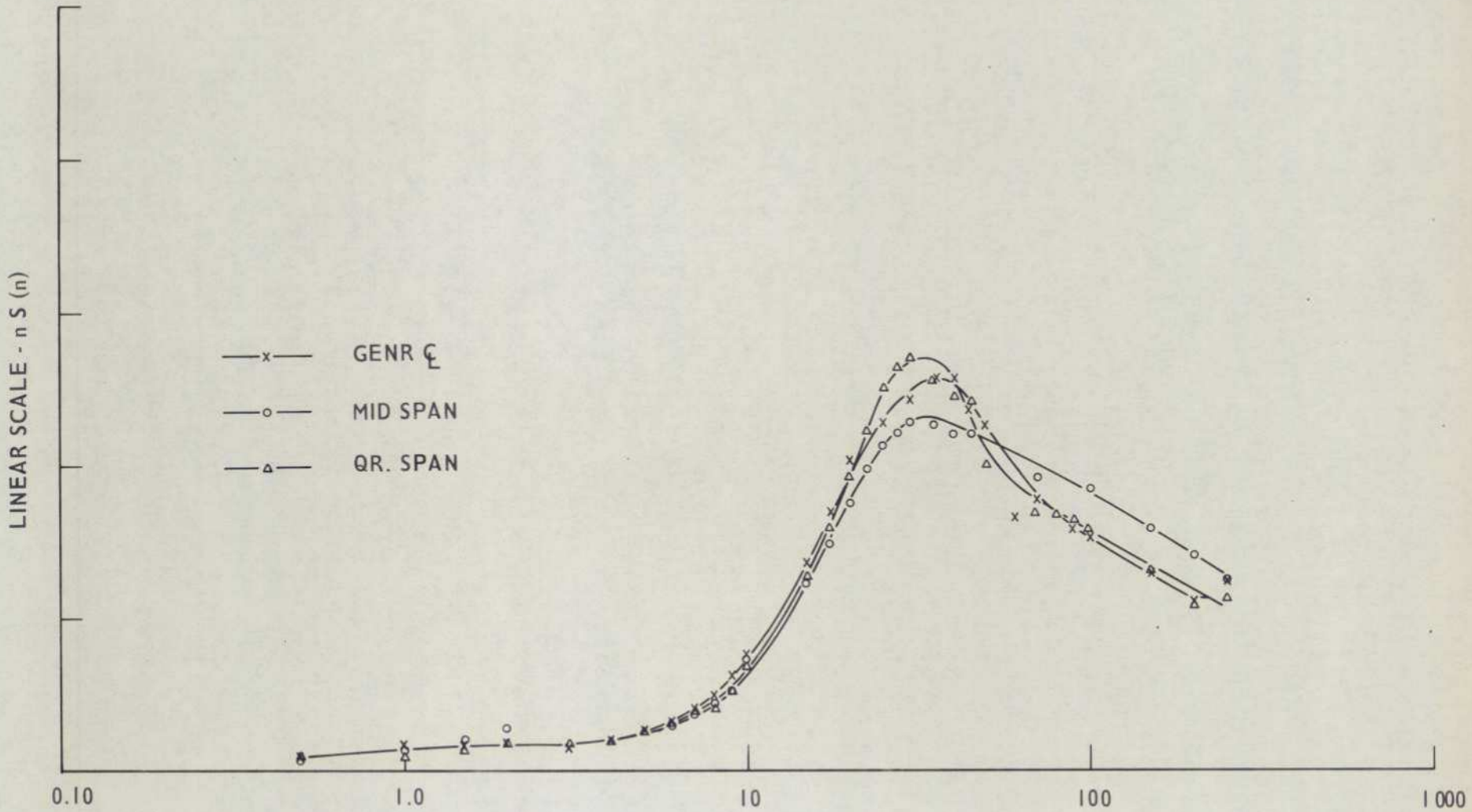


FIG. 80. LATERAL POWER SPECTRA AT h/H = 0.167. 457.0mm (18in) AFT OF V.G. TRAILING EDGE

JC/G.H.LTD (CON) (23.5.69) RL 3.3.1893

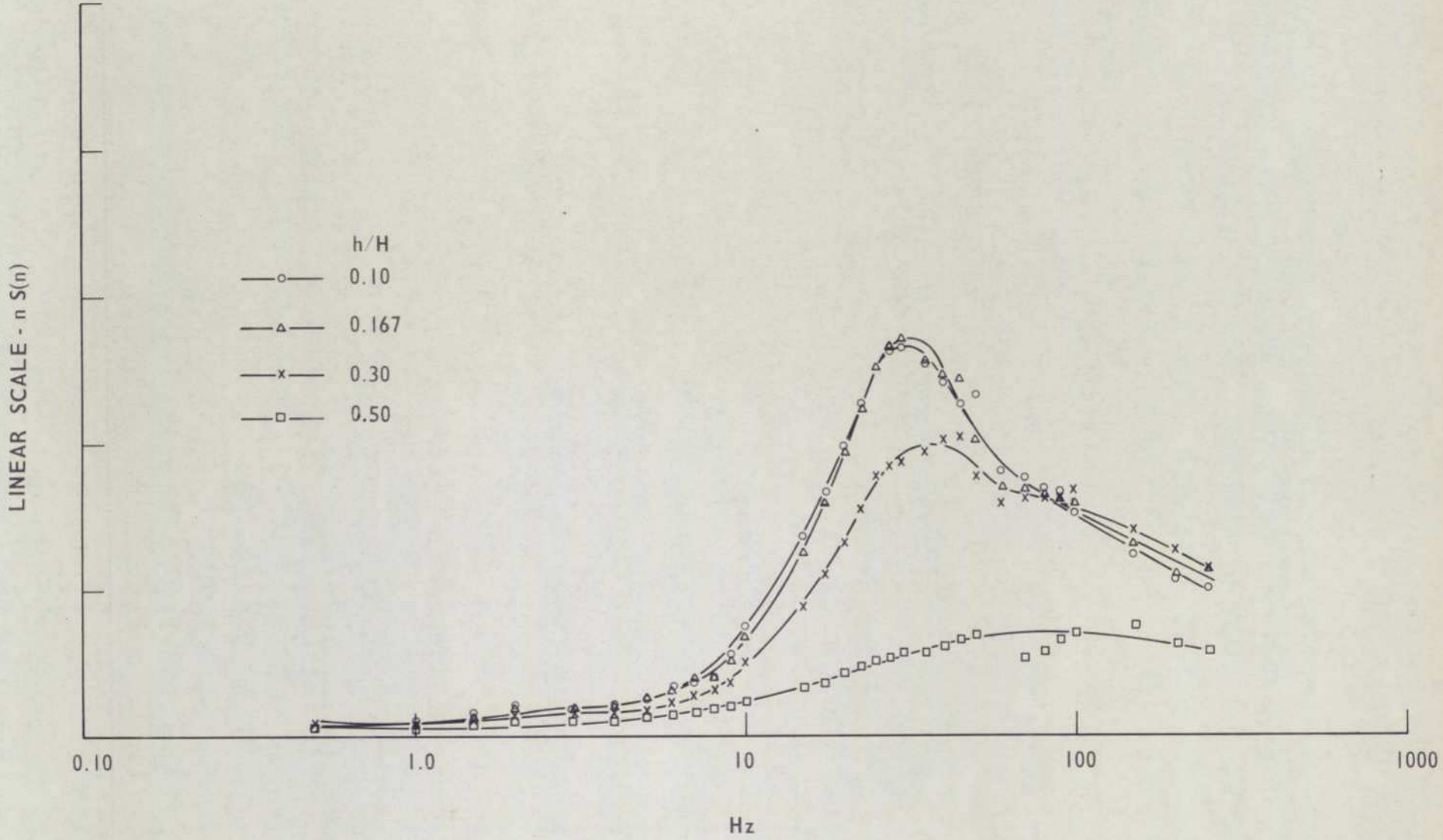


FIG. 81. LATERAL POWER SPECTRA - VARIATION WITH HEIGHT 457mm (18 in) AFT OF V.G. TRAILING EDGE SEMI SPAN ℄

JC/G.H.Ltd.(CON)(23.5.69)RL.3.3.1894

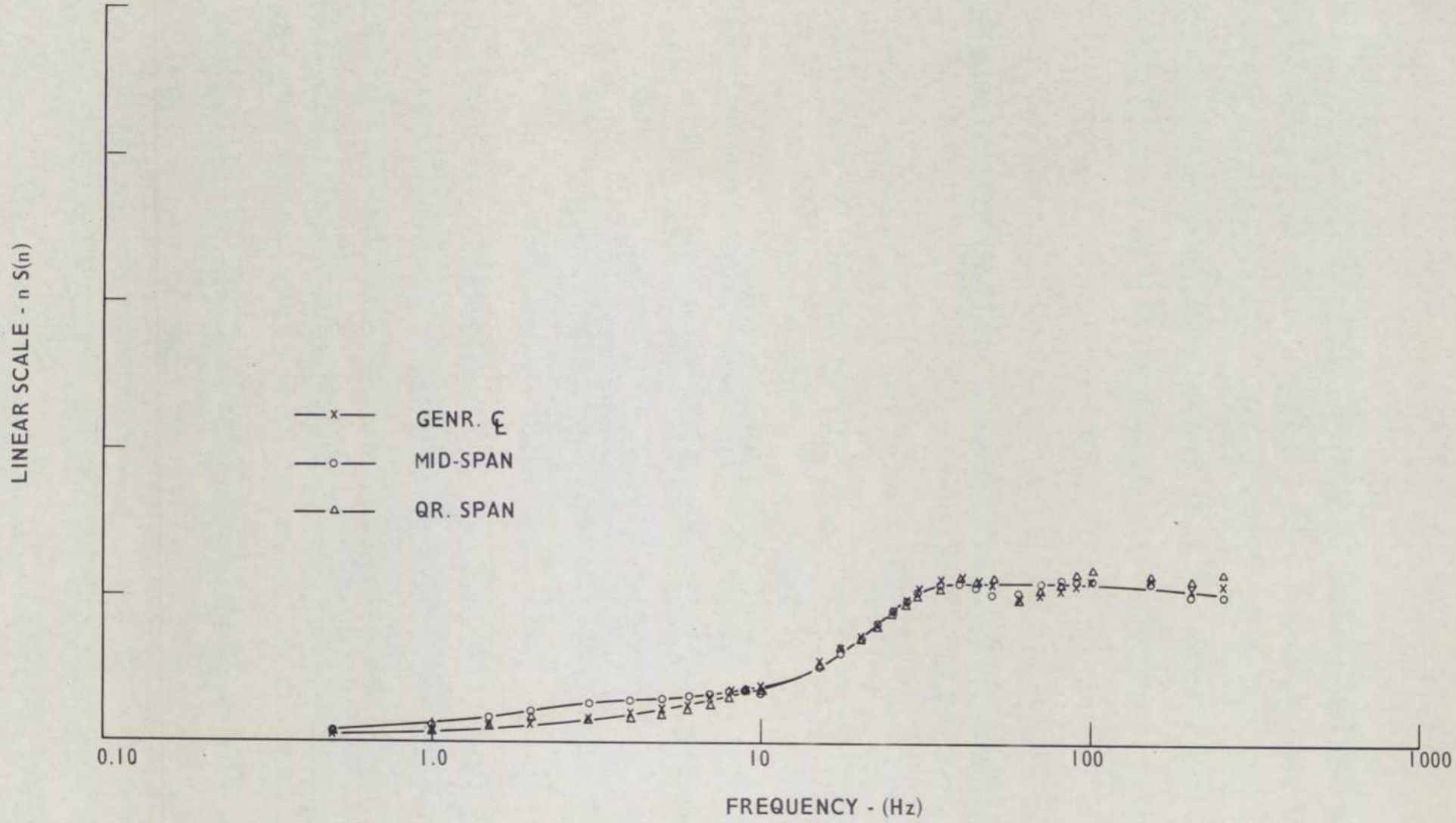


FIG. 82. VERTICAL POWER SPECTRA AT h/H = 0.167. 457.0mm (18in) AFT OF V.G. TRAILING EDGE

JC/G.H.LTD(CON)(23.5.69) RL 3.3.1895

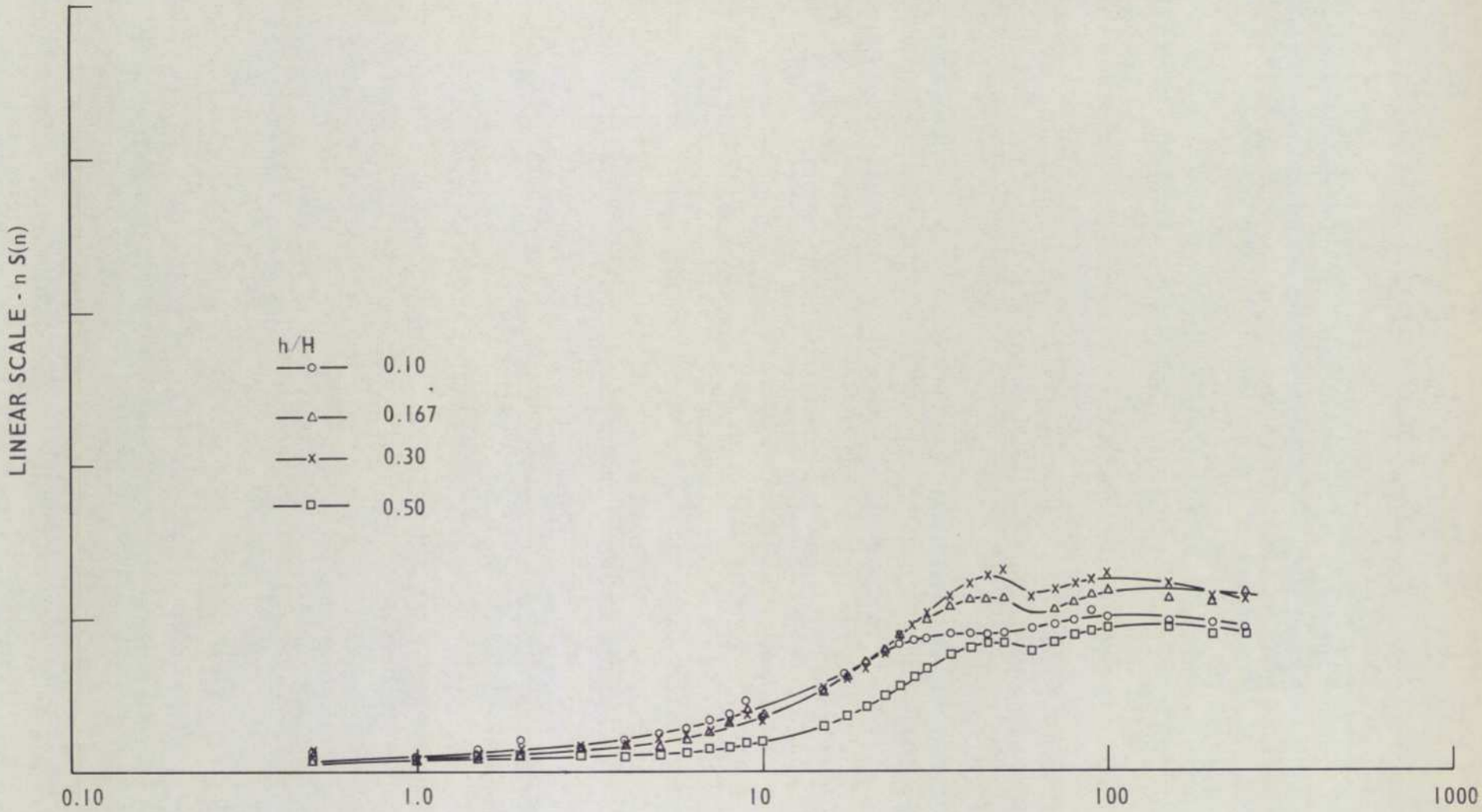


FIG. 83. VERTICAL POWER SPECTRA - VARIATION WITH HEIGHT 457.0mm (18in) AFT OF V.G. TRAILING EDGE SEMI-SPAN ℄

JC/G.H.LTD. (CON)(23.5.69) RL 3.3.1896

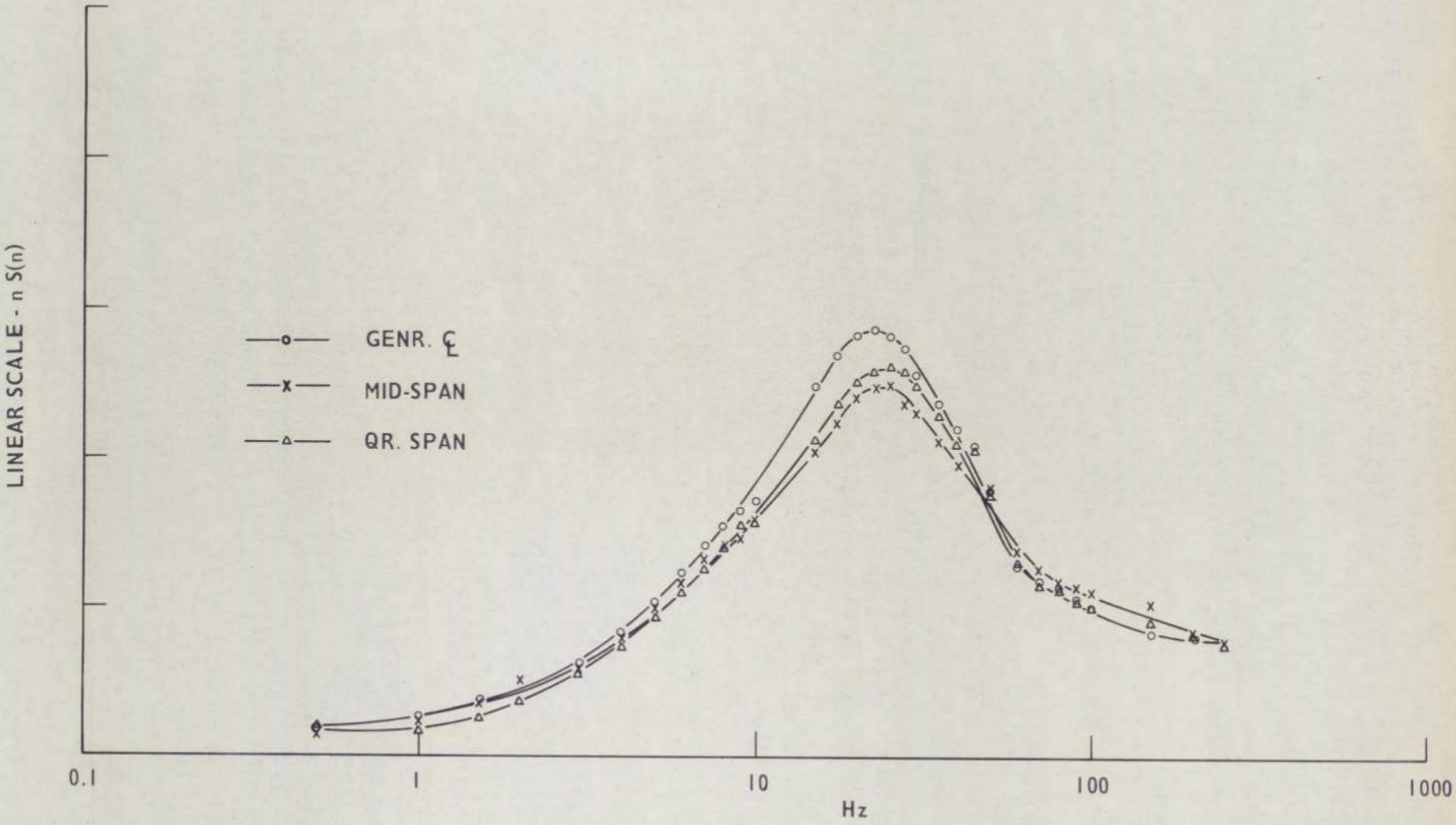


FIG. 84. LONGITUDINAL POWER SPECTRA AT h/H = 0.167 685.0mm(27in) AFT OF V.G. TRAILING EDGE

JC/G.H.LTD (CON)(11.9.69) RL 3.3.1897

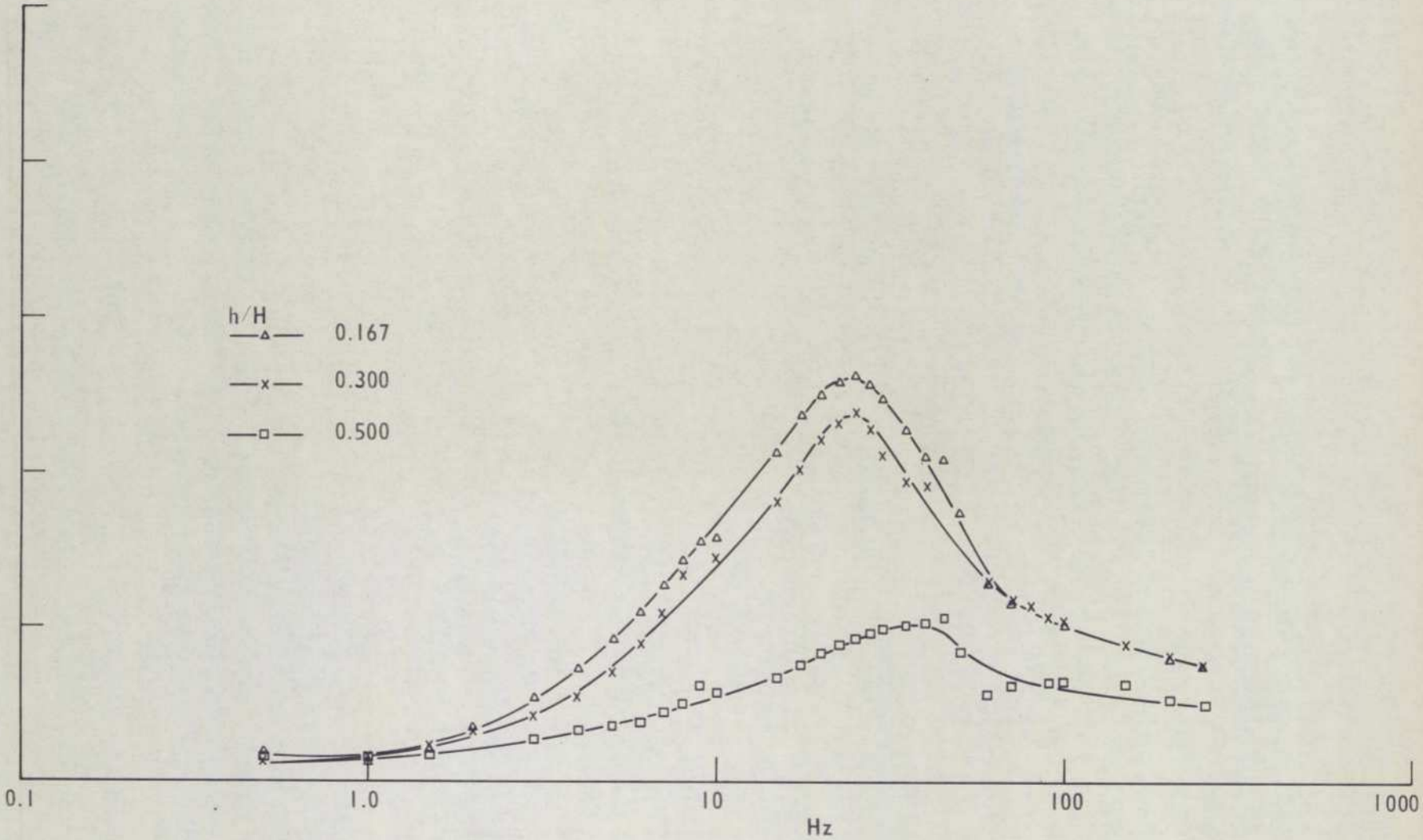


FIG. 8 5. LONGITUDINAL POWER SPECTRA - VARIATION WITH HEIGHT 685.0mm (27in) AFT OF V.G. TRAILING EDGE SEMI-SPAN $\mathcal{C}_L$

JC/G.H.LTD.(CON)(23.5.69) RL 3.3.1898

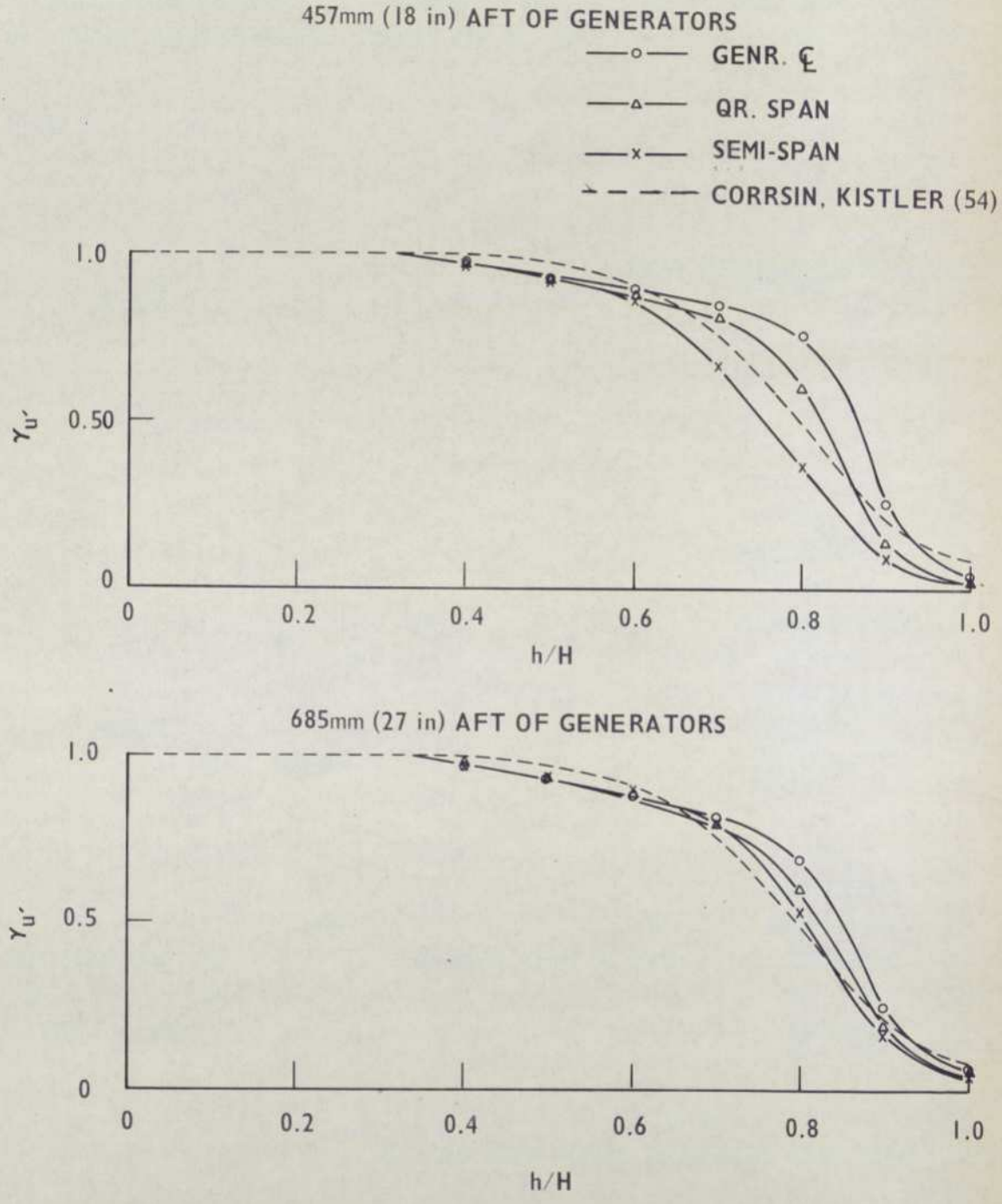


FIG. 86. INTERMITTENCY FACTOR DISTRIBUTION ACROSS THE SIMULATED BOUNDARY LAYER. COMPARISON OF DISTRIBUTIONS 457mm (18 in) AND 685mm (27 in) AFT OF GENERATOR TRAILING EDGES

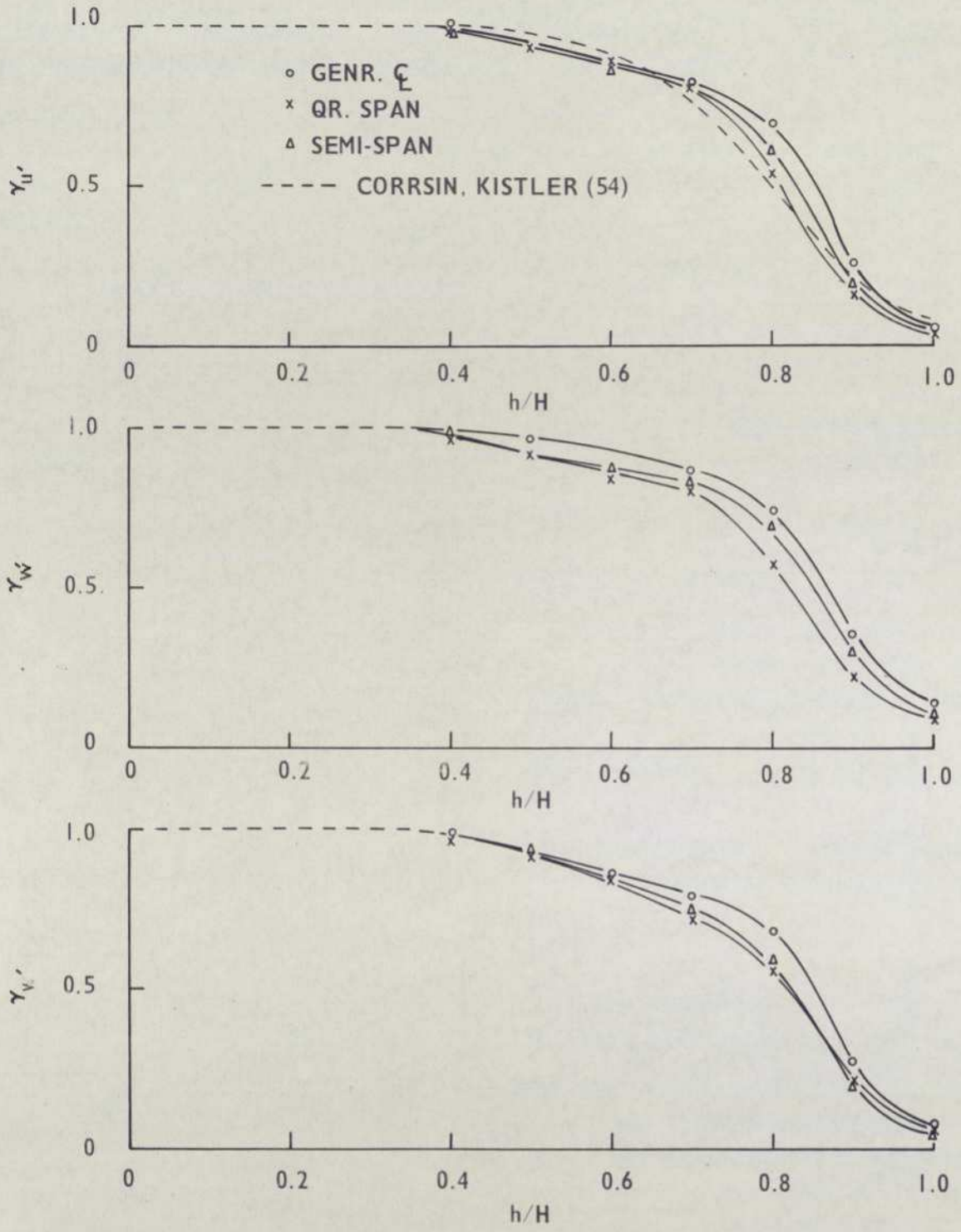


FIG. 87. INTERMITTENCY FACTOR DISTRIBUTION ACROSS THE SIMULATED BOUNDARY LAYER. 685mm (27 in) AFT OF GENERATOR TRAILING EDGES

COMPARISON OF MEASUREMENTS WITH ATMOSPHERIC BOUNDARY LAYER PROFILE SUGGESTED BY HARRIS'S DATA (1968)

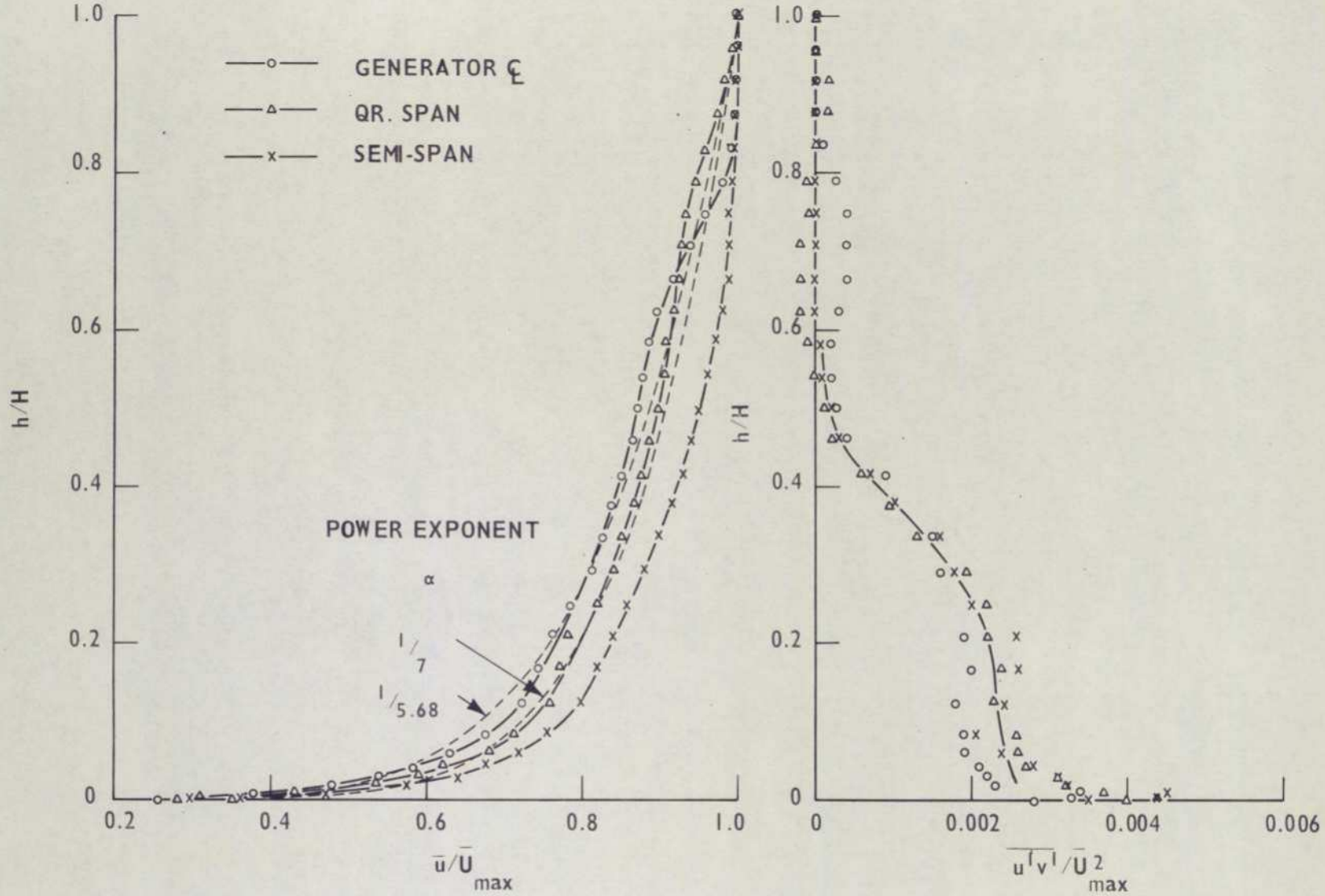


FIG. 88. VELOCITY AND REYNOLDS STRESS PROFILES IN A SIMULATED BOUNDARY LAYER. PLANE OF TRAVERSES: 457mm (18in) AFT OF GENERATOR TRAILING EDGES

JC/G.H.LTD. (CON)(23.5.69) RL 3.3.1901

COMPARISON OF MEASUREMENTS WITH ATMOSPHERICAL BOUNDARY LAYER PROFILE SUGGESTED BY HARRIS'S DATA (1968)

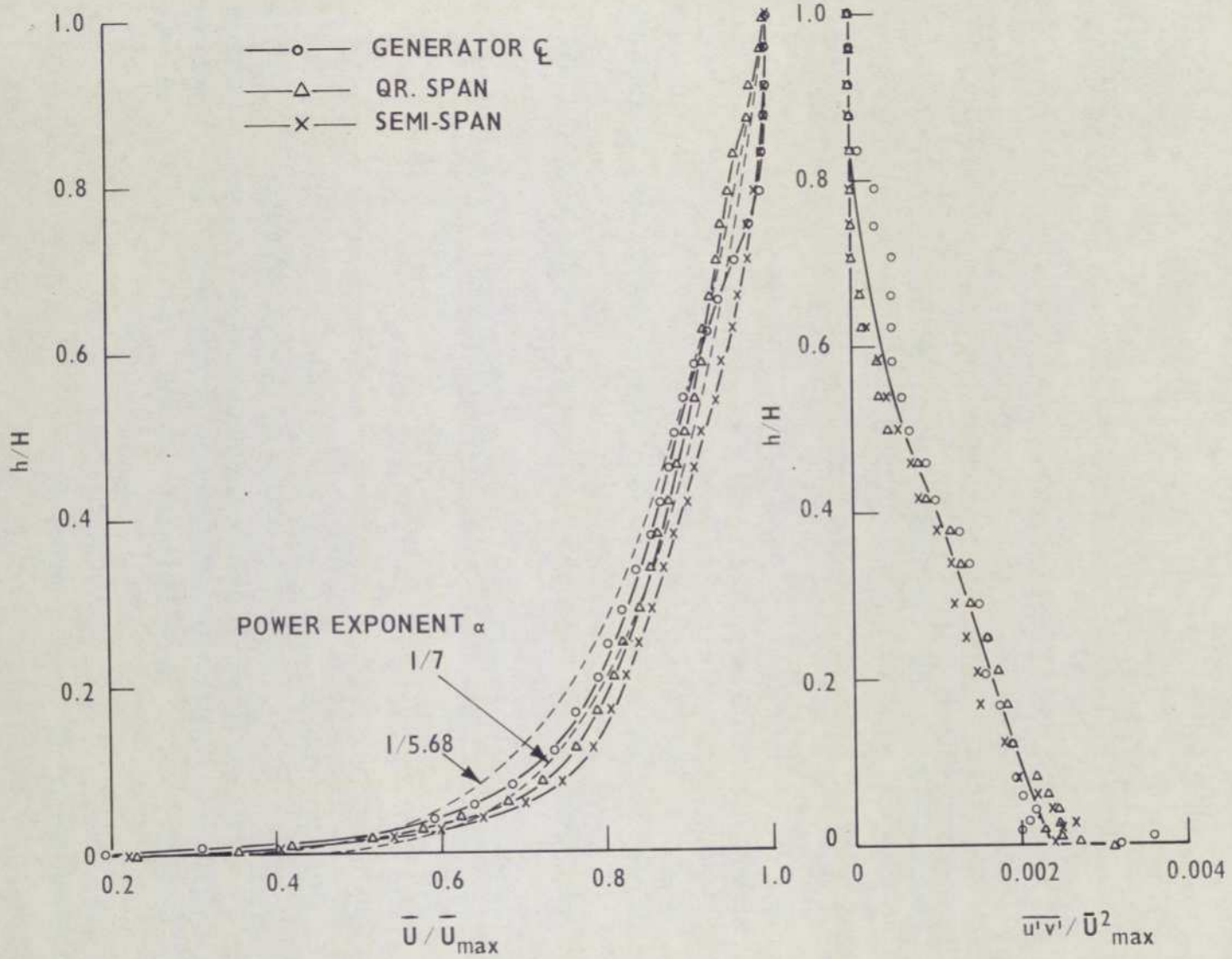


FIG.89. VELOCITY AND REYNOLDS STRESS PROFILES IN A SIMULATED BOUNDARY LAYER.

PLANE OF TRAVERSE: 685 mm(27in.) AFT OF GENERATOR TRAILING EDGES

JC/G.H.Ltd.(CON)(23.5.69)RL.3.3.1902

COMPARISON OF MEASUREMENTS WITH ATMOSPHERIC BOUNDARY LAYER DATA (HARRIS 1968)

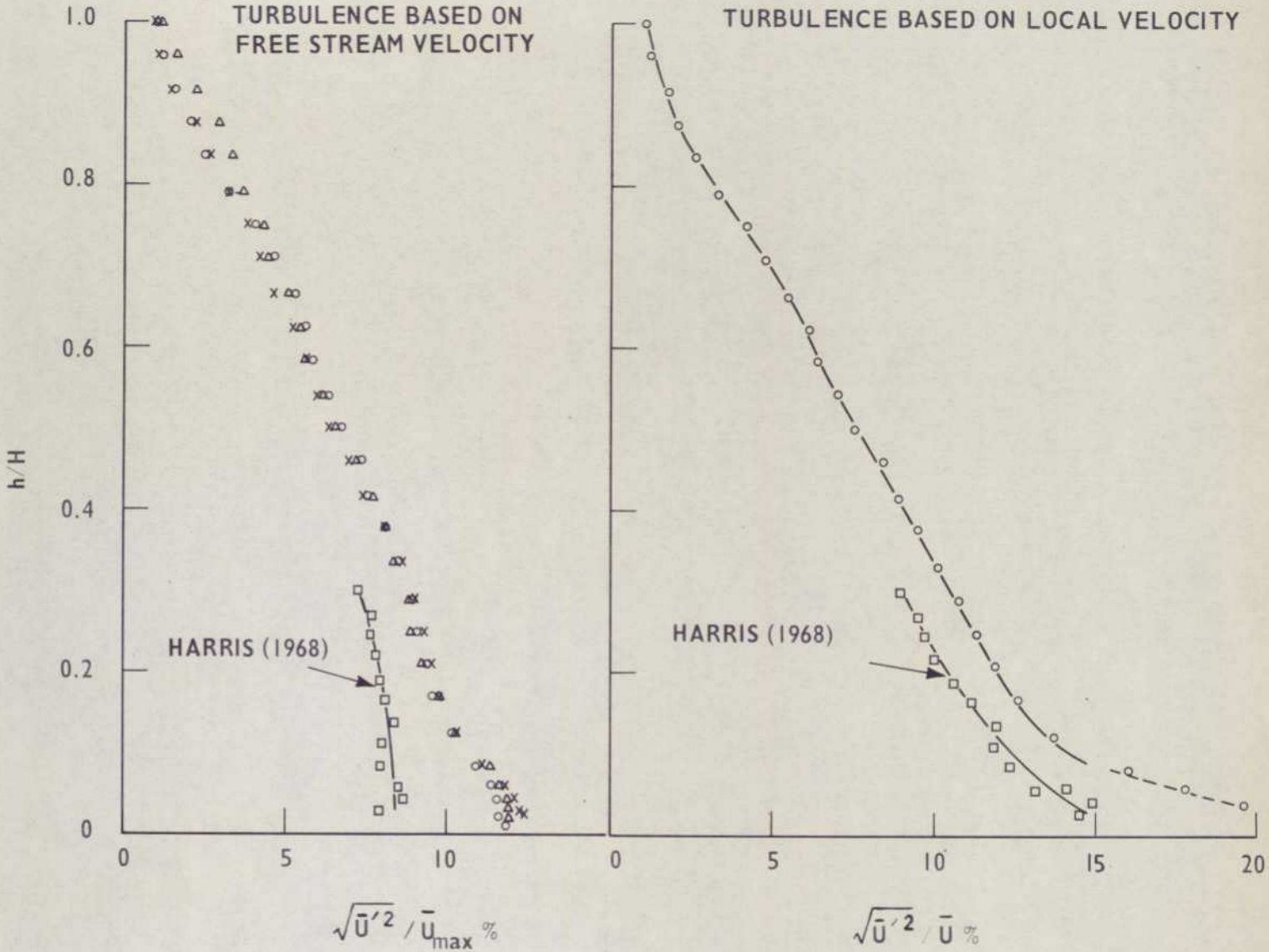


FIG. 90. TURBULENCE INTENSITY PROFILES IN A SIMULATED BOUNDARY LAYER. PLANE OF TRAVERSE: 685 mm (27 in.) AFT OF GENERATOR TRAILING EDGES

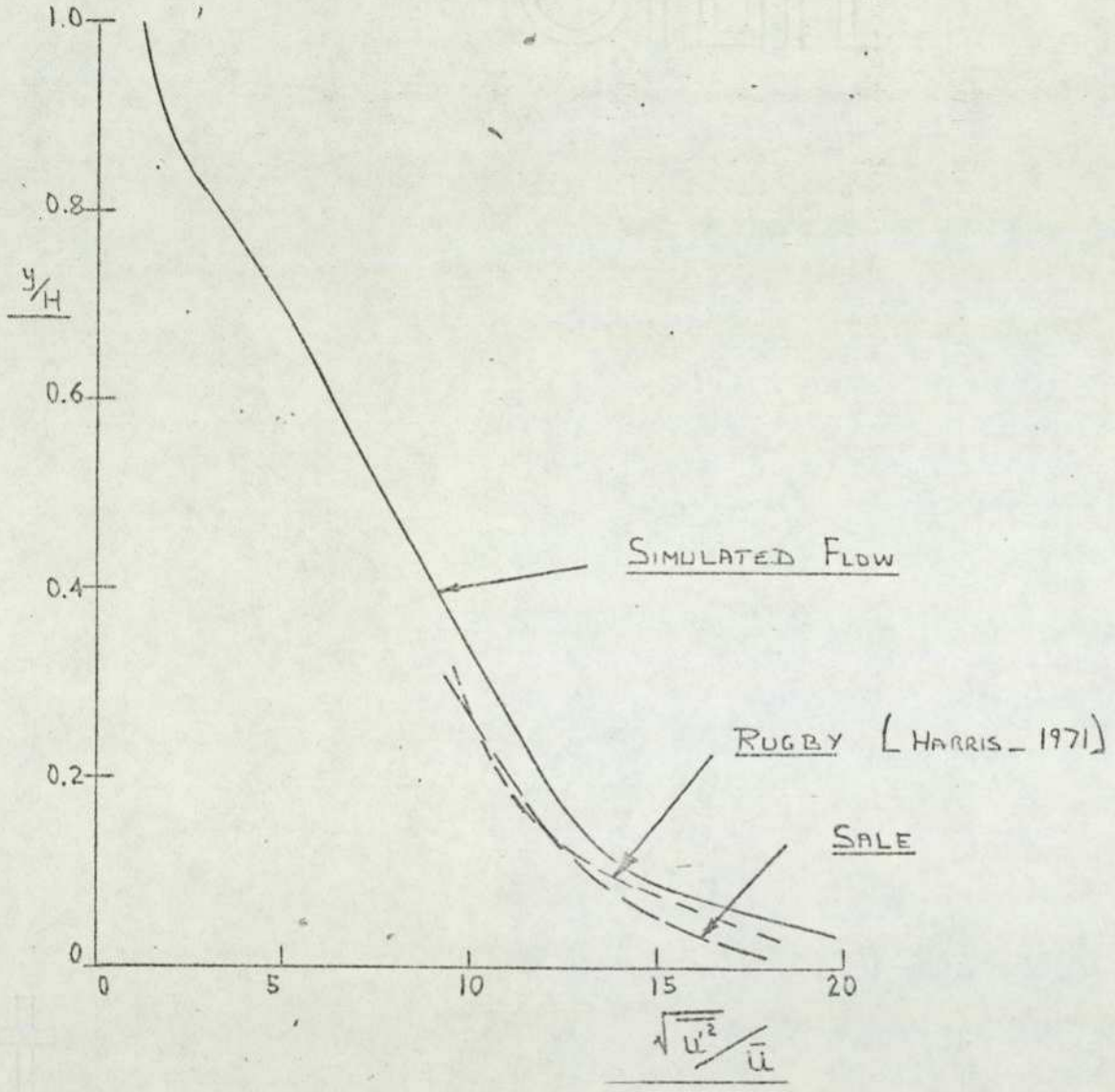
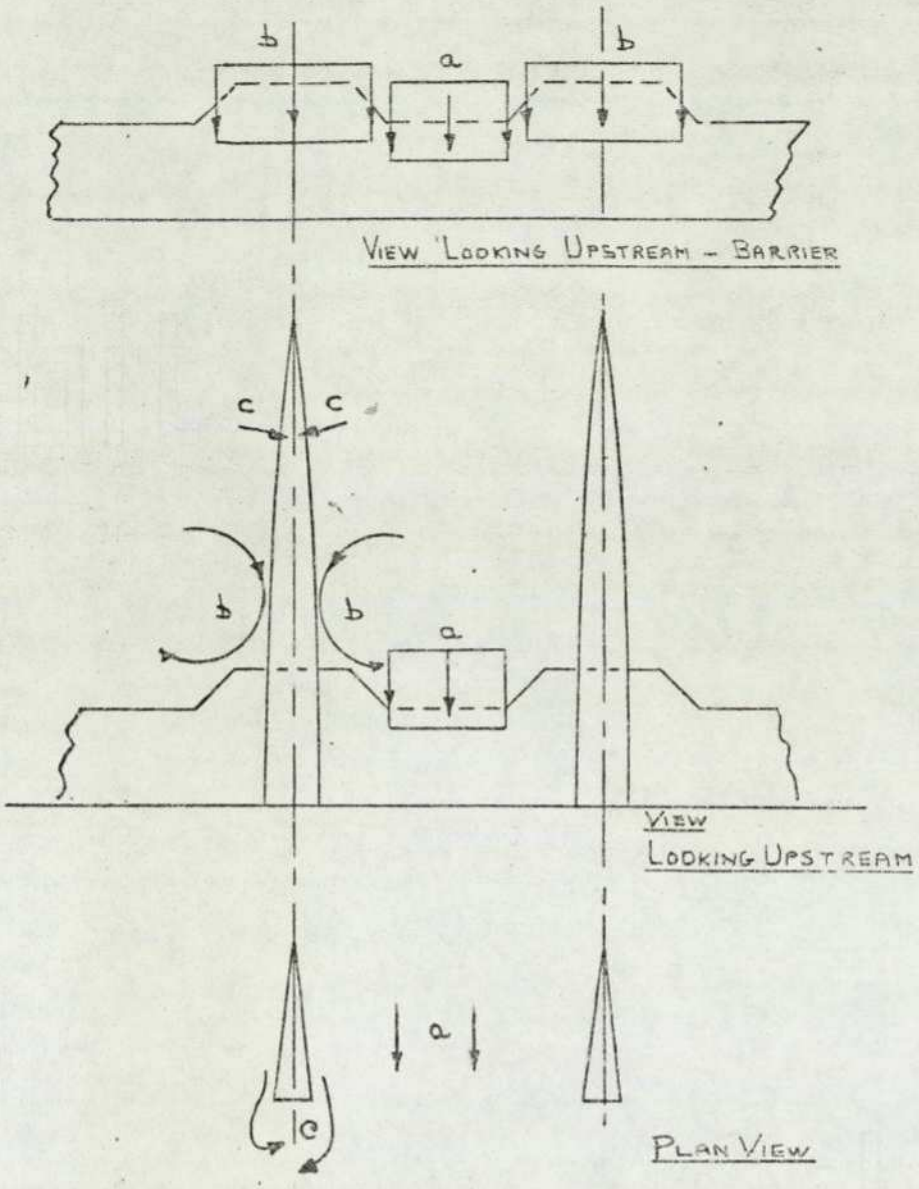


FIG. 91. COMPARISON OF SIMULATED AND FULL SCALE TURBULENCE INTENSITIES



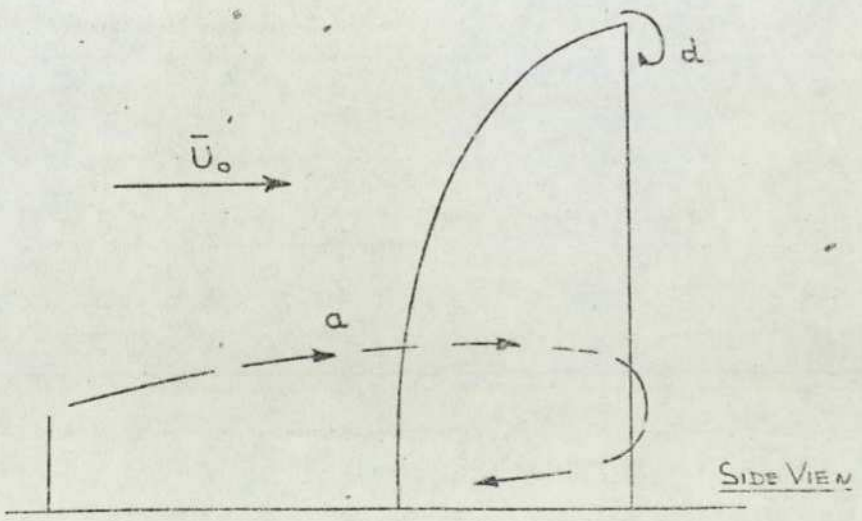


FIG.92 SCHEMATIC REPRESENTATION OF IMMEDIATE FLOW PATTERNS PRODUCED BY BOUNDARY LAYER SIMULATION COMPONENTS.

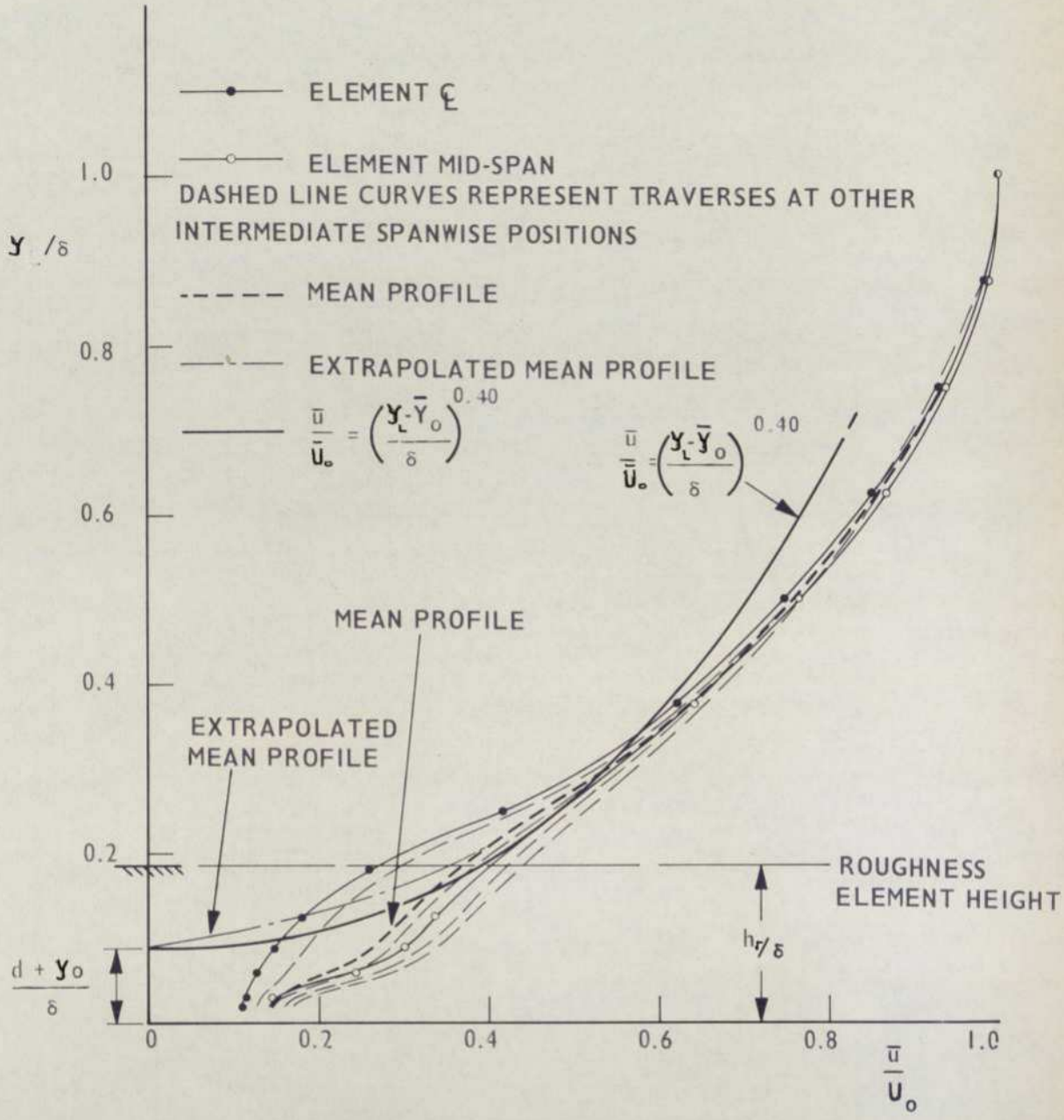


FIG.93. VELOCITY PROFILES FOR TYPICAL ROUGHNESS DISTRIBUTION

$A_R/A = 0.205$

ATMOSPHERIC BOUNDARY LAYER SIMULATION

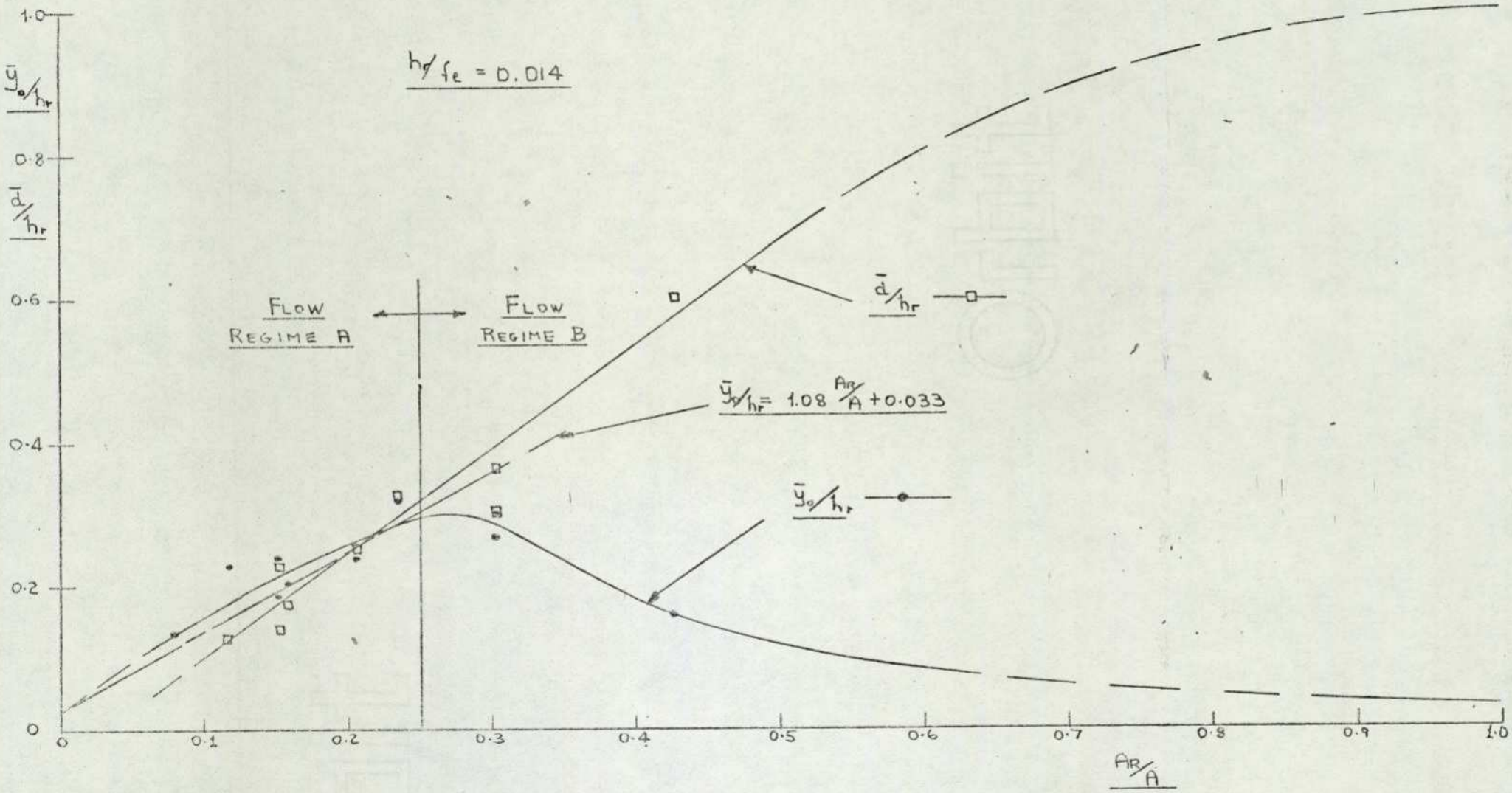


FIG. 94. VARIATION OF ROUGHNESS LENGTH AND ZERO PLANE DISPLACEMENT WITH ROUGHNESS ELEMENT DENSITY

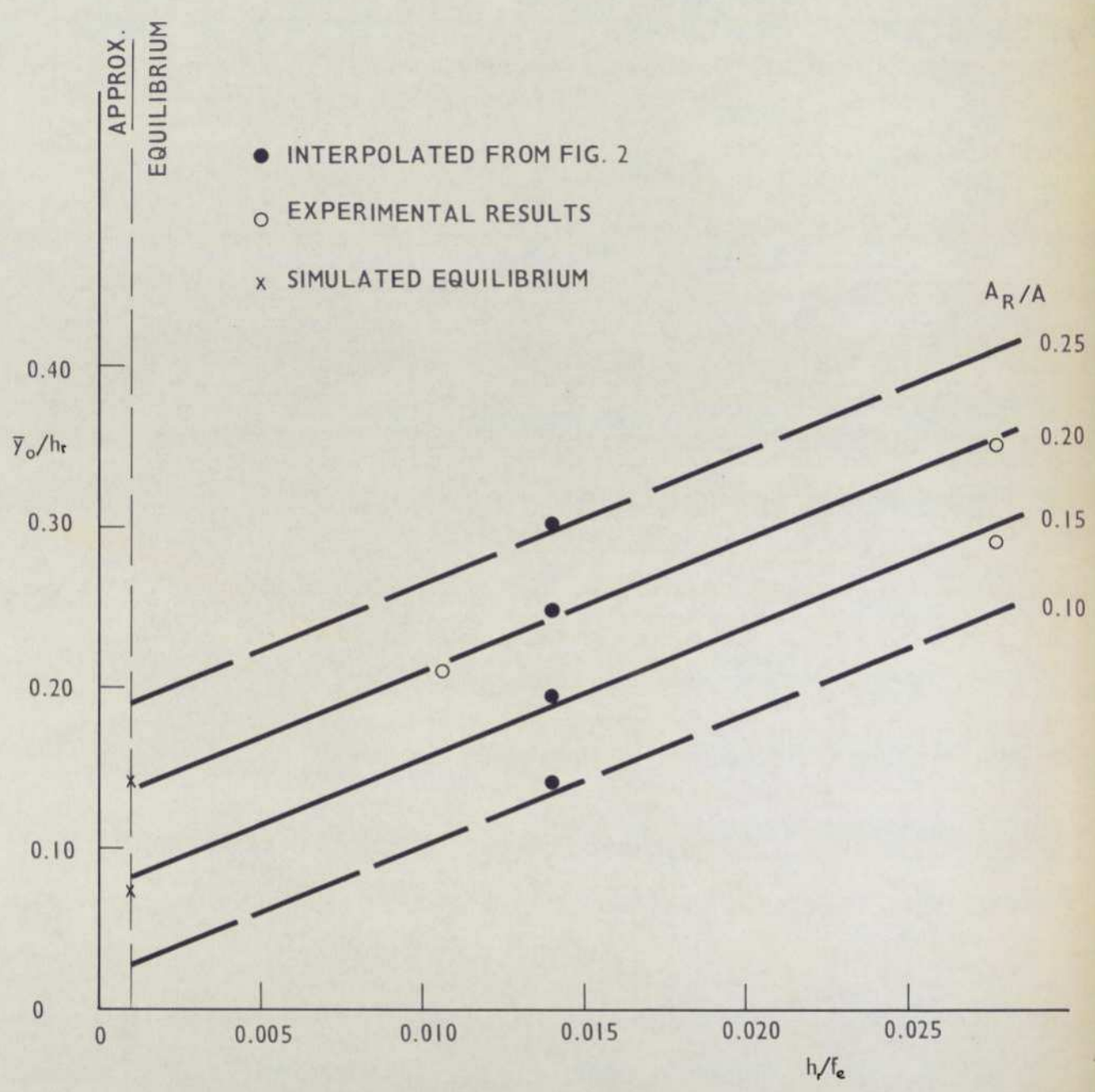


FIG.95. VARIATION OF MEAN ROUGHNESS LENGTH WITH FETCH AND DENSITY DISTRIBUTION OF ROUGHNESS

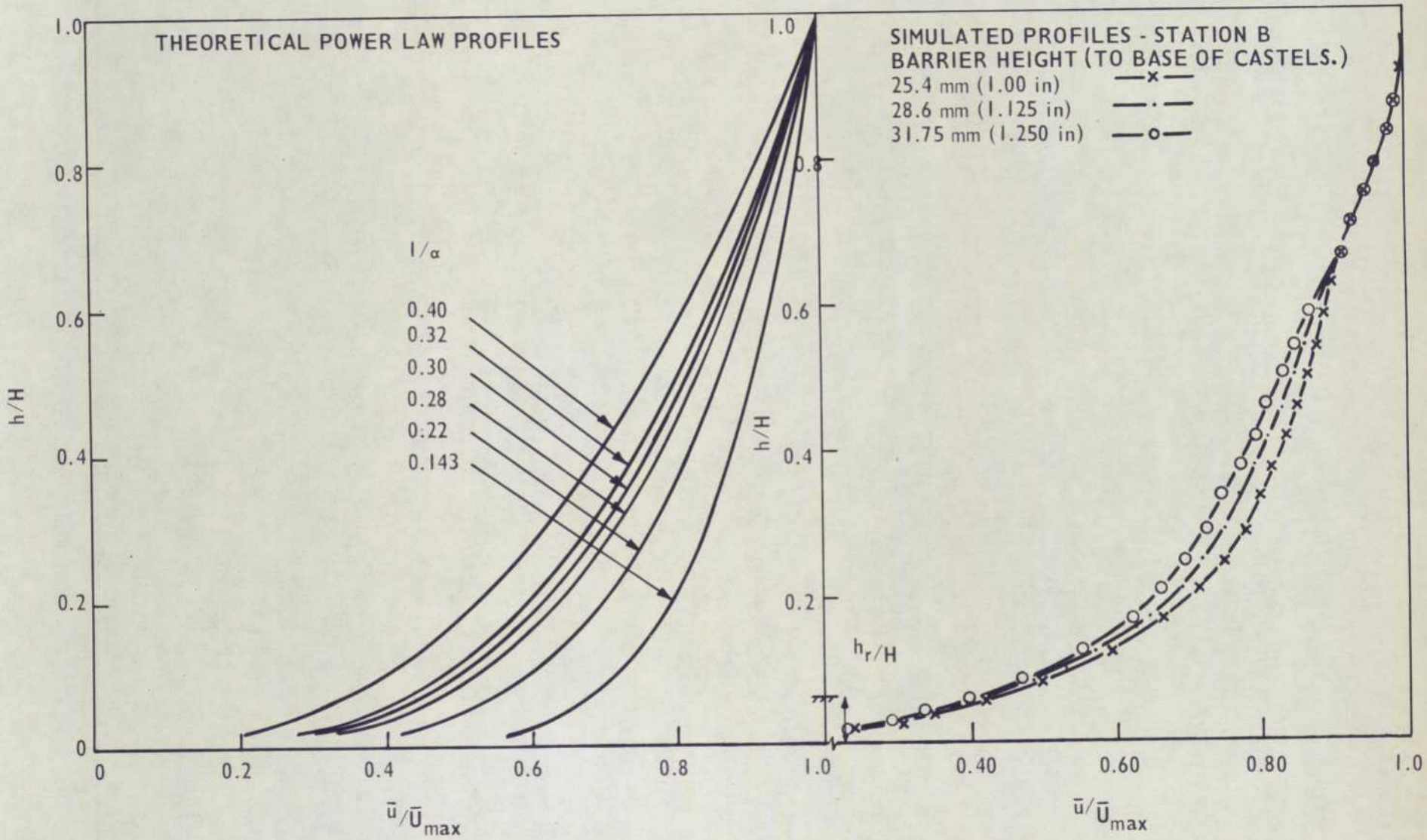


FIG.96. BOUNDARY LAYER SIMULATION - URBAN TERRAIN

JC/D.L.(CON)(5.4.72)RL.3.3.3058

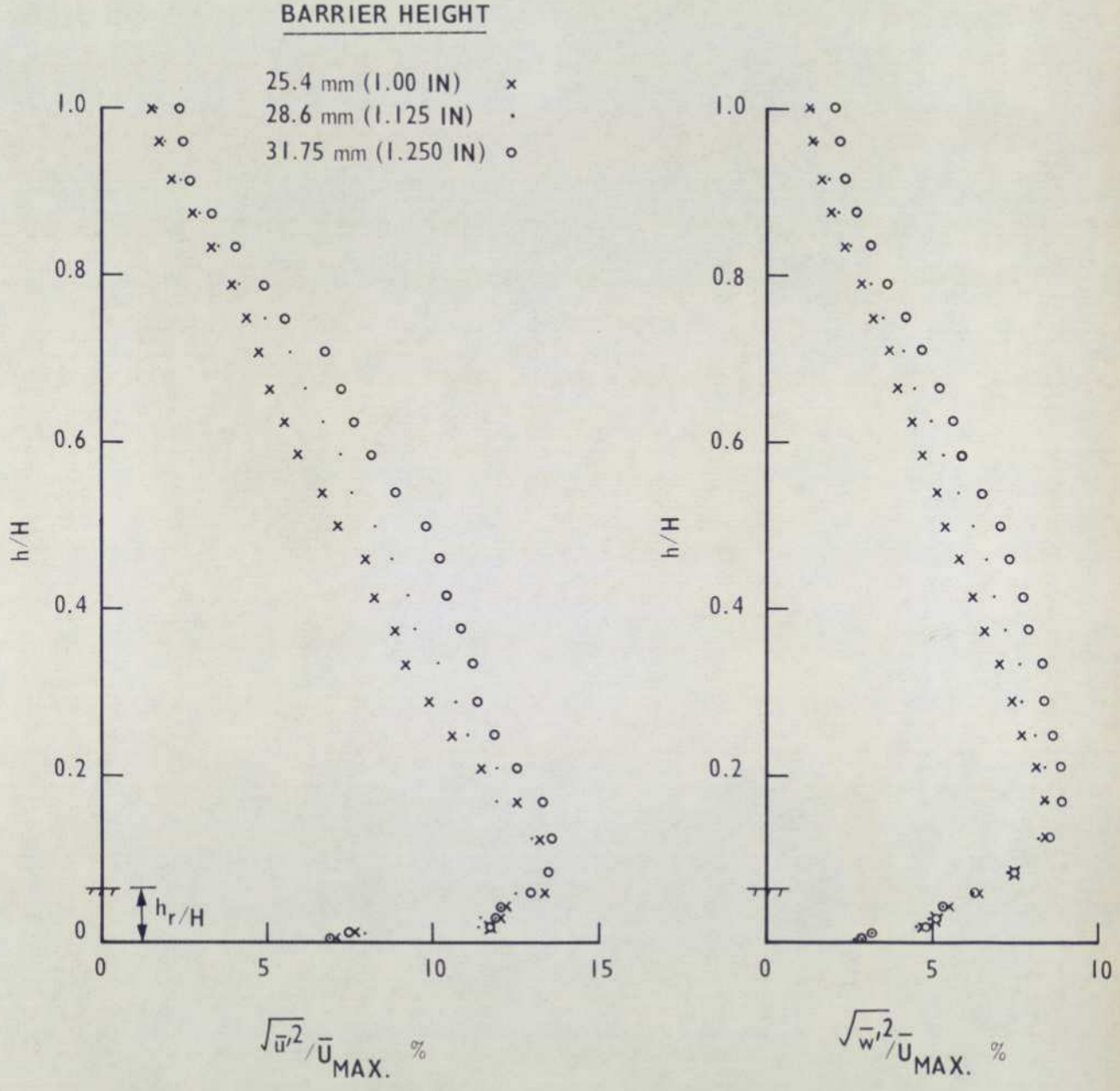


FIG. 97 BOUNDARY LAYER SIMULATION - URBAN TERRAIN, EFFECT OF BARRIER HEIGHT ON TURBULENCE PRODUCTION - STATION B

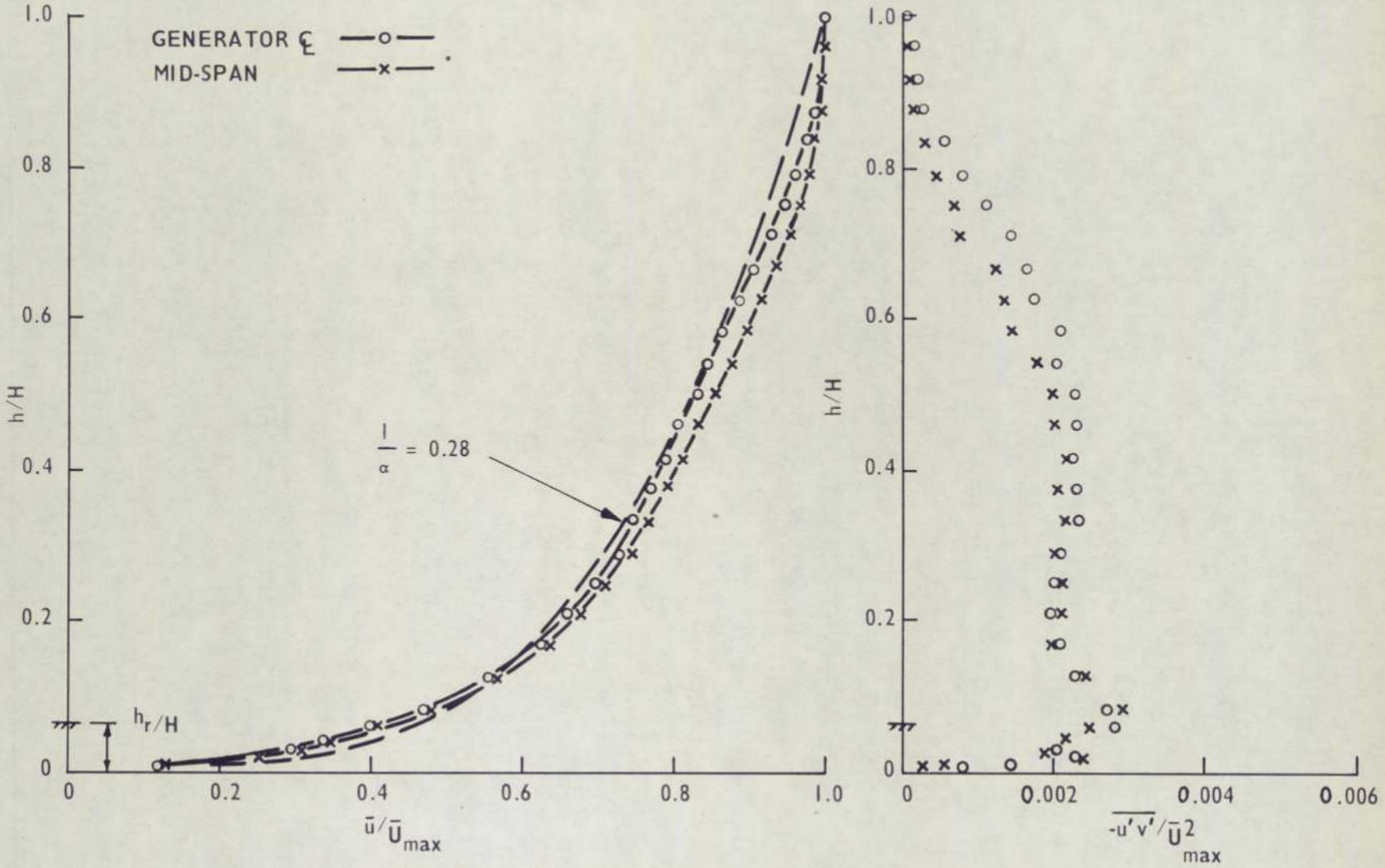


FIG.98. BOUNDARY LAYER SIMULATION - URBAN TERRAIN. STATION B

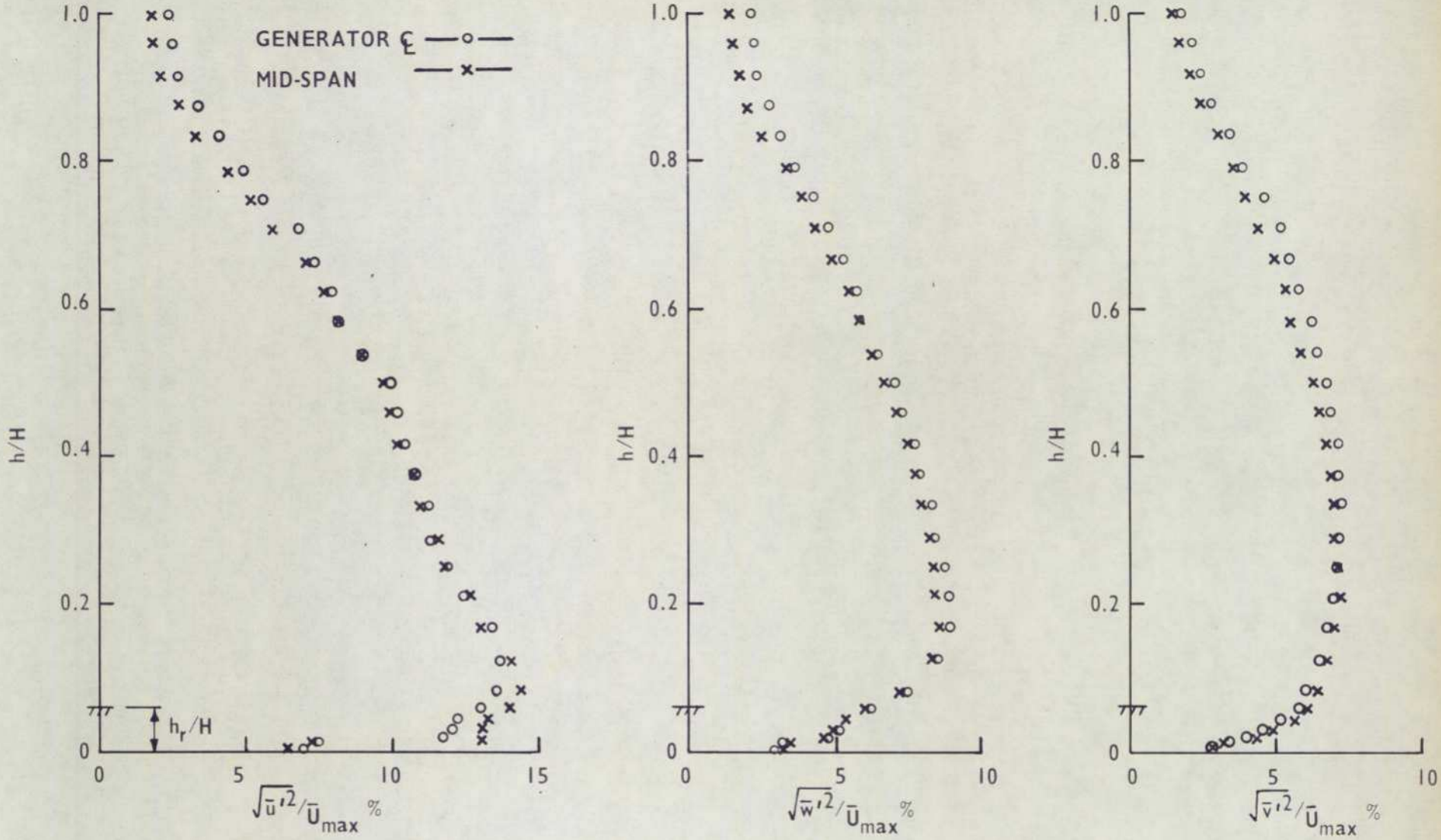


FIG.99. BOUNDARY LAYER SIMULATION - URBAN TERRAIN.STATION B

JC/D.L.(CON)(5.4.72)RL.3.3.3060

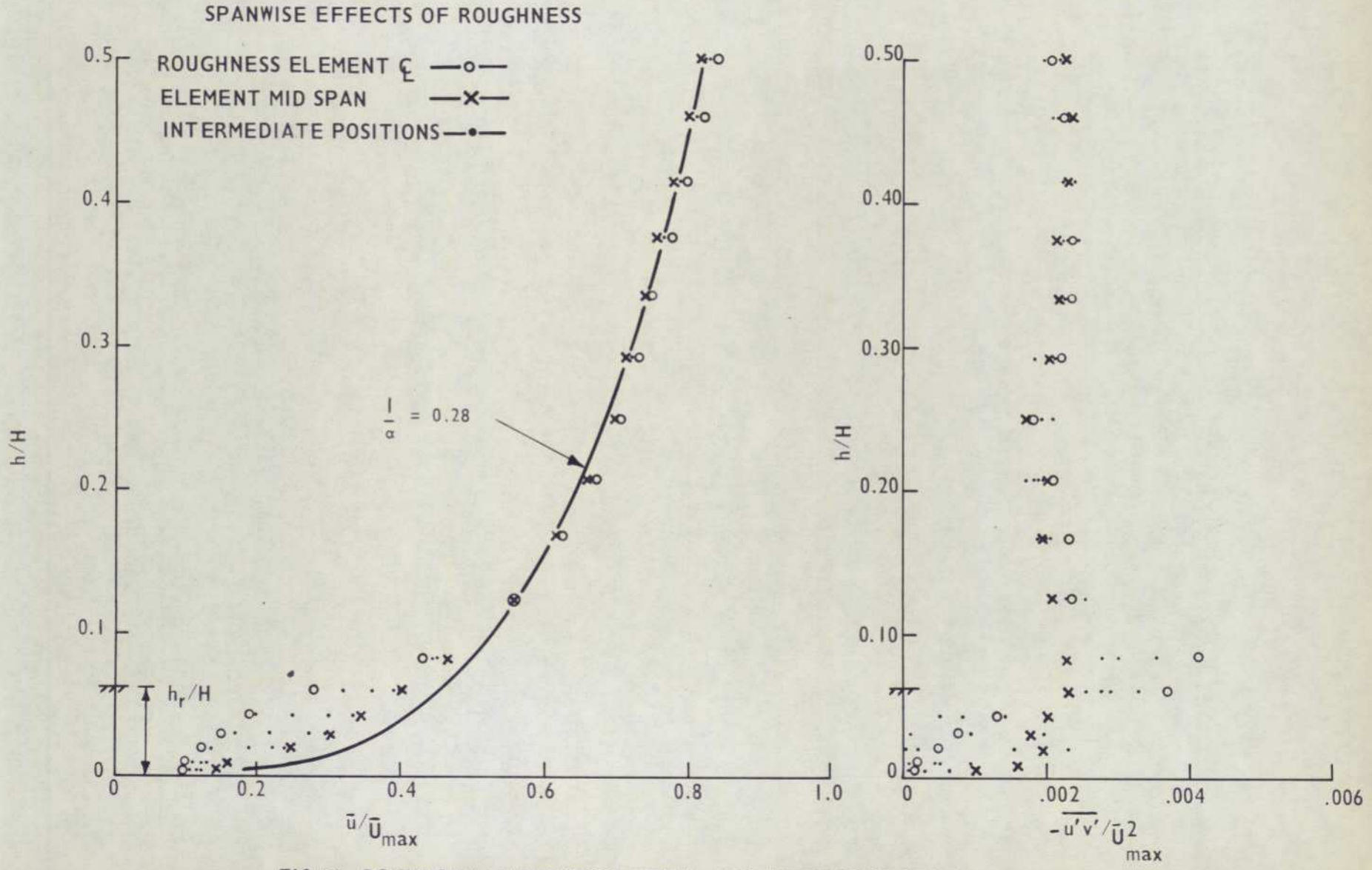


FIG.100. BOUNDARY LAYER SIMULATION - URBAN TERRAIN. STATION B

JC/D.L.(CON)(5.4.72)RL.3.3.3061

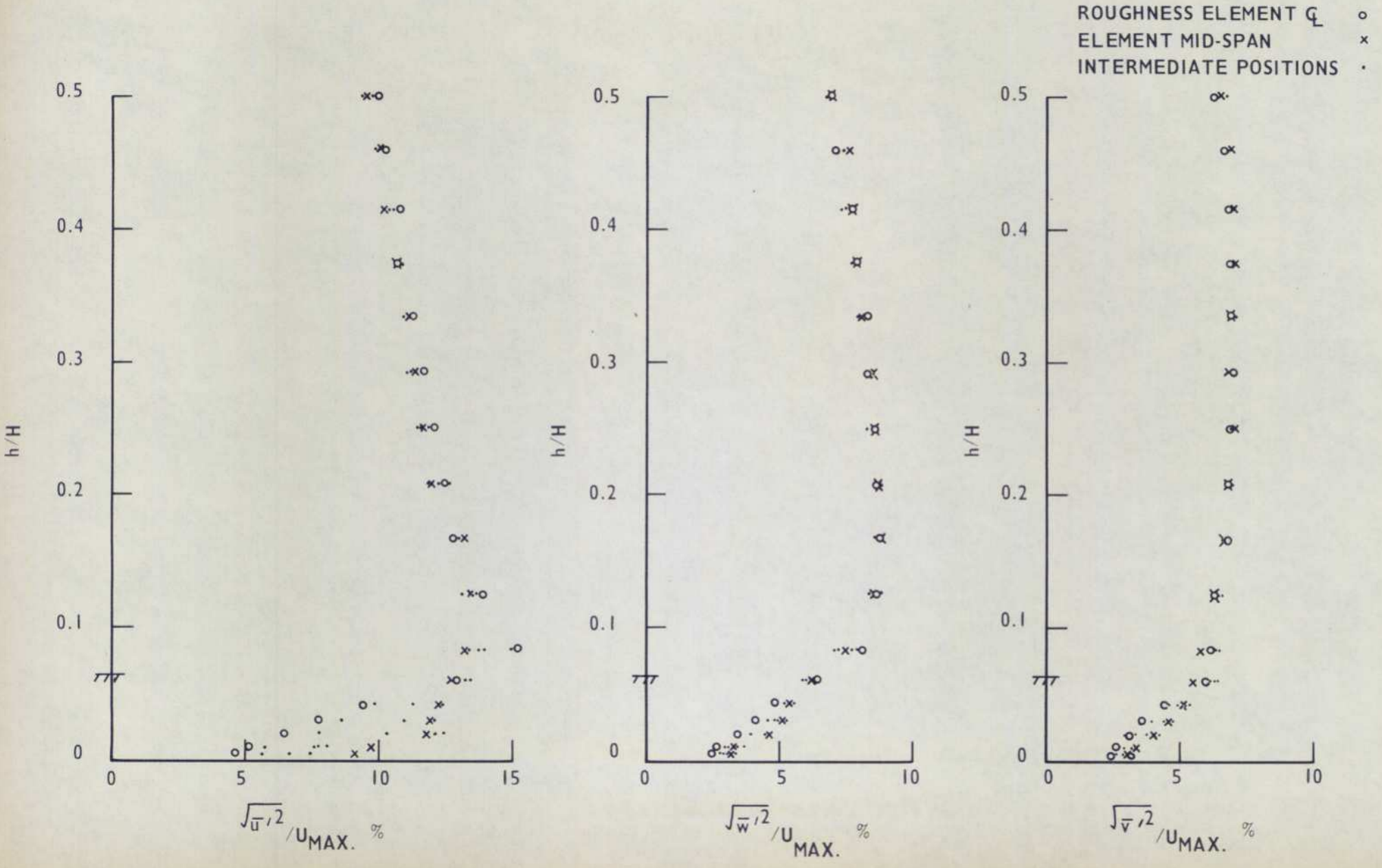


FIG. 101 BOUNDARY LAYER SIMULATION - URBAN TERRAIN, STATION B, SPANWISE EFFECTS OF ROUGHNESS

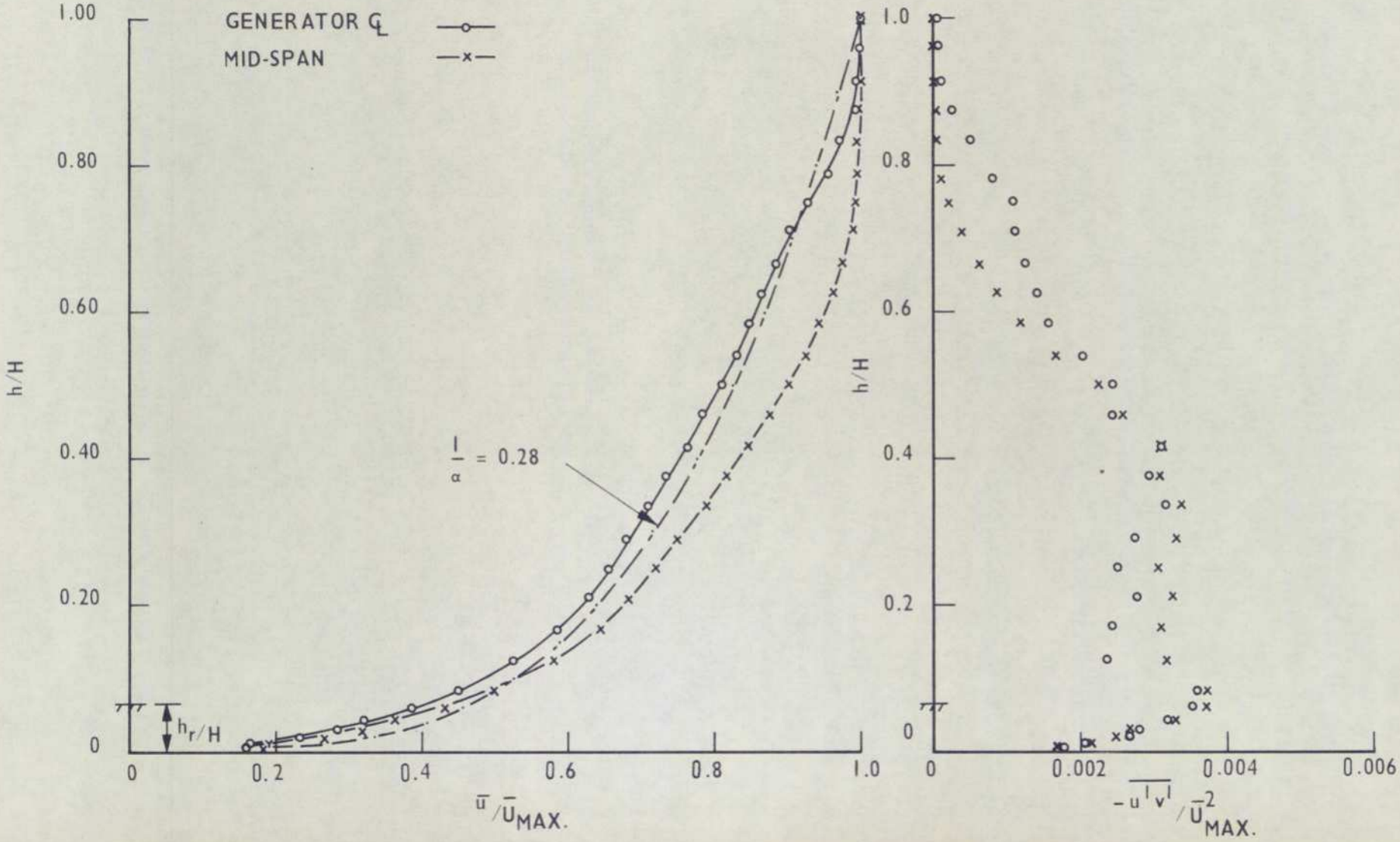


FIG. 102 BOUNDARY LAYER SIMULATION- URBAN TERRAIN, STATION A

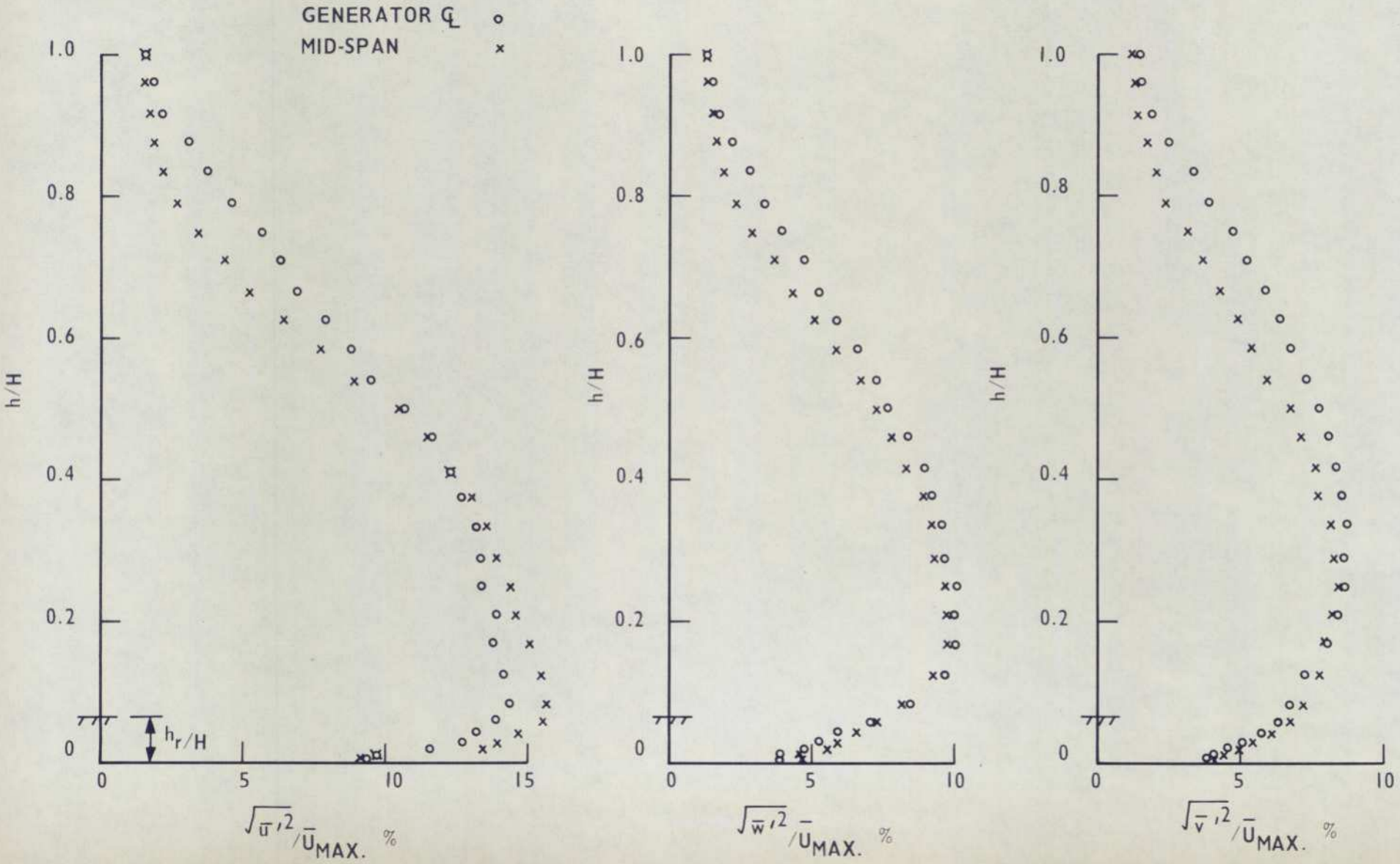


FIG. 103 BOUNDARY LAYER SIMULATION - URBAN TERRAIN, STATION A

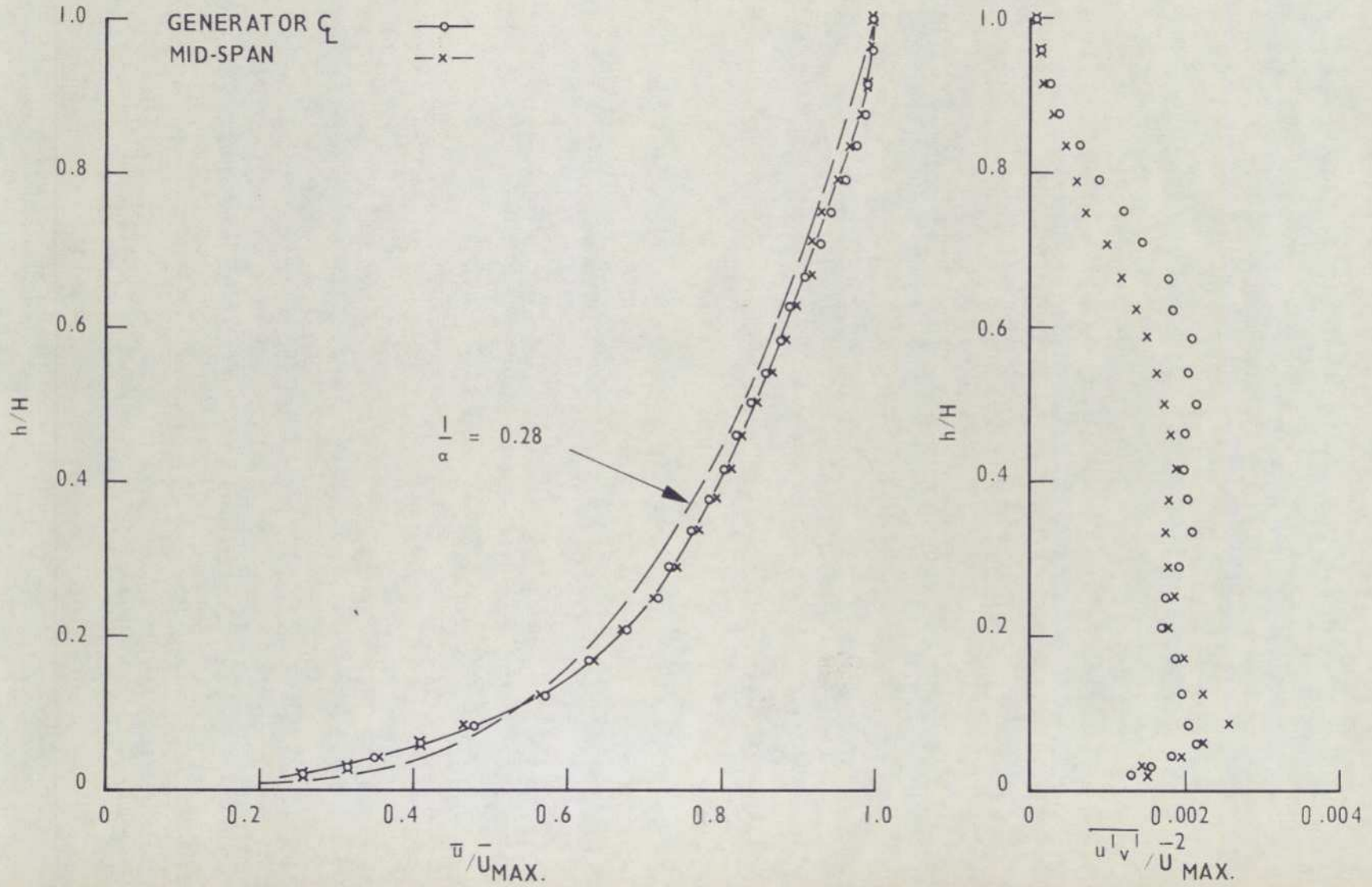


Fig.104. BOUNDARY LAYER SIMULATION - URBAN TERRAIN, STATION C

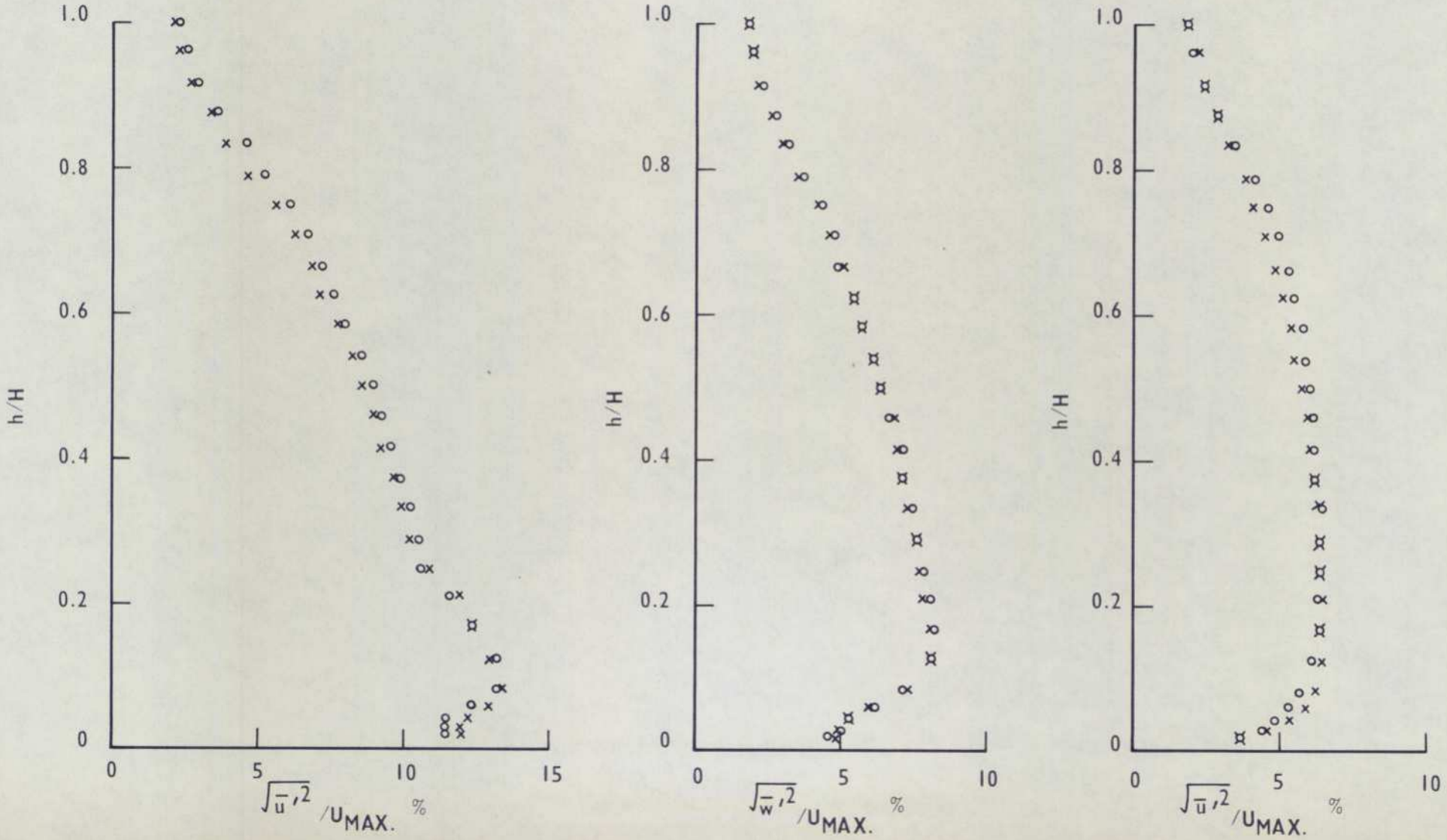


FIG. 105. BOUNDARY LAYER SIMULATION - URBAN TERRAIN, STATION C

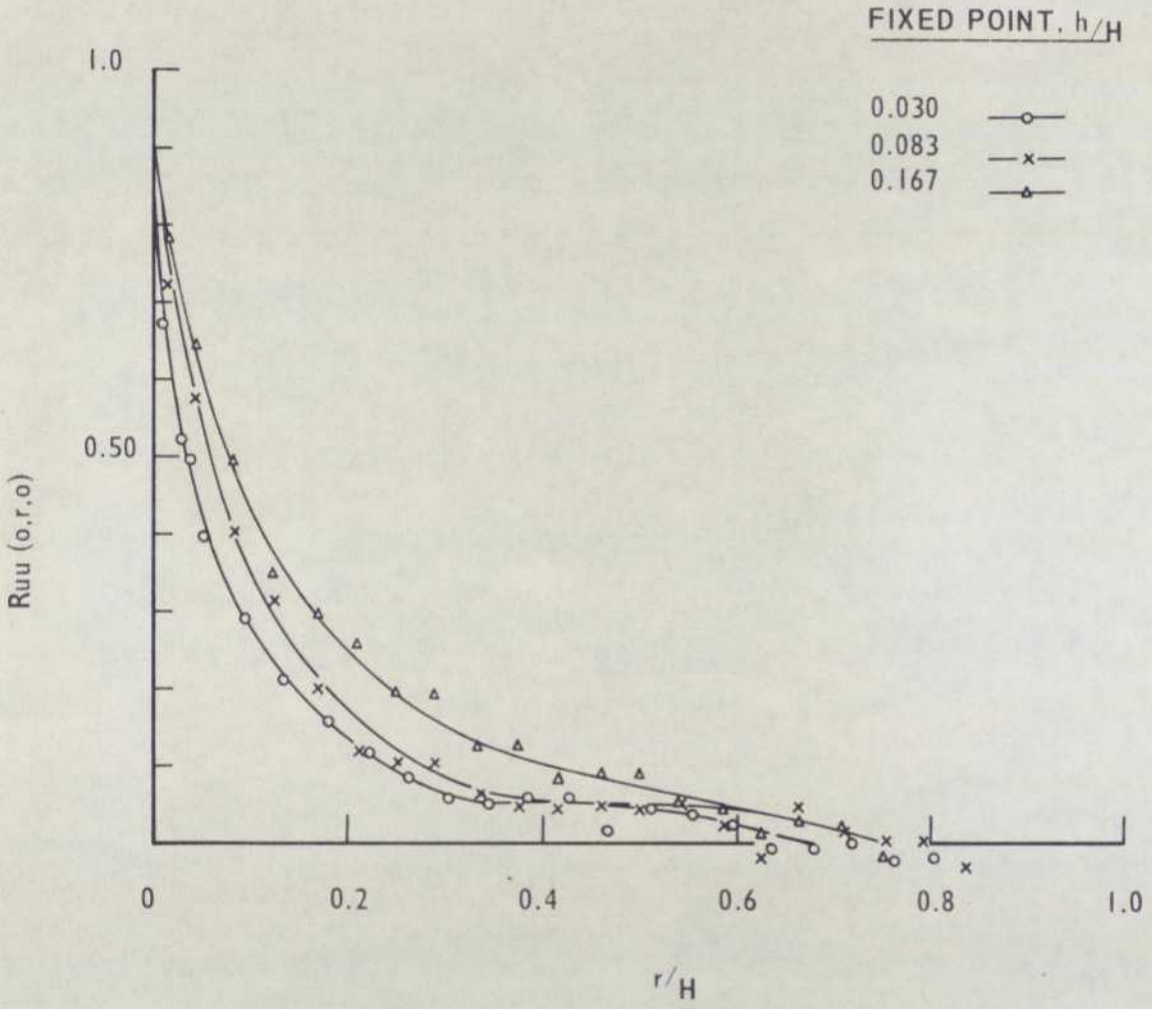


FIG. 106 CORRELATION COEFFICIENT DISTRIBUTION IN A SIMULATED BOUNDARY LAYER 685 mm (27 in) AFT OF VORTICITY GENERATOR TRAILING EDGES. SPANWISE POSITION - GENERATOR $\mathbb{Q}$

URBAN TERRAIN

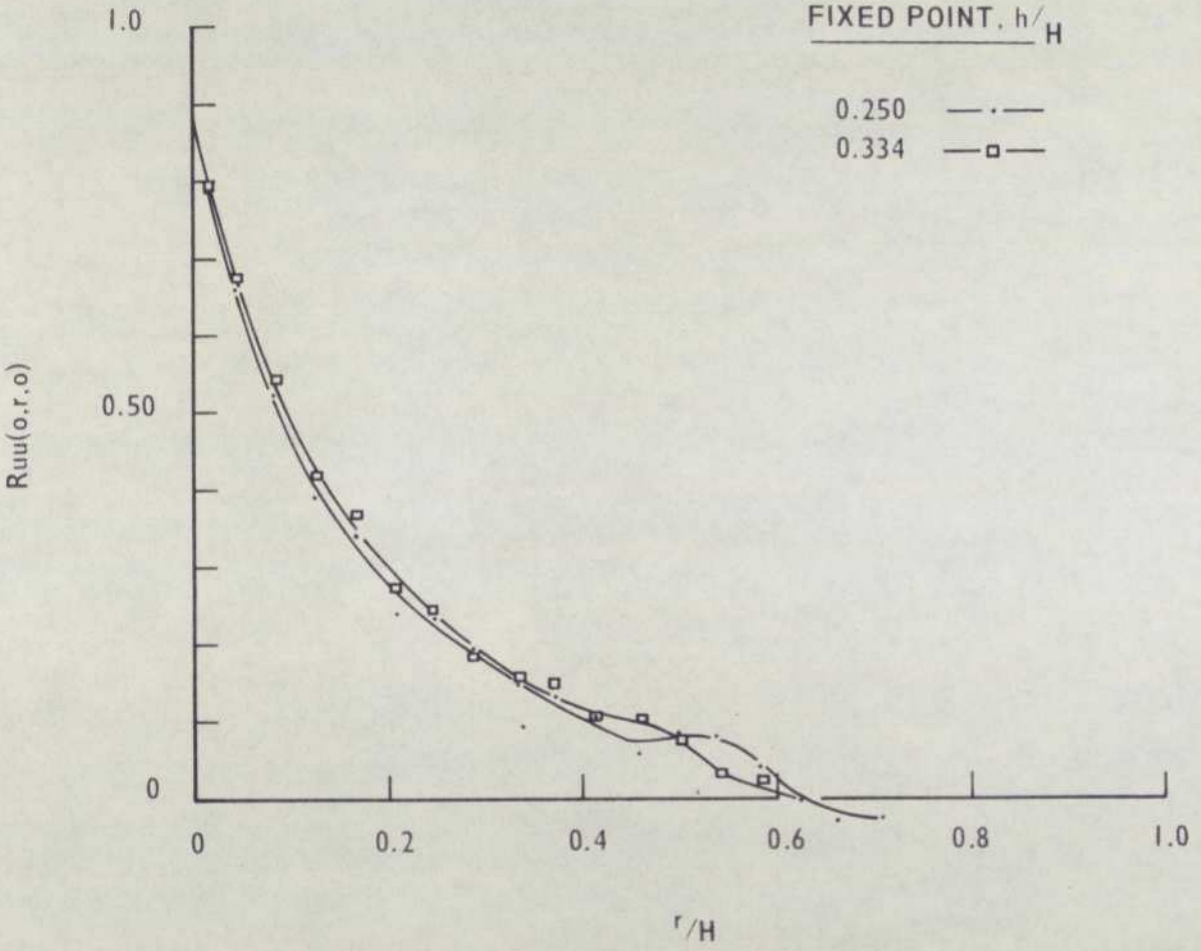


FIG. 107. CORRELATION COEFFICIENT DISTRIBUTION IN A SIMULATED BOUNDARY LAYER. 685 mm (27 in) AFT OF VORTICITY GENERATOR TRAILING EDGES

SPANWISE POSITION - GENERATOR $\mathcal{L}$

URBAN TERRAIN

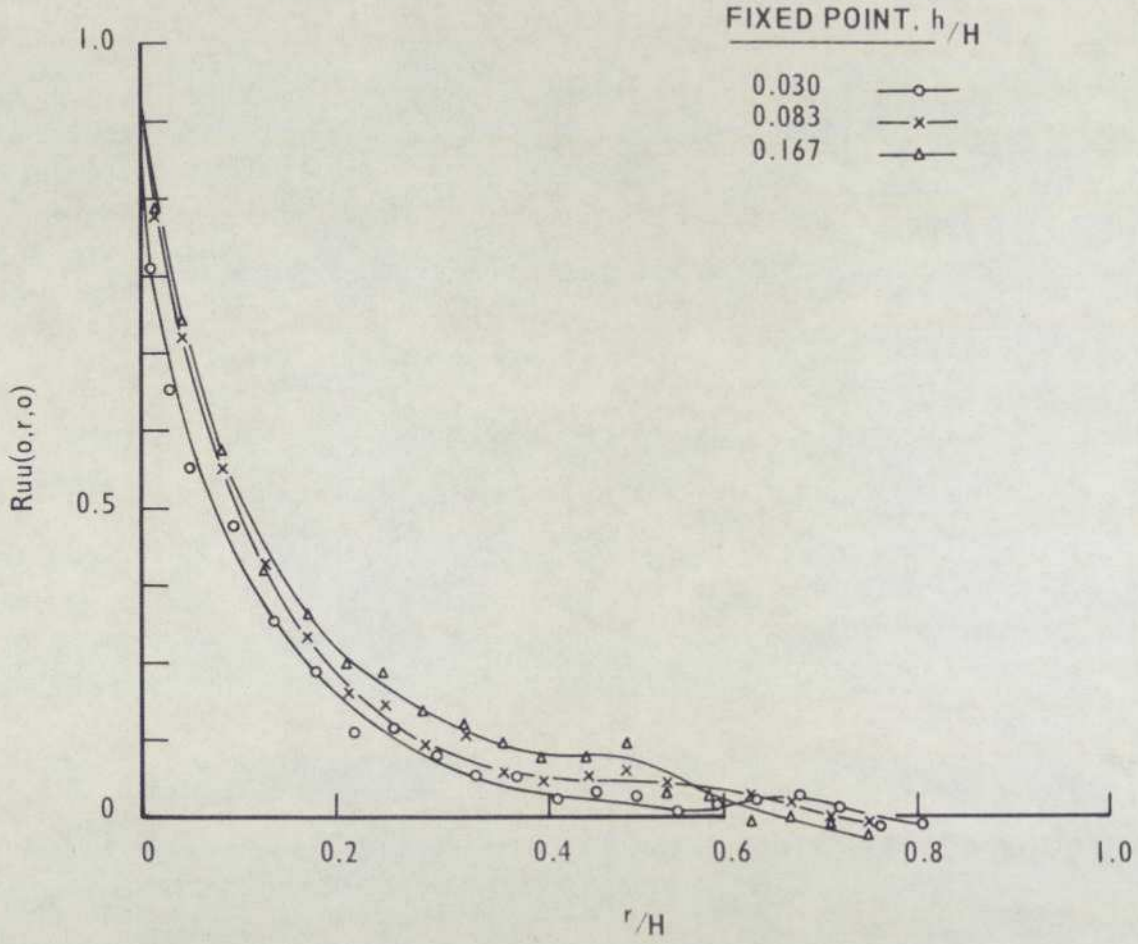


FIG.108. CORRELATION COEFFICIENT DISTRIBUTION IN A SIMULATED BOUNDARY LAYER. 685 mm (27 in) AFT OF VORTICITY GENERATOR TRAILING EDGES. SPANWISE POSITION - GENERATOR MID-SPAN.

URBAN TERRAIN

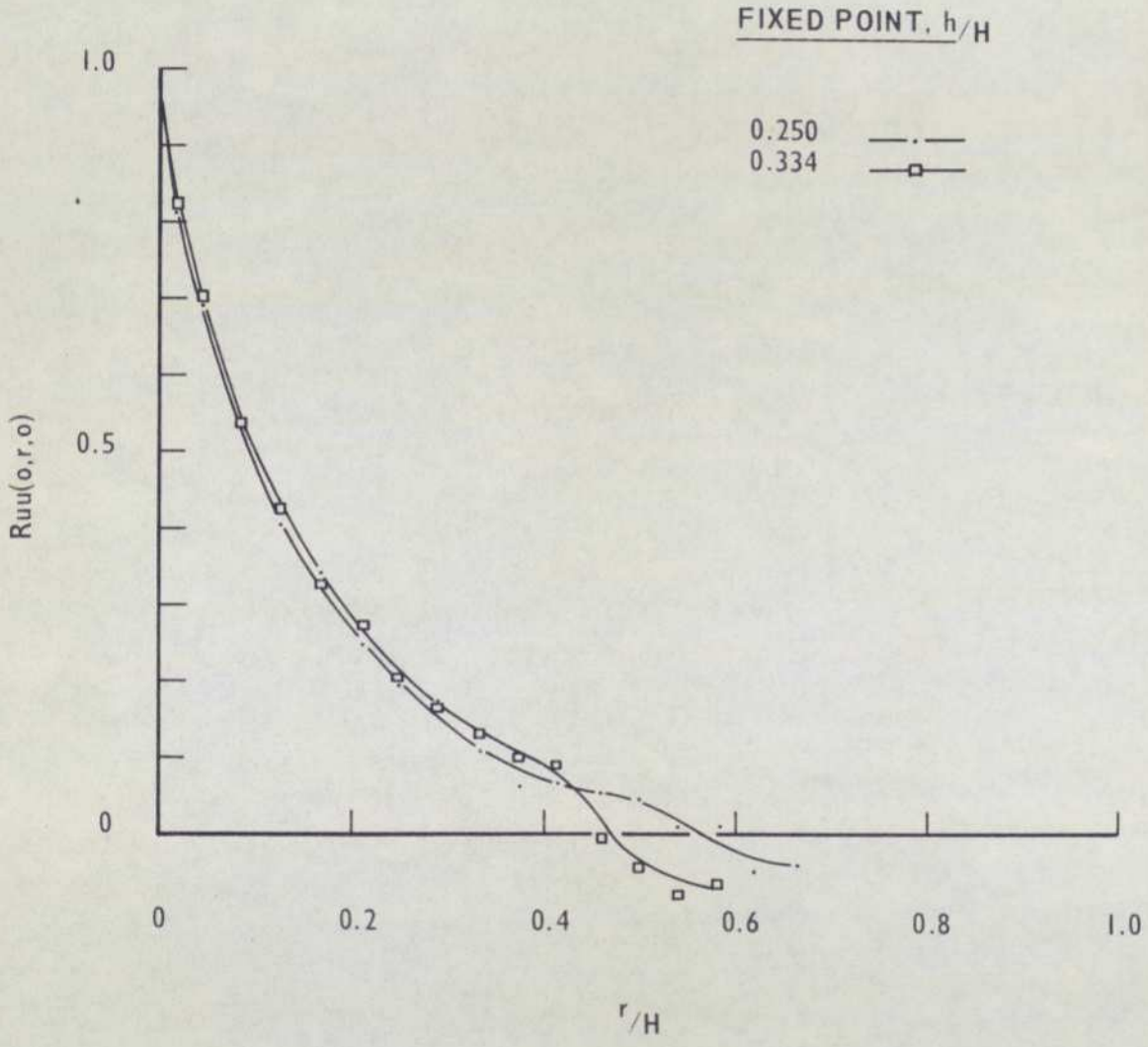


FIG. 109. CORRELATION COEFFICIENT DISTRIBUTION IN A SIMULATED BOUNDARY LAYER. 685 mm (27 in) AFT OF VORTICITY GENERATOR TRAILING EDGES, SPANWISE POSITION - GENERATOR MID-SPAN

URBAN TERRAIN

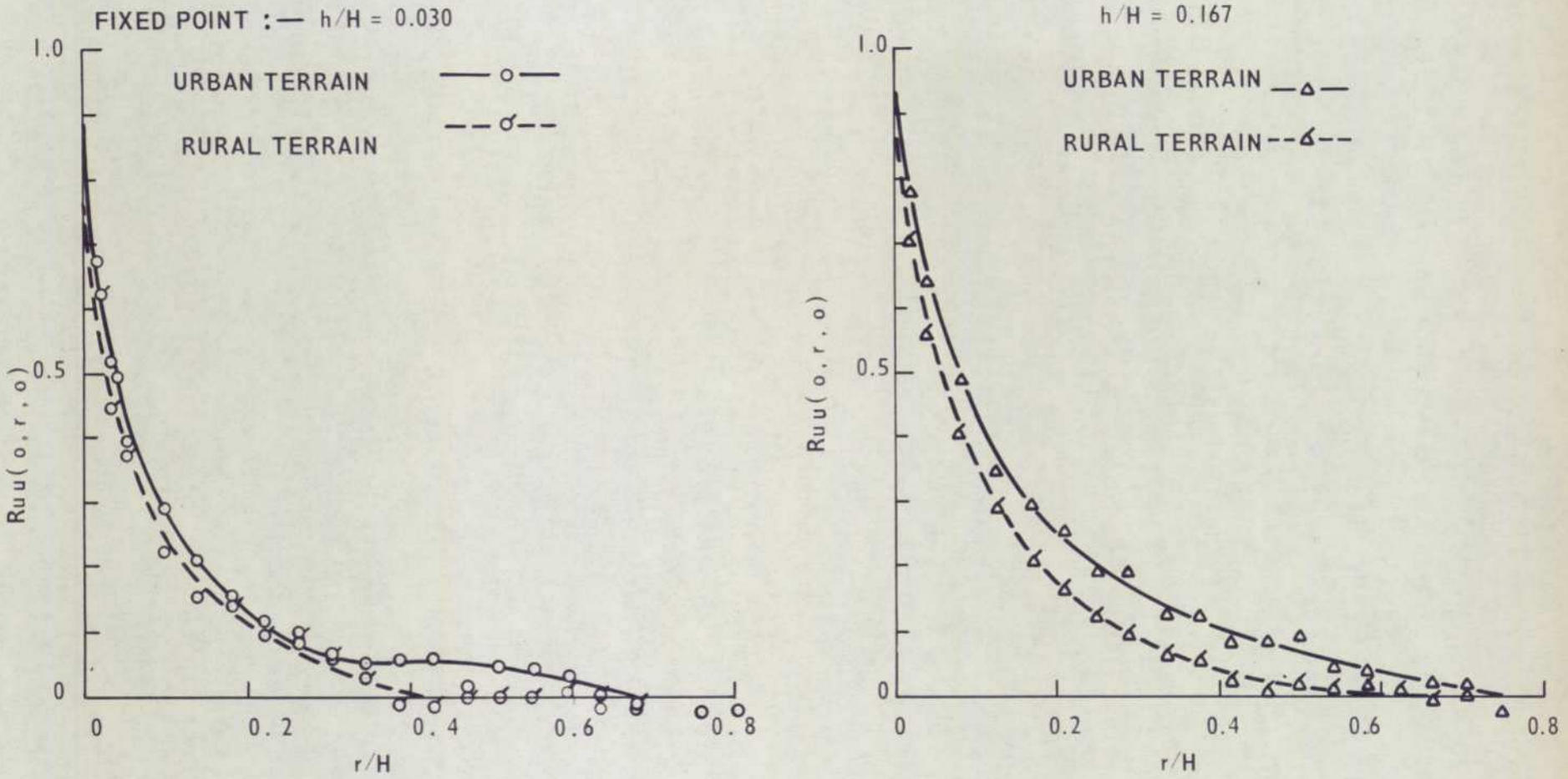


FIG.110.COMPARISON OF CORRELATION COEFFICIENT DISTRIBUTIONS IN SIMULATED BOUNDARY LAYERS.
SPANWISE POSITION: GENERATOR CENTRE-LINE

FIXED POINT: 19.05 mm (0.75 in)
AT $h/H = 0.20$

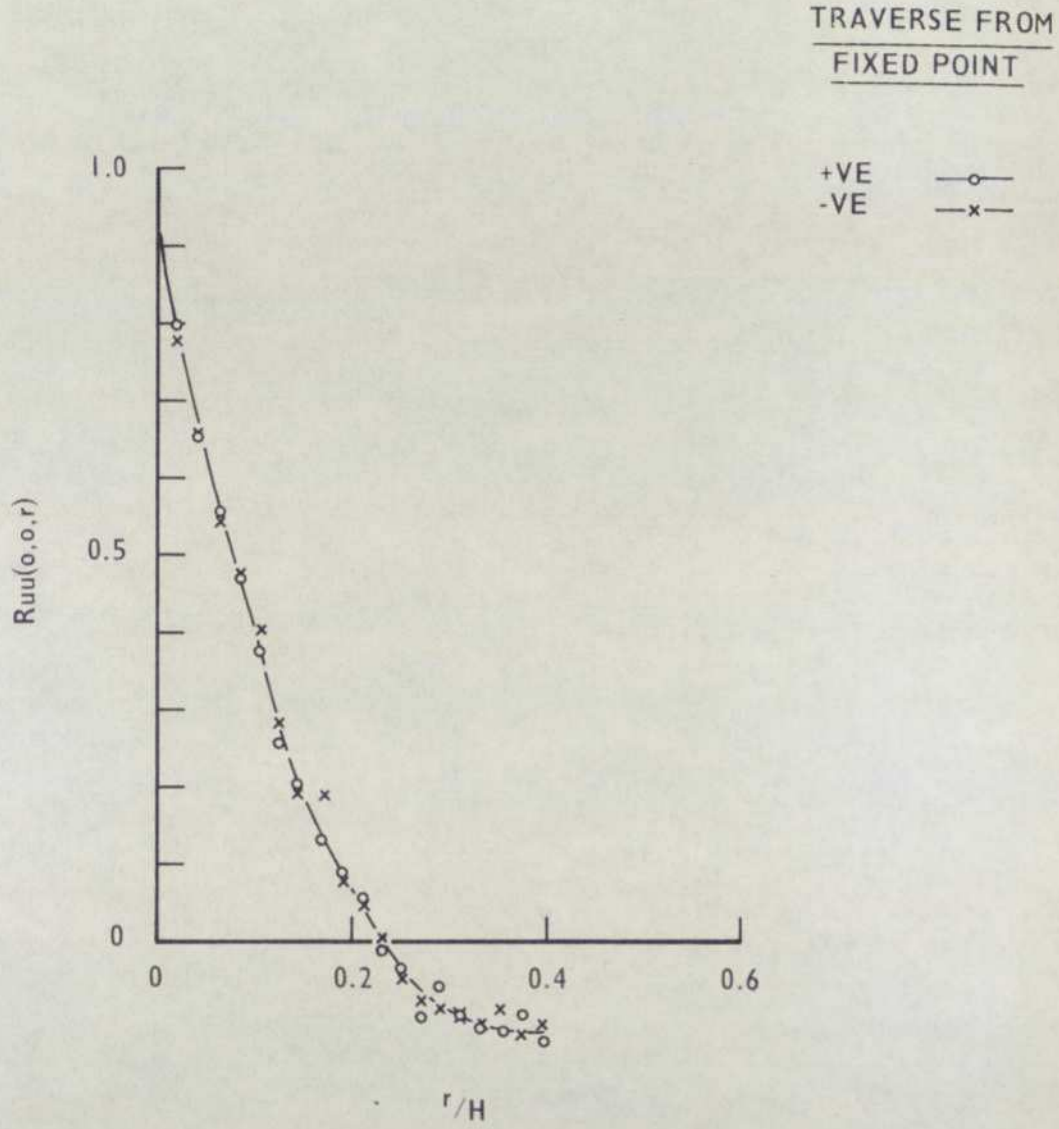


FIG. III. CORRELATION COEFFICIENT DISTRIBUTION IN A SIMULATED BOUNDARY LAYER. 685 mm (27 in) AFT OF VORTICITY GENERATOR TRAILING EDGES

URBAN TERRAIN

FIXED POINT: 0 mm (0 in)

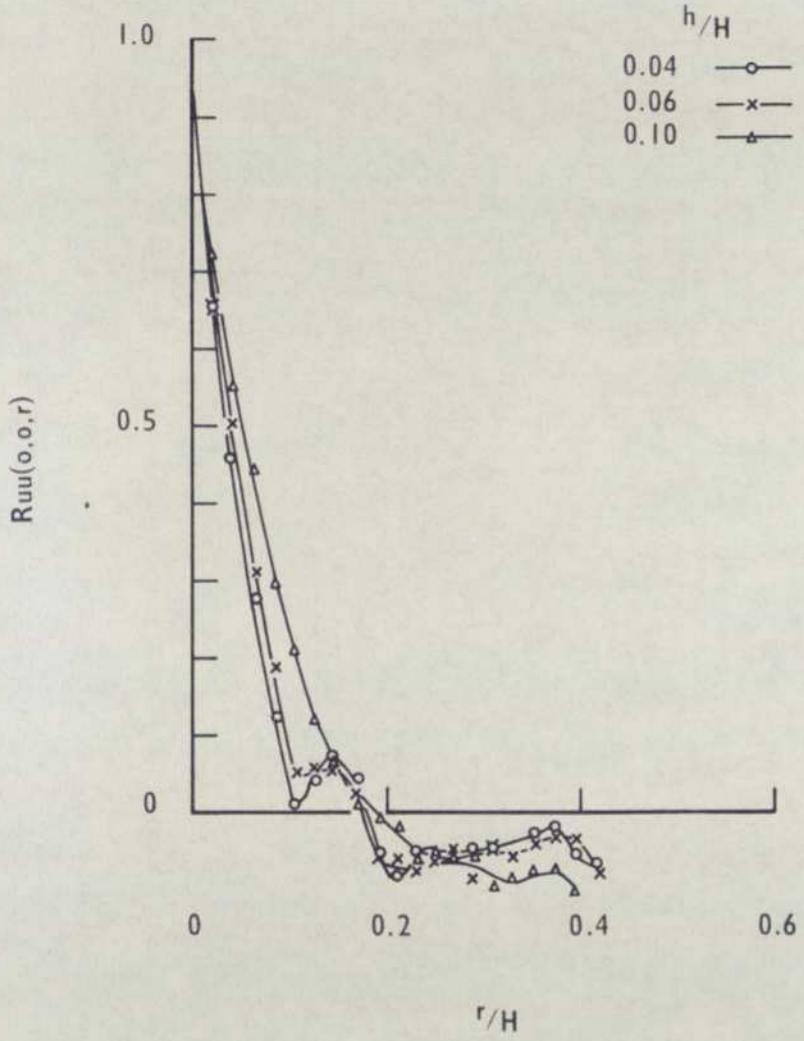


FIG. 112. CORRELATION COEFFICIENT DISTRIBUTION IN A SIMULATED BOUNDARY LAYER. 685 mm (27 in) AFT OF VORTICITY GENERATOR TRAILING EDGES

URBAN TERRAIN

FIXED POINT: 0 mm (0 in)

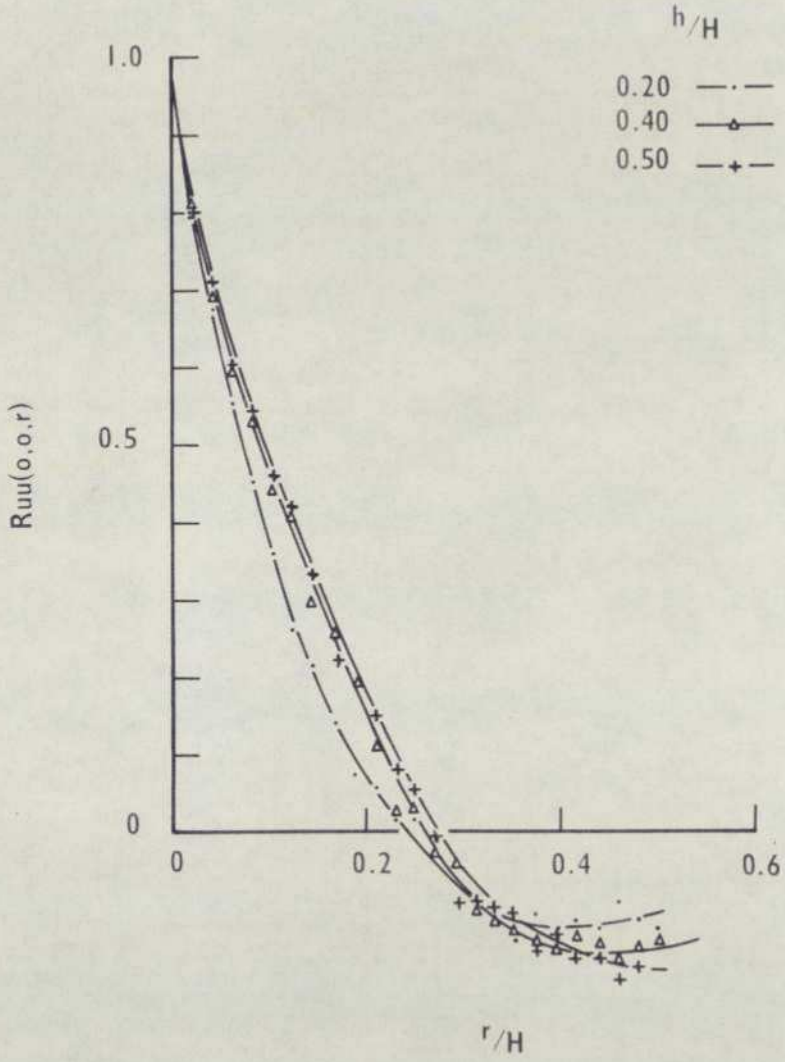


FIG. 113. CORRELATION COEFFICIENT DISTRIBUTION IN A SIMULATED BOUNDARY LAYER. 685 mm (27 in) AFT OF VORTICITY GENERATOR TRAILING EDGES

URBAN TERRAIN

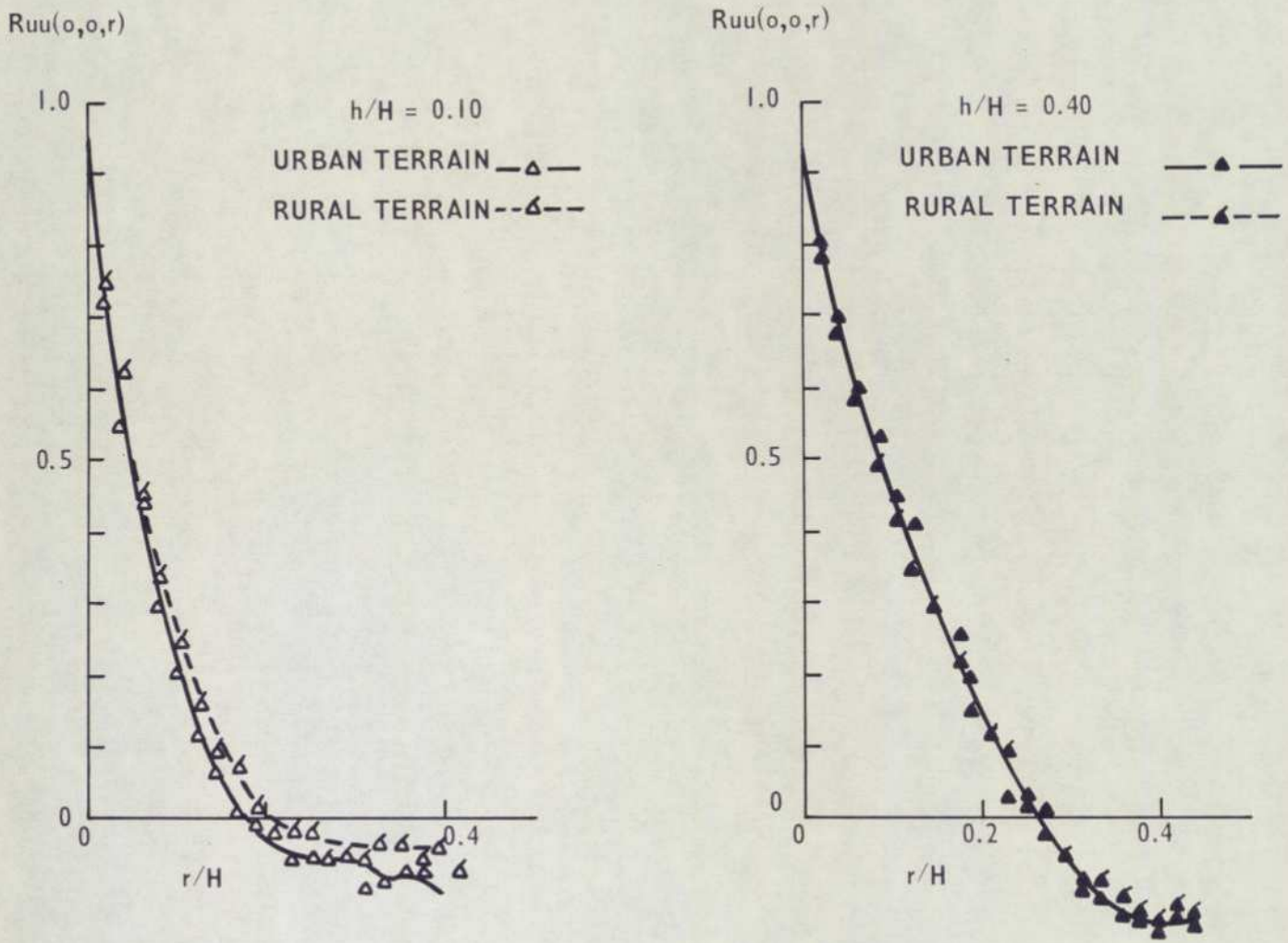


FIG.114 COMPARISON OF CORRELATION COEFFICIENT DISTRIBUTIONS IN SIMULATED BOUNDARY LAYERS.

FIXED POINT: 0 mm (0 in)

JC/D L (CON)(6.4.72)RL 3.3.3063

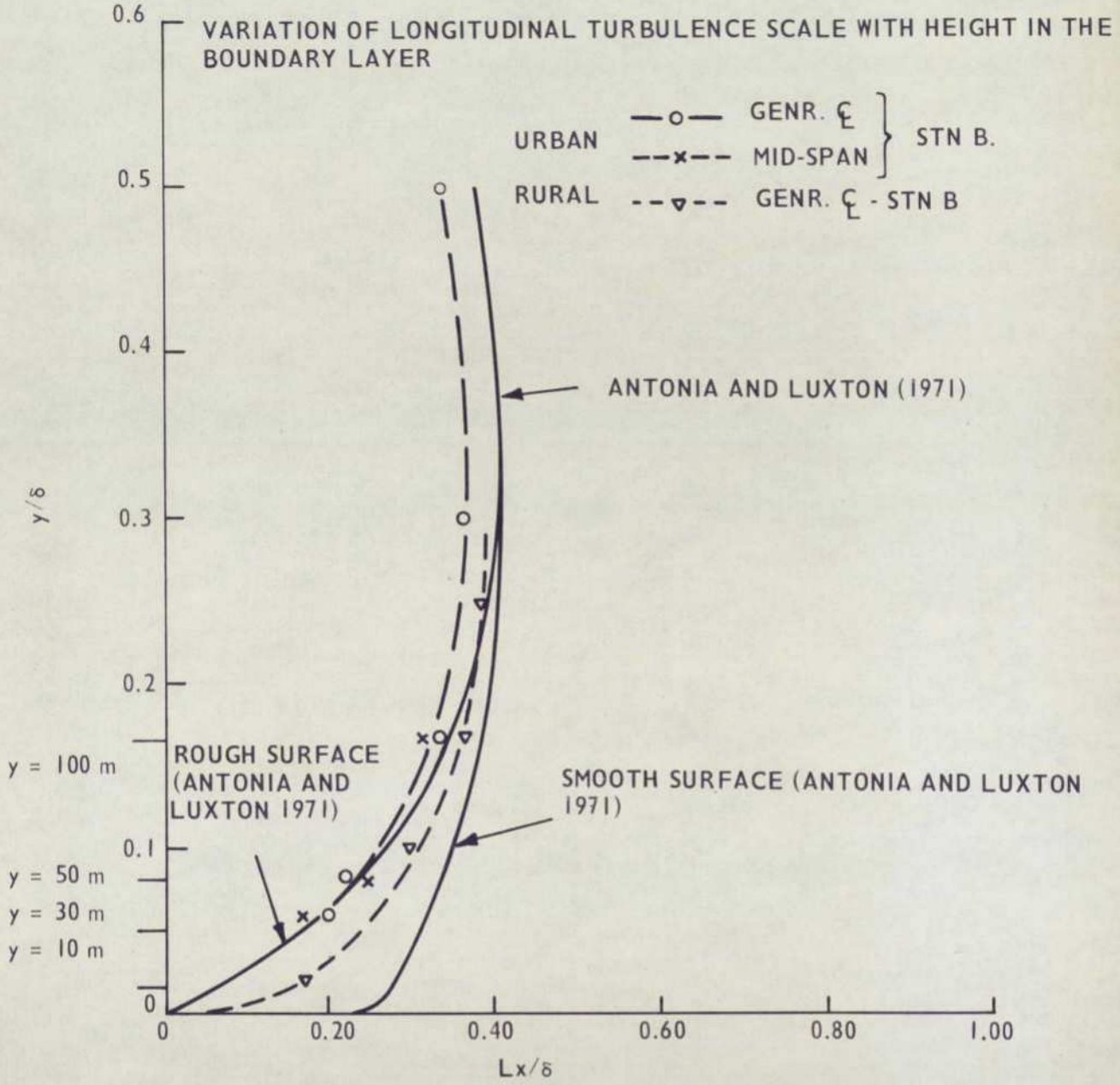


FIG.115. BOUNDARY LAYER SIMULATION - URBAN TERRAIN

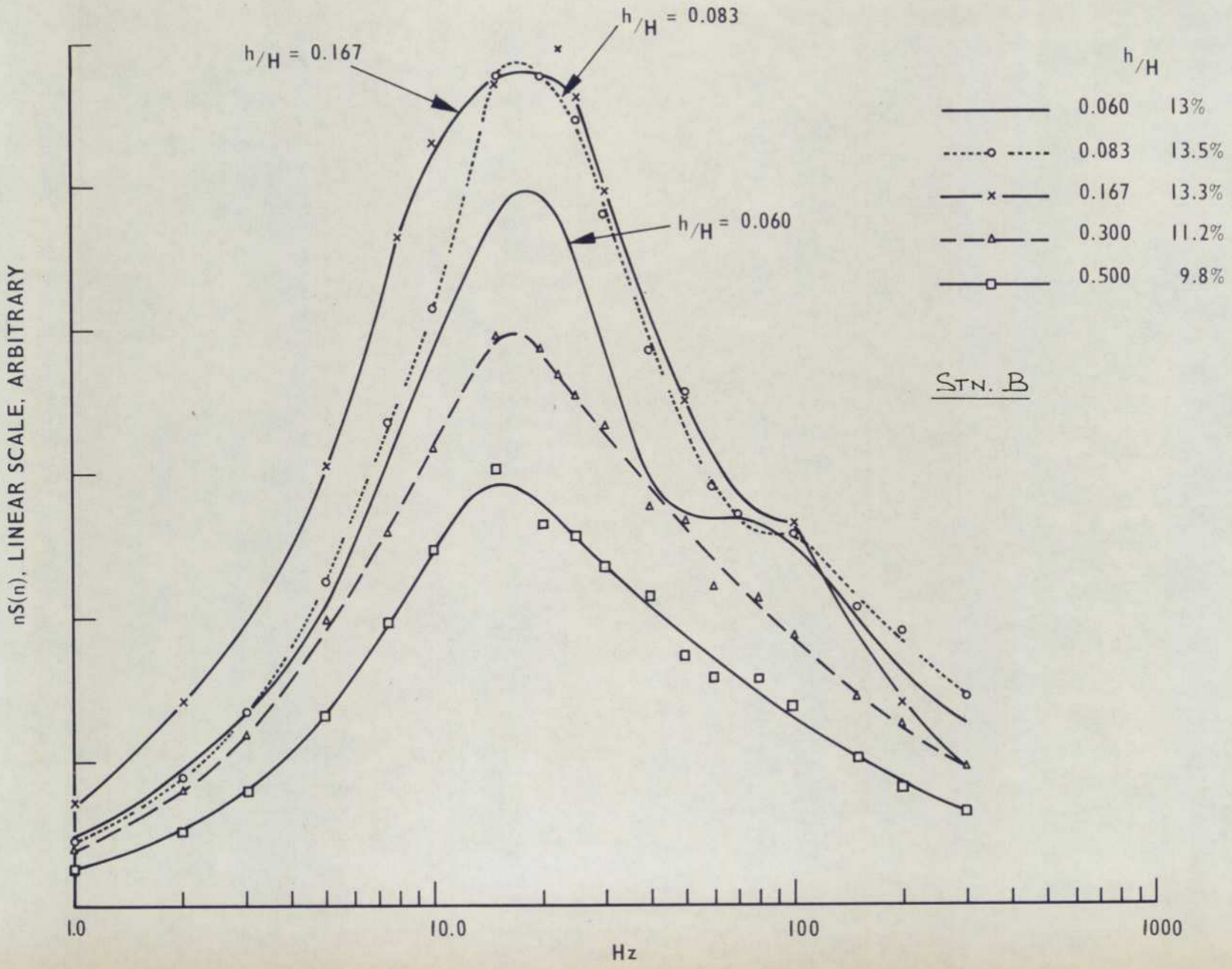


FIG 116. URBAN BOUNDARY LAYER SIMULATION, POWER SPECTRAL DENSITIES OF LONGITUDINAL VELOCITY ON GENR. G

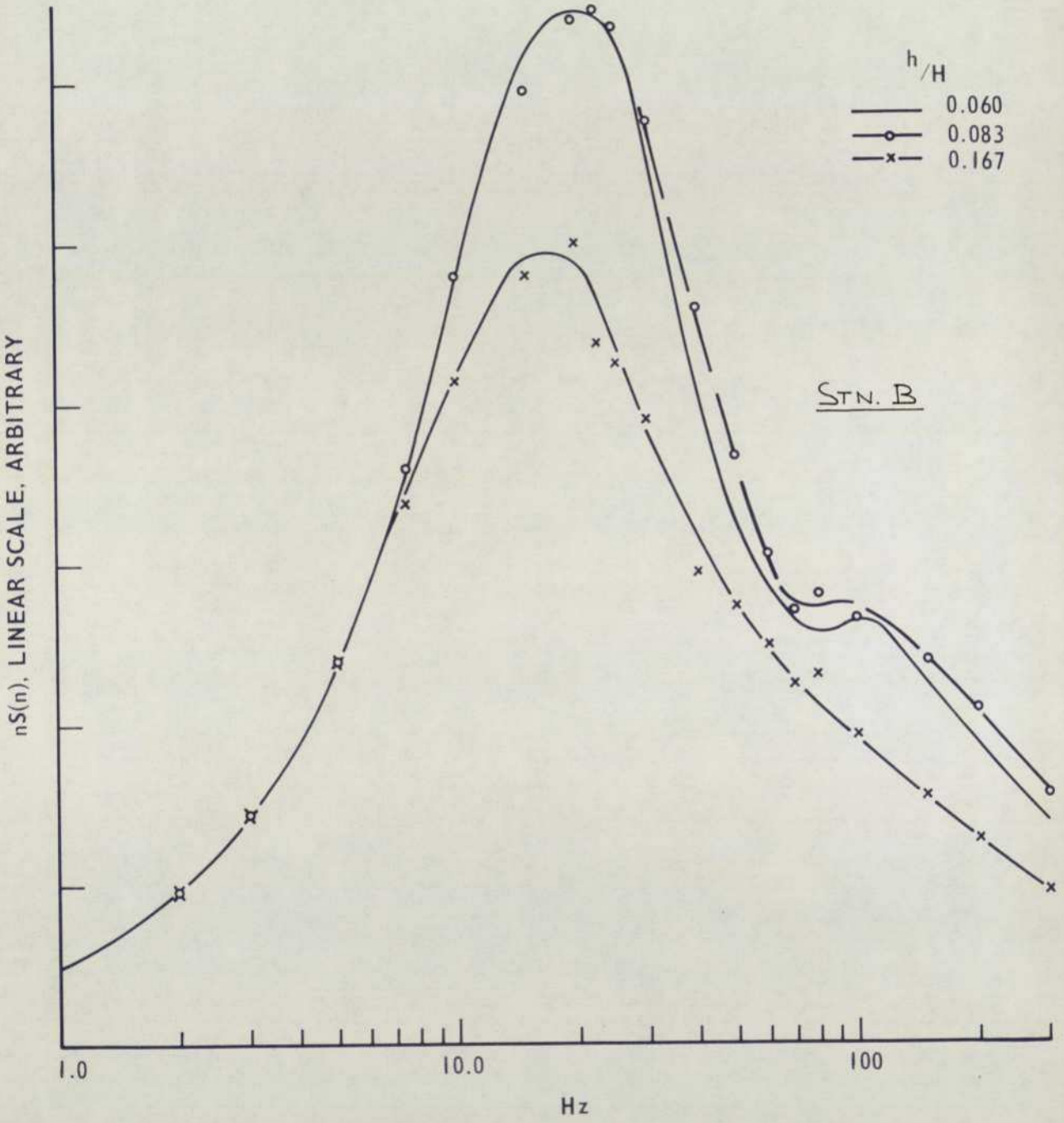


FIG.117 URBAN BOUNDARY LAYER SIMULATION, POWER SPECTRAL DENSITIES OF LONGITUDINAL VELOCITY ON MID-SPAN

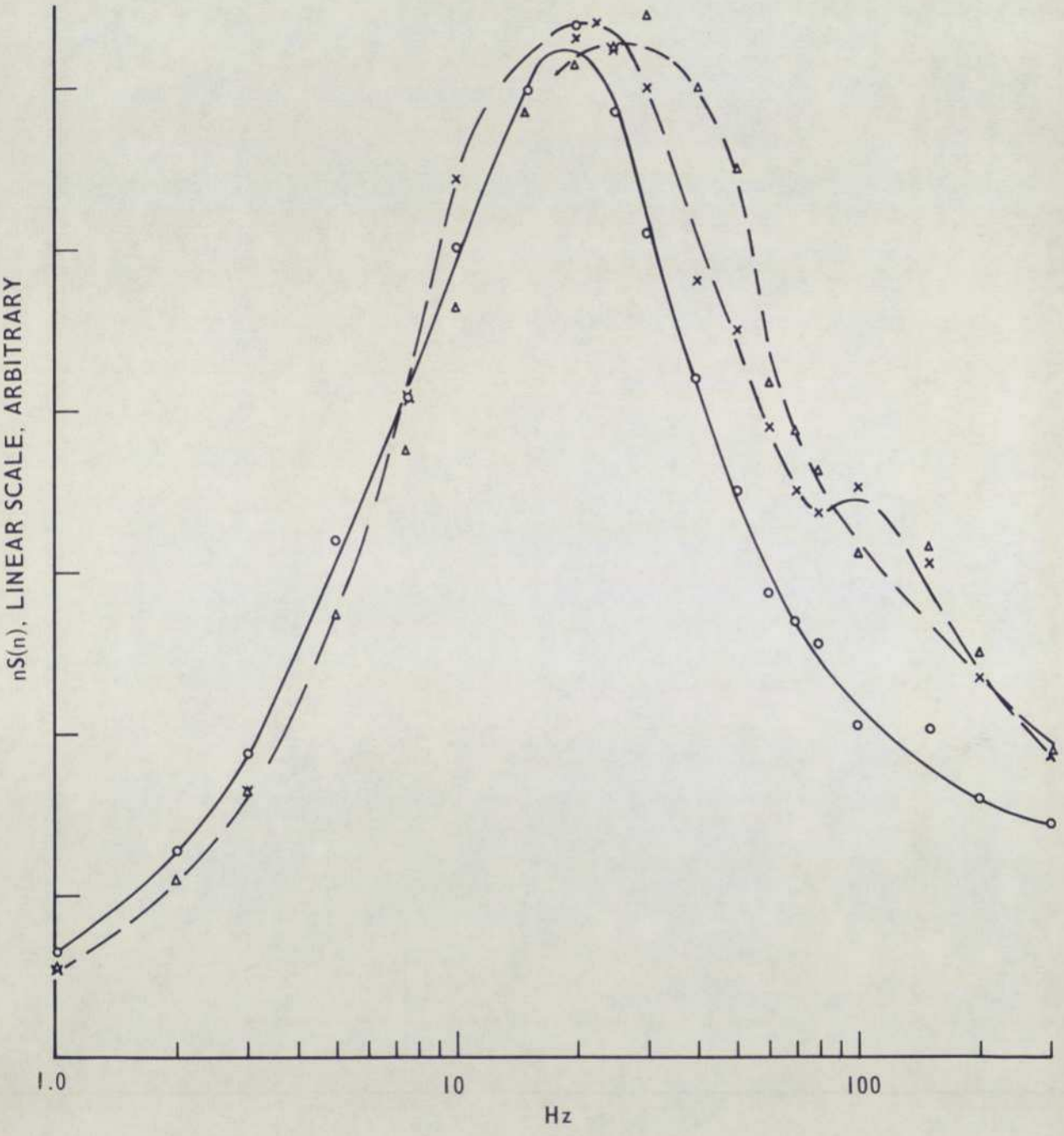


FIG. 118. URBAN BOUNDARY LAYER SIMULATION, POWER SPECTRAL DENSITIES OF LONGITUDINAL VELOCITY AT h/H = 0.083, ROUGHNESS EFFECTS

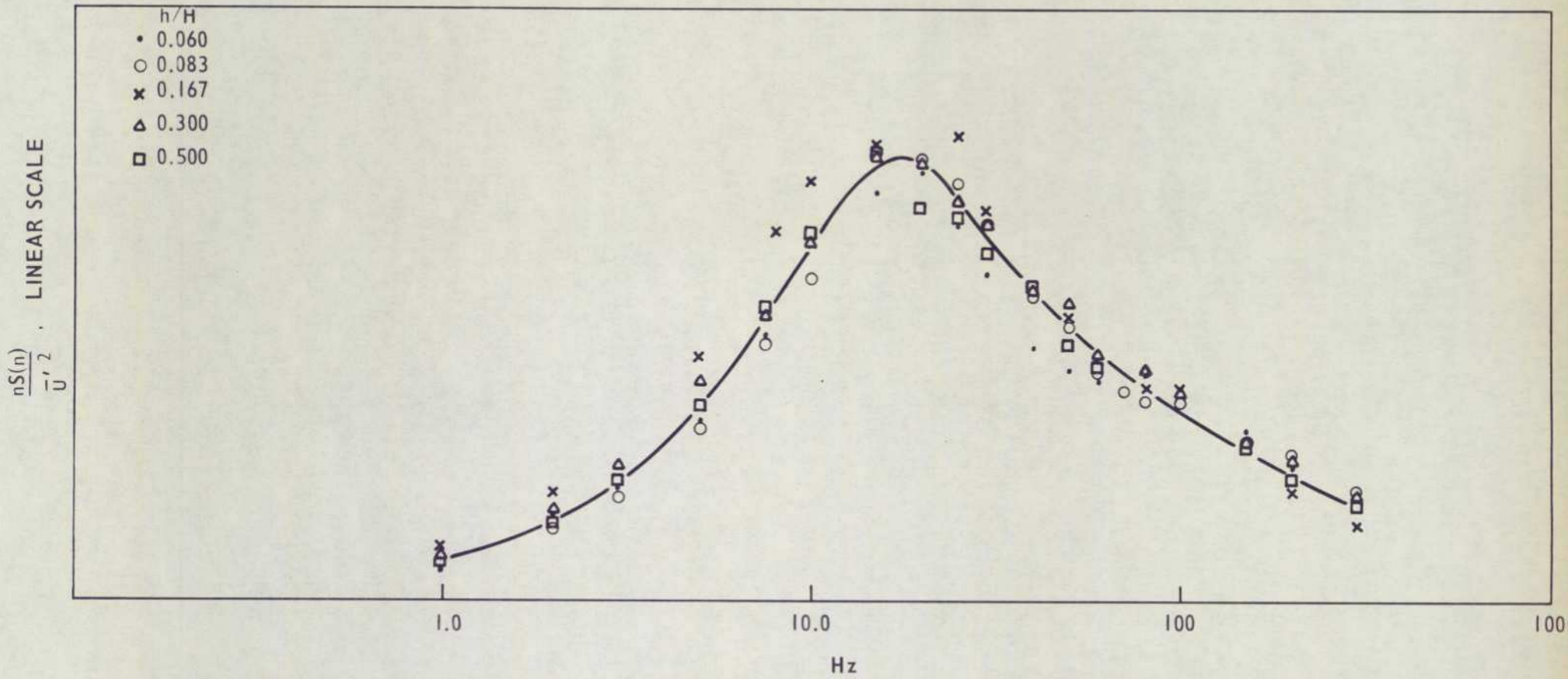


FIG.119 URBAN BOUNDARY LAYER SIMULATION.NORMALISED POWER SPECTRAL DENSITIES OF LONGITUDINAL VELOCITY ON GENERATOR CENTRE-LINE

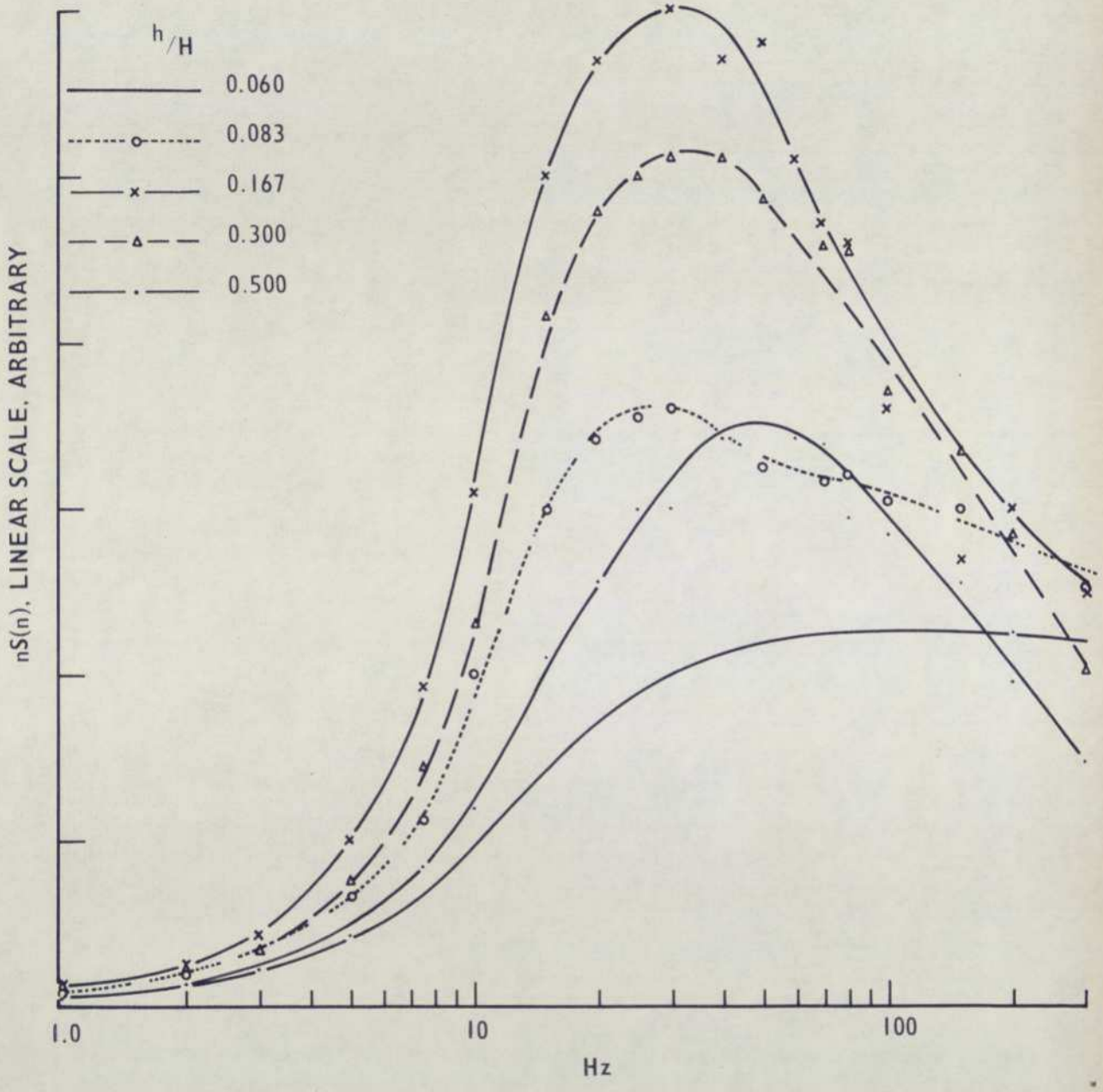


FIG.120. URBAN BOUNDARY LAYER SIMULATION, POWER SPECTRAL DENSITIES OF LATERAL VELOCITY ON GENR. G_L

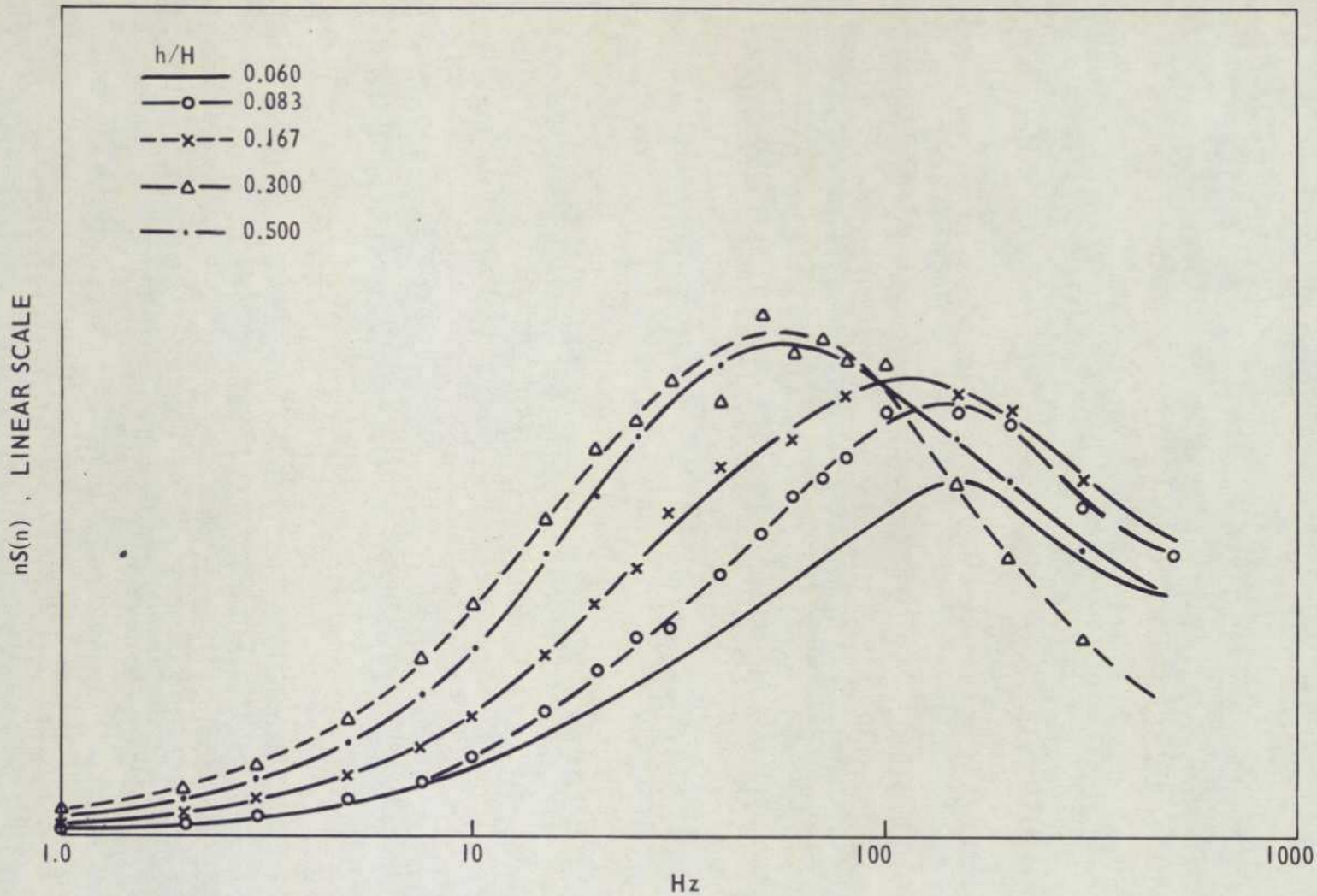


FIG.121.URBAN BOUNDARY LAYER SIMULATION.POWER SPECTRAL DENSITIES OF VERTICAL VELOCITY ON GENERATOR CENTRE LINE

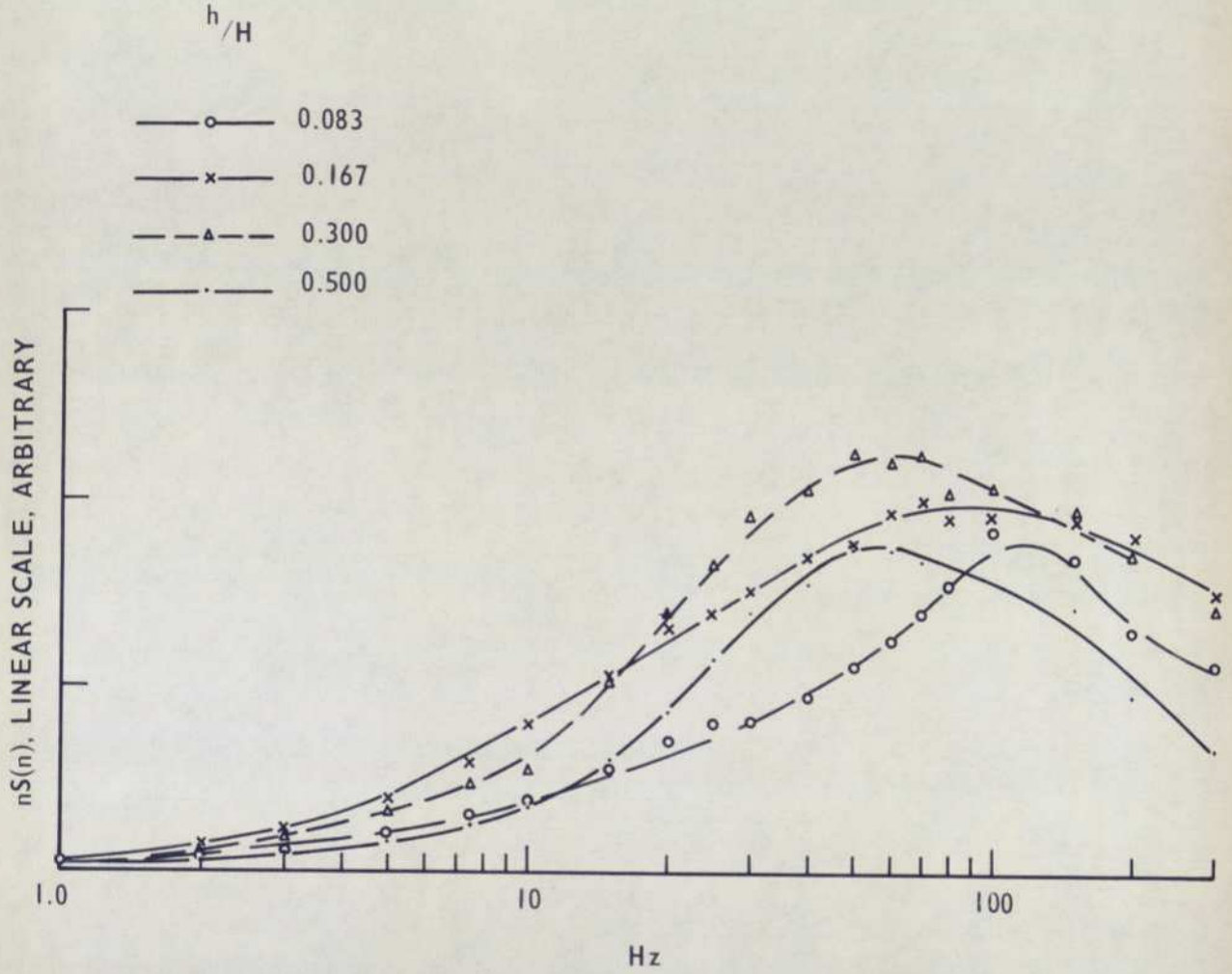


FIG.122 RURAL BOUNDARY LAYER SIMULATION, POWER SPECTRAL DENSITIES OF VERTICAL VELOCITY ON GENR. G

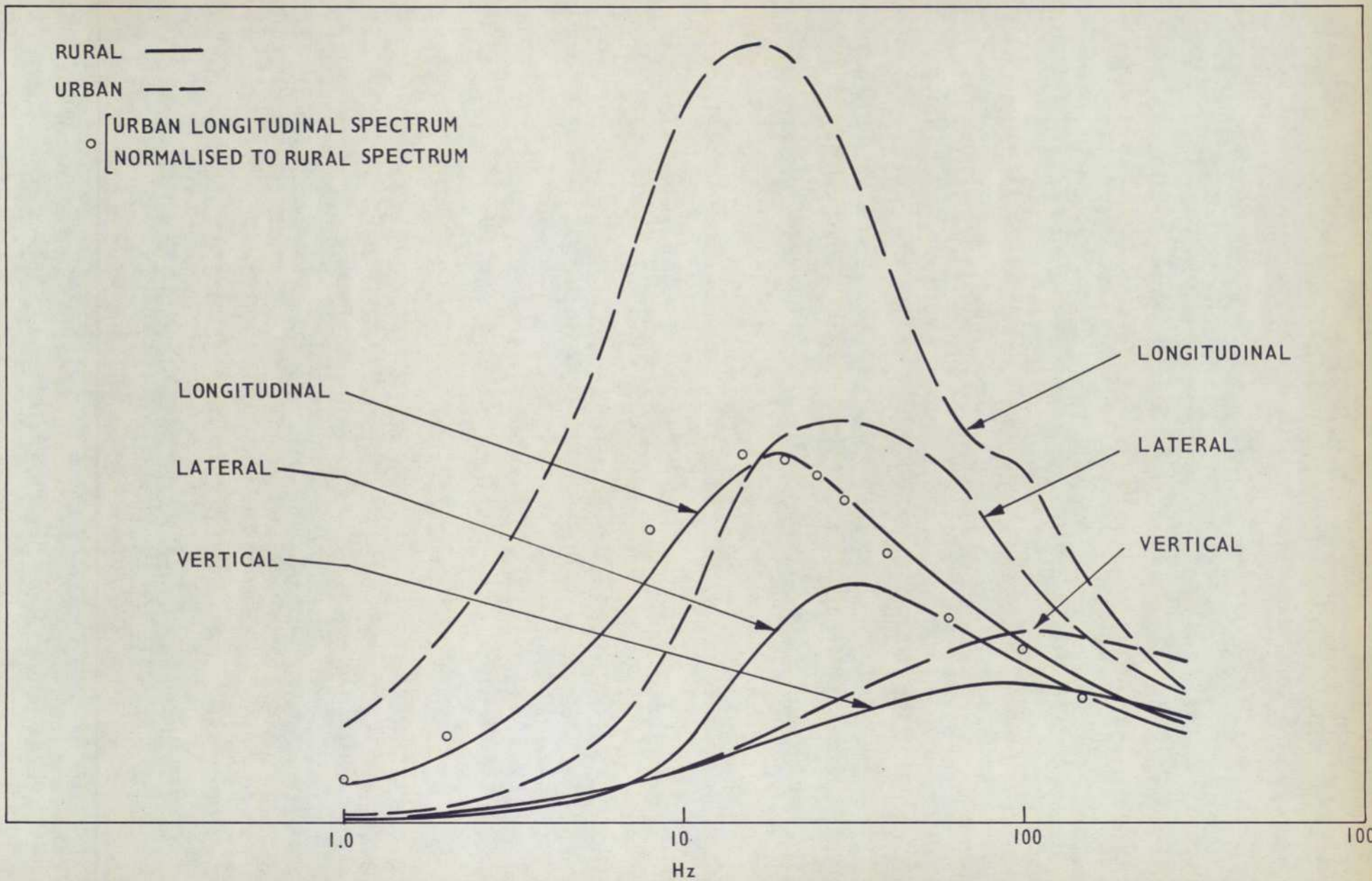


FIG.123. URBAN BOUNDARY LAYER SIMULATION. POWER SPECTRAL DENSITIES OF FLUCTUATING VELOCITIES AT h/H = 0.167

JC/D.L.(CON)(6.4.72)RL.3.3.3065

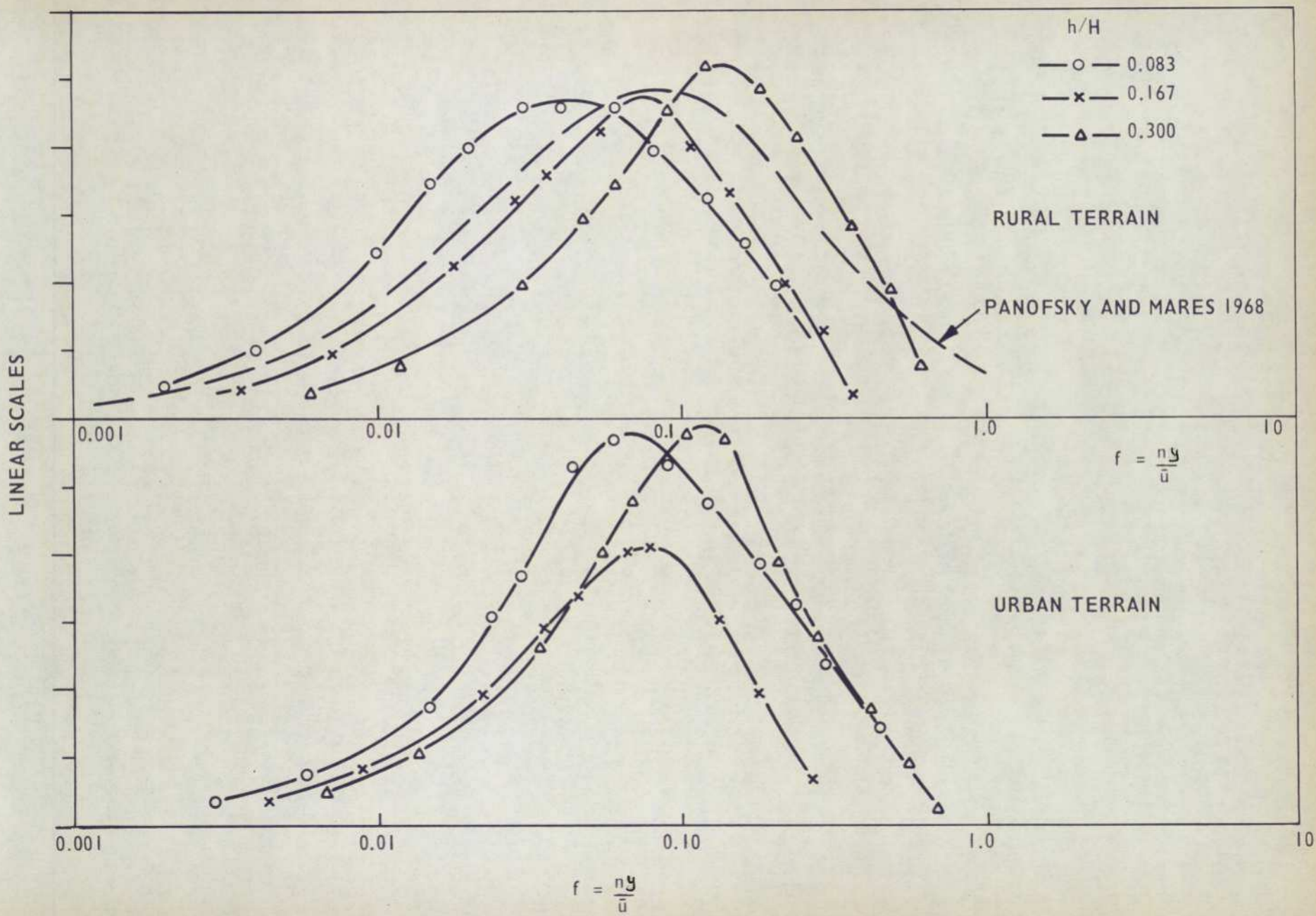


FIG.124 BOUNDARY LAYER SIMULATION: COSPECTRA OF THE LONGITUDINAL AND VERTICAL FLUCTUATING VELOCITIES

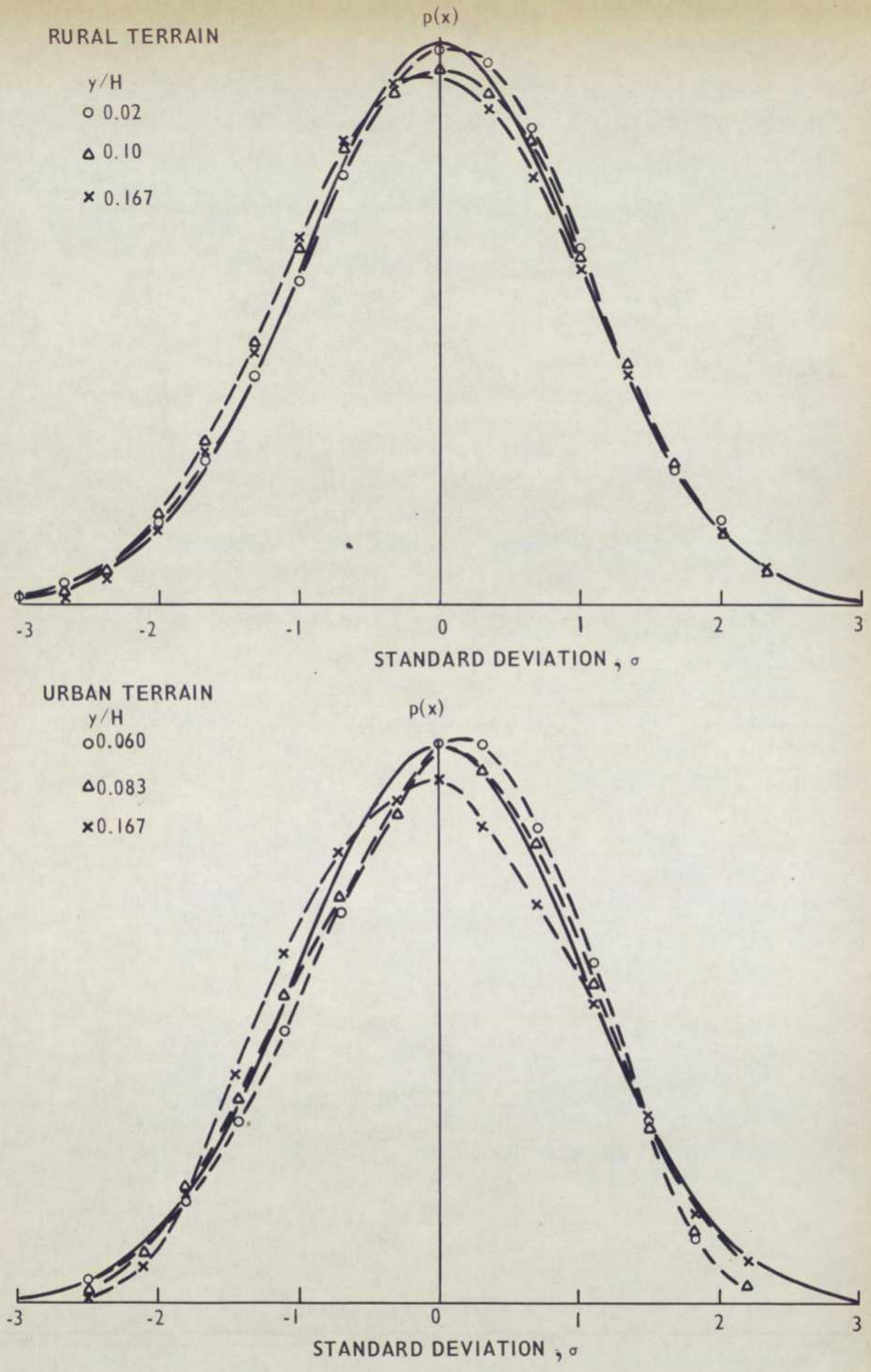


FIG.125. PROBABILITY DENSITY DISTRIBUTION OF THE LONGITUDINAL FLUCTUATING VELOCITY IN SIMULATED RURAL AND URBAN BOUNDARY LAYERS

JC/D.L.(CON)(6.4.72)RL.3.3.3069

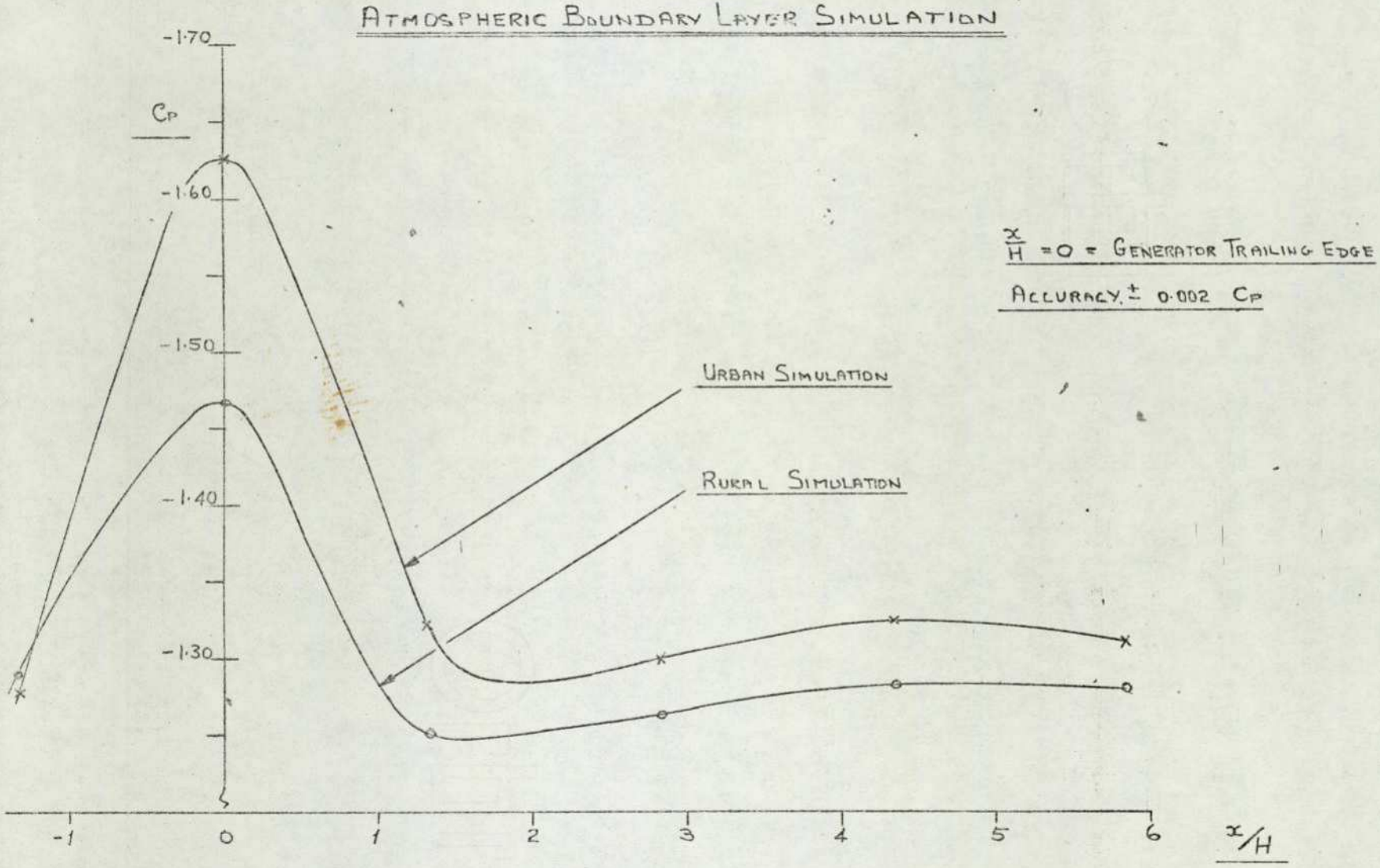


FIG. 126 AXIAL PRESSURE GRADIENT IN BOUNDARY LAYER WIND TUNNEL.

Atmospheric Boundary Layer Structure

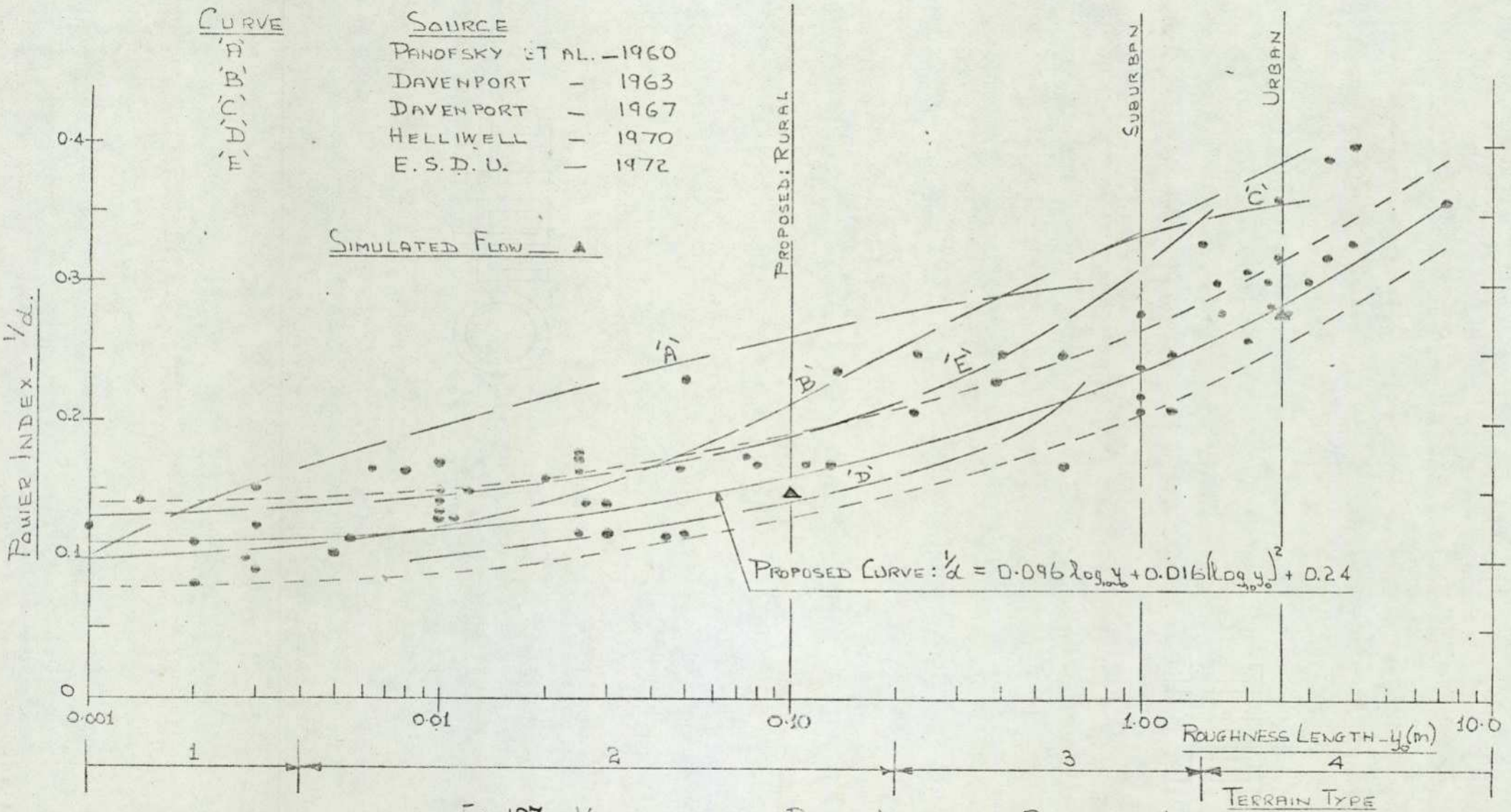


Fig. 127 Variation of the Power Index with Roughness Length

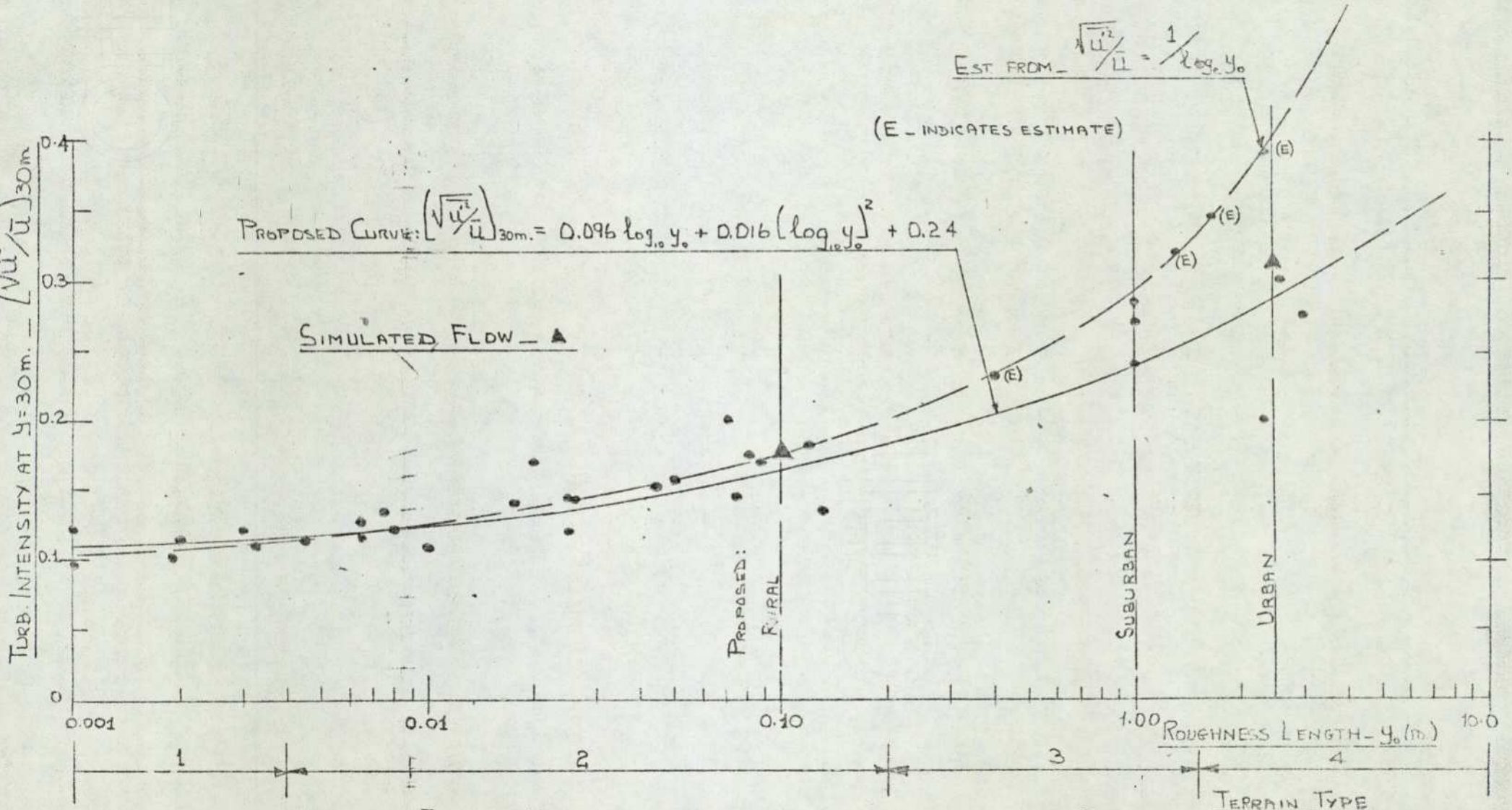


FIG. 12 8 VARIATION OF TURBULENCE INTENSITY WITH ROUGHNESS LENGTH.

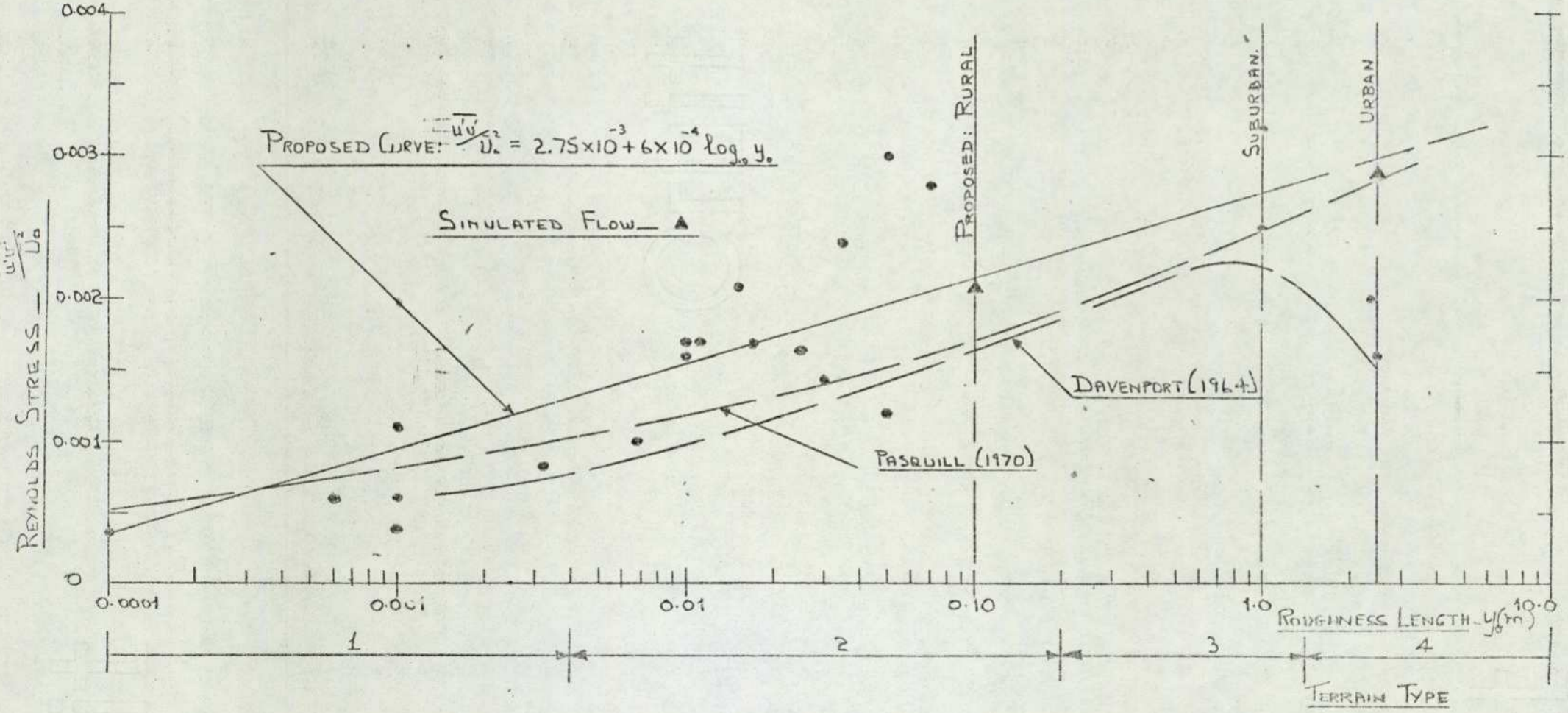


FIG. 129. VARIATION OF REYNOLDS STRESS WITH ROUGHNESS LENGTH.

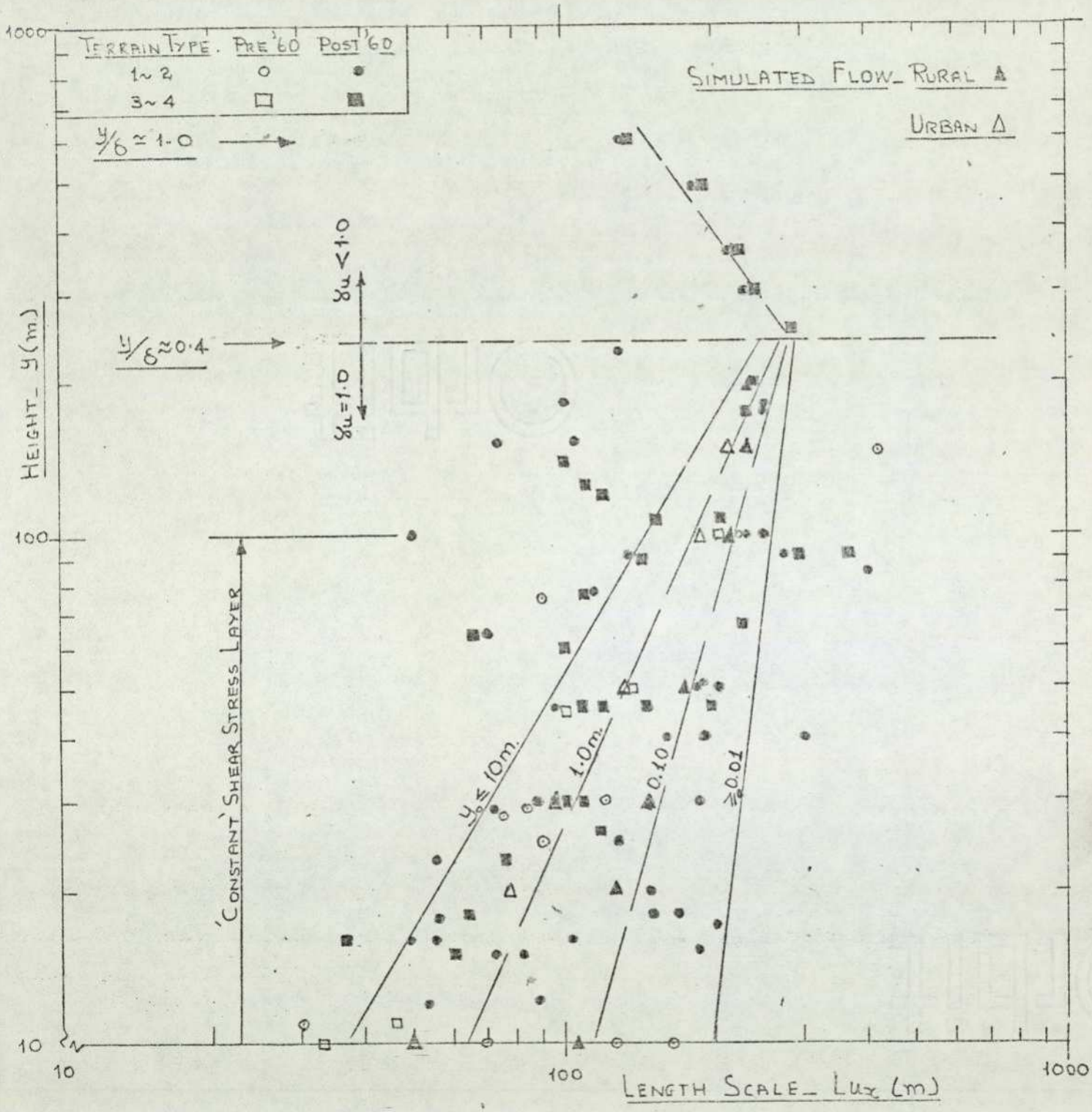


FIG. 130 VARIATION OF LENGTH SCALE WITH HEIGHT AND ROUGHNESS LENGTH.